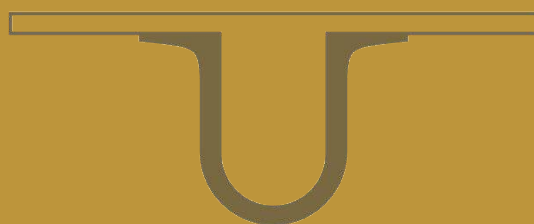




UNIVERSIDADE D
COIMBRA



Lucas Danilo Dias

DEVELOPMENT OF METAL CATALYSTS FOR
ACTIVATION OF CO AND CO₂. SYNTHESIS OF SMALL
RING HETEROCYCLES WITH POTENTIAL
BIOLOGICAL ACTIVITY

Tese no âmbito do Doutoramento em Química, ramo em Catálise e Sustentabilidade orientada pela Professora Doutora Maria Miguéns Pereira, co-orientada pela Professora Doutora Maria Paula Matos Marques Catarro e pelo Doutor Mário José Ferreira Calvete e apresentada ao Departamento de Química da Faculdade de Ciências e Tecnologia da Universidade de Coimbra.

Fevereiro de 2019

Universidade de Coimbra
Departamento de Química – Faculdade de Ciências e Tecnologia

**Development of Metal Catalysts for
Activation of CO and CO₂. Synthesis of Small
Ring Heterocycles with Potential
Biological Activity**

Lucas Danilo Dias

Tese de Doutoramento em Química, ramo de especialização em Catálise e Sustentabilidade, orientada pela Professora Doutora Maria Miguéns Pereira, co-orientada pela Professora Doutora Maria Paula Matos Marques Catarro e pelo Doutor Mário José Ferreira Calvete e apresentada ao Departamento de Química da Faculdade de Ciências e Tecnologia da Universidade de Coimbra.

Coimbra, 2019

“Bem-aventurado o homem que acha a sabedoria, e a pessoa que encontra o entendimento, pois a sabedoria é muito mais proveitosa que a prata, e o lucro que ela proporciona é maior que o acúmulo de ouro fino”
Provérbios 3:13,14

Agradecimentos

Inicialmente, gostaria de prestar os meus sinceros votos de agradecimento à Professora Mariette Pereira, minha orientadora, pela forma única, crítica e construtiva em que se fez presente durante todos estes meus anos de formação académica. Desta forma, deixo aqui o meu muito obrigado por todos os ótimos momentos de convivência, sendo eles de orientação ou de uma simples conversa sobre a vida e claro, por me deixar conhecer um pouco sobre o “universo” das porfirinas. Sou muito grato por todas as oportunidades. Muito obrigado por acreditar em mim.

Agradeço à Professora Maria Paula Marques, minha co-orientadora, por todos os ensinamentos, discussões científicas e por toda simpatia desde o nosso primeiro contacto. Também gostaria de agradecer à Ana Batista de Carvalho, por toda discussão e ensinamento laboratorial no âmbito dos ensaios biológicos.

Agradeço também ao Doutor Mário Calvete, meu co-orientador, por toda ajuda, ensinamentos, conversas e partilha de bons momentos durante estes anos no DQ da Universidade de Coimbra. Obrigado por estar sempre disponível.

A todos os professores do Departamento de Química da Universidade de Coimbra e em especial ao Professor Christopher Brett, diretor do doutoramento em Química da Universidade de Coimbra, por todos os ensinamentos e conversas.

Ao Professor Armando Pombeiro, diretor do Programa de doutoramento Interuniversitário em Catálise e Sustentabilidade (CATSUS).

Gostaria também de agradecer à Professora Liane Rossi, por me receber em seu laboratório na Universidade de São Paulo, de uma forma muito simpática e por me apresentar o fantástico “mundo” das nanopartículas magnéticas. Agradeço ao Jhonatan por toda ajuda no laboratório e a todos os membros do Laboratório de Nanomateriais e Catálise (IQ-USP), nomeadamente ao Bruno, Nágila, Guilherme, Tomaz, Karla, Ofélia, Thalita, Rerison e Adriano.

Agradeço também à Professora Carmen Claver e à Professora Anna M. Masdeu Bultó por me receber no laboratório de Catálise e Química Inorgânica da

Universitat Rovira i Virgili (Tarragona, Espanha) e por toda colaboração no âmbito da ativação de CO₂.

À Professora Doutora Ermelinda Eusébio e à Professora Teresa Roseiro pela colaboração nas análises de TG-DSC. Obrigado por toda ajuda! (谢谢).

À Sílvia Gramacho por todo auxílio e contribuição nas análises de GC-MS.

Ao Professor Rui Brito e ao Pedro Cruz pelo serviço de Ressonância Magnética Nuclear do Centro de Química de Coimbra, relativamente a colaboração na obtenção dos espectros de RMN.

Ao Professor Gilberto Aquino por todas as discussões, conselhos e pela amizade. Obrigado por tudo.

A todos os colegas do Laboratório de Catálise & Química Fina da Universidade de Coimbra (César, Liliana, Carolina, Vanessa, Fábio, Giusi, Rafael, Diana, Andreia) por toda ajuda e partilha de bons momentos de trabalho. Em especial, gostaria de agradecer ao Rui Carrilho por toda ajuda/colaboração durante estes anos.

Aos meus amigos e companheiros (João Pedro, Marcello, Lucas Lino, Ruben, João Paulo, Neto, Ezequiel, ...) pelos momentos de amizade que vivemos e o que iremos viver.

À minha família (Jonathan, Jaison Jr., Vanessa, Jaison, Alex, Marlene, Letícia, Sônia) e os que eu considero como família (Cristiane e Edson), por sempre acreditar em mim. Em especial e com carinho, à minha mãe (Rosilda) por ser a minha base e amiga. Você é peça fundamental nesta conquista.

Gostaria também de agradecer, à Júlia, minha amiga e companheira, pelo amor, carinho, ajuda e pela compreensão durante todos estes anos. Obrigado por tudo.

Por último ao Conselho Nacional de Desenvolvimento Científico e Tecnológico (CNPq – Brasil) pelo apoio financeiro através da concessão da bolsa de doutorado 232620/2014-8 GDE.

Lucas D. Dias

Fevereiro de 2019

Table of Contents

Abstract	i
Resumo	iii
Abbreviations and Symbols	vii
List of Compounds	xi
Nomenclature	xiii
Chapter 1 – Introduction	1
1.1. Catalysis in the Green Chemistry Context	1
1.2. Designing Catalytic Processes	6
1.3. Metalloporphyrins as Bioinspired Catalysts	8
1.3.1 Cytochrome P-450	8
1.3.2 Metalloporphyrins in Epoxidation Reactions	11
1.4. Metalloporphyrins as Catalysts in Sequential Epoxidation/CO ₂ Cycloaddition Reaction	27
1.5. Renewable Terpene-based Raw Materials for the Pharmaceutical Industry	31
1.5.1 Hydroformylation of Terpenes	33
1.6. References	38
Chapter 2 – Synthesis of Metalloporphyrins Catalysts	51
2.1. Introduction	51
2.2. Synthesis of Metalloporphyrins for Homogeneous Catalysis	53
2.3. Synthesis of Hybrid Metalloporphyrins for Heterogeneous Catalysis	62
2.3.1 Synthesis of Magnetite Nanoparticles (MNP)	64
2.3.2 Synthesis of Silica-coated Magnetite Nanoparticles (MNP@SiO ₂)	65
2.3.3 Functionalisation of Silica-coated Magnetite Nanoparticles	70
2.3.4 Synthesis of Hybrid Metalloporphyrins Magnetic Catalysts	73
2.4. Conclusions	80
2.5. References	81

Chapter 3 – Heterobimetallic Dual-Catalyst for Transformation of Olefins into Cyclic Carbonates	83
3.1. Introduction	83
3.2. Catalytic Epoxidation.....	85
3.3. Catalytic CO ₂ Cycloaddition to Epoxides	95
3.4. Sequential Epoxidation/CO ₂ Cycloaddition Reactions	101
3.5. Conclusions	105
3.6. References.....	107

Chapter 4 – Synthesis of Biologically Active Terpenes through Catalytic Processes	109
4.1. Introduction	109
4.2. Catalytic Epoxidation of Terpenes using Molecular Oxygen.....	110
4.2.1 Recyclability and Reusability Tests	117
4.2.2 Scale-up and Experimental Setup for the Recovery of Isobutyric Acid	119
4.3. (–)-Isopulegol Benzyl Ether Derivatives as Potential Anticancer Agents against Osteosarcoma	123
4.3.1 Protection Reaction of (–)-Isopulegol	124
4.3.2 Synthesis of (–)-Isopulegol Benzyl Ether Epoxides	125
4.3.3 Hydroformylation of (–)-Isopulegol Benzyl Ether	131
4.3.4 Epoxide Ring-opening of (–)-Isopulegol Benzyl Ether Epoxide.....	132
4.4. Anticancer Activity of (–)-Isopulegol Benzyl Epoxides against Human Osteosarcoma Cells	133
4.5. Conclusions	137
4.6. References	139

Chapter 5 – Experimental	143
5.1. General Information	144
5.1.1 Solvents and Chemicals	144
5.1.2 Instrumentation and Methodology	145
5.2. Experimental of Chapter 2.....	151
5.2.1 Synthesis of Metalloporphyrins for Homogeneous Catalysis.....	151
5.2.2 Synthesis of Hybrid Metalloporphyrins for Heterogeneous Catalysis	164
5.3. Experimental of Chapter 3.....	170
5.3.1 General Procedures for Catalytic Epoxidation Reaction	171
5.3.2 General Procedures for Catalytic CO ₂ Cycloaddition Reaction.....	173
5.3.3 General Procedures for Sequential Epoxidation/CO ₂ Cycloaddition Reaction	174
5.4. Experimental of Chapter 4.....	180
5.4.1 Catalytic Epoxidation of Terpenes.....	180
5.4.2 Catalytic Hydroformylation of (–)-Isopulegol Benzyl Ether	184
5.4.3 Biological Assays of (–)-Isopulegol Benzyl Ether Epoxides	186
5.5. References.....	190

Abstract

The main goal of the work described in this dissertation was the preparation of homogeneous and heterogeneous metal catalysts (immobilized onto magnetic nanoparticles) of tetrapyrrolic macrocycles (metalloporphyrins), with a view to develop sustainable processes for the synthesis and functionalization of small organic molecules, including terpenes, with potential antiproliferative activity. This written thesis is divided into five chapters.

Chapter 1 presents an historical perspective for the application of Catalysis within the Green Chemistry context, as well as a literature review (last five years) of all the topics focused in the experimental work. From this bibliographical review, we highlight the synthesis of cyclic carbonates *via* sequential epoxidation/CO₂ cycloaddition, using metalloporphyrins as bio-inspired catalysts for activation of CO₂, and O₂ and H₂O₂ as oxidants for epoxidation reactions. Finally, a literature revision is also described for the *one-pot* preparation of terpene-aldehydes, from renewable substrates, *via* CO/H₂ activation (hydroformylation).

Chapter 2 refers to the synthesis and characterization of metalloporphyrin-based catalysts. Regarding the synthesis of symmetrical and non-symmetrical porphyrins, three synthetic approaches were used, namely nitrobenzene, nitrobenzene/NaY and a more sustainable strategy, involving water/microwave irradiation. Therefore, a family of symmetric porphyrins with different functionalities (F, CF₃, Cl) and non-symmetrical porphyrins with appropriate functional groups (NH₂, NO₂) were synthesized. Then, the discussion of their subsequent covalent immobilization onto functionalized magnetic nanoparticles and their full characterization (UV-Vis, FT-IR, TG-DSC, TEM, ICP) are presented.

In **Chapter 3**, we describe the use of heterobimetallic dual-catalytic systems for the implementation of sustainable sequential olefin transformations into high added-value cyclic carbonates, *via* epoxidation followed by CO₂ cycloaddition reaction. The optimization studies regarding central metal and catalyst structure for each catalytic system - epoxidation and CO₂ cycloaddition - is discussed. The catalytic systems (MnOAc-TDCPP **15Mn**/isobutyraldehyde) and MnOAc-TDCPP

15Mn/NH₄OAc gave rise to the most active and selective catalytic systems for the epoxidation of olefins, using O₂ and H₂O₂ as oxidants, respectively. The catalytic system (CrCl-TPP*p*CF₃ **12 Cr**/PPNCl) was found to be the most active and selective system for the synthesis of cyclic carbonates. Finally, the direct synthesis of cyclic carbonates from olefins, using homogeneous and/or heterogeneous sequential methodologies are described. The heterogeneous catalysts (**MNP@SiO₂-NH-17Mn** and **MNP@SiO₂-NH-19Cr**) are the ones that gave rise to the best sequential styrene to cyclic carbonate transformation. A remarkable result was achieved when these immobilized catalysts were reused, in several consecutive cycles, without significant loss of activity and selectivity.

Concerning our interest in the development of sustainable methods for preparation of compounds with potential anti-proliferative activity against osteosarcoma, in **Chapter 4** terpenes were chosen as renewable raw materials to implement selected chemical transformations, namely epoxidation, hydroformylation and epoxide ring-opening reactions. Thus, (–)-isopulegol was used as a model terpene and its epoxide derivative was synthesized, with good yield, using **MNP@SiO₂-NH-17Mn** as an immobilized catalyst and O₂ as the oxidant. The (–)-isopulegol benzyl ether aldehyde derivatives were synthesized through an hydroformylation reaction using Rh(acac)(CO)₂/phosphite as a catalyst. Finally, an (–)-isopulegol amino alcohol was prepared *via* epoxide ring opening, using butylamine as a nucleophile and CrCl-TPP*p*CF₃ (**12Cr**) as a catalyst. Moreover, the antiproliferative and cytotoxic activities of each diastereomer of (–)-isopulegol epoxide were evaluated against the human osteosarcoma cell line (MG-63). The measured IC₅₀ values were significantly lower than those reported in the literature for similar compounds (diastereomer **33**: MTT = 249.8 μM, SRB = 114.8 μM; diastereomer **34**: MTT = 158.2 μM, SRB = 104.0 μM).

Chapter 5 comprises the detailed description of all the experimental techniques and instrumentation, as well as of the synthesis/characterization of the new catalysts and catalytic reaction products.

Keywords: biological activity; carbon monoxide and dioxide; homo-/heterogeneous catalysis; small ring heterocycles; sustainable synthesis.

Resumo

O trabalho desenvolvido nesta dissertação orientou-se no sentido de preparar catalisadores metálicos homogêneos e heterogêneos (imobilizados em nanopartículas magnéticas) do tipo macrociclos tetrapirrólicos (porfirinas) para desenvolver processos sustentáveis de síntese e funcionalização de pequenas moléculas orgânicas, incluindo terpenos, com potencial atividade antiproliferativa.

A presente dissertação encontra-se dividida em cinco capítulos. No **Capítulo 1** apresenta-se uma discussão histórica e de aplicação da Catálise no contexto da Química Verde e uma revisão da literatura (últimos cinco anos) que engloba todos os tópicos desenvolvidos no trabalho. Desta revisão bibliográfica destacou-se a utilização de metaloporfirinas como catalisadores bioinspirados em reações de epoxidação utilizando O_2 e H_2O_2 como oxidantes, e de metaloporfirinas como catalisadores para a ativação de CO_2 em reações sequenciais de epoxidação/cicloadição de CO_2 para a síntese de carbonatos cíclicos. Por fim descreveu-se a utilização de terpenos como substratos renováveis na reação de ativação de CO/H_2 (hidroformilação) para a síntese de aldeídos.

No **Capítulo 2** descreve-se a síntese e caracterização de catalisadores metálicos baseados em porfirinas. Para a síntese das porfirinas simétricas e não-simétricas utilizaram-se três estratégias sintéticas, nomeadamente a do nitrobenzeno, do nitrobenzeno/ NaY e uma estratégia sustentável envolvendo água/micro-ondas. Desta forma, sintetizou-se uma família de porfirinas simétricas com diferentes funcionalidades (F, CF_3 , Cl) e uma série de porfirinas não-simétricas com grupos funcionais apropriados (NH_2 , NO_2) para a sua posterior imobilização covalente em nanopartículas magnéticas funcionalizadas. Além disso, apresentam-se ainda os estudos de otimização para a obtenção de nanopartículas magnéticas funcionalizadas com complexos metálicos de porfirinas e a sua completa caracterização (UV-Vis, FT-IR, TG-DSC, TEM, ICP).

No **Capítulo 3** descreve-se a utilização de sistemas catalíticos duais heterobimetálicos para transformações sustentáveis e sequenciais de olefinas em epóxidos, seguidas de cicloadição com CO_2 para a preparação de carbonatos cíclicos

de elevado valor acrescentado. Neste capítulo, discutem-se ainda os estudos de otimização de cada sistema catalítico, tipo de metal/estrutura do catalisador (epoxidação e cicloadição de CO₂) relativamente ao tipo de metal/estrutura do catalisador e condições reacionais utilizadas. Após otimização, os sistemas catalíticos (MnOAc-TDCPP **15Mn**/isobutiraldeído) e (MnOAc-TDCPP **15Mn**/NH₄OAc) apresentaram-se como os mais ativos e seletivos para a epoxidação de olefinas, utilizando O₂ e H₂O₂ como oxidantes, respetivamente. Relativamente à reação de cicloadição de CO₂ em epóxidos, o catalisador (CrCl-TPP*p*CF₃ **12Cr**/PPNCl) apresentou-se como o mais ativo e seletivo para a síntese de carbonatos cíclicos. Por fim, desenvolveram-se metodologias sequenciais homogéneas e heterogéneas para a síntese de carbonatos cíclicos a partir de olefinas, onde o sistema catalítico heterogéneo (**MNP@SiO₂-NH-17Mn** e **MNP@SiO₂-NH-19Cr**) foi capaz de promover sequencialmente a transformação do estireno em carbonato cíclico. Um resultado notório resulta do facto deste catalisador poder ser reutilizado em vários ciclos consecutivos sem perda significativa de atividade e seletividade.

Atendendo ao nosso interesse no desenvolvimento de métodos sustentáveis para a preparação de compostos com potencial atividade anti-proliferativa contra o osteossarcoma, no **Capítulo 4** foram selecionados terpenos como matérias primas renováveis para efetuar transformações químicas específicas, nomeadamente epoxidação, hidroformilação e reação de abertura de epóxido. Neste estudo, o (-)-isopulegol foi utilizado como terpeno modelo e o seu epóxido foi sintetizado com um bom rendimento, utilizando **MNP@SiO₂-NH-17Mn** como catalisador e O₂ como oxidante. O aldeído derivado do éter benzílico do (-)-isopulegol foi sintetizado através da reação de hidroformilação, utilizando um Rh(acac)(CO)₂/fosfito como catalisador. Por fim, um aminoálcool derivado do (-)-isopulegol foi preparado utilizando CrCl-TPP*p*CF₃ (**12Cr**) como catalisador e butilamina como nucleófilo. Neste capítulo salienta-se ainda a avaliação do(s) epóxido(s) derivados dos dois diastereoisômeros do (-)-isopulegol quanto à sua capacidade antiproliferativa e citotóxica face à linha celular humana de osteossarcoma (MG-63). Os resultados descritos nesta dissertação apresentam valores de IC₅₀ significativamente mais baixos do que os reportados na literatura para compostos análogos (diastereoisômero **33**:

MTT = 249.8 μ M, SRB = 114.8 μ M; diastereoisômero **34**: MTT = 158.2 μ M, SRB = 104.0 μ M).

O **Capítulo 5** contém a descrição detalhada das técnicas experimentais e da instrumentação, bem como todos os processos de síntese/caracterização dos novos catalisadores e produtos resultantes das reações catalíticas desenvolvidos no decorrer deste trabalho.

Palavras-chave: atividade biológica; catálise homo-/heterogénea; monóxido e dióxido de carbono; pequenos anéis heterocíclicos; síntese sustentável.

Abbreviations and Symbols

Å	unit of length equal to 10^{-10} m
s	singlet
d	duplet
dd	douplet of douplets
m	multiplet
J	coupling constant
δ	chemical shifts
λ	wavelength
ϵ	molar absorptivity
$[M]^+$	molecular ion
^1H NMR	proton nuclear magnetic resonance spectroscopy
^{13}C NMR	carbon 13 nuclear magnetic resonance spectroscopy
2-Me-THF	2-Methyltetrahydrofuran
A549 cells	human lung carcinoma
acac	acetylacetonate
Ac ₂ O	ethanoic anhydride
AcOH	ethanoic acid
ACS	American Chemical Society
APTES	(3-Aminopropyl)triethoxysilane
CATSUS	Catalysis and Sustainability
cod	1,5-cyclooctadiene
COSY	correlation spectroscopy in nuclear magnetic resonance
CPTES	(3-Chloropropyl)triethoxysilane
CTAC	cetyltrimethylammonium chloride
DME	1,2-Dimethoxyethane
DMEM	Dulbecco's modified eagle medium
DMF	<i>N,N</i> -dimethylformamide
DMSO	dimethyl sulfoxide

EDTA	ethylenediaminetetraacetic acid
ESI	electrospray ionization
FAAS	flame atomic absorption spectrometry
FBS	fetal bovine serum
FDA	Food and Drug Administration
Formazan	1,3,5-Triphenyltetrazolium formazan
FT-IR	Fourier-transform infrared spectroscopy
GC	gas chromatography
GC-MS	gas chromatography coupled with mass spectrometry
HAT	hydrogen atom transfer
HepG2	human hepatocellular carcinoma
HMBC	heteronuclear multiple-bond correlation
HMQC	heteronuclear multiple-quantum correlation
IBA	isobutyraldehyde
ICP	inductively coupled plasma
Igepal CO-520®	polyoxyethylene (5) nonylphenylether, branched
IR	infrared spectroscopy
IUPAC	International Union of Pure and Applied Chemistry
MG-63	human osteosarcoma cells
MNP	magnetite nanoparticles
MNP@SiO ₂	silica-coated magnetite nanoparticles
MNP@SiO ₂ -NH ₂	amino functionalised nanoparticles
m/z	mass/charge relation
MS	mass spectrometry
MS (MALDI-TOF)	mass spectrometry (matrix assisted laser desorption/ionization)
MTT	3-(4,5-dimethylthiazol-2-yl)-2,5-diphenyltetrazolium bromide
MW	molecular weight
NADH	nicotinamide adenine dinucleotide hydrogen
NADPH	nicotinamide adenine dinucleotide phosphate hydrogen
NMR	nuclear magnetic resonance
NOESY	nuclear overhauser effect spectroscopy

PBS	phosphate-buffered saline
PEN/STREP	penicillin streptomycin
PPA	Pollution Prevent Act
ppm	parts per million
PPNCl	bis(triphenylphosphine)iminium chloride
Ras	protein superfamily of small GTPases
SAR	structure–activity relationship
SRB	Sulforhodamine B
TBAB	tetrabutylammonium bromide
TBHP	<i>tert</i> -Butyl hydroperoxide
TCA	trichloroacetic acid
TDCPP	5,10,15,20-tetra(2,6-dichlorophenyl)porphyrin
TEM	transmission electron microscopy
TEOS	tetraethoxysilane
TG-DSC	thermogravimetry-differential scanning calorimetry
THF	tetrahydrofuran
TLC	thin-layer chromatography
TMS	tetramethylsilane
TON	turnover number
TOF	turnover frequency
TPP p CF ₃	5,10,15,20-tetra(4-trifluoromethylphenyl)porphyrin
U.S.	United States
UV-Vis	Ultraviolet–visible spectroscopy
XPS	X-ray photoelectron spectroscopy

List of Compounds

- 1 5,10,15,20-tetraphenylporphyrin
- 2 5,10,15,20-tetra(4-trifluoromethylphenyl)porphyrin
- 3 5,10,15,20-tetra(2,6-dichlorophenyl)porphyrin
- 4 5,10,15,20-tetra(2,6-difluorophenyl)porphyrin
- 5 5-(4-acetamidephenyl)-10,15,20-tris(2,6-dichlorophenyl)porphyrin
- 6 5-(4-aminephenyl)-10,15,20-tris(2,6-dichlorophenyl)porphyrin
- 7Cu 2-nitro-5,10,15,20-tetra(4-trifluoromethylphenyl)porphyrinato(II) Copper
- 8 2-nitro-5,10,15,20-tetra(4-trifluoromethylphenyl)porphyrin
- 9Mn 5,10,15,20-tetraphenylporphyrinatomanganese(III) Acetate
- 10Cr 5,10,15,20-tetraphenylporphyrinatomanganese(III) Chloride
- 11Mn 5,10,15,20-tetra(4-trifluoromethylphenyl)porphyrinatomanganese(III) Acetate
- 12Cr 5,10,15,20-tetra(4-trifluoromethylphenyl)porphyrinatomanganese(III) Chloride
- 13Mn 5,10,15,20-tetra(2,6-difluorophenyl)porphyrinatomanganese(III) Acetate
- 14Cr 5,10,15,20-tetra(2,6-difluorophenyl)porphyrinatomanganese(III) Chloride
- 15Mn 5,10,15,20-tetra(2,6-dichlorophenyl)porphyrinatomanganese(III) Acetate
- 16Cr 5,10,15,20-tetra(2,6-dichlorophenyl)porphyrinatomanganese(III) Chloride
- 17Mn 5-(4-aminephenyl)-10,15,20-tris(2,6-dichlorophenyl)porphyrinatomanganese(III) Acetate
- 18Mn 2-nitro-5,10,15,20-tetra(4-trifluoromethylphenyl)porphyrinatomanganese(III) Acetate
- 19Cr 2-nitro-5,10,15,20-tetra(4-trifluoromethylphenyl)porphyrinatomanganese(III) Acetate
- 20 Styrene oxide
- 21 1,2-cyclohexene oxide
- 22 1,2-hexene oxide
- 23 β - and α -Pregnenolone acetate oxide
- 24 Styrene carbonate
- 25 4-chlorostyrene carbonate
- 26 2-naphthalene carbonate

- 27 1,2-hexene carbonate
- 28 Cyclooctene oxide
- 29 Isobutyric acid
- 30 α -pinene oxide
- 31 (+)-Limonene oxide
- 32 (-)-Isopulegol benzyl ether
- 33 (-)-Isopulegol-benzyl ether epoxide (Diastereoisomer A)
- 34 (-)-Isopulegol-benzyl ether epoxide (Diastereoisomer B)
- 35 (-)-Isopulegol-benzyl ether aldehyde (Diastereoisomer A)
- 36 (-)-Isopulegol-benzyl ether aldehyde (Diastereoisomer B)
- 37 (-)-Isopulegol-benzyl ether amino alcohol

MNP Magnetite nanoparticles

MNP@SiO₂ Silica-coated magnetite nanoparticles

MNP@SiO₂-NH₂ Amine-functionalised magnetite nanoparticles

MNP@SiO₂-Cl Chloro-functionalised magnetite nanoparticles

MNP@SiO₂-NH-17Mn 17Mn immobilised onto silica-coated magnetite nanoparticles

MNP@SiO₂-NH-18Mn 18Mn immobilised onto silica-coated magnetite nanoparticles

MNP@SiO₂-NH-19Cr 19Cr immobilised onto silica-coated magnetite nanoparticles

Nomenclature

In this thesis, in order to classify the tetrapyrrolic macrocycles, Fischer^[1] and IUPAC^[2] (*International Union of Pure and Applied Chemistry*) nomenclatures were used. For simplicity, porphyrins and their derivatives were named according to Fischer nomenclature, with exclusion of the experimental section (**Chapter 5**), where IUPAC nomenclature was used.

As reported by Fischer^[1], porphyrin (**Figure I, a**) shows the *meso* positions (methylene bridges), referred as α , β , γ and δ , while the β -pyrrolic positions are numbered from 1 to 8 and the pyrrolic rings are designated as A, B, C and D. Moreover, as stated by Fischer, a reduced hydroporphyrin at 7 and 8 positions, is designated by chlorin (**Figure I, b**) and a reduced porphyrin at α , β , γ and δ positions is named porphyrinogen (**Figure I, c**).

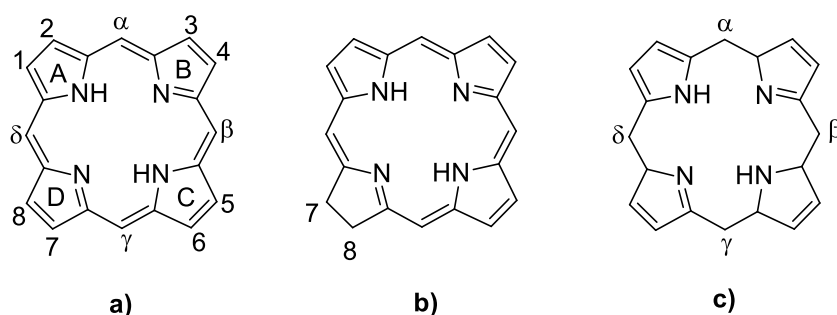


Figure I – Fischer nomenclature: a) *meso* position; b) chlorin; c) porphyrinogen.

On the other hand, using the IUPAC nomenclature,^[2] the tetrapyrrolic macrocycle's carbons are sequentially numbered from 1 to 20 and for the external carbons indices are used, as presented in **figure II**.

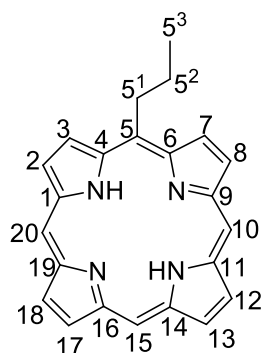
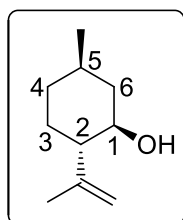
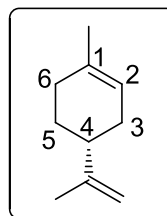


Figure II – IUPAC nomenclature for porphyrins.

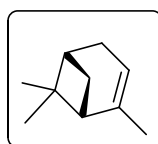
Concerning terpene's nomenclature, the trivial names were used instead of IUPAC nomenclature, for simplicity and historical reasons, as presented in **figure III**.



IUPAC name: (1*R*,2*S*,5*R*)-2-Isopropenyl-5-methylcyclohexanol
Trivial name: (-)-isopulegol



IUPAC name: (*R*)-4-Isopropenyl-1-methyl-1-cyclohexene
Trivial name: (+)-limonene



IUPAC name: 2,6,6-Trimethylbicyclo[3.1.1]hept-2-ene
Trivial name: α -pinene

Figure III – Structures of terpenes and their IUPAC and trivial names.

- [1] O. H. Fischer H., in *Die Chemie des Pyrrols*, Akad. Verlagsges, Germany, **1934**.
 [2] G. P. Moss, *Pure and Applied Chemistry* **1987**, *59*, 779-832.

Chapter 1

Introduction

1.1 Catalysis in the Green Chemistry Context

Uncontrolled industrial development in the United States and worldwide in the 20th century contributed to massive environmental problems/disasters which culminated in the organization of the Pollution Prevention Act of 1990 (PPA),^[1] where industrialists and academics declared that instead of treating and disposing of chemical waste, U.S. national policy should eliminate pollution by improving design (including cost-effective changes in processes and products). This was the birth of the “green chemistry philosophy”,^[2] initially set out in 1998 in the pioneering book *Green Chemistry: Theory and Practice*,^[3] by Paul Anastas and John Warner, where they described the 12 principles of green chemistry (**Figure 1.1**).

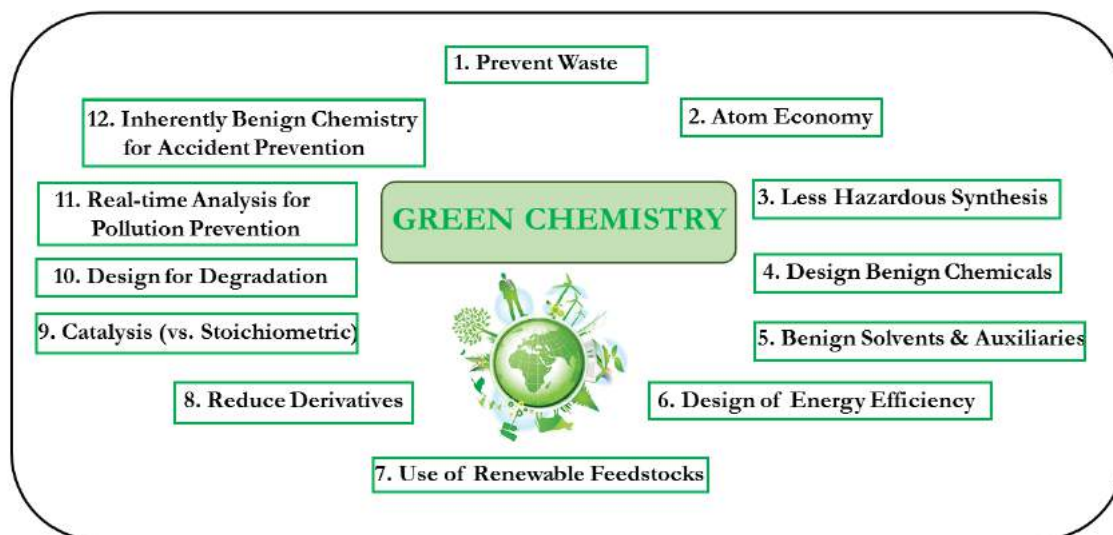


Figure 1.1 – The 12 principles of green chemistry. Adapted from reference [4].

Several preventive actions have been taken worldwide since then, with the aim of decreasing environmental problems and defining future strategies for transforming green chemistry into a real tool to enhance sustainability in its economic, social, and environmental aspects.^[5, 6]

The work described in this thesis is part of the Portuguese inter-university PhD programme on *Catalysis and Sustainability* (CATSUS)^[7] and is strongly engaged with the 12 principles of green chemistry philosophy, as they apply to the development of highly sustainable chemical processes for the preparation of fine chemicals,^[8] using renewable resources.^[9, 10] Among these, we highlight the use of catalytic processes instead of stoichiometric reagents (Principle 9). This indicates several ways in which chemistry can help to increase the sustainability of the planet through: i) reducing energy consumption; ii) substituting toxic stoichiometric reagents; iii) increasing selectivity, and thus minimizing waste; iv) lowering consumption of toxic solvents; v) reutilizing catalysts to minimize waste.

Catalysis can be regarded as a “foundational pillar” of green chemistry,^[11] that significantly contributed to the success of a sustainable chemical industry in the 20th century.^[12] The relevance today of catalysis is clearly demonstrated by the huge number of publications over the last decade (**Figure 1.2**).

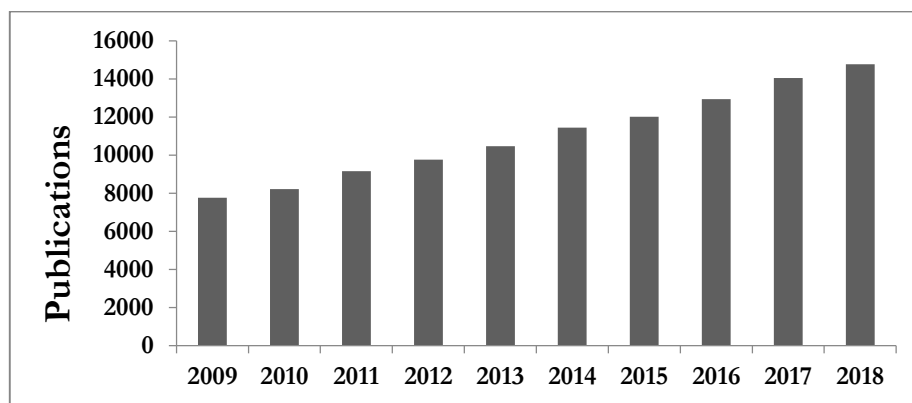


Figure 1.2 – Number of publications on “catalysis” from 2009-2018. Search carried out on Web of Science® search engine using “catalysis”, as search term.

The term “catalysis” was first proposed by Jöns Jakob Berzelius (1779-1848),^[13] who wrote about “...*the property of exerting on other bodies an action which is very different from chemical affinity. By means of this action, they produce decomposition in bodies, and form new compounds into the composition of which they do not enter...*”.^[14] In addition, according to IUPAC^[15] it can be defined as “*a substance that increases the rate of a reaction without modifying the overall standard Gibbs energy change in the reaction; the process is called catalysis*”. Therefore, catalysis is based on the utilization of a substance, the “catalyst”, that reduces energy input and frequently simplifies the final purification processes, due to higher selectivity^[16] (**Figure 1.3**). These features, in combination with the use of renewable feedstocks such as biomass, CO₂, and terpenes transform catalysis into a key tool for decreasing cost and waste, thus making a major contribution to the overall sustainability of the planet.^[17] This is also one of the main goals of the present work.

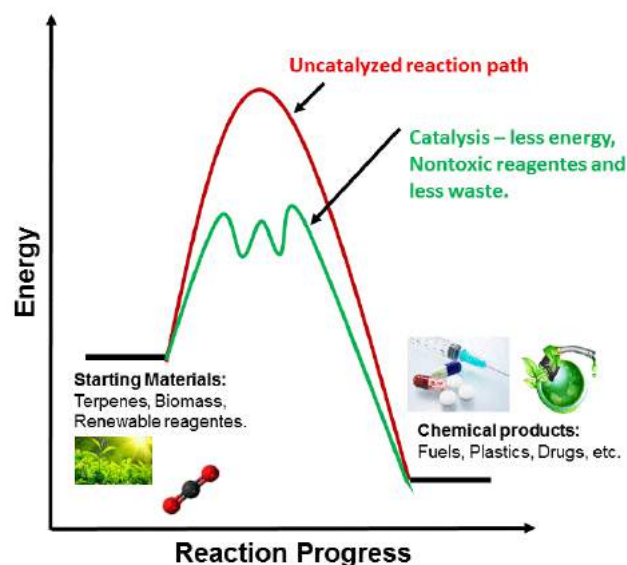


Figure 1.3 – General potential energy diagram showing the effect of a catalyst in a hypothetical reaction.

The relevance of this field is clearly demonstrated by the large number of Chemistry Nobel Prizes (16) awarded by the Royal Swedish Academy of Sciences to scientists who have made relevant contributions to enzymatic or chemical catalysis, which have greatly enhanced both, industrial and economic development.^[18] Of these, we have selected some who have received the Nobel Prize for Chemistry whose ideas, directly or indirectly, are relevant to the work described in this thesis.

In 1912, Victor Grignard and Paul Sabatier, were awarded the Nobel Prize for Chemistry,^[19] for the discovery of stable organo-magnesium compounds, normally called “Grignard reagents”. These organometallic complexes, although mainly used as stoichiometric reagents, have made a great contribution to the development of organic/medicinal chemistry. Furthermore, the results of P. Sabatier may be considered as the first example of the introduction of metals as hydrogenating catalysts of organic compounds.



V. Grignard
(1871-1935)



P. Sabatier
(1854-1941)

Some years later (1930), Hans Fischer was awarded the Nobel Prize in Chemistry^[20] for his research on isolation, synthesis and the characterization of chlorophyll, and haemin (protoporphyrin IX containing a ferric iron).^[21, 22] We can regard Fischer as the “father”



H. Fischer
(1881-1945)

of Porphyrin Chemistry. Porphyrins are the key molecules for developing the new catalysts used in this work.

The Nobel Prize for Chemistry in 2001^[23] was shared by William S. Knowles and Ryoji Noyori to highlight the relevance of their work on chiral catalysed hydrogenation reactions, and K. Barry Sharpless for his work on chiral catalysed oxidation reactions.



W. S. Knowles
(1917-2012)



R. Noyori
(1941)



K. B. Sharpless
(1941)

Sharpless developed a broad set of catalytic oxidation reactions, in particular, chiral epoxidation, asymmetric dihydroxylation and oxyamination. Sharpless's synthetic oxidation methodologies allowed the manufacture of highly efficient antibiotics, anti-inflammatory drugs, and heart medicines, in addition to many chiral agricultural chemicals.^[24-28]

More recently, the Swedish Academy awarded the Chemistry Nobel Prize 2018 to the scientists Frances H. Arnold, George P. Smith and Gregory P. Winter.^[29] In Arnold's work, she performed well-designed chemical modification of enzymes, particularly those of the cytochrome P-450 family, to produce powerful biocatalysts for the production of fine chemicals.^[30-32] The utilization of Arnold's enzymes enables the more environmentally friendly manufacture of various chemical substances such as pharmaceuticals, as well as the production of renewable fuels for a greener transport sector.^[33]



F. H. Arnold
(1956)

The Nobel Prize Lectures of all these scientists have highlighted the relevance of pursuing studies on the development of catalytic reactions to obtain more sustainable chemical industrial processes, preferably using renewable raw materials such as terpenes, CO₂ and O₂. However, many environmental challenges, not to mention problems with industrial development, still lie ahead. The solutions are likely to be given by multidisciplinary studies at the interface between chemistry, engineering, physics, and biology. These encompass the main goal of the work presented and discussed in this thesis.

1.2 Designing Catalytic Processes

As discussed above, the development of multidisciplinary teams has made an enormous contribution towards the design of more sustainable chemical processes. As an example, in the near future the development of alternative modern synthetic chemistry is likely to require the development of sequential catalytic reactions, or bifunctional and/or synergic catalysts, preferentially immobilized onto solid supports.

The use of sequential reactions is a great challenge, but helps to achieve green chemistry goals since they achieve significant waste/solvent minimization, avoid the need for intermediate purification processes, and are, in general, highly atom economic (Principles 1, 2, 4 and 5). These one-pot sequential processes are classified as cascade,^[34] domino,^[35, 36] and tandem reactions^[37, 38] according to the type of reaction and mechanism involved (**Figure 1.4**).

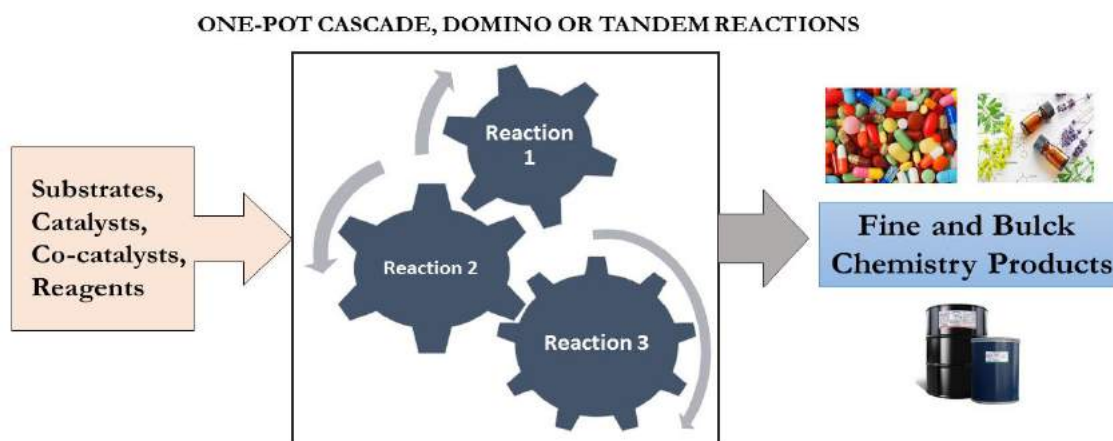
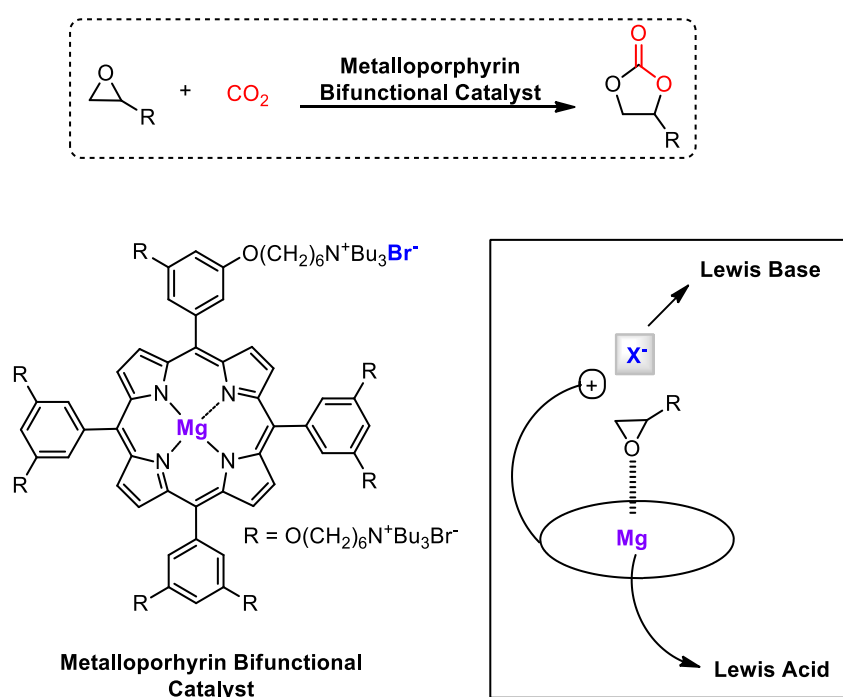


Figure 1.4 – General procedure for one-pot sequential reactions.

The development of heterogeneous bimetallic catalysts is another interesting approach to achieving green chemistry principles since, in general, the use of two metals in the same catalyst increases its activity and selectivity,^[39] and can be applied in multiple catalytic transformations^[40-42] including hydrogenation,^[43-46] and oxidation.^[47-49]

We can highlight bimetallic catalysts where a “synergistic catalysis”^[50-52] occurs, which are characterized by the enhancement of activity and selectivity of the

overall catalytic process,^[53] due to the involvement of two catalysts and two separate catalytic cycles in a single process. As a selected example, Ema and Hasegawa^[54] reported the preparation a set of bifunctional Mg(II)-porphyrin catalysts bearing tetraalkylammonium bromide groups for the synthesis of cyclic carbonates through CO₂ cycloaddition to epoxide. In this case, the bifunctional catalyst acts with acid and basic properties *via* coordination of the epoxide with the magnesium metal, followed by nucleophilic attack of Br⁻ ion on the epoxide, to produce an alkoxide anion *via* a ring-opening reaction, finally yielding the corresponding cyclic carbonate (Scheme 1.1).



Scheme 1.1 – Bifunctional Mg(II)-porphyrin as catalyst for the synthesis of cyclic carbonate from epoxides and CO₂.

Another challenge for achieving green chemistry principles is the combination of the best features of heterogeneous (high stability and easy recovering) and homogeneous (high selectivity) catalysts via immobilization of the latter onto solid supports.^[55] In the literature, several papers describe the immobilization of synthetic or enzymatic homogeneous catalysts onto a variety of solid supports such as polymers,^[56, 57] silica,^[58, 59] mesoporous materials,^[60] carbon materials^[61, 62] and magnetic nanoparticles (MNP)^[63, 64] (Figure 1.5).

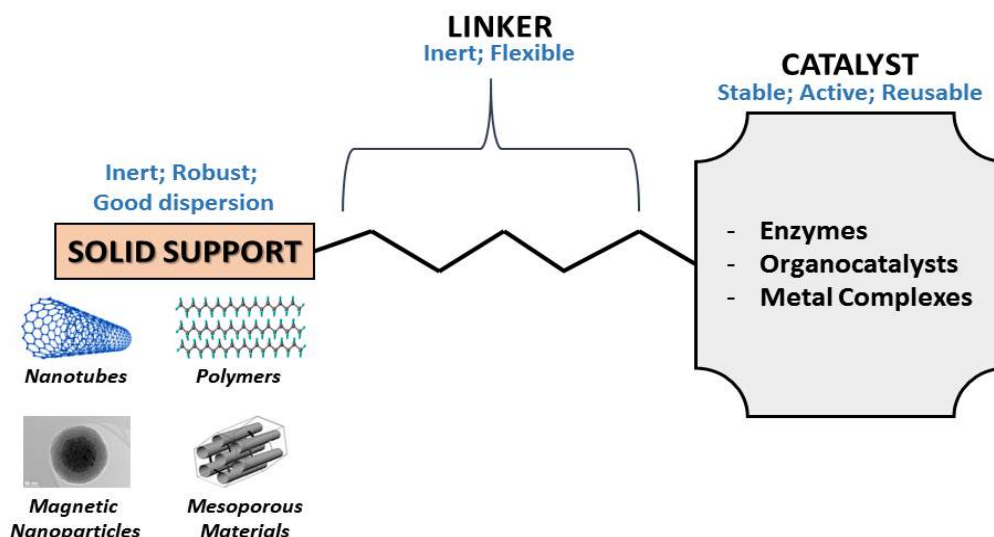


Figure 1.5 – General approach for immobilization of a catalyst.

Among these, we highlight magnetic nanoparticles because of their easy synthesis and chemical modulation, high stability, and ready response to an external magnetic field, which is used for catalyst recovery and reuse.^[65-68] This is, therefore, one of the main goals of this thesis, the results of which are presented in **chapter 2**.

1.3 Metalloporphyrins as Bioinspired Catalysts

Synthetic metalloporphyrins are relevant molecular scaffolds which, because they mimic natural processes, have been used in multiple catalytic transformations, including C-H activation, hydrocarbon oxidation, sulphur, hydroxyl and carbonyl oxidation, halogenation, carbene transfer reactions, reduction and other reactions.^[69-76] Below we present a critical analysis of the accepted mechanism of cytochrome P-450, together with the use of synthetic metalloporphyrins in catalytic epoxidation reactions, one of the aims of this work.

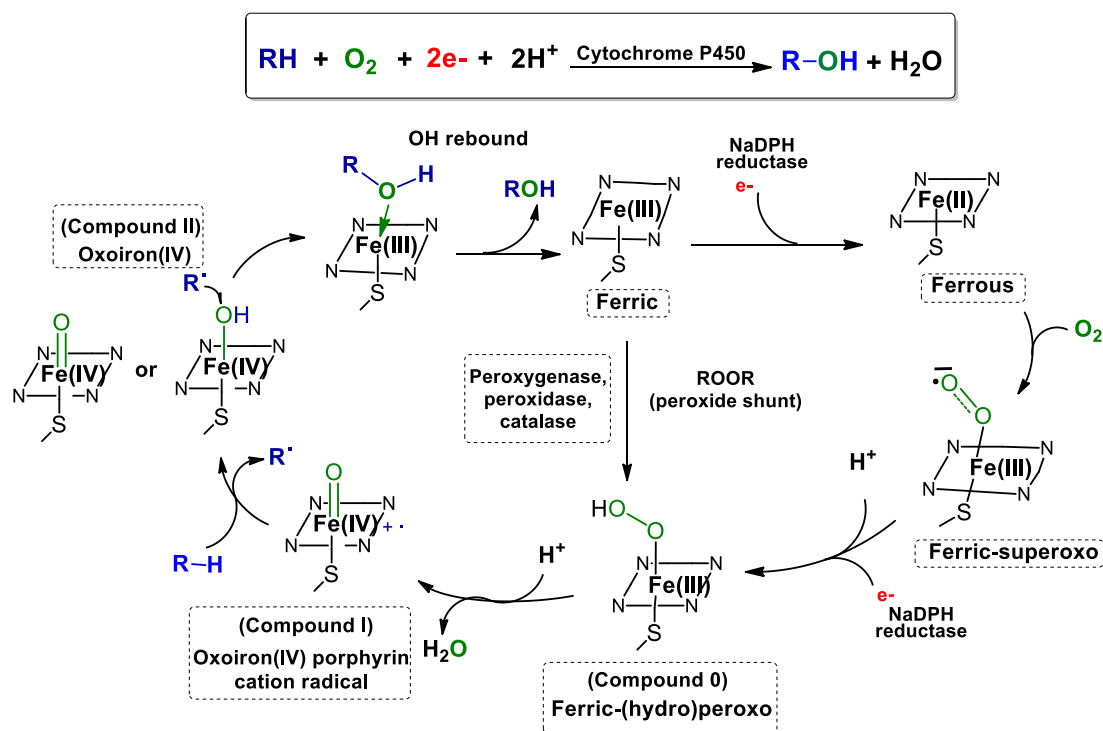
1.3.1 Cytochrome P-450

Metalloporphyrins are types of natural tetrapyrrole macrocycles with a distinct aromatic structure (18π electrons).^[77] They have been studied in detail due to their

vital role in many life processes, such as oxygen-transport in red blood cells,^[78] biotransformation of drugs and xenobiotics in liver,^[79] and storage of oxygen in muscle tissues.^[80, 81]

From the multiple biological processes possible, we will highlight the biomimetic systems involving the enzyme family of cytochrome P-450. This enzyme was discovered by Garfinkel and Klingenberg in 1958^[82] and identified by Sato in 1962.^[83] Since then, numerous biochemical and synthetic advances have been made in the understanding of cytochrome P-450's *in vivo* action, as well as its function as catalyst in the degradation and synthesis of biocompounds.^[84-89]

In the mechanism of action, it is generally accepted that mono-oxygenase-mediated biological oxygenation involves two-electron reduction provided by NADPH reductase^[71, 90] (**Scheme 1.2**).



Scheme 1.2 – Catalytic cycle of molecular oxygen activation by cytochrome P-450. Adapted with permission from ref [90]. Copyright 2018 ACS.

Initially, a first electron is used to reduce the Fe(III) ferric species to an Fe(II) ferrous species. Then, an electron is transferred from Fe(II) to O₂, thus forming the ferric-superoxo intermediate. Subsequently, a second electron from NADPH and a proton are transferred to the ferric-superoxo intermediate, yielding a ferric-

(hydro)peroxo intermediate (compound 0) that is able to generate the oxo-iron(IV) porphyrin cation radical intermediate (compound I). In an alternative route, known as the peroxide shunt, the ferric-(hydro)peroxo intermediate (compound 0) can be produced *via* H₂O₂ binding to the ferric species. This intermediate is accepted as one of the active species of biomimetic epoxidation reactions using H₂O₂ as oxidant.^[91] The formation of an oxo-iron(IV) porphyrin cation radical (compound I) is then performed by protonation of compound 0 at the distal oxygen, followed by heterolytic scission of the O–O bond and water elimination. Next, the oxoiron(IV) porphyrin cation radical (compound I) promotes the activation of C–H substrates via hydrogen atom transfer (HAT). Following this, the incipient substrate radical (R•) recombines with the oxo-iron(IV) (compound II) via oxygen rebound to afford the desired hydroxylation products.

With the aim of mimicking the high activity and selectivity of the cytochrome P-450 in industrial processes, a wide variety of one-pot methods for synthesizing *meso*-tetra-substituted porphyrins have been implemented over the years; these include the pioneering work of Rothemund,^[92, 93] Adler and Longo,^[94-96] supplemented by Gonsalves and Pereira's nitrobenzene method.^[97]

Synthetic advances were achieved with the remarkable development of the two-step approach reported by Pereira^[98] for *meso*-tetraalkylporphyrin synthesis, and extended by the Lindsey group to the synthesis of *meso*-tetrarylporphyrins.^[99-103] More recently, with the aim of improving these one- and/or two-step methodologies, several synthetic processes have been described, using alternative catalysts,^[104-110] alternative solvents/heating processes,^[111-116] and also flow chemistry.^[117] The great achievements seen so far in the synthesis of *meso*-tetrarylporphyrins have been crucial to understanding porphyrin-based natural systems, and to promoting their transposition as bioinspired catalysts from natural systems to laboratory levels and/or industrial scale.^[90]

The foregoing is a brief introduction to green chemistry, catalysis, the design of catalytic processes, and the mechanism of cytochrome P-450 oxidation catalysis. The use of metalloporphyrins as catalysts in epoxidation reaction, using O₂ and H₂O₂ as oxidants is one of the main goals of this work, and a systematic literature review (last 5 years) is provided in the next section.

1.3.2 Metalloporphyrins in Epoxidation Reactions

When discussing the design and development of biomimetic oxidative catalytic systems based on metalloporphyrins, we should highlight the work of Groves^[71] and Goldberg,^[118] who reviewed the mechanism of hydroxylation and epoxidation of olefins with synthetic porphyrins and natural processes. In addition, as previously mentioned, we must include Arnold's work on the modification of cytochrome P-450 type enzymes for application in multiple chemical transformations, including epoxidation.^[25]

The effects of the porphyrin central metal, macrocycle structure, and oxygen donor in biomimetic systems have been extensively described.^[69, 90, 119-122] The oxygen sources described in the literature include sodium hypochlorite (NaOCl),^[123] iodosylbenzene (PhIO),^[124] alkyl peroxides (ROOH),^[125] molecular oxygen (O₂)^[90] and hydrogen peroxide (H₂O₂).^[126] However, if we focus the search on green chemistry aspects, the last examples are considered to be the most attractive for epoxidation reactions (**Chapter 3** and **4**) and a literature review of these is given in detail below.

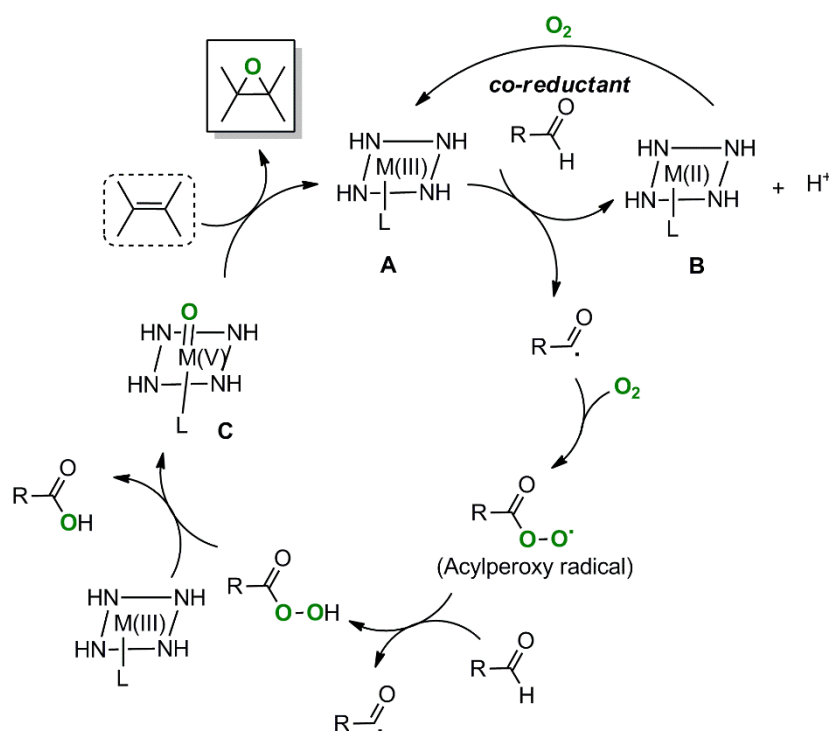
O₂ as oxidant

The use of O₂ as oxidant in biomimetic oxidation processes is highly challenging,^[127] since its high stability in triplet state^[128] requires the presence of an electron donor, which, in biological systems such as cytochrome P-450, is performed by NADPH.^[129]

This electron source can be provided by the appropriate metalloporphyrins, as described by Groves in his seminal work (in which he used ruthenium(VI) porphyrins,^[130] and aldehydes, according to Mukaiyama-type mechanisms,^[131, 132] and others.^[133, 134] Aldehydes are the most commonly used co-reductors applied so far for O₂ activation in selective epoxide formation.^[131]

The mechanism of this reaction was first proposed by Mukaiyama and is generally accepted as presented in **scheme 1.3**. It involves the reaction of the M(III)

catalytic species (**A**) with the aldehyde generating the acyl radical ($\text{RCO}\cdot$) and the M(II) species (**B**), which can be reoxidized to M(III) by oxygen (**A**). The acyl radical then reacts with oxygen to give the acylperoxy radical ($\text{RC(O)OO}\cdot$), which reacts with M(III) catalyst to form the M(V) -oxo active catalytic species (**C**). This can selectively transfer oxygen to the olefin, yielding the desired epoxide and the original M(III) catalyst. It should also be noted that in the Mukaiyama epoxidation mechanism, the involvement of a secondary non-catalytic pathway, based on the direct epoxidation with the peracid obtained from direct autooxidation of the aldehyde, can also occur.^[132]

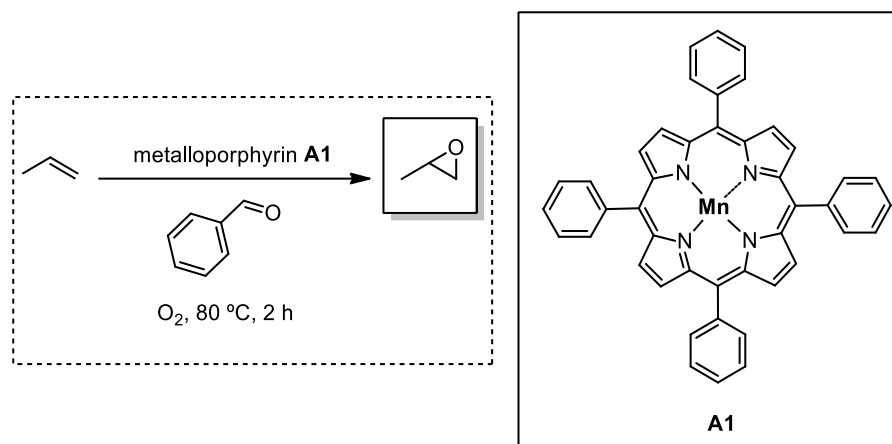


Scheme 1.3 – General mechanism for Mukaiyama aerobic epoxidation of alkenes.

To place this work in context, we describe below literature reports from the last 5 years on homogeneous and heterogeneous metalloporphyrin-based catalysts in epoxidation reactions using O_2 and H_2O_2 as oxidant.

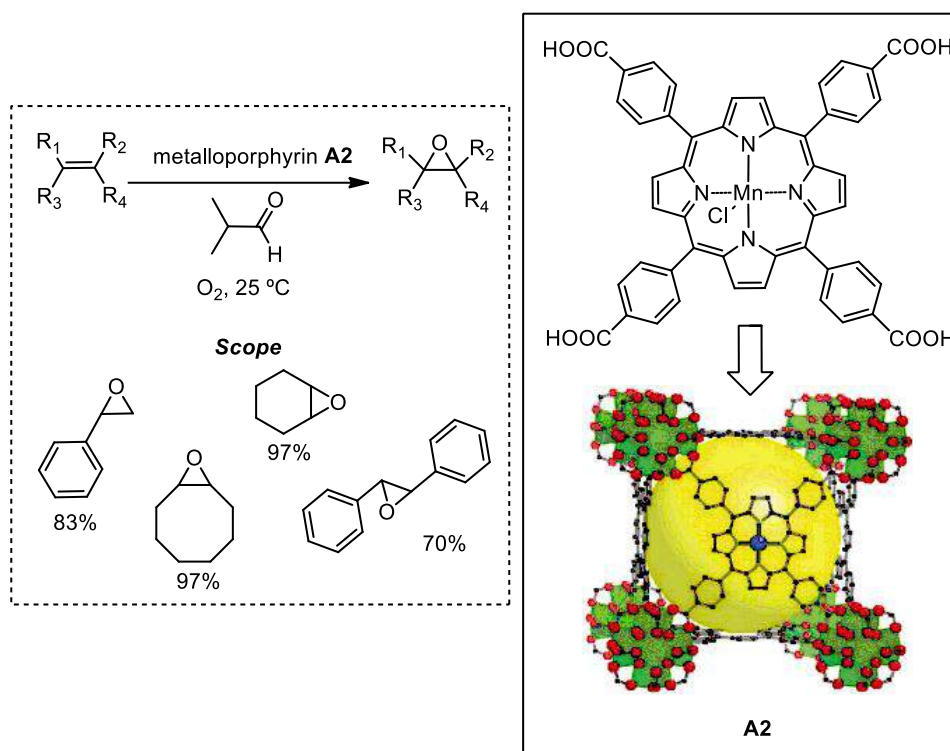
In 2015, Ji^[135] reported a study of the liquid phase catalytic epoxidation of propylene, using O_2 as oxidant, a manganese complex of *meso*-tetraphenylporphyrin **A1** as catalyst, and benzaldehyde as co-reductant. The conversion of propylene was only 38% and the selectivity toward propylene oxide reached 80%. The authors

provided experimental evidence (*in situ* IR, *in situ* UV and MS) for the involvement of Mn(IV)-oxo species during propylene epoxidation (**Scheme 1.4**).



Scheme 1.4 – Direct aerobic liquid phase epoxidation of propylene catalysed by Mn(III)-porphyrin.

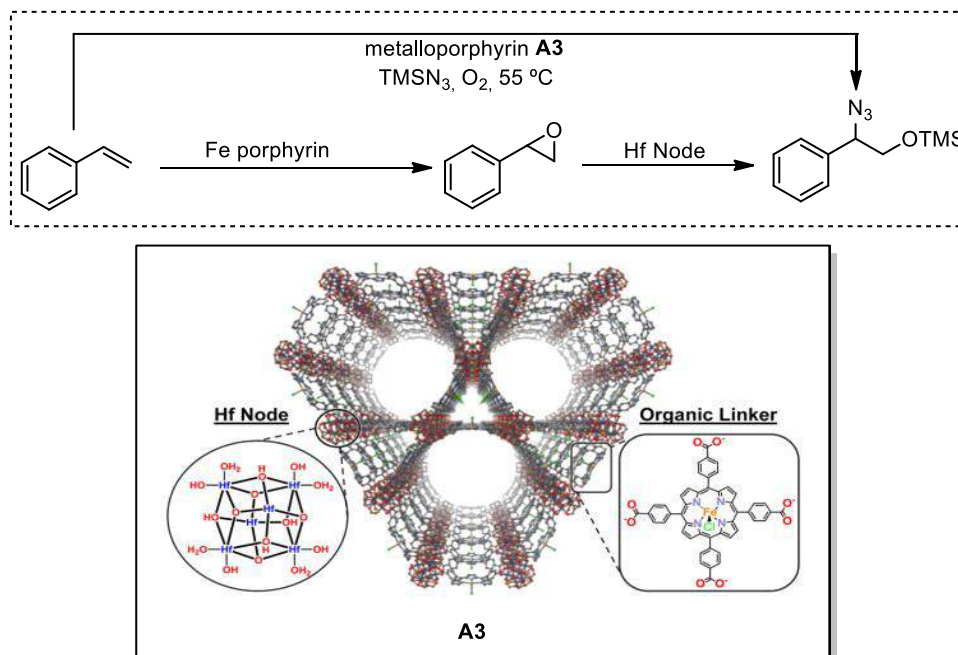
Bouchard^[136] prepared MOF-type catalysts, **A2**, containing a manganese(III) porphyrin as template to generate MOF $[Zr_6O_4(OH)_4(MgC_{48}H_{24}O_8N_4Cl)_3]$. The catalyst was synthesized by reacting Mn(III) *meso*-tetra(4-carboxyphenyl)porphyrinato chloride with zirconyl chloride octahydrate, in DMF, using ultrasound. The zirconium MOF **A2** was obtained upon adding acetic acid and further heating. It was evaluated as epoxidation catalyst for several alkenes, using O_2 as oxidant. The reaction was kept at $25\text{ }^\circ\text{C}$ for 2.5–4 h and 70–97% of conversion was reported. The catalyst could be reused for up to five catalytic cycles. It showed minimal deactivation and had retained its structural stability and crystallinity at the end of the catalytic cycle. Moreover, the kinetic studies of styrene epoxidation are in agreement with theoretical and experimental studies of homogeneous reactions with the same porphyrin unit, suggesting that the heterogeneous catalyst operates with a similar mechanism to its homogeneous counterpart (**Scheme 1.5**).



Scheme 1.5 – Epoxidation of alkenes catalysed by a manganese porphyrin-based metal-organic framework. Catalyst **A2** structure was adapted with permission from ref [136]. Copyright 2015 Elsevier.

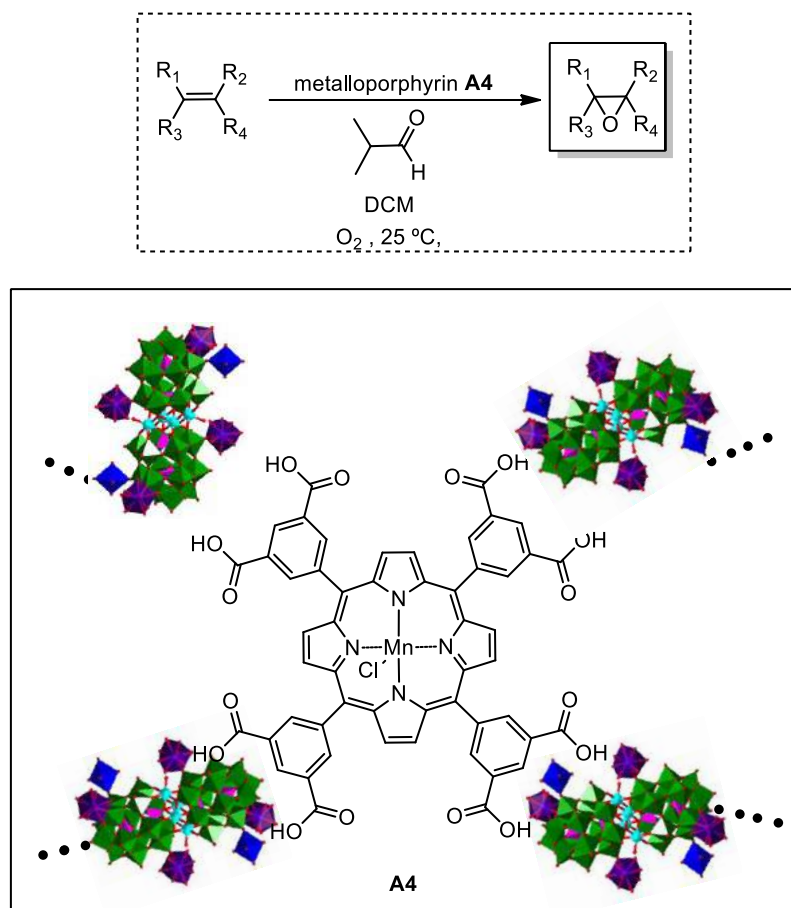
The *meso*-tetra(4-carboxyphenyl)porphyrin was also used as structural motif for the construction of Hf6 heterobimetallic metal organic framework Hf6-MOF **A3**.^[137] For the catalyst synthesis, the Hf node was first prepared, and then reacted with *meso*-tetra(4-carboxyphenyl)porphyrinato iron(III) chloride in DMF for 2 days, to produce **A3**. This catalyst was then applied in tandem epoxidation/ring opening reactions using styrene as substrate. In the same autoclave, the authors mixed acetonitrile as solvent, the catalyst Hf6-MOF **A3**, styrene, isobutyraldehyde as co-reductant, and azido trimethylsilane (TMSN₃) as nucleophile (**Scheme 1.6**). The autoclave was pressurized with O₂ (0.5 MPa) for 10 h, at 80 °C. The catalyst Hf6-MOF **A3** was able both to transfer oxygen to styrene, yielding the epoxide, and also to act as Lewis acid to catalyse the epoxide ring-opening, yielding the trimethylsilyl ether of phenyl azidohydrin (100%). The azidohydrin product is an important intermediate for α -amino alcohols synthesis. This regioselectivity was promoted by the concerted presence of Fe-decorated Hf6 nodes and the Fe-porphyrin struts. This report is a

good example of tandem catalysis using a recyclable heterogeneous bimetallic catalyst as described above.



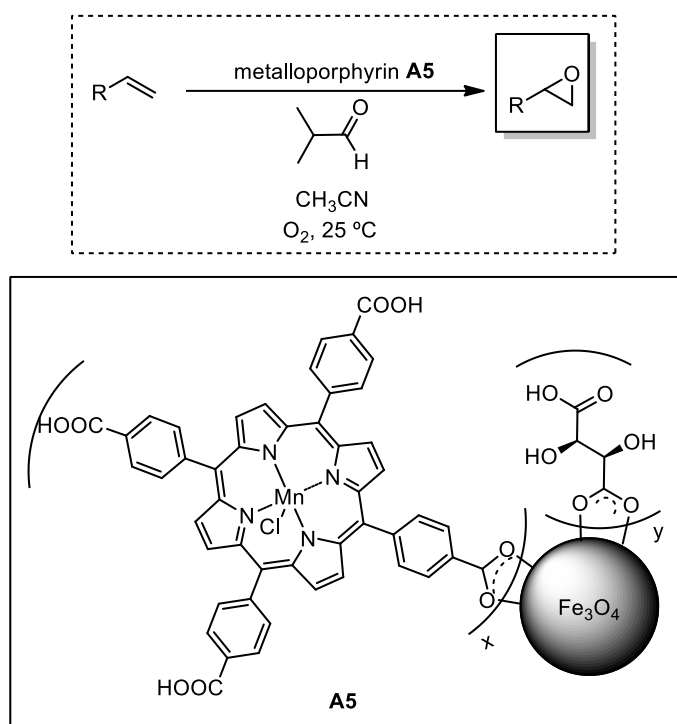
Scheme 1.6 – Hafnium-based metal-organic framework as a catalyst in styrene conversion to the trimethylsilyl ether of phenyl azidoalcohol. Catalyst **A3** structure was adapted with permission from ref [137]. Copyright 2015 ACS.

Wu^[138] reported the synthesis of a hybrid material, **A4**, involving inorganic polyoxometalates (POMs) + metalloporphyrins), and its application as heterogeneous catalyst in epoxidation reactions (**Scheme 1.7**). This hybrid material was developed by a “step-by-step” aggregation strategy, starting with the reaction of the POM units with metal ions to bind metal nodes on their surfaces, followed by the reaction of the resulting POM derivatives with metalloporphyrin. These experiments demonstrated that the hybrid material was able to catalyse the oxidation of diverse olefins, with up to 97% conversion, high epoxide selectivity (up to 99%), high turnover number (up to 220 000), and high turnover frequency (up to 22 000 h^{-1}). Moreover, **A4** could be reused six times with almost no loss of activity/selectivity (**Scheme 1.7**).



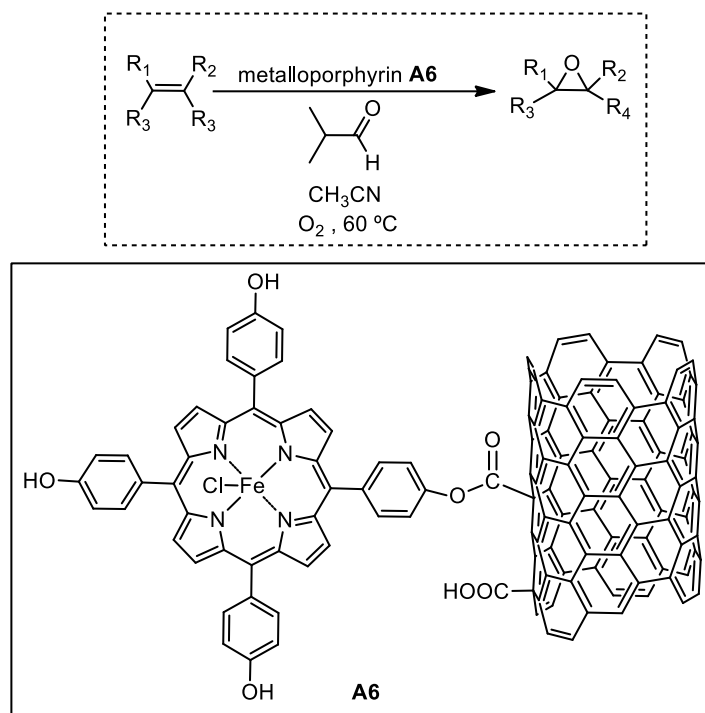
Scheme 1.7 – Metalloporphyrin-polyoxometalate hybrid material as catalyst in epoxidation of olefins using O₂ as oxidant. Catalyst **A4** structure was adapted with permission from ref [138]. Copyright 2016 ACS.

Hosseini-Monfared^[139] reported the immobilization of manganese *meso*-tetra(4-carboxyphenyl)porphyrin onto the chiral surface of magnetite nanoparticles coated with tartaric acid. The new heterogeneous catalyst **A5** (**Scheme 1.8**) was applied to the epoxidation reactions of pro-chiral olefins with molecular oxygen as oxidant, again using isobutyraldehyde as co-reductant and acetonitrile as solvent, at a temperature of 25 °C, for 8 h (**Scheme 1.7**). The reaction showed good conversions (68–100%), reasonable-to-good selectivity for epoxide (47–100%), and variable enantioselectivity (11–100%), depending on the olefin structure (terminal, cyclic, and aromatic olefins), with the best results being obtained with cyclic aliphatic olefins. The catalyst showed little deactivation, and was readily recovered by magnetic filtration. The authors described the easy reutilization, with an external magnet, up to four times with little loss in activity and selectivity.



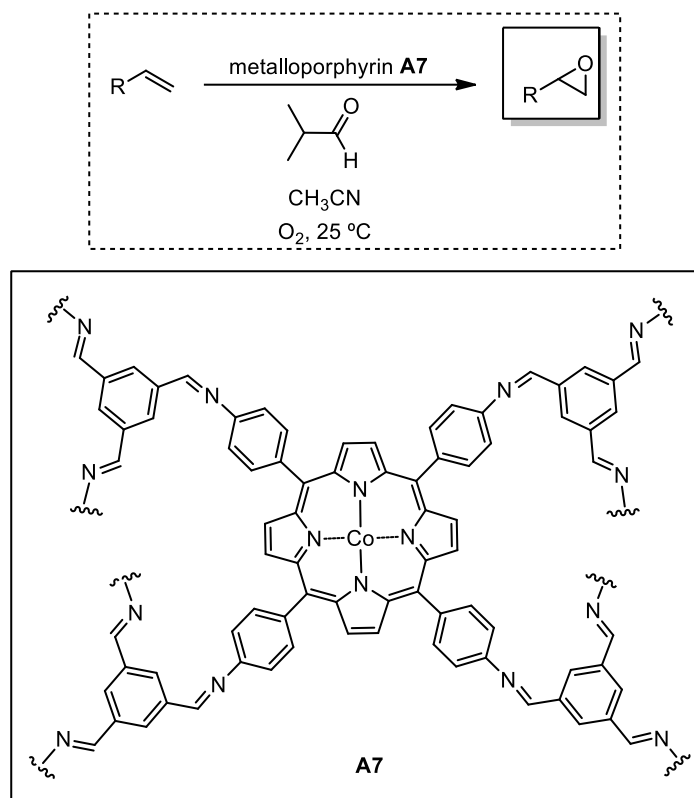
Scheme 1.8 – Recyclable Mn-Porphyrin as catalyst in epoxidation of olefins using molecular oxygen.

Rayati^[140] reported the synthesis of catalyst **A6**, produced by covalent anchoring of *meso*-tetrakis(4-hydroxyphenyl)porphyrinate iron(III) chloride onto multiwalled carbon nanotubes (**Scheme 1.9**). The catalyst was evaluated in aerobic oxidation of olefins (using isobutyraldehyde as co-reductant) and the desired epoxides were obtained with up to 100% conversion and selectivity. The heterogeneous nanocatalyst was reutilized for seven cycles without leaching or loss of activity.



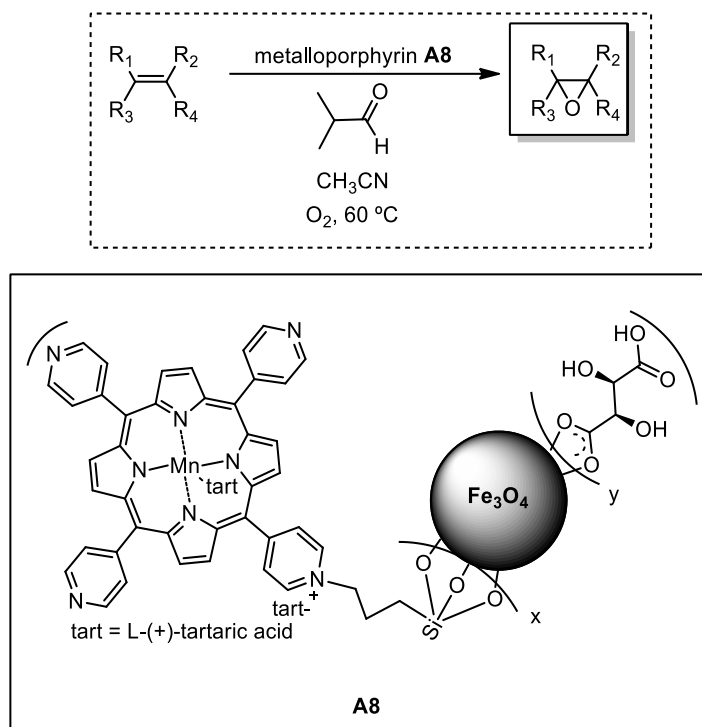
Scheme 1.9 – Fe(III)-porphyrins immobilized onto multiwalled carbon nanotubes for epoxidation of olefins.

Wu^[141] developed a new 3D covalent porphyrinic framework, synthesized by condensation of a four branched tetraphenylamine porphyrin and the trigonal 1,3,5-triformylbenzene, based on the principle of reticular chemistry, followed by metalation with cobalt(II) acetate. This hybrid material catalyst was evaluated in epoxidation reaction of olefins under mild conditions, and >99% conversion, 93% epoxide selectivity, TON = 29 215, and TOF = 3434 h⁻¹ were observed, using styrene as model substrate (**Scheme 1.10**). The authors extended this work to several other substrates, seeking for higher conversions toward epoxide formation for cyclic olefins. The new heterogeneous catalyst exhibited higher stability than its homogeneous counterparts and could be reused for up to 15 cycles without loss of activity/selectivity.



Scheme 1.10 – A covalent-porphyrinic framework as catalyst in aerobic epoxidation of olefins.

The same authors^[142] reported a magnetic hybrid metalloporphyrin catalyst, **A8**, prepared by covalent attachment of a manganese complex of *meso*-tetra(4-pyridyl)porphyrin onto magnetic nanoparticles stabilized with chiral L-(+)-tartaric acid (tart). The catalyst was evaluated in the enantioselective epoxidation of acyclic and cyclic olefins, using molecular oxygen as oxidant and isobutyraldehyde as co-reductant. The immobilized cationic system showed high activity (up to 100%) and selectivity (up to 90%) for the epoxidation of olefins (*cis*- and *trans*-stilbene, styrene, 1-decene, and 1-phenyl-1-cyclohexene), with enantiomeric excess up to 97% (**Scheme 1.11**). Remarkably, the catalyst could be reused for several runs using styrene as substrate without loss of activity, and the selectivity for epoxide was up to 100%.



Scheme 1.11 – Recyclable manganese-porphyrin as catalyst in asymmetric epoxidation of olefins.

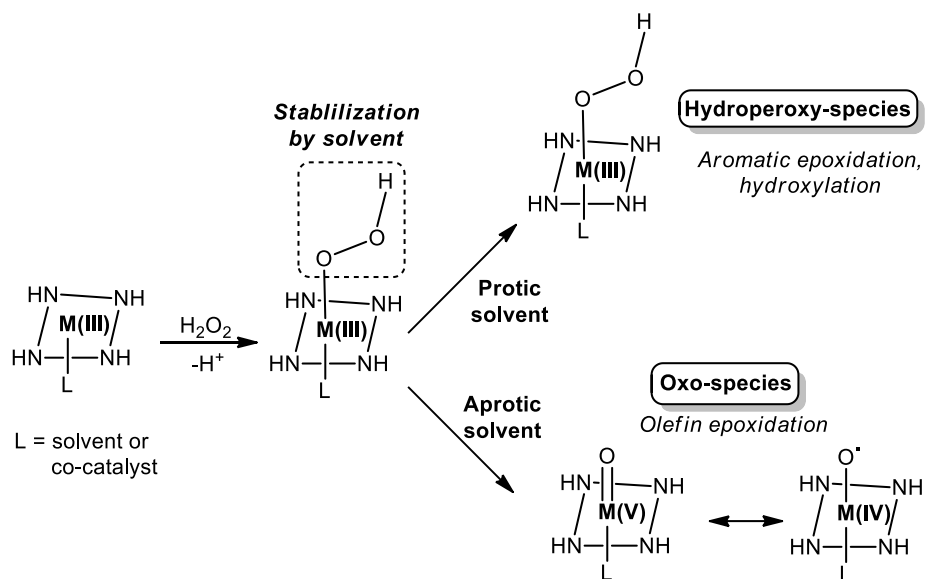
It can be generally concluded that co-reductants like aldehydes are normally used to promote the transformation of olefins to epoxides, and in this case Mn(III) porphyrins are the most promising catalysts. Moreover, the use of Co(III) and Fe(III) porphyrins is less recommended due to the concomitant occurrence of an autooxidation pathway. In sum, in the last 5 years, is notable the use of heterogeneous catalysts for epoxidation of olefins using O₂ as oxidant showing high stability and recyclability.

H₂O₂ as oxidant

H₂O₂ is an excellent alternative oxygen source since its oxidation level does not require the presence of an extra electron donor (co-reductant). As previously described, the oxidative catalytic cycle with H₂O₂ and metalloporphyrins (shunted peroxide cycle - **scheme 1.2**) involves various active catalytic species e.g. ferric-(hydro)peroxo, oxoiron(IV)porphyrin cation radical and oxoiron(IV), each possessing various levels of oxidising ability.^[143]

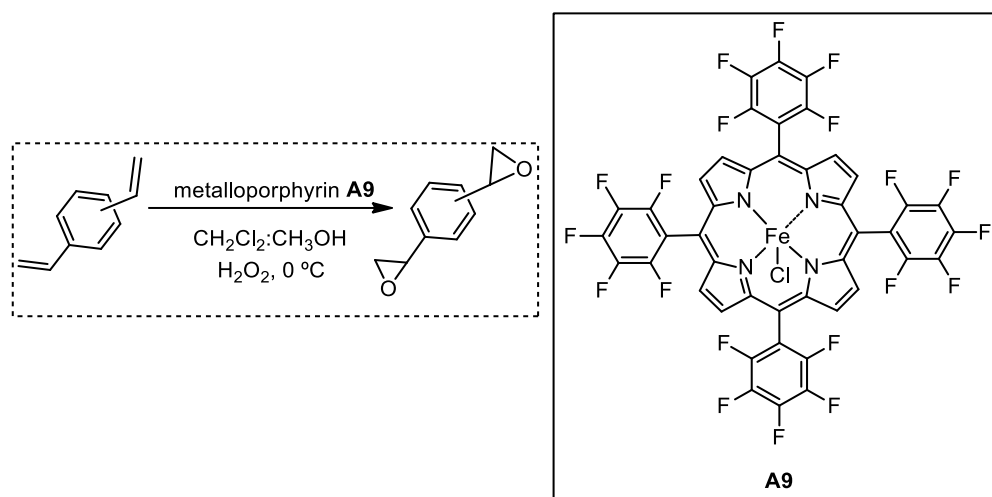
However, there are a number of problems regarding the use of hydrogen peroxide as oxidant, in particular the stability of metalloporphyrins towards the reaction conditions,^[144, 145] and its dismutation (catalase pathway).^[146] Some publications have highlighted the importance of catalyst stability in hydrogen peroxide oxidations, but many studies have either simply not considered this problem or circumvented it by performing the reactions in the presence of an excess of substrate relative to the amount of hydrogen peroxide used.^[147]

In the mechanism of oxidation reactions catalysed by metalloporphyrins/H₂O₂, it is accepted that the central metal, porphyrin structure, solvent and co-catalyst (axial ligand) used all have a notable influence on the formation and stabilization of the catalytic active species (hydroperoxo type species and/or oxo-species). Thus, the catalytic system and reaction conditions are key parameters when aiming to achieve high selectivity for epoxide formation (**Scheme 1.12**). For example, when metalloporphyrins bearing highly electron withdrawing groups in the phenyl ring (e.g. fluorine) are used, with Fe(III) as central metal and a protic solvent (methanol), the hydroperoxy-species is preferentially formed, and shows high selectivity for aromatic epoxidation and formation of hydroxylation products. In contrast, in the catalytic systems based on metalloporphyrins bearing less electron withdrawing (e.g. chlorine), with Mn(III) as central metal, aprotic solvents and strong donating axial ligand, epoxidation products are favoured, due to the preferential formation of active oxo-species.



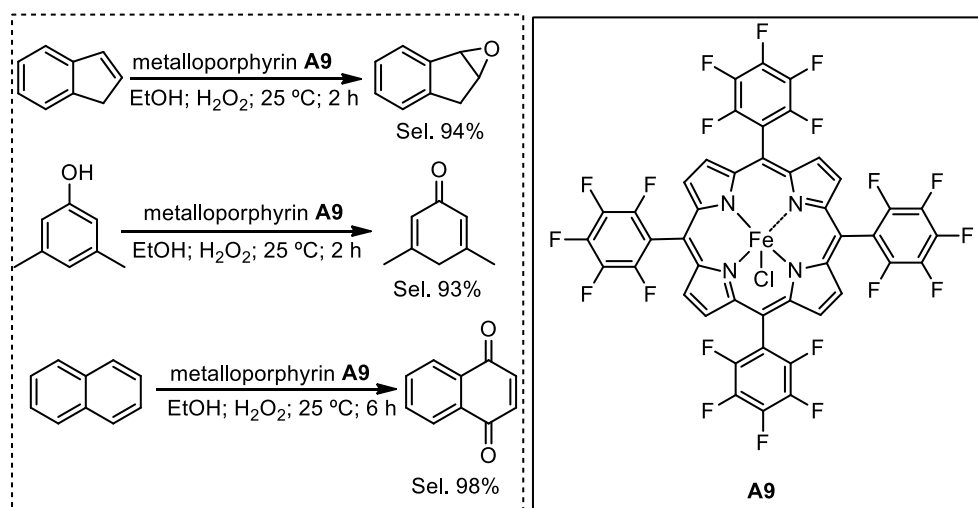
Scheme 1.12 – Effects of the solvent and co-catalyst on the general mechanisms.

Farha^[148] noted a strong influence of solvent and porphyrin structure on the activity and selectivity for double epoxidation of divinylbenzene (DVB) to divinylbenzene dioxide (DVBDO), a product of major interest for epoxy resin preparation. Considering the catalyst performance, the best conditions are: phenylfluorinated iron(III)-porphyrin **A9** as catalyst; CH₂Cl₂:MeOH (1:3) as solvent, room temperature, and the slow addition of H₂O₂. Under optimized reaction conditions the double epoxidation was found to have 77% yield and TON of 600 (**Scheme 1.13**). The authors observed that electron-withdrawing groups make the catalyst more robust, but the higher Lewis acidity also contributes to lowering the selectivity for epoxide formation due to epoxide ring opening.



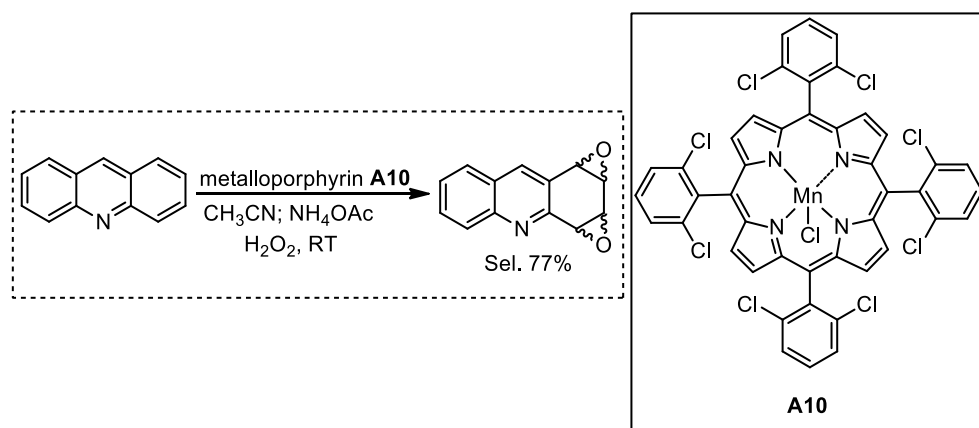
Scheme 1.13 – Epoxidation of the commercially relevant divinylbenzene catalysed by phenylfluorinated iron(III)-porphyrin.

Rebello^[149] studied the effect of substrate structure on the selectivity for epoxide formation using iron(III)-pentafluoroporphyrin **A9** as catalyst and ethanol as a green solvent. She observed that at room temperature, for 2-6 h, indene was selectively transformed into indene 1,2-oxide and 3,5-dimethylphenol, while naphthalene was selectively oxidized to the corresponding quinones. These results indicate that it is more likely that the mechanism proceeds through a porphyrin iron(V) active oxo- species, rather than *via* hydroperoxy ones (**Scheme 1.14**).



Scheme 1.14 – Evaluation of substrate structure in oxidation reaction using iron(III)-porphyrin as catalyst and H_2O_2 as oxidant.

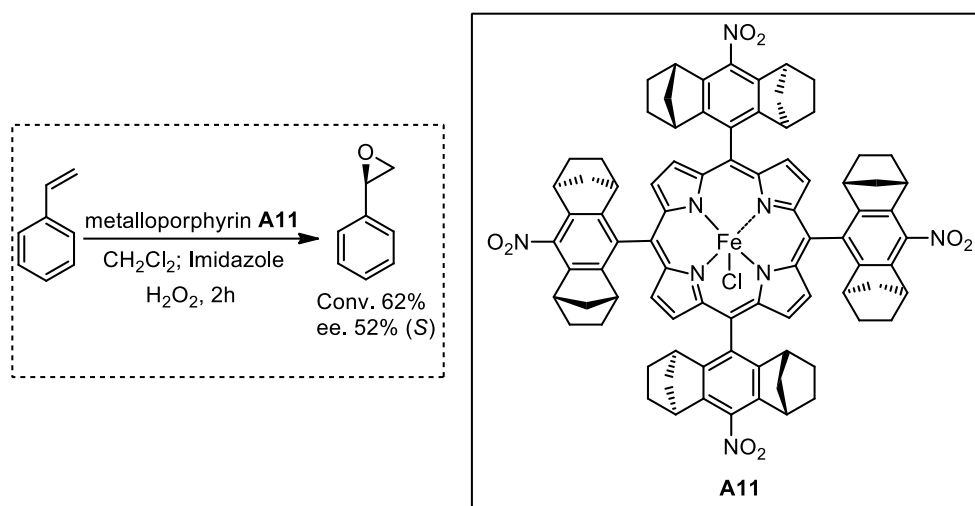
Rebelo^[150] also reported the direct epoxidation of acridine, using a different catalytic system: **A10**; H₂O₂/CH₃CN; NH₄OAc. In this case, the author observed the progressive dearomatization and epoxidation of the azatricyclic structure, with di, and tetra-epoxides being isolated (77%) and characterized (**Scheme 1.15**).



Scheme 1.15 – Epoxidation of acridine catalysed by Mn(III)-porphyrin and using H₂O₂ as oxidant.

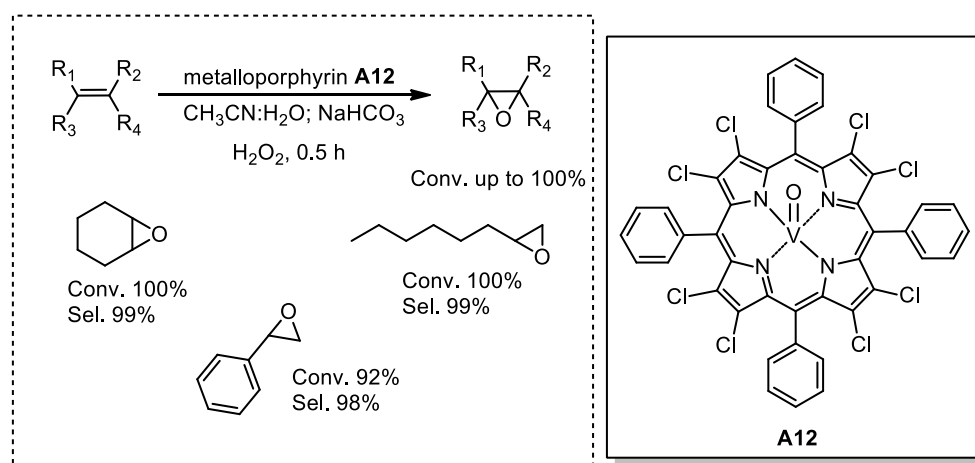
Jiang^[151] studied the influence of the central metal on the solventless epoxidation of unsaturated fatty acid methyl esters (FAMEs), using H₂O₂ as oxidant and concluded that its presence in metalloporphyrins has a strong influence on the catalytic performance, following the order: Mn(III)=Fe(III)>Co(II)>Ni(II)>Zn(II). To carry out the epoxidation in multi gram scale (20 g), the authors selected Mn(III), without any co-catalyst (axial ligand) and H₂O₂ as oxygen donor. Under these reaction conditions they obtained a low conversion (33%) and very low epoxide yield (12%).

Simonneaux^[152] reported the synthesis of the chiral metalloporphyrin **A11**, which was evaluated in the asymmetric epoxidation of styrene derivatives, with H₂O₂ as oxidant and imidazole as axial ligand. Using CH₂Cl₂/MeOH mixture (0.5:0.5) as solvent, the authors obtained styrene epoxide with 62% yield and 52% e.e. for the *S*-enantiomer (**Scheme 1.16**).



Scheme 1.16 – Chiral iron porphyrin as catalyst in epoxidation reaction.

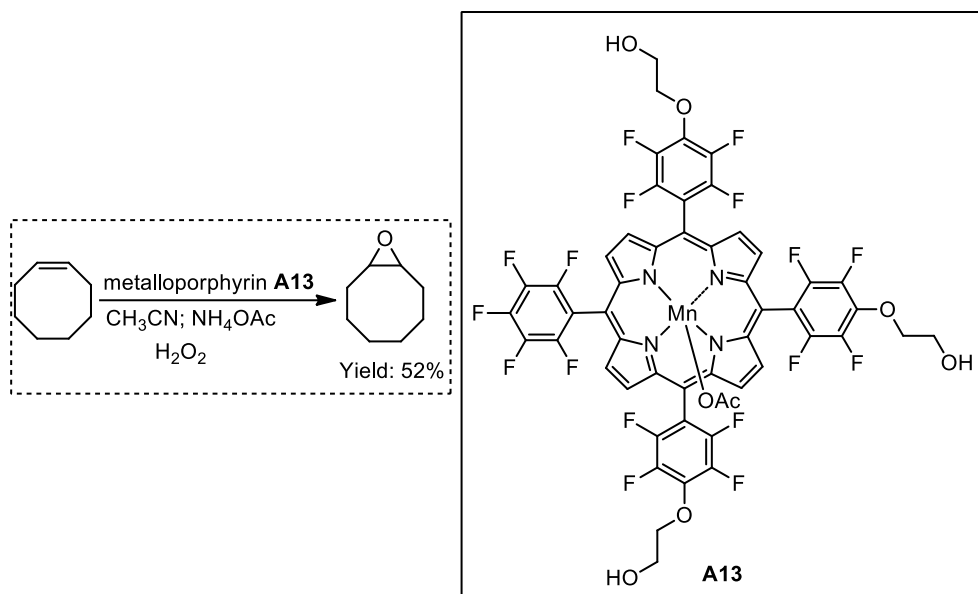
Sankar and Maurya^[153] synthesized a vanadium(IV) octachloro-porphyrin **A12** and applied it as catalyst to the epoxidation of various olefins, using H_2O_2 as oxidant, NaHCO_3 as axial ligand, in a mixture of $\text{CH}_3\text{CN}/\text{H}_2\text{O}$ (3:2) as solvent, for 30 min. The authors obtained very high epoxide selectivity (98–100 %), along with very high activity, independent of the olefin structure (e.g. 100% for both cyclohexene and 1-octene) (**Scheme 1.17**).



Scheme 1.17 – β -octachlorovanadylporphyrin as catalyst in epoxidation of olefins.

Simões and Nakagaki^[154] studied the influence of the number of ethylene glycol substituents on perfluorinated manganese(III) complexes of *meso*-phenyl substituted porphyrins in the oxidation of *cis*-cyclooctene, using H_2O_2 as oxidant,

acetonitrile as solvent, at room temperature. The authors concluded that ammonium acetate was the best axial ligand, while Mn(III) complex **A13**, bearing three ethylene glycol was found to be the most efficient catalyst. This catalytic system yielded epoxide in 52% yield, using a catalyst/oxidant/substrate (**A13**/H₂O₂/cyclooctene) molar ratio of 1:1200:600 and a reaction time of 1 h (**Scheme 1.18**).



Scheme 1.18 – Ethylene glycol substituted porphyrin manganese(III) as catalyst in epoxidation of olefins.

To sum up, in the design and development of a catalytic system for epoxidation reaction using H₂O₂ as oxidant, Fe(III) and Mn(III) can be accepted as the most appropriate metals. The combination of solvent and co-catalyst used could control the catalytic species formed, and act to regulate the product selectivity. Considering the porphyrin structure, the second-generation porphyrins containing halogen atoms in the phenyl rings are shown to be the most active and selective catalysts. Finally, immobilization of metalloporphyrins is a good way to prevent degradation *via* inactive μ -oxo dimer formation and to promote catalyst reutilization.

1.4 Metalloporphyrins as Catalysts in Sequential Epoxidation/ CO₂ Cycloaddition Reaction

The current demand by the chemical industry for renewable raw materials is a crucial issue for the development of sustainable chemistry.^[155, 156] Because of this, the conversion of CO₂ into high value chemicals and materials for fine and bulk chemical industry has become a topic of increasing relevance in economic and environmental terms.^[157-160]

As a direct consequence of the marked growth of CO₂ levels in the atmosphere,^[161, 162] a major effort is being directed to developing processes and technologies towards the reduction of carbon emissions through capture and transformation processes.^[163-165] Many catalytic processes have used CO₂ as a practical chemical feedstock to produce value-added products, including urea, salicylic acid (Kolbe-Schmitt process), organic carbonates, polymers and so forth.^[160, 166] This has resulted in the consumption of approximately 116 million tons of CO₂ per year.^[167] Nevertheless, only a small proportion (1%) of the total abundance of CO₂ on Earth is currently used by the chemical industry,^[168] due to its high thermodynamic and kinetic stability.^[169]

One of the various transformations using CO₂ as a feedstock, its cycloaddition to epoxides, is an atom economical approach to preparing cyclic carbonates,^[170-173] or polymeric materials. These products are widely used as aprotic polar solvents, fine chemical intermediates, and sources for polymer and engineering plastic synthesis (**Figure 1.7**).^[174-178]

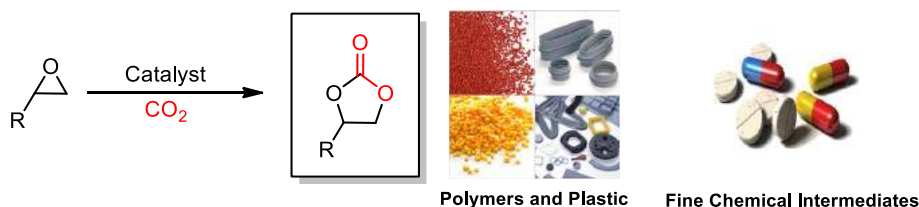
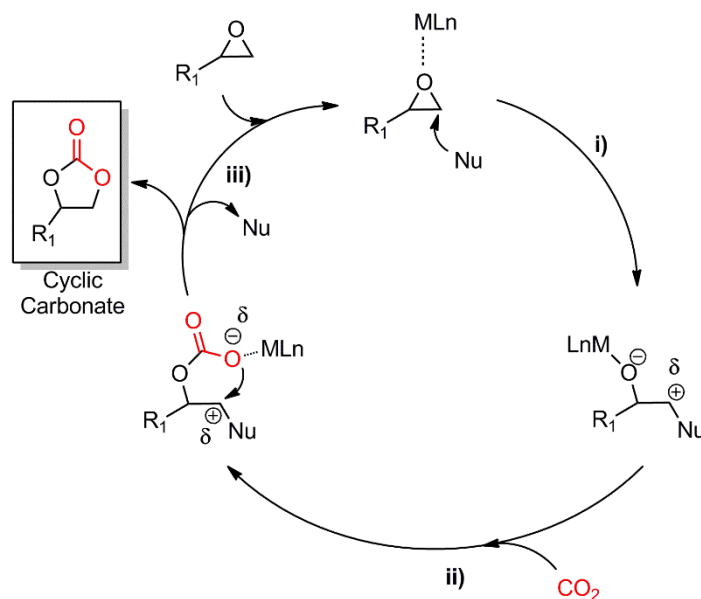


Figure 1.7 – Synthesis cyclic carbonates and their general applications.

It is generally accepted that the mechanism of the CO₂ cycloaddition reaction to epoxide is catalysed by a nucleophile and a Lewis acid metal complex,^[179, 180] and involves the following steps: i) epoxide activation by the metal centre and ring opening by nucleophilic attack; ii) CO₂ insertion into the metal alkoxy-bond generated by ring opening; iii) formation of the carbonate by cyclization and release of the products (**Scheme 1.19**).



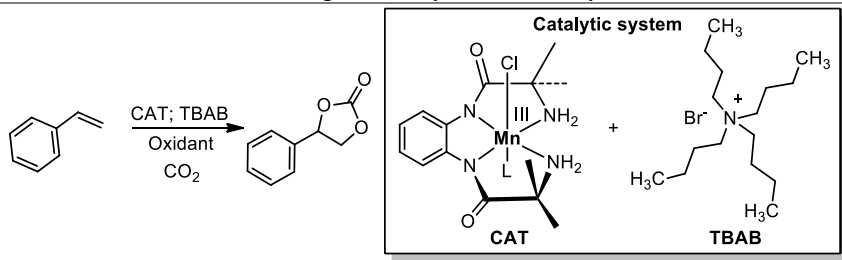
Scheme 1.19 – General mechanism of CO₂ cycloaddition reaction to epoxide catalysed by a nucleophile and a Lewis acidic metal complex.^[180]

These coupling reactions of CO₂ with epoxides have been catalysed by various systems, including organocatalysts,^[171, 181, 182] ionic liquids,^[183, 184] and metal catalysts,^[185, 186] in particular, those based on metalloporphyrins.^[187-189] However, the search for selective sequential catalytic systems capable of sequentially promoting olefin epoxidation, followed by CO₂ addition to generate cyclic carbonates, is still a major challenge.^[190-200] This is one of the studies described in **chapter 3**. Because of this, we are presenting a systematic review for the last 5 years on the utilization of sequential catalytic systems able to promote the synthesis of cyclic carbonates from olefins.

In 2015, Ghosh and co-authors^[201] evaluated the effect of the oxidant-type on the sequential synthesis of styrene carbonate from styrene using a manganese(III) amido-amine complex as catalyst and TBAB as co-catalyst (**Table 1.1**). TBHP was

shown to be the best oxidant for the synthesis of styrene carbonate, with 34% yield (**Table 1.1; entry 1**). With the other oxidants, low yields were found. This was possibly due to demetallation of the catalyst in the cases of peracetic acid and H₂O₂ (**Table 1.1; entry 2-3**), while with PhIO as oxidant it was probably due to its poor solubility (**Table 1.1, entry 4**). Pyridine *N*-oxide was seen to be a poor oxidant, and might not be able oxidize the manganese(III) complex to the high-valent manganese-oxo species (**Table 1.1, entry 5**). Finally, in the case of *m*-CPBA, no styrene carbonate was observed, which could be due to the poor miscibility of *m*-CPBA in styrene (**Table 1.1, entry 6**).

Table 1.1 – Oxidant evaluation in sequential synthesis of cyclic carbonate from olefin.^a



Entry	Oxidant	Styrene oxide	Styrene carbonate	Benzaldehyde
1	TBHP	16	34	23
2	H ₂ O ₂	6	11	19
3	CH ₃ COOOH	18	5	9
4	PhIO	32	21	7
5	Py- <i>N</i> -Oxide	12	-	2
6	<i>m</i> -CPBA	22	-	4

^a**Reaction conditions:** Catalyst-TBAB-alkene = 1:2:500; CO₂ (17 bar), 80 °C; oxidant: 1.5 equivalent; Acetonitrile: 2.5 mL.

In 2015, Launay and co-authors^[202] reported the attempted application of the catalytic system (manganese(III)salen + choline chloride) to direct synthesis of styrene carbonate from styrene at 80 °C and 120 °C (**Table 1.2, entry 1.2**). However, no styrene carbonate formation was found in either case. At 80 °C, the authors observed full conversion of styrene, but only 25% styrene oxide selectivity, and no formation of styrene carbonate was detected (**Table 1.2, entry 1**). When the reaction was performed at 120 °C, no styrene oxide or styrene carbonate was observed

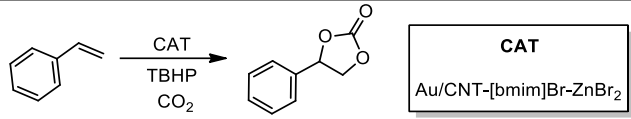
(**Table 1.2, entry 2**). The authors reported that this result at 120 °C might be due to a possible polymerization reaction. In both cases, many by-products with benzoyl fragments were found.

Table 1.2 – Attempted synthesis of styrene carbonate from styrene catalysed by a Mn(salen) and choline chloride.^a

Entry	Oxidant	Temperature (°C)	Conv. (%)	Styrene oxide	Styrene carbonate
1	O ₂ + IBA	80	100	25	0
2	O ₂ + IBA	120	100	3	1

^a**Reaction conditions:** styrene (8.7 mmol), isobutyraldehyde (IBA) (25 mmol), benzonitrile (20 mL), catalyst (7.9 μmol), choline chloride (0.145 mmol) and internal standard *n*-dodecane (4.6 mmol) for 23 h.

In 2016, Krawczyk and co-authors^[203] examined the effect of CO₂ pressure (1.2-2.0 MPa) and temperature (100-120 °C) in one-pot synthesis of styrene carbonate from styrene using a gold nanoparticle supported on multiwalled carbon nanotubes (Au/CNT) and [bmim]Br/ZnBr₂ as catalysts (**Table 1.3**). The authors observed that a decrease of CO₂ pressure led to an increase in the styrene carbonate yield. The Au/CNT reutilization was also studied and no loss of activity was observed in up to 5 catalytic cycles.

Table 1.3 – One-pot synthesis of styrene carbonate from styrene catalysed by nanogold-ionic liquid.


Entry	CO ₂ pressure (MPa)	Temperature (°C)	Conv. (%)	Styrene carbonate (%)	Benzaldehyde
1	1.2	120	100	60	9
2	2	120	99	33	10
3	2	100	100	27	8
4	1.2	100	100	56	12
5	1.2	120	99	58	9

^a**Reaction conditions:** styrene (32 mmol); anhydrous TBHP (64 mmol); ratio of substrate: Au/CNT (100 mmol/g); molar ratio of [bmim]Br:ZnBr₂:substrate (22:1:357).

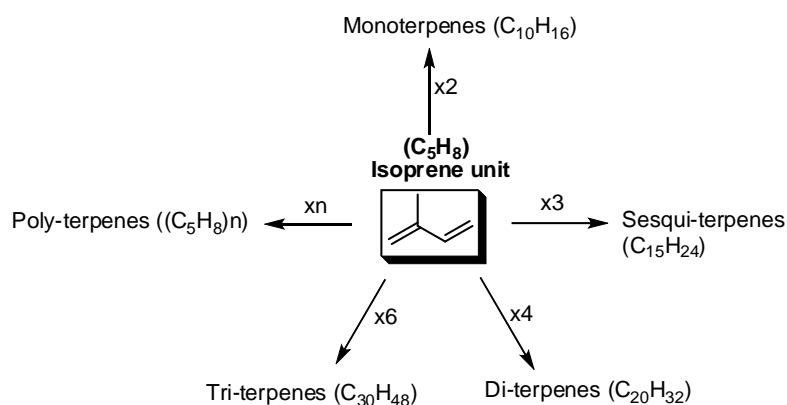
In sum, to the best of our knowledge there are no reports using a recyclable heterogeneous catalytic system based on metalloporphyrins to promote sequential transformation of olefins into cyclic carbonates, using green oxidants such as O₂ or H₂O₂. In this context, in this thesis (**Chapter 3**), we reported the application of hybrid manganese(III) and chromium(III) porphyrin magnetic nanocomposite as reusable catalysts in olefin epoxidation using O₂ and H₂O₂ and sequential epoxidation/CO₂ cycloaddition reaction to epoxide, yielding a family of cyclic carbonates.

1.5 Renewable Terpene-based Raw Materials for the Pharmaceutical Industry

The use of renewable raw materials, from agro-resources to products for fine^[204] and bulk industry,^[205-207] has aroused great interest within the research community.^[208] Among the various renewable raw materials proposed, terpenes and terpenoids appear particularly attractive,^[209] due to their low toxicity,^[210, 211] structurally diverse scaffolds that have built-in olefinic bonds,^[205] interesting pharmacological properties,^[212-214] etc.

Terpenes, in the strictest sense, refer to a series of isomeric, unsaturated hydrocarbons of the general formula (C₅H₈) and are found in almost all life forms,

where they carry out a myriad of functions ranging from primarily structural ones, to involvement in photosynthesis.^[215] Their production in plants depends both on their species and on environmental conditions.^[216, 217] An isoprene unit (C_5H_8) is the basic chemical entity of terpenes for the structural transformations during biosynthesis, and it undergoes rearrangements and can be readily oxidized to yield a wide family of mono-, sesqui-, tri-, di-, and tetra-terpenes^[218] (**Scheme 1.20**).



Scheme 1.20 – Biotransformation and general classification of terpenes.^[217]

In their classification, monoterpenes possess two isoprene units ($C_{10}H_{16}$), sesquiterpenes have three isoprene units ($C_{15}H_{24}$). Higher terpenes, such as diterpenes, have four isoprene units ($C_{20}H_{32}$), triterpenes have six ($C_{30}H_{48}$), tetraterpenes have eight ($C_{40}H_{64}$), while terpenes having $>C_{40}$ are called polyterpenes.^[219]

Terpenes are an abundant feedstock, and are inexpensive, which makes them ideal small molecule building blocks for many applications,^[220] such as fuels,^[221] monomers for polymer synthesis,^[222] biochemical-signalling agents,^[223] sources of chirality for synthetic reagents and catalysts,^[224] and starting material for organic synthesis. In addition to these applications, terpenes display a wide array of pharmacological properties, including antimicrobial,^[225, 226] antioxidant,^[227] anticancer,^[228] antiarrhythmic,^[229] anti-inflammatory,^[230] anti-histaminic,^[231] anti-spasmodic^[232] and anti-diabetic.^[233] Because of this, the past 50 years have seen an explosion in synthetic terpene research resulting in the total synthesis of many complex terpene natural products,^[234, 235] the rise of the semisynthetic steroid field,

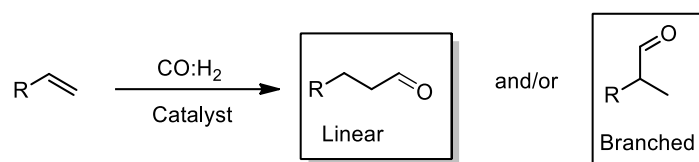
and the U.S. Food and Drug Administration (FDA) approval of a variety of terpene-based drugs.^[236]

In this thesis, we highlight anti-cancer agents among the many drugs developed, since cancer is a major cause of morbidity and mortality;^[237] and is expected to rise from 14 million new cases in 2012 to 24 million in 2035.^[238] Within the variety of malignant cancer cells, osteosarcoma is one of the most common primary malignant bone cancers to occur in childhood and adolescence, and shows a very poor prognosis for patients with metastatic or recurrent disease (survival < 20%).^[239] There are several studies in the literature and there is clearly considerable interest in the development and use of natural products against osteosarcoma cells, including terpenes and others, e.g. alkaloids,^[240, 241] saponins such as diosgenin,^[242] curcumin (polyphenol),^[241] and sulforaphane (organosulfur).^[243]

One way to access an array of synthetic and semi-synthetic terpene-based osteosarcoma drugs is through the development and utilization of efficient and selective catalytic processes. There are numerous catalytic approaches which can promote the synthesis and transformation of terpenes, and that can modulate properties such as their flavour or pharmacological activity. These can involve oxidation,^[244, 245] reduction,^[246] cross coupling,^[247] hydroaminomethylation,^[248] hydroformylation,^[249] epoxidation,^[250] alkoxylation,^[251] etc. We highlight here the hydroformylation reaction as a powerful tool to transform an olefin into an aldehyde.

1.5.1 Hydroformylation of Terpenes

The hydroformylation reaction (oxo synthesis) is one of the most important industrial processes involving homogenous catalysis.^[252, 253] This reaction was discovered in 1938 by Otto Roelen (1897-1993), and involves the utilization of syngas (hydrogen and carbon monoxide) to be added across the carbon-carbon double bond of alkenes (or alkynes), yielding linear and branched aldehydes^[254, 255] (**Scheme 1.21**).

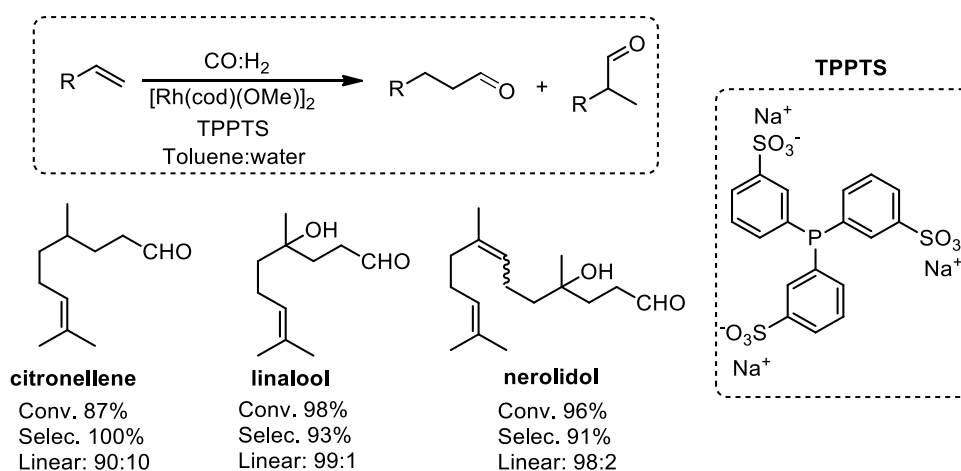


Scheme 1.21 – General reaction of hydroformylation.

Aldehydes (or oxo chemicals) have been used as raw materials in the production of many chemical products, including solvents, coatings, plasticizers, alcohols, resins, detergent alcohols, and as intermediates leading to pharmaceuticals and agrochemicals.^[253] Their consumption in 2017 was approximately 14 million metric tons.^[256]

We highlight here the application of the hydroformylation process to promote the structural modification of terpenes, with the aim of modulating their flavour or biological properties,^[248, 249, 257-272] and present a systematic review of the literature from the last 5 years (2014-2018).

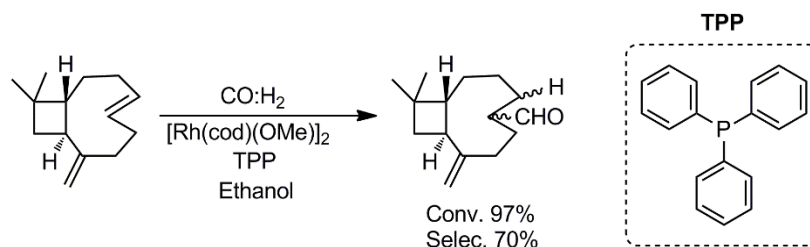
In 2015, Gusevskaya and co-authors^[259] reported the hydroformylation of a set of acyclic terpenes, β -citronellene, linalool and nerolidol, in a water/toluene biphasic medium, using $[\text{Rh}(\text{cod})(\text{OMe})_2]$ as the catalyst precursor and a water-soluble tris(3-sulfonatophenyl)phosphine as ligand (**Scheme 1.22**). In this study, the authors evaluated the effect of CO/H_2 pressure, temperature, the amount of substrate/catalyst and the use of a cationic surfactant, cetylmethylammonium chloride (CTAC), on the reaction rates.



Scheme 1.22 – Hydroformylation of acyclic terpenes in a biphasic system.

After an optimization study, a notable increase was observed in the conversion (up to 98%) and selectivity for aldehydes (up to 100%) in hydroformylation of all three terpenes, due to the addition of the cationic surfactant (CTAC). Several aldehydes were obtained from the terpenes using a biphasic system as an eco-friendly medium, in which rhodium catalyst can be easily separated from the reaction medium.

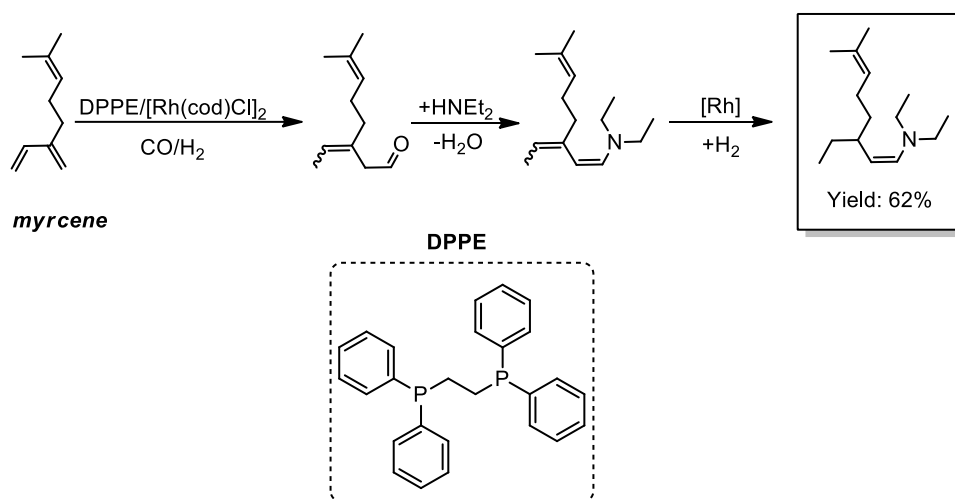
In 2016, Gusevskaya and dos Santos^[249] carried out the hydroformylation of β -caryophyllene, one of the most widespread sesquiterpenes, using various phosphines and bulk monophosphites as ligands, and toluene or ethanol as solvent. The authors evaluated the effect of the phosphorous ligand/rhodium ratio, reaction time, and temperature on conversion and selectivity for aldehyde. They observed that temperatures above 60 °C avoided the substrate decomposition; the decrease of selectivity may be due to substrate isomerization following by hydroformylation of the isomers. The endocyclic double bond showed much higher reactivity towards its hydroformylation, leading to the major primary aldehyde formation. After optimization studies, the catalytic system ($\text{PPh}_3 + [\text{Rh}(\text{cod})(\text{OMe})_2]$) and ethanol as solvent was able to promote the hydroformylation of β -caryophyllene, showing 97% conversion and 70% selectivity for aldehyde formation (**Scheme 1.23**).



Scheme 1.23 – Hydroformylation of β -caryophyllene catalysed by Rh/phosphorous ligands.

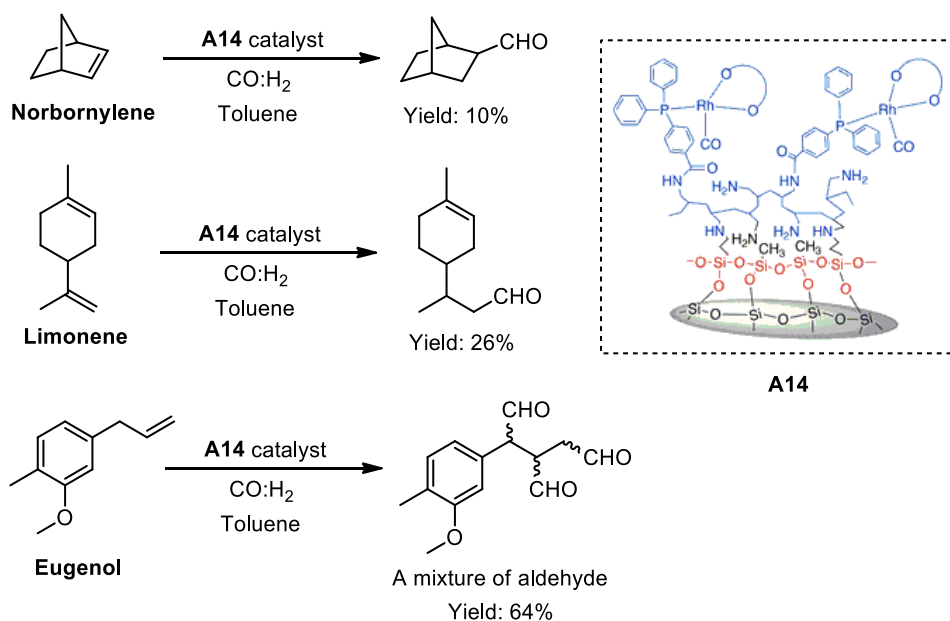
In 2017, Vorholt and co-authors^[248] developed a catalytic hydroamino-methylation system with the aim of obtaining renewable building blocks for surfactants from terpenes (1,3-dienes) through hydroformylation and enamine condensation steps, followed by hydrogenation. The authors tested the effects of temperature, syngas pressure and composition, metal-ligand ratio on conversion and selectivity, for each step separately. For the optimized reaction conditions, the hydroformylation of myrcene was performed using (Rh/1,2-bis(diphenylphosphino)

ethane), for 3 hours, and showed a high yield (70%) and the highest TOF values (739 mol mol⁻¹ h⁻¹) for hydroformylation of 1,3-dienes so far. For the tandem reaction, the combination of [Rh(cod)Cl]₂ with the 1,2-bis(diphenylphosphino)ethane (dppe) ligand was found to be the best catalytic system, yielding the enamine with 62% in 18 h (**Scheme 1.24**).



Scheme 1.24 – Tandem hydroaminomethylation of myrcene.

More recently, in 2018, Rosenberg and co-authors^[258] studied the immobilization of Rh complexes onto silica gel containing covalently anchored poly(allylamine) chains (SPC) and their application in hydroformylation of unsaturated compounds, including terpenes. These new Rh heterogeneous catalysts were characterized by solid-state NMR spectroscopy, IR, XPS, TEM, and elemental analysis. The hydroformylation catalytic system was optimized using 1-octene as model substrate and the covalent-coupled catalyst **A14** was recovered and reused for 3 catalytic cycles without loss of activity. The optimized heterogeneous catalytic system was then applied in hydroformylation of a set of terpenes (norbornylene, limonene and engenol) yielding 10%, 26% and 64% for aldehydes, respectively (**Scheme 1.25**).



Scheme 1.25 – Rh complexes immobilized onto silica polyamine composite as catalyst in the hydroformylation of terpenes. Adapted with permission from ref [258]. Copyright 2018 ACS.

The relevance of terpenes as renewable raw material, led us to use catalytic processes, like epoxidation, hydroformylation and epoxide ring-opening to promote the synthesis of derivatives for Medicinal Chemistry application, and the results are presented and discussed in **chapter 4**.

1.6 References

- [1] <https://www.epa.gov/laws-regulations/summary-pollution-prevention-act>
Access: 03/02/2019.
- [2] P. T. Anastas, *Origins and Early History of Green Chemistry*, World Scientific Singapore, **2018**.
- [3] P. Anastas, J. Warner, *Green Chemistry: Theory and Practice*, University Press, Oxford, **1998**.
- [4] P. T. Anastas, M. M. Kirchhoff, *Accounts of Chemical Research* **2002**, *35*, 686-694.
- [5] J. H. Clark, *Green and Sustainable Medicinal Chemistry: Methods, Tools and Strategies for the 21st Century Pharmaceutical Industry*, Royal Soc Chemistry, Cambridge, **2016**.
- [6] J. H. Clark, *Green Chemistry and Environmentally Friendly Technologies*, Blackwell Science Publ, Oxford, **2005**.
- [7] <http://catsus.tecnico.ulisboa.pt/> Access: 03/02/2019.
- [8] M. M. Pereira, M. J. F. Calvete, *Sustainable Synthesis of Pharmaceuticals: Using Transition Metal Complexes as Catalysts*, Royal Society of Chemistry, Oxford, **2018**.
- [9] J. C. Serrano-Ruiz, R. M. West, J. A. Durnesic, *Catalytic Conversion of Renewable Biomass Resources to Fuels and Chemicals*, Annual Reviews, Palo Alto, **2010**.
- [10] E. L. Scott, J. P. M. Sanders, A. Steinbuchel, *Perspectives on Chemicals from Renewable Resources*, Springer, New York, **2010**.
- [11] P. T. Anastas, M. M. Kirchhoff, T. C. Williamson, *Applied Catalysis a-General* **2001**, *221*, 3-13.
- [12] J. L. Casci, C. M. Lok, M. D. Shannon, *Catalysis Today* **2009**, *145*, 38-44.
- [13] B. Lindstrom, L. J. Pettersson, *Cattech* **2003**, *7*, 130-138.
- [14] J. J. Berzelius, *Jahres-Bericht* **1835**, *14*, 237.
- [15] K. J. Laidler, *Pure and Applied Chemistry* **1996**, *68*, 149-192.
- [16] J. Wisniak, *Educación Química* **2010**, *21*, 60-69.
- [17] K. M. Nichólas, *Selective Catalysis for Renewable Feedstocks and Chemicals*, Springer International Publishing, Heidelberg, New York, Dordrecht, London, **2014**.
- [18] A. M. Echavarren, *ChemCatChem* **2010**, *2*, 1331-1332.
- [19] <https://www.nobelprize.org/prizes/chemistry/1912/summary/>
Access: 21/12/2018.
- [20] <https://www.nobelprize.org/prizes/chemistry/1930/summary/>
Access: 22/12/2018.
- [21] H. Fischer, *Org. Synth* **1955**, *3*, 351-X.
- [22] H. Fischer, H. Orth, *Die Chemie des Pyrrols*, Leipzig, **1934**.
- [23] <https://www.nobelprize.org/prizes/chemistry/2001/summary/>
Access: 24/12/2018.

- [24] T. Katsuki, K. B. Sharpless, *Journal of the American Chemical Society* **1980**, *102*, 5974-5976.
- [25] D. B. Sun, B. Pedersen, J. A. Ellman, *Chemical Science* **2019**, *10*, 535-541.
- [26] S. Gahalawat, S. K. Pandey, *Tetrahedron Letters* **2017**, *58*, 2898-2900.
- [27] C. Berube, C. Carpentier, N. Voyer, *Tetrahedron Letters* **2017**, *58*, 2334-2336.
- [28] A. Riera, M. Moreno, *Molecules* **2010**, *15*, 1041-1073.
- [29] <https://www.nobelprize.org/prizes/chemistry/2018/summary/>
Access: 24/12/2018.
- [30] R. J. K. Zhang, K. Chen, X. Y. Huang, L. Wohlschlager, H. Renata, F. H. Arnold, *Nature* **2019**, *565*, 67-72.
- [31] P. J. Almhjell, C. E. Boville, F. H. Arnold, *Chemical Society Reviews* **2018**, *47*, 8980-8997.
- [32] K. Chen, S. Q. Zhang, O. F. Brandenburg, X. Hong, F. H. Arnold, *Journal of the American Chemical Society* **2018**, *140*, 16402-16407.
- [33] F. H. Arnold, *Angewandte Chemie-International Edition* **2018**, *57*, 4143-4148.
- [34] L. Q. Lu, J. R. Chen, W. J. Xiao, *Accounts of Chemical Research* **2012**, *45*, 1278-1293.
- [35] A. Grossmann, D. Enders, *Angewandte Chemie-International Edition* **2012**, *51*, 314-325.
- [36] L. F. Tietze, T. Kinzel, C. C. Brazel, *Accounts of Chemical Research* **2009**, *42*, 367-378.
- [37] M. M. Hussain, P. J. Walsh, *Accounts of Chemical Research* **2008**, *41*, 883-893.
- [38] J. C. Wasilke, S. J. Obrey, R. T. Baker, G. C. Bazan, *Chemical Reviews* **2005**, *105*, 1001-1020.
- [39] W. T. Yu, M. D. Porosoff, J. G. G. Chen, *Chemical Reviews* **2012**, *112*, 5780-5817.
- [40] M. K. Birhanu, M. C. Tsai, A. W. Kahsay, C. T. Chen, T. S. Zeleke, K. B. Ibrahim, C. J. Huang, W. N. Su, B. J. Hwang, *Advanced Materials Interfaces* **2018**, *5*, 1800919-X.
- [41] W. L. Zhu, B. M. Tackett, J. G. G. Chen, F. Jiao, *Topics in Current Chemistry* **2018**, *376*.
- [42] S. K. Singh, *Asian Journal of Organic Chemistry* **2018**, *7*, 1901-1923.
- [43] L. Wang, F. X. Li, Y. J. Chen, J. X. Chen, *Journal of Energy Chemistry* **2019**, *29*, 40-49.
- [44] Q. H. Fang, J. H. Fu, F. Wang, Z. X. Qin, W. G. Ma, J. W. Zhang, G. Li, *New Journal of Chemistry* **2019**, *43*, 28-36.
- [45] N. K. Chaudhari, J. Joo, B. Kim, B. Ruqia, S. I. Choi, K. Lee, *Nanoscale* **2018**, *10*, 20073-20088.
- [46] M. M. J. Li, S. C. E. Tsang, *Catalysis Science & Technology* **2018**, *8*, 3450-3464.
- [47] M. S. Xaba, J. H. Noh, R. Meijboom, *Applied Surface Science* **2019**, *467*, 868-880.
- [48] K. Gupta, R. K. Rai, S. K. Singh, *ChemCatChem* **2018**, *10*, 2326-2349.

- [49] E. Nowicka, M. Sankar, *Journal of Zhejiang University-Science A* **2018**, *19*, 5-20.
- [50] Q. H. Yang, Q. Xu, H. L. Jiang, *Chemical Society Reviews* **2017**, *46*, 4774-4808.
- [51] Y. B. Huang, J. Liang, X. S. Wang, R. Cao, *Chemical Society Reviews* **2017**, *46*, 126-157.
- [52] S. Sun, J. M. He, M. G. Qu, K. S. Li, *Chinese Journal of Organic Chemistry* **2015**, *35*, 1250-1259.
- [53] A. E. Allen, D. W. C. MacMillan, *Chemical Science* **2012**, *3*, 633-658.
- [54] T. Ema, Y. Miyazaki, J. Shimonishi, C. Maeda, J. Hasegawa, *Journal of the American Chemical Society* **2014**, *136*, 15270-15279.
- [55] E. Rafiee, S. Eavani, *RSC Advances* **2016**, *6*, 46433-46466.
- [56] I. Aranaz, N. Acosta, A. Heras, *Biocatalysis and Biotransformation* **2018**, *36*, 89-101.
- [57] J. C. Pessoa, M. R. Maurya, *Inorganica Chimica Acta* **2017**, *455*, 415-428.
- [58] A. Kumar, G. D. Park, S. K. S. Patel, S. Kondaveeti, S. Otari, M. Z. Anwar, V. C. Kalia, Y. Singh, S. C. Kim, B. K. Cho, J. H. Sohn, D. R. Kim, Y. C. Kang, J. K. Lee, *Chemical Engineering Journal* **2019**, *359*, 1252-1264.
- [59] R. Zhong, A. C. Lindhorst, F. J. Groche, F. E. Kuhn, *Chemical Reviews* **2017**, *117*, 1970-2058.
- [60] J. S. Chang, J. S. Hwang, S. E. Park, *Research on Chemical Intermediates* **2003**, *29*, 921-938.
- [61] M. Adeel, M. Bilal, T. Rasheed, A. Sharma, H. M. N. Iqbal, *International Journal of Biological Macromolecules* **2018**, *120*, 1430-1440.
- [62] A. Soozanipour, A. Taheri-Kafrani, *Enzyme Nanoarchitectures: Enzymes Armored with Graphene*, Elsevier Academic Press Inc, San Diego, **2018**.
- [63] M. B. Gawande, P. S. Branco, R. S. Varma, *Chemical Society Reviews* **2013**, *42*, 3371-3393.
- [64] L. M. Rossi, N. J. S. Costa, F. P. Silva, R. Wojcieszak, *Green Chemistry* **2014**, *16*, 2906-2933.
- [65] M. Bilal, Y. P. Zhao, T. Rasheed, H. M. N. Iqbal, *International Journal of Biological Macromolecules* **2018**, *120*, 2530-2544.
- [66] M. Iranmanesh, J. Hulliger, *Chemical Society Reviews* **2017**, *46*, 5925-5934.
- [67] Y. H. Zhu, L. P. Stubbs, F. Ho, R. Z. Liu, C. P. Ship, J. A. Maguire, N. S. Hosmane, *ChemCatChem* **2010**, *2*, 365-374.
- [68] A. Schatz, O. Reiser, W. J. Stark, *Chemistry-A European Journal* **2010**, *16*, 8950-8967.
- [69] M. J. F. Calvete, M. Pineiro, L. D. Dias, M. M. Pereira, *ChemCatChem* **2018**, *10*, 3615-3635.
- [70] M. M. Q. Simoes, D. T. G. Gonzaga, M. F. C. Cardoso, L. D. M. Forezi, A. Gomes, F. D. da Silva, V. F. Ferreira, M. Neves, J. A. S. Cavaleiro, *Molecules* **2018**, *23*.
- [71] X. Y. Huang, J. T. Groves, *Chemical Reviews* **2018**, *118*, 2491-2553.

- [72] C. F. Pereira, M. M. Q. Simoes, J. P. C. Tome, F. A. A. Paz, *Molecules* **2016**, *21*, 1348-1366.
- [73] K. Rybicka-Jasinska, L. W. Ciszewski, D. T. Gryko, D. Gryko, *Journal of Porphyrins and Phthalocyanines* **2016**, *20*, 76-95.
- [74] G. Simonneaux, H. Srour, P. Le Maux, S. Chevance, D. Carrie, *Symmetry-Basel* **2014**, *6*, 210-221.
- [75] Q. Liu, C. C. Guo, *Science China-Chemistry* **2012**, *55*, 2036-2053.
- [76] D. Mansuy, *Comptes Rendus Chimie* **2007**, *10*, 392-413.
- [77] J. C. Barona-Castano, C. C. Carmona-Vargas, T. J. Brocksom, K. T. de Oliveira, *Molecules* **2016**, *21*, 310-337.
- [78] S. Severance, I. Hamza, *Chemical Reviews* **2009**, *109*, 4596-4616.
- [79] C. J. Omiecinski, J. P. V. Heuvel, G. H. Perdew, J. M. Peters, *Toxicological Sciences* **2011**, *120*, S49-S75.
- [80] D. Ostfeld, M. Tsutsui, *Accounts of Chemical Research* **1974**, *7*, 52-58.
- [81] G. A. Ordway, D. J. Garry, *Journal of Experimental Biology* **2004**, *207*, 3441-3446.
- [82] D. Garfinkel, *Archives of Biochemistry and Biophysics* **2003**, *409*, 7-15.
- [83] T. Omura, R. Sato, *Journal of Biological Chemistry* **1964**, *239*, 2370-X.
- [84] I. Tabushi, M. Kodera, M. Yokoyama, *Journal of the American Chemical Society* **1985**, *107*, 4466-4473.
- [85] J. T. Groves, Y. Watanabe, *Journal of the American Chemical Society* **1988**, *110*, 8443-8452.
- [86] D. Mansuy, J. F. Bartoli, P. Battioni, D. K. Lyon, R. G. Finke, *Journal of the American Chemical Society* **1991**, *113*, 7222-7226.
- [87] J. P. Collman, X. M. Zhang, V. J. Lee, E. S. Uffelman, J. I. Brauman, *Science* **1993**, *261*, 1404-1411.
- [88] R. Neumann, M. Dahan, *Nature* **1997**, *388*, 353-355.
- [89] P. A. Williams, J. Cosme, V. Sridhar, E. F. Johnson, D. E. McRee, *Molecular Cell* **2000**, *5*, 121-131.
- [90] M. M. Pereira, L. D. Dias, M. J. F. Calvete, *ACS Catalysis* **2018**, *8*, 10784-10808.
- [91] S. L. H. Rebelo, M. M. Pereira, M. M. Q. Simoes, M. Neves, J. A. S. Cavaleiro, *Journal of Catalysis* **2005**, *234*, 76-87.
- [92] P. Rothemund, *Journal of the American Chemical Society* **1935**, *57*, 2010-2011.
- [93] P. Rothemund, *Journal of the American Chemical Society* **1936**, *58*, 625-627.
- [94] A. D. Adler, Shergali.W, F. R. Longo, *Journal of the American Chemical Society* **1964**, *86*, 3145-3149.
- [95] A. D. Adler, F. R. Longo, J. D. Finarelli, Goldmach.J, J. Assour, Korsakof.L, *Journal of Organic Chemistry* **1967**, *32*, 476-476.
- [96] F. R. Longo, M. G. Finarelli, J. B. Kim, *Journal of Heterocyclic Chemistry* **1969**, *6*, 927-931.
- [97] A. Gonsalves, J. Varejao, M. M. Pereira, *Journal of Heterocyclic Chemistry* **1991**, *28*, 635-640.

- [98] A. Gonsalves, M. M. Pereira, *Journal of Heterocyclic Chemistry* **1985**, *22*, 931-933.
- [99] J. S. Lindsey, H. C. Hsu, I. C. Schreiman, *Tetrahedron Letters* **1986**, *27*, 4969-4970.
- [100] J. S. Lindsey, I. C. Schreiman, H. C. Hsu, P. C. Kearney, A. M. Marguerettaz, *Journal of Organic Chemistry* **1987**, *52*, 827-836.
- [101] R. W. Wagner, D. S. Lawrence, J. S. Lindsey, *Tetrahedron Letters* **1987**, *28*, 3069-3070.
- [102] J. S. Lindsey, R. W. Wagner, *Journal of Organic Chemistry* **1989**, *54*, 828-836.
- [103] J. S. Lindsey, *Accounts of Chemical Research* **2010**, *43*, 300-311.
- [104] C. A. Henriques, N. P. F. Goncalves, A. R. Abreu, M. J. F. Calvete, M. M. Pereira, *Journal of Porphyrins and Phthalocyanines* **2012**, *16*, 290-296.
- [105] M. Silva, A. Fernandes, S. S. Bebiano, M. J. F. Calvete, M. F. Ribeiro, H. D. Burrows, M. M. Pereira, *Chemical Communications* **2014**, *50*, 6571-6573.
- [106] M. J. F. Calvete, L. D. Dias, C. A. Henriques, S. M. A. Pinto, R. M. B. Carrilho, M. M. Pereira, *Molecules* **2017**, *22*, 741-752.
- [107] T. Shinoda, Y. Izumi, M. Onaka, *Journal of the Chemical Society-Chemical Communications* **1995**, 1801-1802.
- [108] C. M. Drain, X. C. Gong, *Chemical Communications* **1997**, *0*, 2117-2118.
- [109] F. Algarra, M. A. Esteves, V. Fornes, H. Garcia, J. Primo, *New Journal of Chemistry* **1998**, *22*, 333-338.
- [110] S. Kitaoka, K. Nobuoka, Y. Ishikawa, *Chemical Communications* **2004**, *0*, 1902-1903.
- [111] C. A. Henriques, S. M. A. Pinto, G. L. B. Aquino, M. Pineiro, M. J. F. Calvete, M. M. Pereira, *ChemSusChem* **2014**, *7*, 2821-2824.
- [112] C. A. Henriques, S. M. A. Pinto, M. Pineiro, J. Canotilho, M. E. S. Eusebio, M. M. Pereira, M. J. F. Calvete, *RSC Advances* **2015**, *5*, 64916-64924.
- [113] S. M. A. Pinto, C. A. Henriques, V. A. Tome, C. S. Vinagreiro, M. J. F. Calvete, J. M. Dabrowski, M. Pineiro, L. G. Arnaut, M. M. Pereira, *Journal of Porphyrins and Phthalocyanines* **2016**, *20*, 45-60.
- [114] A. Petit, A. Loupy, P. Maillard, M. Momenteau, *Synthetic Communications* **1992**, *22*, 1137-1142.
- [115] B. F. O. Nascimento, M. Pineiro, A. Gonsalves, M. R. Silva, A. M. Beja, J. A. Paixao, *Journal of Porphyrins and Phthalocyanines* **2007**, *11*, 77-84.
- [116] R. Lucas, J. Vergnaud, K. Teste, R. Zerrouki, V. Sol, P. Krausz, *Tetrahedron Letters* **2008**, *49*, 5537-5539.
- [117] P. B. Momo, B. S. Bellele, T. J. Brocksom, R. de Souza, K. T. de Oliveira, *RSC Advances* **2015**, *5*, 84350-84355.
- [118] R. A. Baglia, J. P. T. Zaragoza, D. P. Goldberg, *Chemical Reviews* **2017**, *117*, 13320-13352.
- [119] M. Chino, L. Leone, G. Zambrano, F. Pirro, D. D'Alonzo, V. Firpo, D. Aref, L. Lista, O. Maglio, F. Nastri, A. Lombardi, *Biopolymers* **2018**, *109*, e23107-X.

- [120] G. M. Ucoski, V. H. A. Pinto, G. DeFreitas-Silva, J. S. Reboucas, R. M. da Silva, I. Mazzaro, F. S. Nunes, S. Nakagaki, *Microporous and Mesoporous Materials* **2018**, *265*, 84-97.
- [121] C. D. Wu, M. Zhao, *Advanced Materials* **2017**, *29*, 1605446-X.
- [122] A. Gonsalves, M. M. Pereira, *Journal of Molecular Catalysis a-Chemical* **1996**, *113*, 209-221.
- [123] J. Skarzewski, R. Siedlecka, *Organic Preparations and Procedures International* **1992**, *24*, 623-647.
- [124] J. Bernadou, B. Meunier, *Advanced Synthesis & Catalysis* **2004**, *346*, 171-184.
- [125] R. Neumann, A. M. Khenkin, *Inorganic Chemistry* **1995**, *34*, 5753-5760.
- [126] H. Srour, P. Le Maux, S. Chevance, G. Simonneaux, *Coordination Chemistry Reviews* **2013**, *257*, 3030-3050.
- [127] A. Gavriilidis, A. Constantinou, K. Hellgardt, K. K. Hii, G. J. Hutchings, G. L. Brett, S. Kuhn, S. P. Marsden, *Reaction Chemistry & Engineering* **2016**, *1*, 595-612.
- [128] X. Liu, Y. Ryabenkova, M. Conte, *Physical Chemistry Chemical Physics* **2015**, *17*, 715-731.
- [129] M. Sono, M. P. Roach, E. D. Coulter, J. H. Dawson, *Chemical Reviews* **1996**, *96*, 2841-2887.
- [130] C. M. Che, J. S. Huang, *Chemical Communications* **2009**, *0*, 3996-4015.
- [131] L. Vanoye, J. Wang, M. Pablos, C. de Bellefon, A. Favre-Reguillon, *Catalysis Science & Technology* **2016**, *6*, 4724-4732.
- [132] B. B. Wentzel, P. L. Alsters, M. C. Feiters, R. J. M. Nolte, *Journal of Organic Chemistry* **2004**, *69*, 3453-3464.
- [133] P. Zucca, A. Rescigno, A. C. Rinaldi, E. Sanjust, *Journal of Molecular Catalysis A-Chemical* **2014**, *388*, 2-34.
- [134] H. B. Ji, X. T. Zhou, *Biomimetic Epoxidation of Olefins Catalyzed by Metalloporphyrins with Molecular Oxygen*, IntechOpen, London, **2011**.
- [135] Y. Li, X. T. Zhou, S. Y. Chen, R. C. Luo, J. Jiang, Z. X. Liang, H. B. Ji, *RSC Advances* **2015**, *5*, 30014-30020.
- [136] J. W. Brown, Q. T. Nguyen, T. Otto, N. N. Jarenwattananon, S. Glogglar, L. S. Bouchard, *Catalysis Communications* **2015**, *59*, 50-54.
- [137] M. H. Beyzavi, N. A. Vermeulen, A. J. Howarth, S. Tussupbayev, A. B. League, N. M. Schweitzer, J. R. Gallagher, A. E. Platero-Prats, N. Hafezi, A. A. Sarjeant, J. T. Miller, K. W. Chapman, J. F. Stoddart, C. J. Cramer, J. T. Hupp, O. K. Farha, *Journal of the American Chemical Society* **2015**, *137*, 13624-13631.
- [138] S. L. Zhu, X. Xu, S. Ou, M. Zhao, W. L. He, C. D. Wu, *Inorganic Chemistry* **2016**, *55*, 7295-7300.
- [139] A. Farokhi, H. Hosseini-Monfared, *New Journal of Chemistry* **2016**, *40*, 5032-5043.
- [140] S. Rayati, F. Nejabat, *New Journal of Chemistry* **2017**, *41*, 7987-7991.

- [141] M. Zhao, C. D. Wu, *Catalysis Communications* **2017**, *99*, 146-149.
- [142] K. Berijani, H. Hosseini-Monfared, *Molecular Catalysis* **2017**, *433*, 136-144.
- [143] C. Hammond, I. Hermans, N. Dimitratos, *ChemCatChem* **2015**, *7*, 434-440.
- [144] R. De Paula, M. M. Q. Simoes, M. Neves, J. A. S. Cavaleiro, *Journal of Molecular Catalysis A-Chemical* **2011**, *345*, 1-11.
- [145] A. C. Serra, E. C. Marcalo, A. Gonsalves, *Journal of Molecular Catalysis A-Chemical* **2004**, *215*, 17-21.
- [146] I. D. Cunningham, T. N. Danks, J. N. Hay, I. Hamerton, S. Gunathilagan, *Tetrahedron* **2001**, *57*, 6847-6853.
- [147] Y. Iamamoto, M. D. Assis, K. J. Ciuffi, C. M. C. Prado, B. Z. Prellwitz, M. Moraes, O. R. Nascimento, H. C. Sacco, *Journal of Molecular Catalysis A-Chemical* **1997**, *116*, 365-374.
- [148] K. N. Zhang, Y. Yu, S. T. Nguyen, J. T. Hupp, L. J. Broadbelt, O. K. Farha, *Industrial & Engineering Chemistry Research* **2015**, *54*, 922-927.
- [149] S. L. H. Rebelo, A. M. N. Silva, C. J. Medforth, C. Freire, *Molecules* **2016**, *21*, 481-493.
- [150] M. Linhares, S. L. H. Rebelo, K. Biernacki, A. L. Magalhaes, C. Freire, *Journal of Organic Chemistry* **2015**, *80*, 281-289.
- [151] W. J. Zhang, P. P. Jiang, J. H. Wu, P. B. Zhang, K. L. Jiang, *Reaction Kinetics Mechanisms and Catalysis* **2014**, *112*, 147-158.
- [152] N. Amiri, P. Le Maux, H. Srour, H. Nasri, G. Simonneaux, *Tetrahedron* **2014**, *70*, 8836-8842.
- [153] R. Kumar, N. Chaudhary, M. Sankar, M. R. Maurya, *Dalton Transactions* **2015**, *44*, 17720-17729.
- [154] K. Castro, F. H. C. de Lima, M. M. Q. Simoes, M. Neves, F. A. A. Paz, R. F. Mendes, S. Nakagaki, J. A. S. Cavaleiro, *Inorganica Chimica Acta* **2017**, *455*, 575-583.
- [155] F. G. Calvo-Flores, M. J. Monteagudo-Arrebola, J. A. Dobado, J. Isac-Garcia, *Topics in Current Chemistry* **2018**, *376*.
- [156] S. Perathoner, G. Centi, *Journal of the Chinese Chemical Society* **2014**, *61*, 719-730.
- [157] M. M. Zain, A. R. Mohamed, *Renewable & Sustainable Energy Reviews* **2018**, *98*, 56-63.
- [158] J. Artz, T. E. Muller, K. Thenert, J. Kleinekorte, R. Meys, A. Sternberg, A. Bardow, W. Leitner, *Chemical Reviews* **2018**, *118*, 434-504.
- [159] J. J. Wu, X. D. Zhou, *Chinese Journal of Catalysis* **2016**, *37*, 999-1015.
- [160] S. Saedi, N. A. S. Amin, M. R. Rahimpour, *Journal of CO2 Utilization* **2014**, *5*, 66-81.
- [161] A. Mardani, D. Streimikiene, F. Cavallaro, N. Loganathan, M. Khoshnoudi, *Science of the Total Environment* **2019**, *649*, 31-49.
- [162] M. Aghaie, N. Rezaei, S. Zendeheboudi, *Renewable & Sustainable Energy Reviews* **2018**, *96*, 502-525.

- [163] Z. G. Hu, Y. X. Wang, B. B. Shah, D. Zhao, *Advanced Sustainable Systems* **2019**, *3*, 1970002.
- [164] J. Leclaire, D. J. Heldebrant, *Green Chemistry* **2018**, *20*, 5058-5081.
- [165] J. Y. Hu, H. Z. Liu, B. X. Han, *Science China-Chemistry* **2018**, *61*, 1486-1493.
- [166] Q. Liu, L. P. Wu, R. Jackstell, M. Beller, *Nature Communications* **2015**, *6*, 1.
- [167] A. Otto, T. Grube, S. Schiebahn, D. Stolten, *Energy & Environmental Science* **2015**, *8*, 3283-3297.
- [168] M. Cokoja, C. Bruckmeier, B. Rieger, W. A. Herrmann, F. E. Kuhn, *Angewandte Chemie-International Edition* **2011**, *50*, 8510-8537.
- [169] T. Sakakura, J. C. Choi, H. Yasuda, *Chemical Reviews* **2007**, *107*, 2365-2387.
- [170] A. A. Chaugule, A. H. Tamboli, H. Kim, *Fuel* **2017**, *200*, 316-332.
- [171] M. Alves, B. Grignard, R. Mereau, C. Jerome, T. Tassaing, C. Detrembleur, *Catalysis Science & Technology* **2017**, *7*, 2651-2684.
- [172] Q. X. Han, L. Wang, Z. H. Shi, C. Xu, Z. Dong, Z. L. Mou, W. S. Liu, *Chemistry-an Asian Journal* **2017**, *12*, 1364-1373.
- [173] H. Buttner, L. Longwitz, J. Steinbauer, C. Wulf, T. Werner, *Topics in Current Chemistry* **2017**, *375*.
- [174] W. S. Guo, J. E. Gomez, A. Cristofol, J. N. Xie, A. W. Kleij, *Angewandte Chemie-International Edition* **2018**, *57*, 13735-13747.
- [175] D. C. Webster, *Progress in Organic Coatings* **2003**, *47*, 77-86.
- [176] F. Suriano, R. Pratt, J. P. K. Tan, N. Wiradharma, A. Nelson, Y. Y. Yang, P. Dubois, J. L. Hedrick, *Biomaterials* **2010**, *31*, 2637-2645.
- [177] V. M. Lombardo, E. A. Dhulst, E. K. Leitsch, N. Wilmot, W. H. Heath, A. P. Gies, M. D. Miller, J. M. Torkelson, K. A. Scheidt, *European Journal of Organic Chemistry* **2015**, 2791-2795.
- [178] A. W. Kleij, C. J. Whiteoak, *ChemCatChem* **2015**, *7*, 51-53.
- [179] M. North, R. Pasquale, *Angewandte Chemie-International Edition* **2009**, *48*, 2946-2948.
- [180] V. D'Elia, J. D. A. Pelletier, J. M. Basset, *ChemCatChem* **2015**, *7*, 1906-1917.
- [181] M. Cokoja, M. E. Wilhelm, M. H. Anthofer, W. A. Herrmann, F. E. Kuhn, *Chemsuschem* **2015**, *8*, 2436-2454.
- [182] C. J. Whiteoak, A. Nova, F. Maseras, A. W. Kleij, *ChemSusChem* **2012**, *5*, 2032-2038.
- [183] Q. He, J. W. O'Brien, K. A. Kitselman, L. E. Tompkins, G. C. T. Curtis, F. M. Kerton, *Catalysis Science & Technology* **2014**, *4*, 1513-1528.
- [184] V. B. Saptal, B. M. Bhanage, *ChemCatChem* **2016**, *8*, 244-250.
- [185] X. H. Ji, N. N. Zhu, J. G. Ma, P. Cheng, *Dalton Transactions* **2018**, *47*, 1768-1771.
- [186] S. S. Yu, X. H. Liu, J. G. Ma, Z. Niu, P. Cheng, *Journal of CO2 Utilization* **2016**, *14*, 122-125.

- [187] Y. Chen, R. C. Luo, Q. H. Xu, W. Y. Zhang, X. T. Zhou, H. B. Ji, *ChemCatChem* **2017**, *9*, 767-773.
- [188] Z. F. Dai, Q. Sun, X. L. Liu, C. Q. Bian, Q. M. Wu, S. X. Pan, L. Wang, X. J. Meng, F. Deng, F. S. Xiao, *Journal of Catalysis* **2016**, *338*, 202-209.
- [189] F. Zadehahmadi, F. Ahmadi, S. Tangestaninejad, M. Moghadam, V. Mirkhani, I. Mohammadpoor-Baltork, R. Kardanpour, *Journal of Molecular Catalysis A-Chemical* **2015**, *398*, 1-10.
- [190] L. Cuesta-Aluja, A. M. Masdeu-Bulto, *ChemistrySelect* **2016**, *1*, 2065-2070.
- [191] J. S. Sun, L. Liang, J. M. Sun, Y. Q. Jiang, K. F. Lin, X. Z. Xu, R. W. Wang, *Catalysis Surveys from Asia* **2011**, *15*, 49-54.
- [192] N. Eghbali, C. J. Li, *Green Chemistry* **2007**, *9*, 213-215.
- [193] J. M. Sun, S. Fujita, B. M. Bhanage, M. Arai, *Catalysis Today* **2004**, *93-5*, 383-388.
- [194] M. Aresta, E. Quaranta, A. Ciccarese, *Journal of Molecular Catalysis* **1987**, *41*, 355-359.
- [195] D. S. Bai, H. W. Jing, *Green Chemistry* **2010**, *12*, 39-41.
- [196] M. Aresta, A. Dibenedetto, *Journal of Molecular Catalysis A-Chemical* **2002**, *182*, 399-409.
- [197] M. Aresta, A. Dibenedetto, I. Tommasi, *Applied Organometallic Chemistry* **2000**, *14*, 799-802.
- [198] D. Xiang, X. F. Liu, J. S. Sun, F. S. Xiao, J. M. Sun, *Catalysis Today* **2009**, *148*, 383-388.
- [199] J. L. Wang, J. Q. Wang, L. N. He, X. Y. Dou, F. Wu, *Green Chemistry* **2008**, *10*, 1218-1223.
- [200] J. M. Sun, S. Fujita, B. M. Bhanage, M. Arai, *Catalysis Communications* **2004**, *5*, 83-87.
- [201] P. Ramidi, C. M. Felton, B. P. Subedi, H. Zhou, Z. R. Tian, Y. Gartia, B. S. Pierce, A. Ghosh, *Journal of CO2 Utilization* **2015**, *9*, 48-57.
- [202] C. C. Rocha, T. Onfroy, F. Launay, *Comptes Rendus Chimie* **2015**, *18*, 270-276.
- [203] K. Jasiak, T. Krawczyk, M. Pawlyta, A. Jakobik-Kolon, S. Baj, *Catalysis Letters* **2016**, *146*, 893-901.
- [204] J. L. Bicas, A. P. Dionisio, G. M. Pastore, *Chemical Reviews* **2009**, *109*, 4518-4531.
- [205] A. W. Kleij, *ChemSusChem* **2018**, *11*, 2842-2844.
- [206] M. R. Thomsett, J. C. Moore, A. Buchard, R. A. Stockman, S. M. Howdle, *Green Chemistry* **2019**, *21*, 149-156.
- [207] E. A. Baroncini, S. K. Yadav, G. R. Palmese, J. F. Stanzione, *Journal of Applied Polymer Science* **2016**, *133*.
- [208] E. Borre, T. H. Dinh, F. Caijo, C. Crevisy, M. Mauduit, *Synthesis-Stuttgart* **2011**, 2125-2130.

- [209] N. F. Salakhutdinov, K. P. Volcho, O. I. Yarovaya, *Pure and Applied Chemistry* **2017**, *89*, 1105-1117.
- [210] S. A. Mendanha, S. S. Moura, J. L. V. Anjos, M. C. Valadares, A. Alonso, *Toxicology in Vitro* **2013**, *27*, 323-329.
- [211] R. Paduch, M. Kandefler-Szerszen, M. Trytek, J. Fiedurek, *Archivum Immunologiae Et Therapiae Experimentalis* **2007**, *55*, 315-327.
- [212] A. C. S. Rabelo, D. C. Costa, *Chemico-Biological Interactions* **2018**, *296*, 65-75.
- [213] P. Reveglia, A. Cimmino, M. Masi, P. Nocera, N. Berova, G. Ellestad, A. Evidente, *Chirality* **2018**, *30*, 1115-1134.
- [214] R. Kiyama, *European Journal of Pharmacology* **2017**, *815*, 405-415.
- [215] E. Oldfield, F. Y. Lin, *Angewandte Chemie-International Edition* **2012**, *51*, 1124-1137.
- [216] S. Munne-Bosch, L. Alegre, K. Schwarz, *European Food Research and Technology* **2000**, *210*, 263-267.
- [217] A. Smolander, S. Kanerva, B. Adamczyk, V. Kitunen, *Plant and Soil* **2012**, *350*, 1-26.
- [218] M. Aqil, A. Ahad, V. Sultana, A. Ali, *Drug Discovery Today* **2007**, *12*, 1061-1067.
- [219] E. Pichersky, R. A. Raguso, *New Phytologist* **2018**, *220*, 692-702.
- [220] Z. G. Brill, M. L. Condakes, C. P. Ting, T. J. Maimone, *Chemical Reviews* **2017**, *117*, 11753-11795.
- [221] M. A. Rude, A. Schirmer, *Current Opinion in Microbiology* **2009**, *12*, 274-281.
- [222] P. A. Wilbon, F. X. Chu, C. B. Tang, *Macromolecular Rapid Communications* **2013**, *34*, 8-37.
- [223] E. Breitmaier, *Terpenes: Flavors, Fragrances, Pharmaca, Pheromones*; Wiley-VCH, Weinheim, Germany, **2006**.
- [224] H. U. Blaser, *Chemical Reviews* **1992**, *92*, 935-952.
- [225] M. Aziz, S. Karboune, *Critical Reviews in Food Science and Nutrition* **2018**, *58*, 486-511.
- [226] S. A. Zacchino, E. Butassi, M. Di Liberto, M. Raimondi, A. Postigo, M. Sortino, *Phytomedicine* **2017**, *37*, 27-48.
- [227] E. Gonzalez-Burgos, M. P. Gomez-Serranillos, *Current Medicinal Chemistry* **2012**, *19*, 5319-5341.
- [228] M. Huang, J. J. Lu, M. Q. Huang, J. L. Bao, X. P. Chen, Y. T. Wang, *Expert Opinion on Investigational Drugs* **2012**, *21*, 1801-1818.
- [229] J. Li, D. Hu, X. L. Song, T. Han, Y. H. Gao, Y. W. Xing, *Biomed Research International* **2017**, *1*, 1-10.
- [230] Q. Q. Zhao, S. F. Wang, Y. Li, Q. Y. Song, K. Gao, *Fitoterapia* **2016**, *111*, 87-94.
- [231] A. V. O. Deurbina, M. L. Martin, M. J. Montero, R. Carron, M. A. Sevilla, L. S. Roman, *Journal of Pharmacy and Pharmacology* **1990**, *42*, 295-296.

- [232] H. Sadraei, G. R. Asghari, V. Hajhashemi, A. Kolagar, M. Ebrahimi, *Phytomedicine* **2001**, *8*, 370-376.
- [233] T. Nuutinen, *European Journal of Medicinal Chemistry* **2018**, *157*, 198-228.
- [234] S. Y. Pan, S. C. Chen, G. B. Dong, *Angewandte Chemie-International Edition* **2018**, *57*, 6333-6336.
- [235] Y. Zou, A. B. Smith, *Journal of Antibiotics* **2018**, *71*, 185-204.
- [236] D. J. Newman, G. M. Cragg, *Journal of Natural Products* **2016**, *79*, 629-661.
- [237] R. Duffy, C. Wade, R. Chang, *Drug Discovery Today* **2012**, *17*, 942-953.
- [238] B. W. Stewart, F. Bray, D. Forman, H. Ohgaki, K. Straif, A. Ullrich, C. P. Wild, *Carcinogenesis* **2016**, *37*, 2-9.
- [239] S. J. Taran, R. Taran, N. B. Malipatil, *Indian Journal of Medical and Paediatric Oncology* **2017**, *38*, 33-43.
- [240] X. Hu, D. H. Li, C. Chu, X. Li, X. H. Wang, Y. Jia, H. M. Hua, F. X. Xu, *International Journal of Molecular Sciences* **2018**, *19*, 3403-3434.
- [241] J. A. McCubrey, K. Lertpiriyapong, L. S. Steelman, S. L. Abrams, L. V. Yang, R. M. Murata, P. L. Rosalen, A. Scalisi, L. M. Neri, L. Cocco, S. Ratti, A. M. Martelli, P. Laidler, J. Dulinska-Litewka, D. Rakus, A. Gizak, P. Lombardi, F. Nicoletti, S. Candido, M. Libra, G. Montalto, M. Cervello, *Aging-Us* **2017**, *9*, 1477-1536.
- [242] G. Sethi, M. K. Shanmugam, S. Warriar, M. Merarchi, F. Arfuso, A. P. Kumar, A. Bishayee, *Nutrients* **2018**, *10*, 645-657.
- [243] M. F. Ullah, S. H. Bhat, E. Husain, F. Abu-Duhier, S. M. Hadi, F. Sarkar, A. Ahmad, *Phytochemistry Reviews* **2014**, *13*, 811-833.
- [244] W. L. Wang, D. Agustin, R. Poll, *Molecular Catalysis* **2017**, *443*, 52-59.
- [245] M. D. Costa, A. L. P. de Meireles, E. V. Gusevskaya, *Asian Journal of Organic Chemistry* **2017**, *6*, 1628-1634.
- [246] M. L. Casella, G. F. Santori, A. Moglioni, V. Vetere, J. F. Ruggera, G. M. Iglesias, O. A. Ferretti, *Applied Catalysis A-General* **2007**, *318*, 1-8.
- [247] A. Abad, C. Agullo, A. C. Cunat, D. Jimenez, R. H. Perni, *Tetrahedron* **2001**, *57*, 9727-9735.
- [248] T. A. Fassbach, T. Gaide, M. Terhorst, A. Behr, A. J. Vorholt, *ChemCatChem* **2017**, *9*, 1359-1362.
- [249] K. C. B. Oliveira, A. D. Faria, A. C. Monteiro, E. N. dos Santos, E. V. Gusevskaya, *Applied Catalysis A-General* **2016**, *523*, 139-145.
- [250] J. Silvestre-Albero, M. E. Domine, J. L. Jorda, M. T. Navarro, F. Rey, F. Rodriguez-Reinoso, A. Corma, *Applied Catalysis A-General* **2015**, *507*, 14-25.
- [251] J. E. Castanheiro, I. M. Fonseca, A. M. Ramos, J. Vital, *Microporous and Mesoporous Materials* **2017**, *249*, 16-24.
- [252] Y. C. Deng, H. Wang, Y. H. Sun, X. Wang, *ACS Catalysis* **2015**, *5*, 6828-6837.
- [253] R. Franke, D. Selent, A. Borner, *Chemical Reviews* **2012**, *112*, 5675-5732.
- [254] E. V. Gusevskaya, J. Jimenez-Pinto, A. Borner, *ChemCatChem* **2014**, *6*, 382-411.

- [255] P. van Leeuwen, P. C. J. Kamer, C. Claver, O. Pamies, M. Dieguez, *Chemical Reviews* **2011**, *111*, 2077-2118.
- [256] <https://ihsmarkit.com/products/oxo-chemical-economics-handbook.html>.
Access: 12/11/2018.
- [257] F. G. Delolo, K. C. B. Oliveira, E. N. dos Santos, E. V. Gusevskaya, *Molecular Catalysis* **2019**, *462*, 1-9.
- [258] D. Gorbunov, D. Safronova, Y. Kardasheva, A. Maximov, E. Rosenberg, E. Karakhanov, *Acs Applied Materials & Interfaces* **2018**, *10*, 26566-26575.
- [259] C. G. Vieira, M. C. de Freitas, K. C. B. de Oliveira, A. D. Faria, E. N. dos Santos, E. V. Gusevskaya, *Catalysis Science & Technology* **2015**, *5*, 960-966.
- [260] M. C. de Freitas, C. G. Vieira, E. N. dos Santos, E. V. Gusevskaya, *ChemCatChem* **2013**, *5*, 1884-1890.
- [261] C. G. Vieira, M. C. de Freitas, E. N. dos Santos, E. V. Gusevskaya, *ChemCatChem* **2012**, *4*, 795-801.
- [262] D. S. Melo, S. S. Pereira, E. N. dos Santos, *Applied Catalysis A-General* **2012**, *411*, 70-76.
- [263] A. Behr, A. J. Vorholt, in *Organometallics and Renewables, Vol. 39* (Eds.: M. A. R. Meier, B. M. Weckhuysen, P. C. A. Bruijninx), Springer-Verlag Berlin, Berlin, **2012**, pp. 103-127.
- [264] C. G. Vieira, J. G. da Silva, C. A. A. Penna, E. N. dos Santos, E. V. Gusevskaya, *Applied Catalysis A-General* **2010**, *380*, 125-132.
- [265] J. G. da Silva, C. G. Vieira, E. N. dos Santos, E. V. Gusevskaya, *Applied Catalysis A-General* **2009**, *365*, 231-236.
- [266] H. J. V. Barros, J. G. da Silva, C. C. Guimaraes, E. N. dos Santos, E. V. Gusevskaya, *Organometallics* **2008**, *27*, 4523-4531.
- [267] C. S. Graebin, V. L. Eifler-Lima, R. G. da Rosa, *Catalysis Communications* **2008**, *9*, 1066-1070.
- [268] E. V. Gusevskaya, E. N. dos Santos, R. Augusti, A. D. Dias, C. M. Foca, *Journal of Molecular Catalysis A-Chemical* **2000**, *152*, 15-24.
- [269] L. Kollar, G. Bodi, *Chirality* **1995**, *7*, 121-127.
- [270] J. Bakos, B. Heil, L. Kollar, S. Toros, *Magyar Kemiai Folyoirat* **1994**, *100*, 394-402.
- [271] L. Kollar, J. Bakos, B. Heil, P. Sandor, G. Szalontai, *Journal of Organometallic Chemistry* **1990**, *385*, 147-152.
- [272] W. H. Clement, M. Orchin, *Industrial & Engineering Chemistry Product Research and Development* **1965**, *4*, 283.

Chapter 2

Synthesis of Metalloporphyrins Catalysts

2.1 Introduction

The search for efficient and selective catalysts for olefin epoxidation reactions is a topic of great interest for bulk^[1] and fine chemicals industry^[2], namely in the preparation of propylene oxide (5 million tons per year)^[3] and for the pharmaceutical compounds as, for instance, carfilzomib (anti-myeloma drug) and fragrances, e.g. in the production of limonene oxide. However, the processes used in the preparation of epoxides do not always meet the current green chemistry requirements and there is still a growing interest in the design and synthesis of efficient, selective and reusable catalysts to activate non-polluting oxidants such as O₂ or H₂O₂.

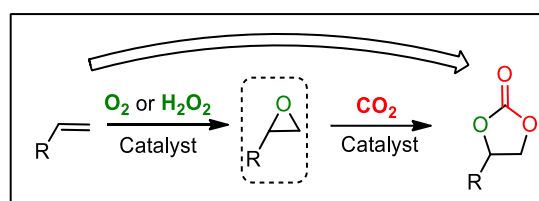
Among them, as mentioned in the introduction (**Chapter 1**), we highlight the use of biomimetic catalysts of the metalloporphyrins family, since these are described as active and selective catalysts in several types of oxidative transformations,^[4] easily accessible by synthesis and easily mouldable.

In this context, based on the critical analysis of the literature presented in the introduction (**Chapter 1**), we decided to synthesize porphyrins containing halogen

atoms at the ortho positions of the phenyl groups, known as second generation porphyrin catalysts,^[5] developed to increase the stability and activity of oxidation catalysts, which was a limitation found for metalloporphyrins catalysts of the first generation (based on *meso*-tetraphenylporphyrin). This strategy has been followed by the *Catalysis & Fine Chemistry Group - University of Coimbra*, which has hypothesised to place electron-attracting groups on the periphery of porphyrin to increase the Lewis acidity of the central metal and to evaluate the effect of different metals (Cr, Mn etc) on the synthesis of cyclic carbonates.^[6, 7]

Furthermore, manganese was chosen as the central metal because it is described that this metal easily forms active and selective catalytic species for Mn(V) type epoxides.^[8] Finally, to allow the reuse of the catalysts, we have designed molecules bearing nitro substituents at the *beta* positions, capable of undergoing *ipso*-nitro substitution with amine-functionalised magnetite nanoparticles.

Nevertheless, the main objective of the work presented here was not limited to the development of homogeneous and heterogeneous catalysts for the synthesis of epoxides, but also intended to develop biomimetic catalysts of the metalloporphyrins type and reusable to transform olefins to cyclic carbonates using epoxides as intermediates (**Scheme 2.1**), since cyclic carbonates are extensively used as intermediates for fine and bulk chemistry industry, as aprotic polar solvents, precursors for biomedical applications and raw materials for engineering plastics.^[9]



Scheme 2.1 – Synthesis of cyclic carbonates using epoxides as intermediates.

We again hypothesize the immobilisation of metalloporphyrins so that we could develop an active, selective and reusable catalytic system, capable of sustainably transform olefins into cyclic carbonates using renewable raw materials such as O₂ and CO₂. Thus, we proceeded to the structural design of reusable catalysts of the metalloporphyrin type, in order to develop catalysts for the activation of O₂, H₂O₂

and CO₂, specifically in reactions of epoxidation and cycloaddition of CO₂ in epoxides (Figure 2.1).

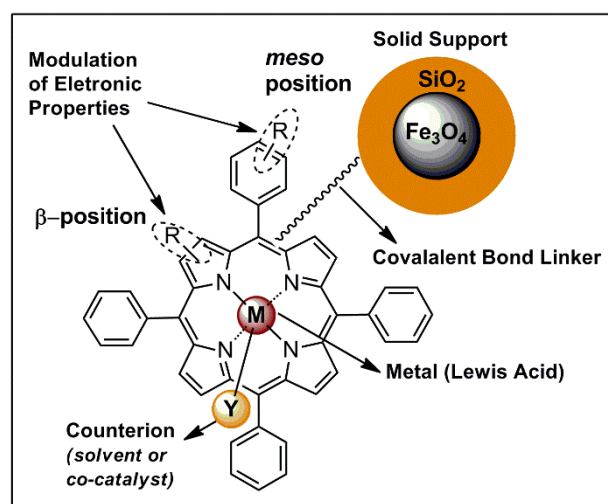


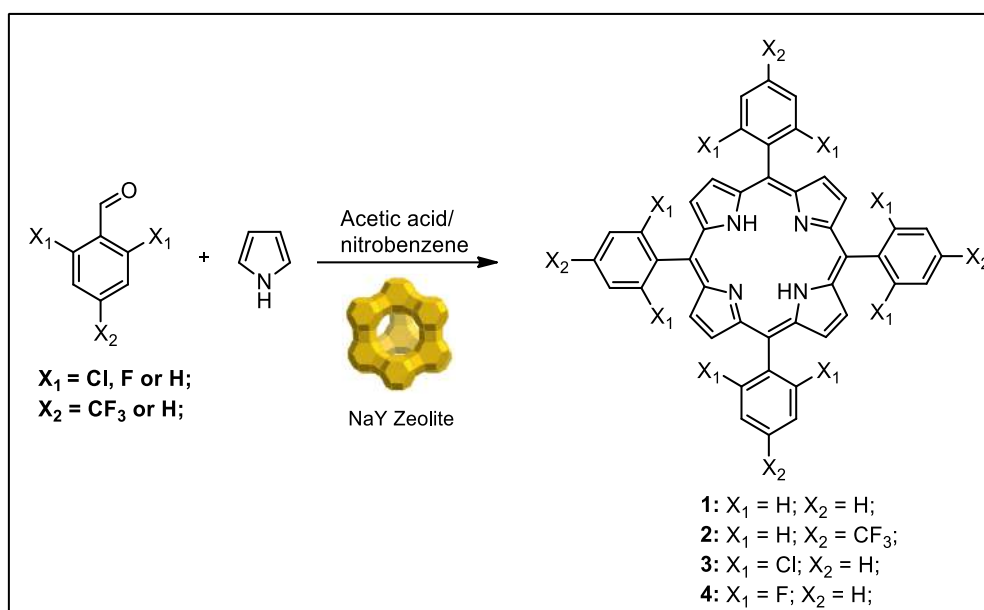
Figure 2.1 – Main features of homogeneous and heterogeneous metalloporphyrin catalysts developed in this work.

In this chapter, the synthesis of a family of manganese and chromium metalloporphyrins for homogeneous and heterogeneous catalysis (immobilized catalysts) is described, along with the optimisation and synthesis of silica-coated magnetite nanoparticles.

2.2 Synthesis of Metalloporphyrins for Homogeneous Catalysis

Aiming the preparation of metalloporphyrin catalysts in multi-gram scale under sustainable conditions, we selected the one-pot synthetic approaches reported by Gonsalves-Pereira^[10, 11] and Pereira-Calvete,^[12] since they allow the preparation of halogenated porphyrins in the absence of toxic quinones as oxidants.^[13]

In a typical procedure, the *meso*-tetraarylporphyrins were synthesised through one-pot reaction of pyrrole with equimolar amounts of halogenated benzaldehyde, in a mixture of acetic acid/nitrobenzene (2:1), in the absence or presence of NaY zeolite as solid Lewis catalyst. The reaction was heated at 140 °C along 2 h, after which, upon cooling, methanol was added to the crude to induce porphyrin precipitation (Scheme 2.2).



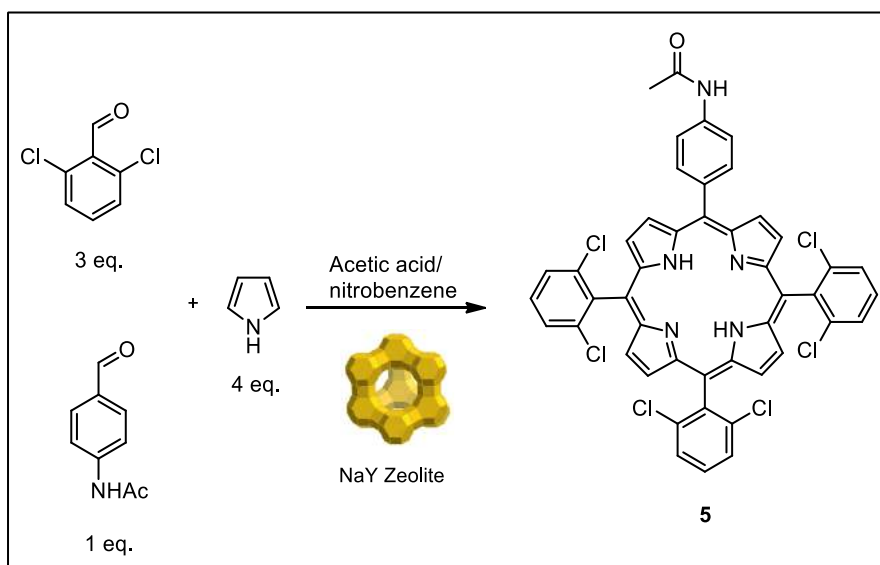
Scheme 2.2 – Synthesis of porphyrins (1-4) using the nitrobenzene and NaY/nitrobenzene methods.

The yields obtained using the nitrobenzene and NaY/nitrobenzene methods for the synthesis of the several porphyrins are presented in **table 2.1**.

Table 2.1 – Yields obtained by nitrobenzene and NaY/nitrobenzene methods for the synthesis of porphyrin (1-4).

Entry	Porphyrin	Method	Yield (%)
1	1	Nitrobenzene	24
2		NaY/Nitrobenzene	35
3	2	Nitrobenzene	8
4		NaY/Nitrobenzene	17
5	3	Nitrobenzene	6
6		NaY/Nitrobenzene	11
7	4	Nitrobenzene	8
8		NaY/Nitrobenzene	17

Then, aiming the preparation of non-symmetric porphyrins bearing suitable groups for linkage to functionalised magnetite nanoparticles, we also used the NaY/nitrobenzene method, as reported by Calvete-Pereira,^[14] for the preparation of 5-(4-acetylamino-phenyl)-10,15,20-tris(2,6-dichlorophenyl) porphyrin (**5**) (**Scheme 2.3**). NaY (0.016 M) was added to 2,6-dichlorobenzaldehyde (3 equivalents), 4-acetamidobenzaldehyde (1 equivalent), and pyrrole (4 equivalents) in a mixture of acetic acid and nitrobenzene (2:1), providing the non-symmetric porphyrin **5**.



Scheme 2.3 – Synthesis of porphyrin **5** using the NaY/nitrobenzene method.

In this methodology, the NaY zeolite acts as an efficient catalyst for the activation of aldehydes following their condensation revealing high potential for the multi-gram scale preparation and being possible the NaY zeolite reutilisation in several catalytic cycles. In this context, we evaluated its reutilisation in the synthesis of non-symmetric porphyrin **5** (**Figure 2.2**).

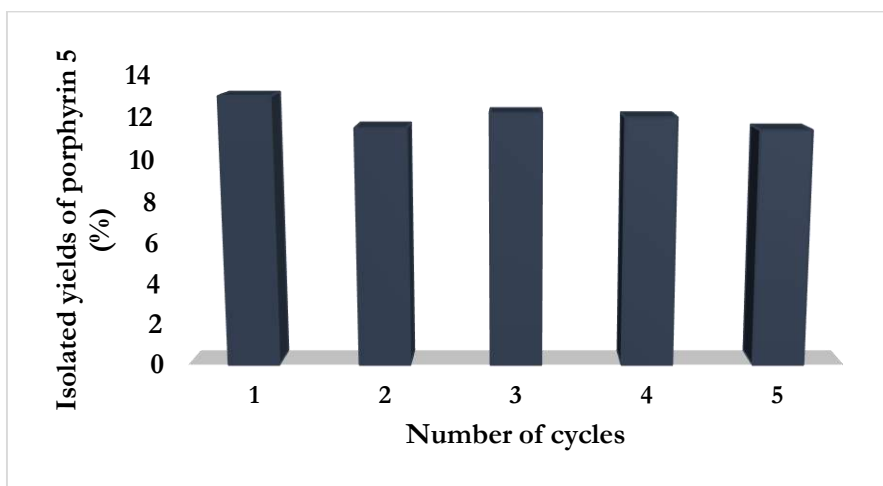


Figure 2.2 – Reutilization of NaY catalyst on the synthesis of porphyrin **5**.

After each cycle, the NaY catalyst was recovered by filtration, washed several times with dichloromethane and tetrahydrofuran, following by drying at 150 °C, for 12 hours. The subsequent cycles were performed using the recovered solid and reactivation procedure was similar for each reutilisation.

Then, to evaluate the effect of the presence and the ratio between NaY and all reagents (pyrrole and aldehydes) and assuming NaY MW = 12,752 g/mol,^[15] we performed the synthesis of porphyrin **5** using different ratios (**Figure 2.3**).

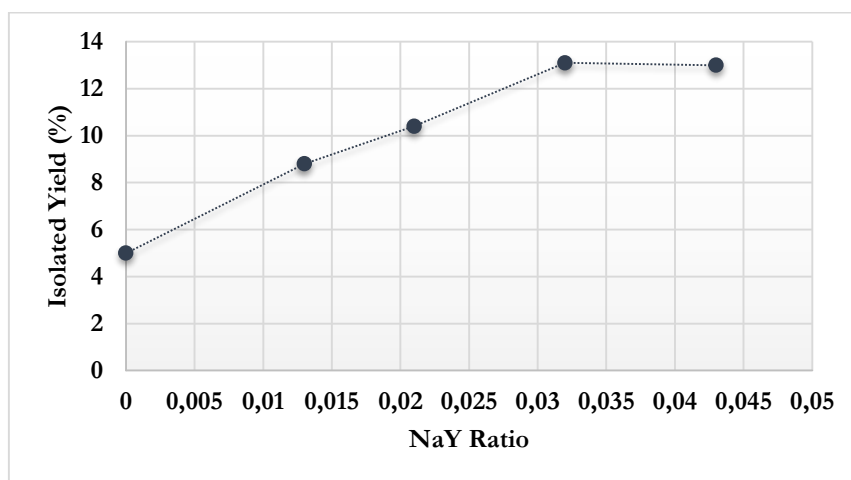


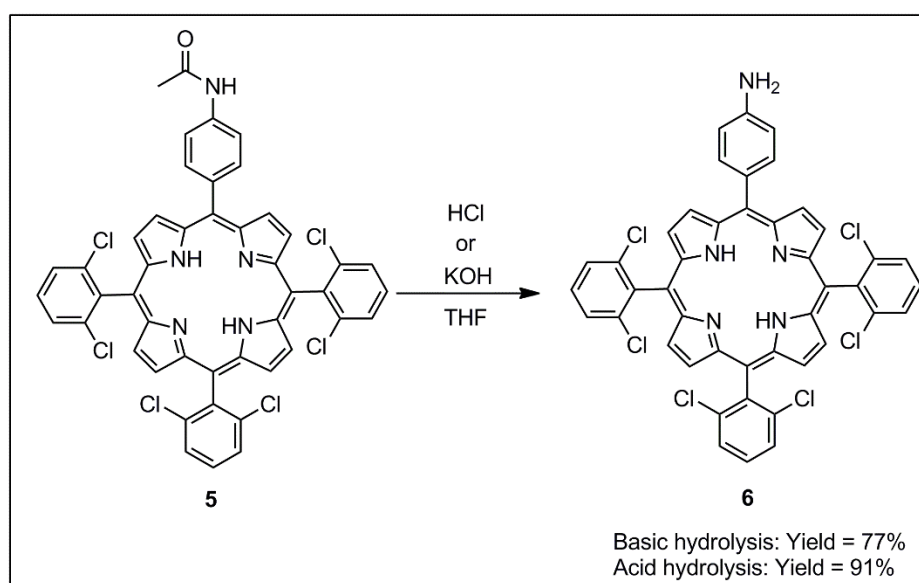
Figure 2.3 – Isolated yields of porphyrin **5** vs. the NaY amount. When NaY ratio = 0, it represents the isolated yields using the nitrobenzene method.

The analysis of **table 2.1** and the **figure 2.3** led us to conclude that the presence and the amount of NaY had a positive influence on the overall isolated yields. When a 1.3 and 2.1 mol% of NaY were used, the yield of porphyrin **5** were

8.8% and 10.4%, respectively. While a yield of 13.1% was obtained when the ratio was increased to 4.3 mol%, similar to the 13.0% yield, when a 3.2% amount of NaY catalyst was used.

According to Pereira and Calvetel^[2] the pKa and the presence of an acid (organic or solid – Lewis or Brønsted) like NaY, are determining factors for activation of aldehyde and pyrrole condensation and consequently to increase porphyrin synthetic yields. The compounds were characterised by ¹H-NMR spectroscopy (details can be found in experimental section - **Chapter 5**) and are in good agreement with the previously reported.^[16-18]

Then, in order to obtain the corresponding porphyrin with an amine group for linkage to functionalised magnetic nanoparticles, the synthesis of non-symmetric porphyrin **6** was carried out by hydrolysis of **5** in acidic and basic medium (**Scheme 2.4**).



Scheme 2.4 – Synthesis of porphyrin **6** through basic and acid hydrolysis of **5**.

Porphyrin **6** was purified by column chromatography in silica gel, using a *n*-hexane/ethyl acetate (1:5) mixture as eluent, giving the 5-(4-aminophenyl)-10,15,20-tri(2,6-dichlorophenyl)porphyrin **6** in 77% and 91% in basic and acidic medium, respectively. The ¹H-NMR spectrum of porphyrin **6** does not show a singlet signal at $\delta = 2.31$ ppm (methyl protons) (**Figure 2.4**), confirming the hydrolysis of the porphyrin's amine protecting acetyl group in **5**.

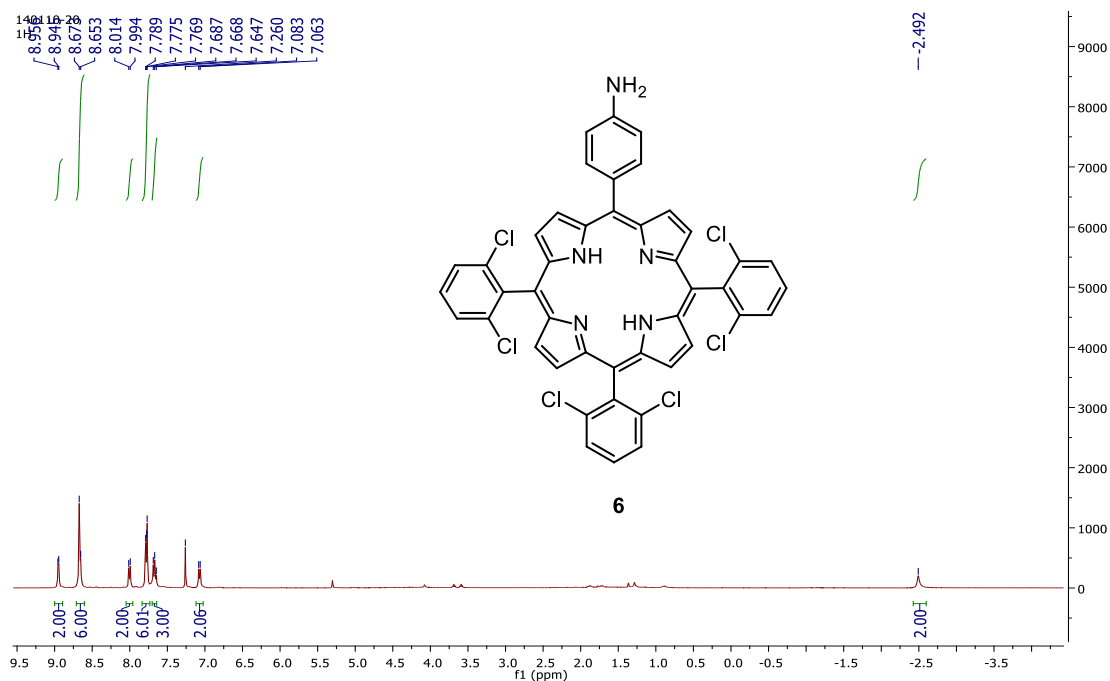
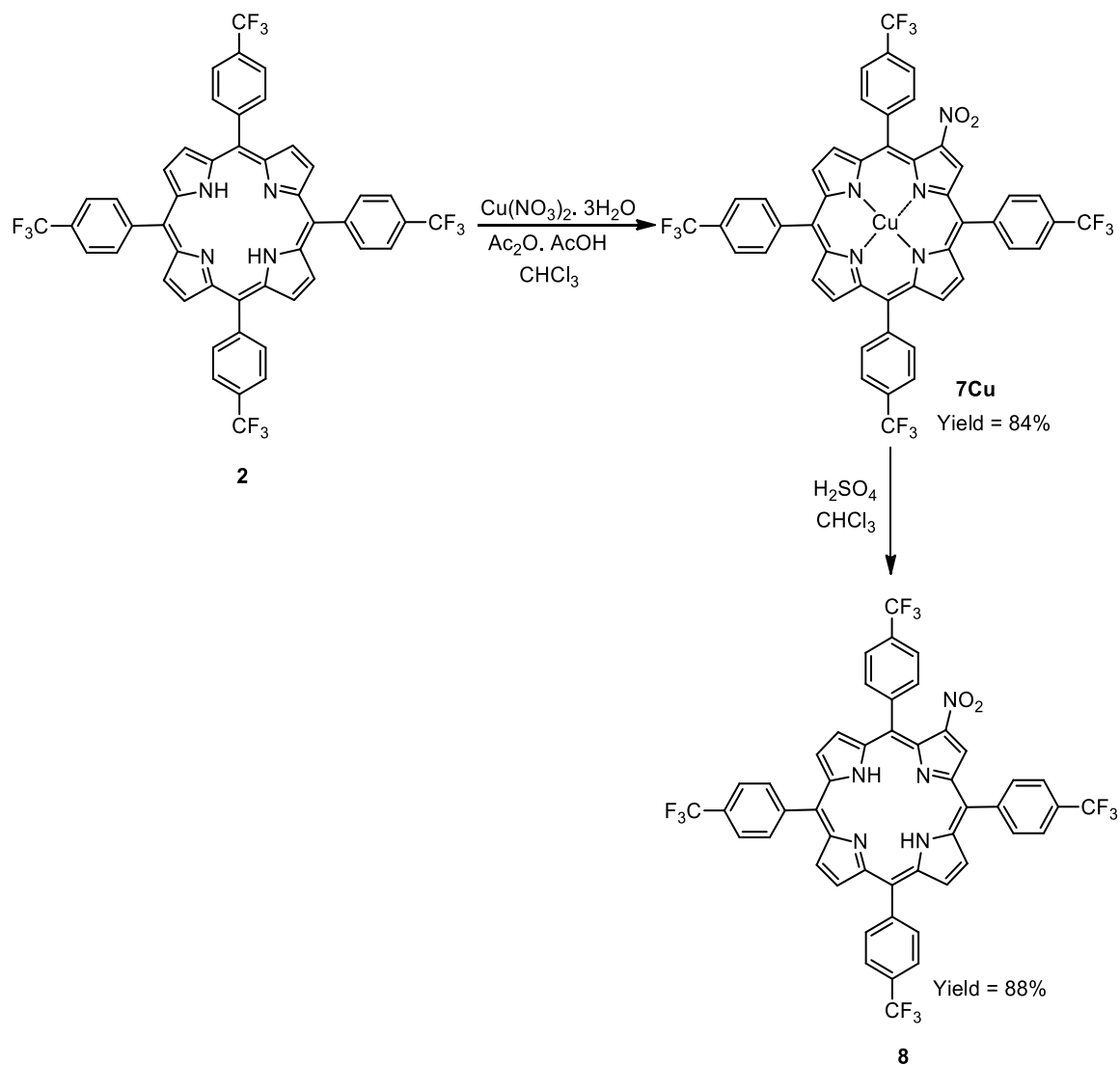


Figure 2.4 – ¹H-NMR spectrum of porphyrin **6**.

Additionally, the β -nitration of porphyrin **2** with copper(II) nitrate in an acetic anhydride/acetic acid mixture, followed by demetallation in acidic medium was performed, yielding porphyrin **8**, which could be used further to promote the covalent attachment to aminopropyl-functionalised silica-coated magnetite nanoparticles (Scheme 2.5).



Scheme 2.5 – Synthesis of porphyrin **8** through β -nitration of porphyrin **2** followed by demetallation of **7Cu** in acidic medium.

Porphyrin **8** was purified by column chromatography in silica gel, using a dichloromethane/*n*-hexane (2:1) mixture as the eluent, giving the β -nitro-*meso*-tetra(4-(trifluoromethyl)phenyl)porphyrin **8** in 88% yield. The $^1\text{H-NMR}$ spectrum of porphyrin **8** shows clearly a singlet signal at $\delta = 9.01$ ppm, attributed to the β -H next to the nitro group and two multiplet signals at $\delta = 8.96$ - 8.86 ppm and $\delta = 8.70$ - 8.67 ppm corresponding to the others β -H (7H) (**Figure 2.5**). Thus, the change in the signal corresponding to β -H when compared to the β -H signal of porphyrin precursor **2** and the presence of a singlet signal at $\delta = 9.01$ ppm with integration 1H confirms the formation of β -nitro-*meso*-tetra(4-(trifluoromethyl)phenyl)porphyrin **8**.

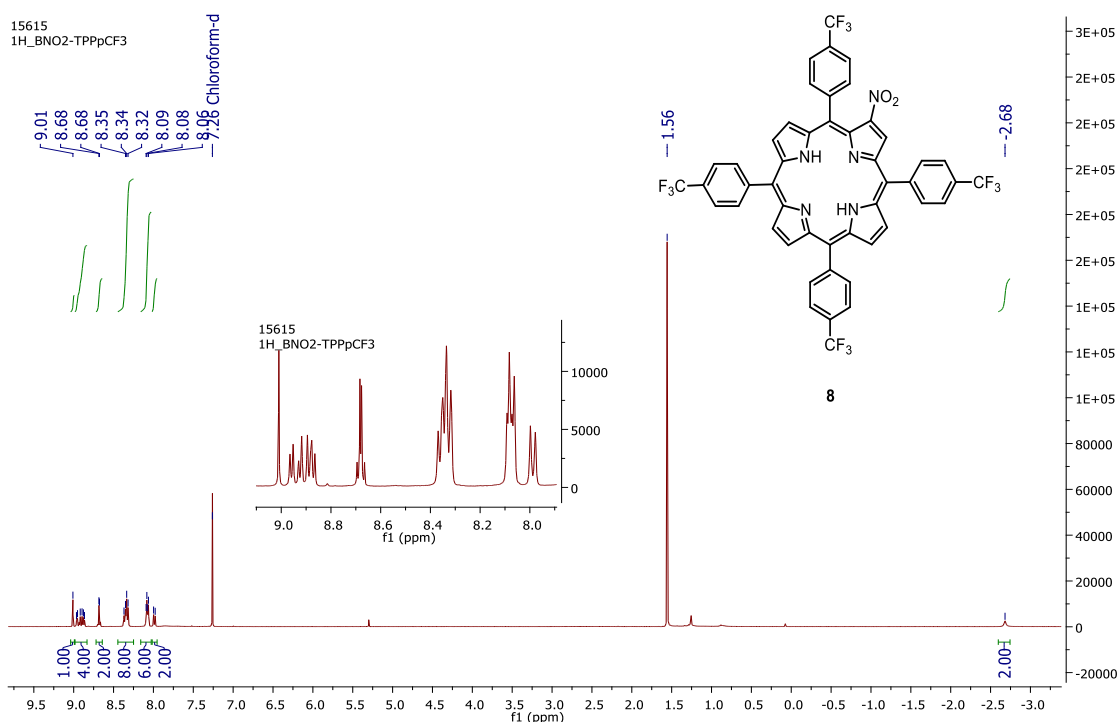
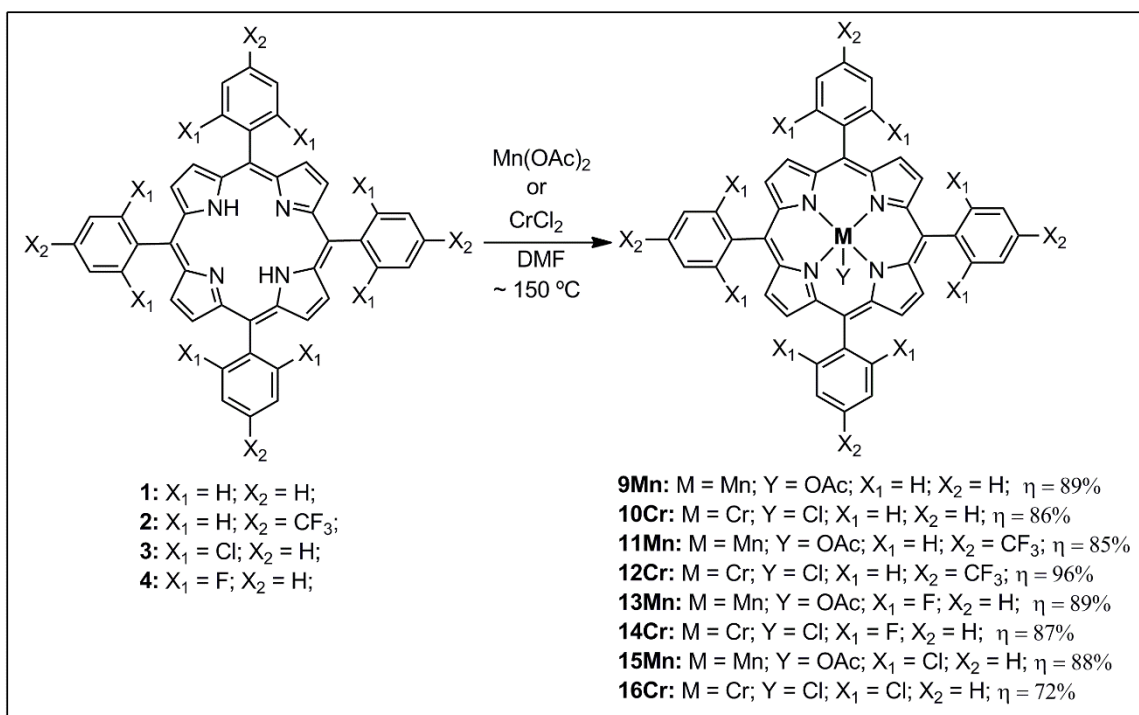


Figure 2.5 – ^1H -NMR spectrum of porphyrin **8**.

To obtain the desired metalloporphyrins, the symmetric *meso*-tetraarylporphyrins **1-4** and the non-symmetric porphyrin **8** were submitted to a complexation reaction using Mn(II) and Cr(II) salts. Among the various methods for metalloporphyrin synthesis described in the literature,^[8, 19] we have chosen the Adler's DMF method^[20] because the DMF easily dissolves both the porphyrin and the metallic salts and has a high boiling point.

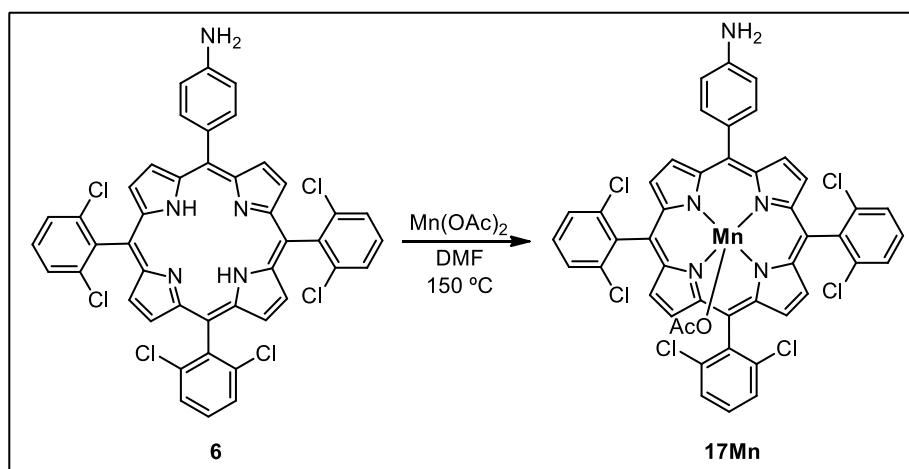
Thus, in a typical reaction, the desired porphyrin was dissolved in the minimum amount of DMF, heated at reflux temperature, followed by addition of an excess of the desired metallic salt (manganese(II) acetate tetrahydrate or chromium(II) chloride) (**Scheme 2.6**), monitoring by UV-Vis (**Chapter 5**).



Scheme 2.6 – Synthesis of metalloporphyrins (**9-16**).

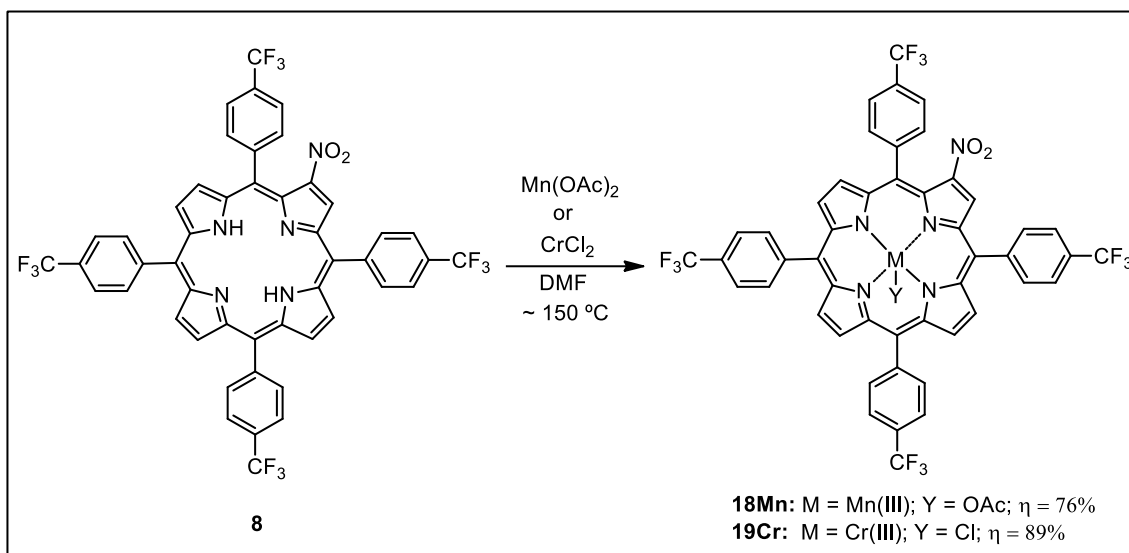
Upon the corresponding work-up, the metalloporphyrin catalysts **9Mn**, **11Mn**, **13Mn**, and **15Mn** were obtained in 89%, 85%, 89%, and 88% isolated yield, respectively (**Scheme 2.6**). Additionally, also metalloporphyrin catalysts **10Cr**, **12Cr**, **14Cr**, and **16Cr** were produced, in 86%, 96%, 87%, and 72% yield, respectively.

The non-symmetric porphyrin **6** also submitted to complexation reaction through DMF method, using manganese(II) acetate tetrahydrate yielding the metalloporphyrin **17Mn** in 78% yield (**Scheme 2.7**).



Scheme 2.7 – Synthesis of metalloporphyrin **17Mn**.

Moreover, the non-symmetric porphyrin **8** was submitted to complexation reaction through DMF method, using manganese(II) acetate tetrahydrate and chromium chloride yielding the metalloporphyrins **18Mn** and **19Cr** in 76% and 89% yield, respectively (**Scheme 2.8**).



Scheme 2.8 – Synthesis of metalloporphyrins **18Mn** and **19Cr**.

All synthesised porphyrins and metalloporphyrins were fully characterised by NMR and mass spectrometry, and the characterisation data is in agreement with the literature (**Chapter 5**).

2.3 Synthesis of Hybrid Metalloporphyrins for Heterogeneous Catalysis

As previously discussed, the immobilisation of metalloporphyrins is a great strategy to avoid degradation of the homogeneous catalysts and to promote catalyst reutilisation. From recent literature, several successful approaches have been developed to attach metalloporphyrins to solid supports, including silica,^[21] carbon material,^[22] and inorganic nanoparticles^[23], allowing efficient reutilisations up to several cycles. However, for general application, the supported metalloporphyrin catalyst should have the following characteristics: stable against oxidation; resistant to physical abrasion; resistant to metalloporphyrin leaching or removal; suitable for

batch or continuous flow systems; suitable for use in a wide range of solvents and conditions; and capable of being “tailor-made” for selective oxidations.^[4]

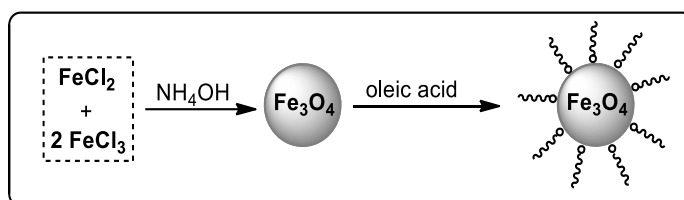
Among the known solid support, we have selected magnetic nanoparticles, specifically magnetite (**Fe₃O₄**) as supports, given their easy recovery and reutilisation by using an external magnet. Fe₃O₄ is a ferromagnetic mineral which containing atoms of Fe(II) and Fe(III) occupying octahedral and tetrahedral sites of coordination when the oxide anions are arranged as a cubic close packed lattice.^[24] The ferrimagnetism in magnetite is defined by the arrangement of the spins in Fe(II) that are antiparallel to the Fe(III) spins, while the interactions of the iron ions in different coordination sites result in incomplete cancellation of spin moments and a strong magnetization. These ferromagnetic nanoparticles (**Fe₃O₄**) have been calling much attention of the scientific community due to the low toxicity and their superparamagnetic performance, which can be applied in different fields, namely in medicinal chemistry and in catalytic processes as solid supports, as well.^[25]

However, magnetite nanoparticles with size less than 20 nm suffer from instability due to oxidation, generally leading to loss of magnetism and dispersion. Hence, it is necessary to protect the magnetic nanoparticles with organic molecules for many applications, such as surfactants, polymers, carbon, or inorganic layers, based on silica or metals to avoid the loss of its magnetic properties.^[26-29] Besides promoting the stabilisation of the nanoparticles, coating can also be used for further functionalisation and subsequent anchorage of other molecules. In this context, one of the goals of the described work in this thesis is to promote the synthesis of magnetite Fe₃O₄, its coating using silica and further functionalisation, in order to allow subsequent covalent attachment of metalloporphyrins, thus providing a new family of hybrid-metalloporphyrin catalysts.

In this section, we present the results of the synthesis and functionalisation of the silica-coated magnetic nanoparticles, as well as their attachment to the metalloporphyrins and their characterisations.

2.3.1 Synthesis of Magnetite Nanoparticles (MNP)

Aiming the preparation of hybrid magnetic materials, we promoted the synthesis of the magnetite nanoparticles (**MNP**) cores, using Fe^{2+} and Fe^{3+} ions, following the co-precipitation method.^[30] In a standard reaction, a mixture of aqueous solution of 1M FeCl_3 and a 2M HCl solution of FeCl_2 were added to 1M NH_4OH and mechanically stirred along 30 min. Then, the **MNP** were recovered using an external magnetic field, washed with distilled water and dispersed in water, after which oleic acid was added to stabilize the **MNP**. The resulting precipitate was magnetically separated, washed, centrifuged and stocked to provide a stock solution containing 45 mg of **MNP** mL^{-1} in cyclohexane (**Scheme 2.9**).



Scheme 2.9 – Synthesis of magnetite magnetic nanoparticles (**MNP**).

The oleic acid stabilized **MNP** were then characterised by transmission electron microscopy (TEM), for which the samples were prepared by slow evaporation of one drop of colloidal solution in isopropyl alcohol deposited on a carbon covered copper grid. The size distributions of the nanoparticles were determined through a manual analysis of amplified micrographs using ImageToll software version 3.0® to obtain the statistical distribution of the diameter. The mean curve fit, obtained using the Gaussian line shape, showed an **MNP** diameter size distribution of 7 ± 2 nm (**Figure 2.6**).

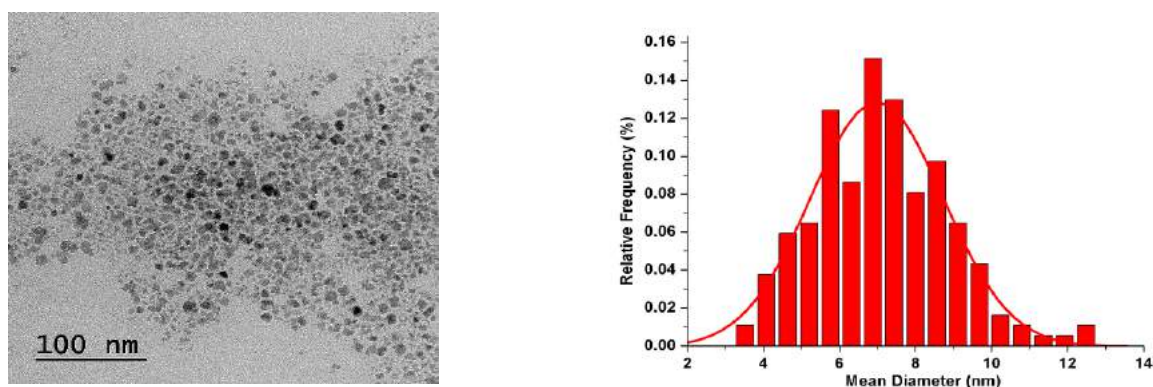
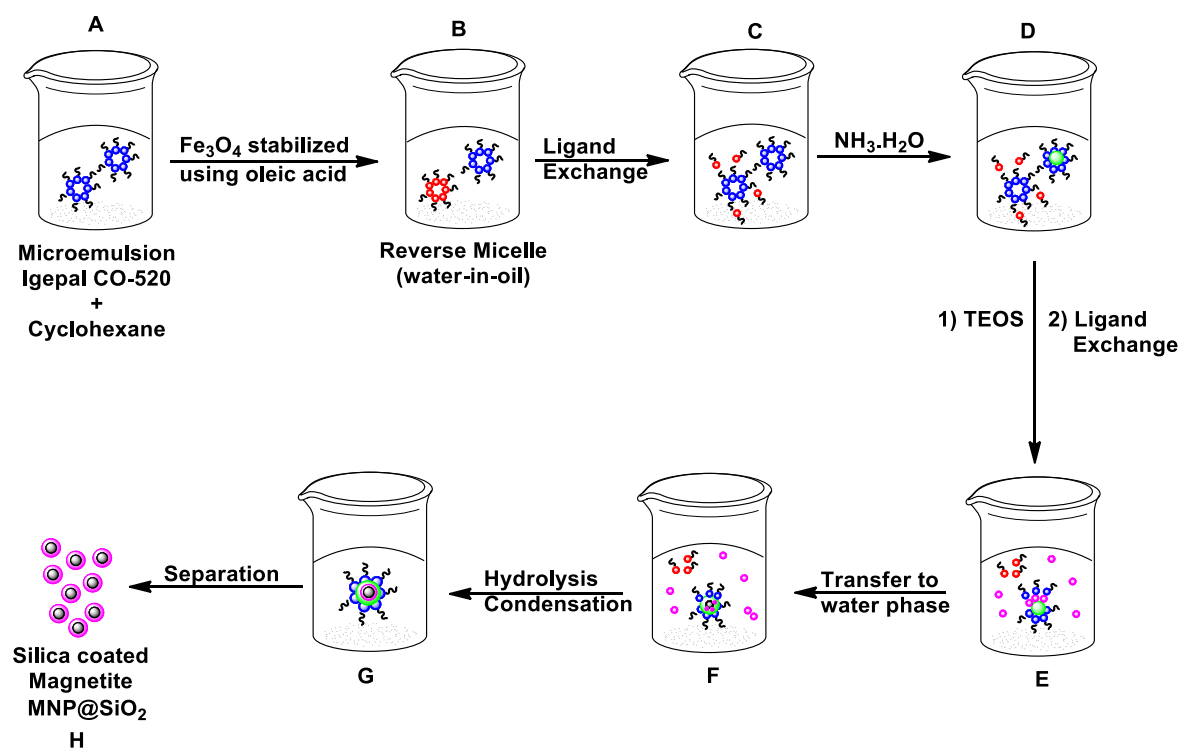


Figure 2.6 – Transmission electron microscopy (TEM) images and the corresponding particle size distribution histograms of **MNP**.

2.3.2 Synthesis of Silica-coated Magnetite Nanoparticles (**MNP@SiO₂**)

The optimisation of the coating process of the magnetic nanoparticles was carried out following the method of microemulsion (**Scheme 2.10**).^[31, 32]



Scheme 2.10 – General procedure for the synthesis of silica-coated magnetite nanoparticles (**MNP@SiO₂**).

First, surfactant Igepal CO-520® (Polyoxyethylene (5) branched nonylphenyl ether) was dispersed in cyclohexane, at room temperature, leading to formation of micelles (**A**; **Scheme 2.10**). Then, the **MNPs**, previously stabilised with oleic acid, were added to this solution to promote ligand exchange between oleic acid and Igepal CO-520® (**C**; **Scheme 2.10**). Posteriorly, an aqueous solution of ammonium hydroxide was added, filling the interior of the remaining micelles of Igepal CO-520® (**D**; **Scheme 2.10**). Finally, the addition of tetraethyl orthosilicate (TEOS), the crucial size control step, was carried out (**E**; **Scheme 2.10**). Therefore, in this step, we evaluated the effect of reaction time (8-16 h) and TEOS addition on the resulting nanoparticle size. The obtained material was then centrifuged, washed with ethanol and dried in air for 24 hours, at room temperature. The silica-coated magnetite nanoparticles (**MNP@SiO₂**) were further calcined in an oven to remove the surfactants from the silica surface, yielding the magnetic material (**H**). The nanoparticles obtained in different reaction times were characterized by electron microscopy transmission (TEM), presenting their images and particle diameter distribution histograms in **figures 2.7-2.12**.

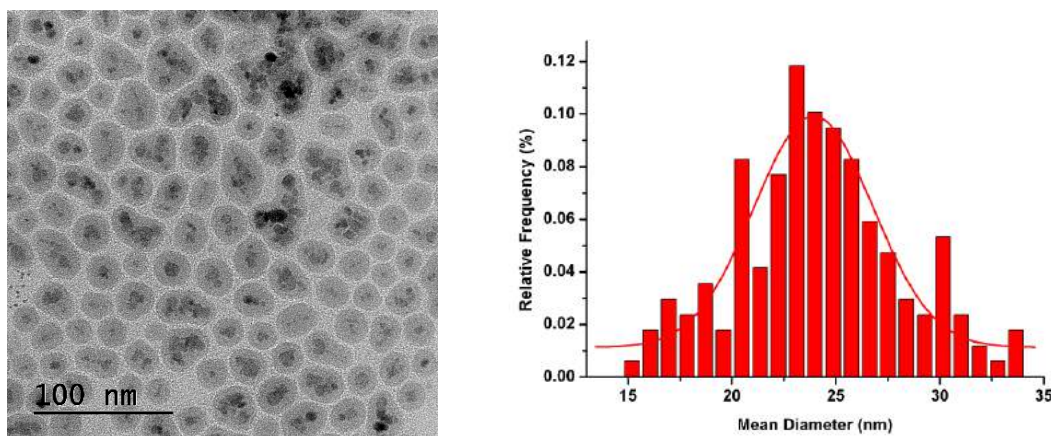


Figure 2.7 – Transmission electron microscopy (TEM) images and the corresponding particle size histograms for fabricating **MNP@SiO₂** using TEOS (30.8 mL) in 6 h.

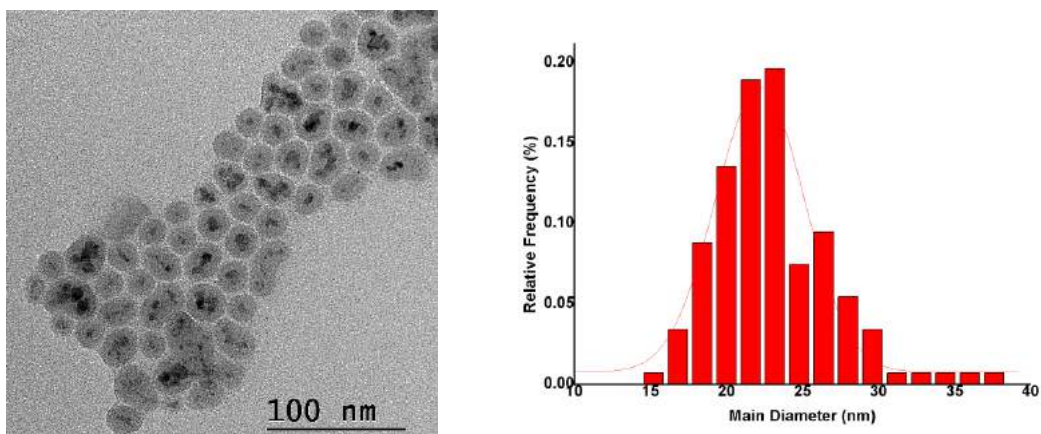


Figure 2.8 – Transmission electron microscopy (TEM) images and the corresponding particle size histograms for fabricating MNP@SiO_2 using TEOS (30.8 mL) in 8 h.

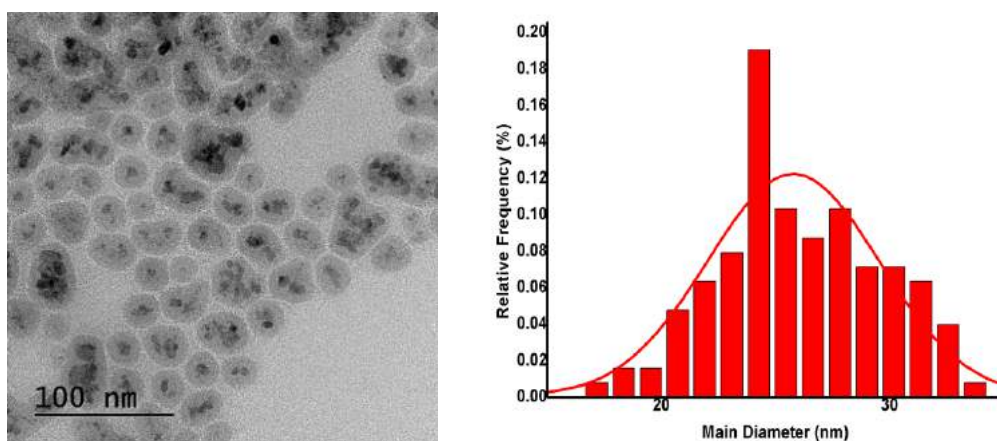


Figure 2.9 – Transmission electron microscopy (TEM) images and the corresponding particle size histograms for fabricating MNP@SiO_2 using TEOS (30.8 mL) in 10 h.

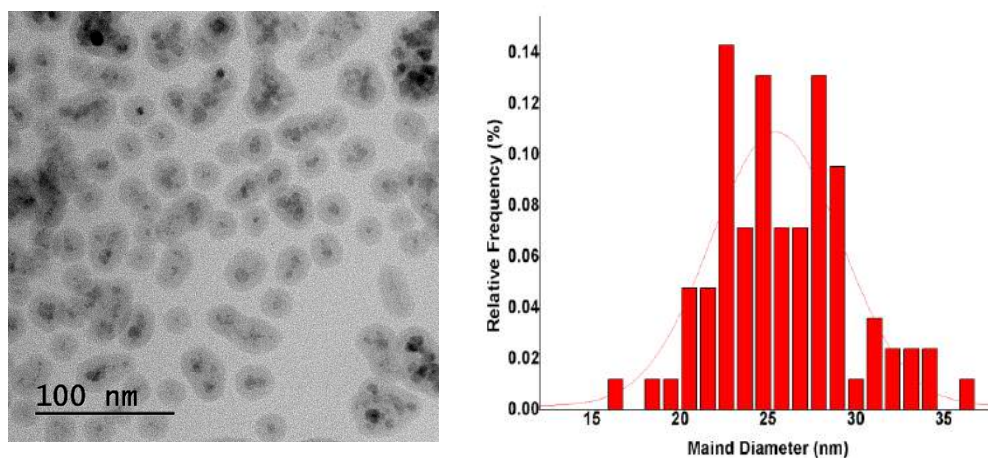


Figure 2.10 – Transmission electron microscopy (TEM) images and the corresponding particle size histograms for fabricating **MNP@SiO₂** using TEOS (30.8 mL) in 12 h.

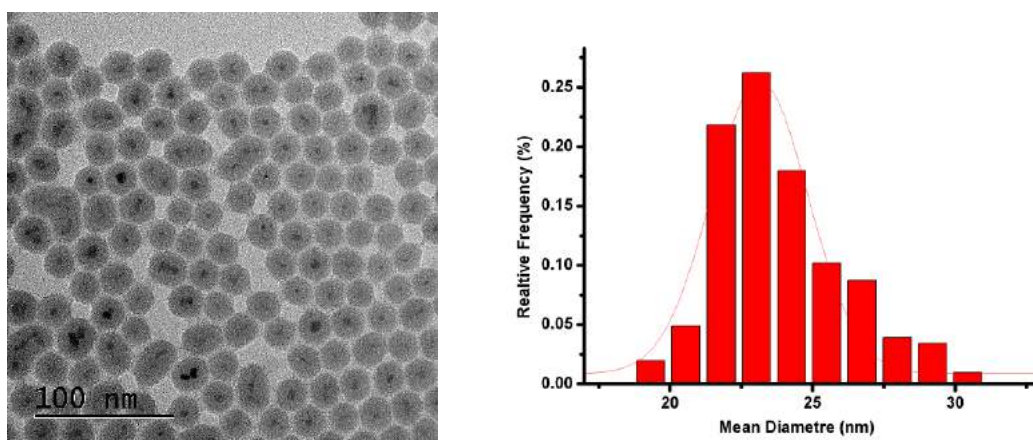


Figure 2.11 – Transmission electron microscopy (TEM) images and the corresponding particle size histograms for fabricating **MNP@SiO₂** using TEOS (30.8 mL) in 14 h.

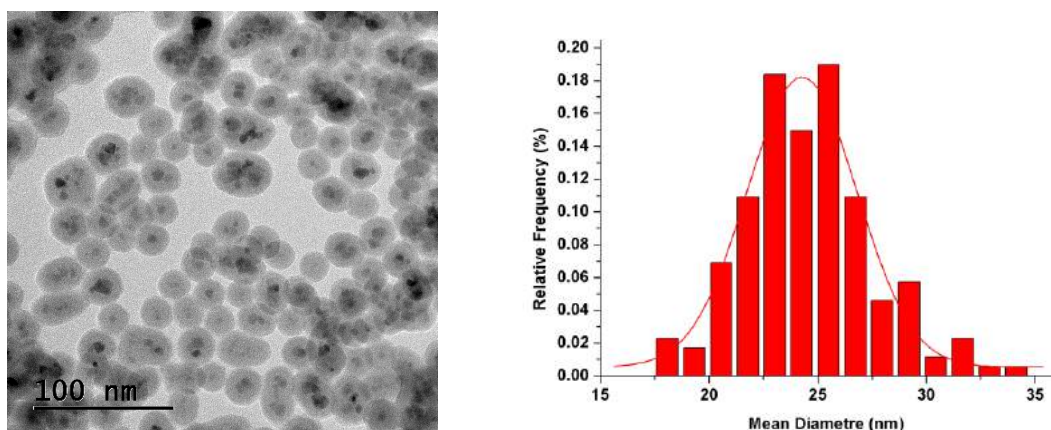


Figure 2.12 – Transmission electron microscopy (TEM) images and the corresponding particle size histograms for fabricating MNP@SiO_2 using TEOS (30.8 mL) in 16 h.

Upon TEM image analysis (**Figures 2.7-2.12**), the shell thickness size and core-shell size are presented in **table 2.2**.

Table 2.2 – Time parameters for fabricating MNP@SiO_2 .

Entry	Time (h)	Shell Thickness (nm)	Core-shell Size (nm)
1	6	17.0	23 ± 2.8
2	8	15.2	22 ± 2.9
3	10	18.8	25 ± 3.7
4	12	18.5	25 ± 3.6
5	14	16.2	23 ± 1.7
6	16	17.3	24 ± 2.5

It should be emphasised that we did not observe core-free silica particles, which states the relevance of this methodology to avoid the formation of core-free silica particles. Regarding particle size, aggregation and homogeneity of the silica-coated magnetite nanoparticles (MNP@SiO_2), we can conclude that 14 h is clearly the best reaction time to prepare MNP@SiO_2 with a shell thickness and a core-shell

size of 16.2 nm and 23.1 ± 1.7 nm, respectively (**Table 2.2, entry 5**). The **MNP@SiO₂** obtained in 14 h were characterized by thermogravimetry differential scanning calorimetry (TG-DSC) and Fourier-transform infrared spectroscopy (FT-IR), as show in **figure 2.13** (a) and (b), respectively.

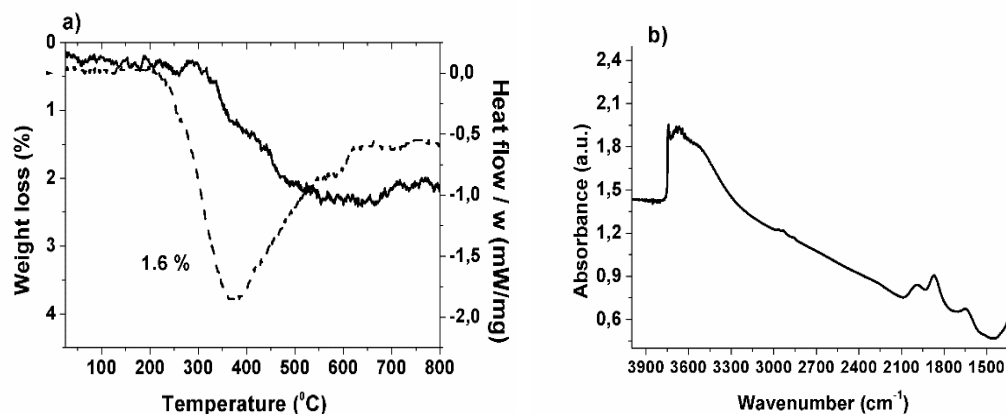


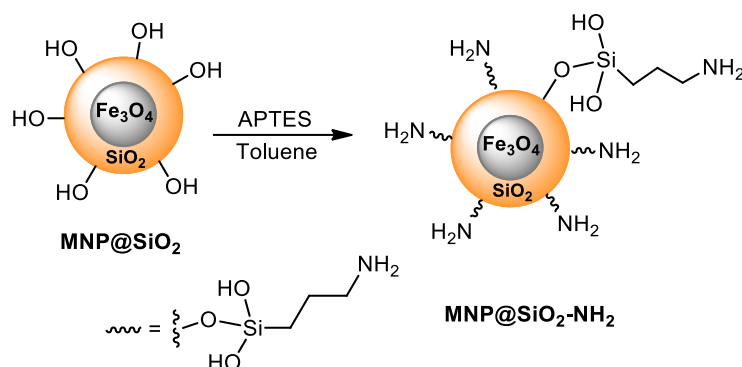
Figure 2.13 – a) TG-DSC curves (weight loss – solid line; heat flow – dashed line) of **MNP@SiO₂**; b) Infrared spectra of **MNP@SiO₂**.

From the analysis of **MNP@SiO₂** thermogram (**Figure 2.13; a**) an endothermic peak between 50 °C and 150 °C is observed, which is attributed to weight loss of physically adsorbed water and solvents. Another 1.6% weight loss of occurring between 200 and 800 °C is attributed to the decomposition of silanol groups grafted at the surface of **MNP@SiO₂**.^[33] In addition, the coating process was confirmed by infrared analysis 4000-1500 cm⁻¹ of the **MNP@SiO₂** (**Figure 2.13; b**). We also observed broad bands between 3750-3300 cm⁻¹, which are typical of terminal silanol and hydroxyl groups, and additional signals at 2950-2850 cm⁻¹, characteristic of C–H stretching vibrations. Furthermore, peaks at 2000 and 1870 cm⁻¹ are attributed to Si–O–Si elongation harmonic and the 1640 cm⁻¹ band is typical of O–H deformation of silica-coated magnetite nanoparticles.^[34, 35]

2.3.3 Functionalisation of Silica-coated Magnetite Nanoparticles

The silica-coated nanoparticle (**MNP@SiO₂**) previously prepared were then functionalized by Grobet’s method using different approaches.^[36] In a typical experiment, **MNP@SiO₂** was reacted with a solution of aminopropyltriethoxysilane

(APTES) 1% (v/v) in refluxing dry toluene, yielding the desired amino-functionalised nanoparticles after work-up (**Scheme 2.11**).



Scheme 2.11 – Synthesis of amino-functionalised nanoparticles ($\text{MNP@SiO}_2\text{-NH}_2$).

The amino functionalised nanoparticles ($\text{MNP@SiO}_2\text{-NH}_2$) were characterised by thermogravimetry/differential scanning calorimetry (TG-DSC) and Fourier-transform infrared spectroscopy (FT-IR). The **figure 2.14** shows the thermogram (**a**) and infrared spectrum (**b**) of $\text{MNP@SiO}_2\text{-NH}_2$.

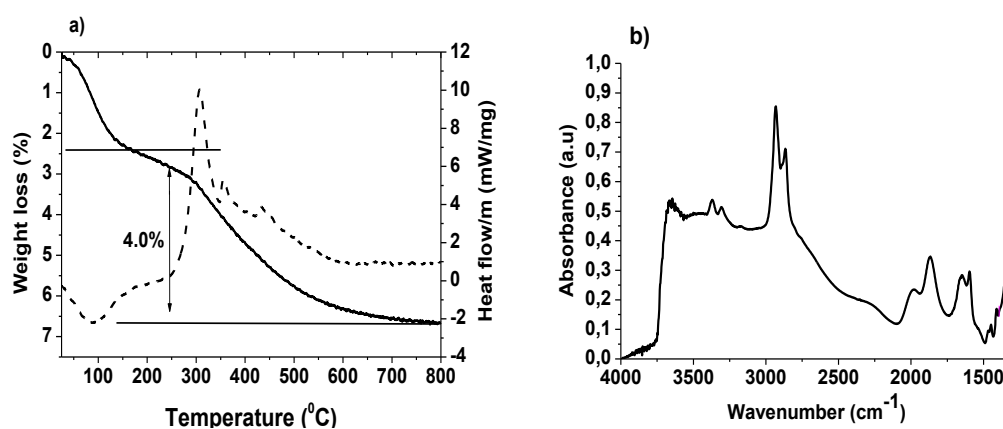
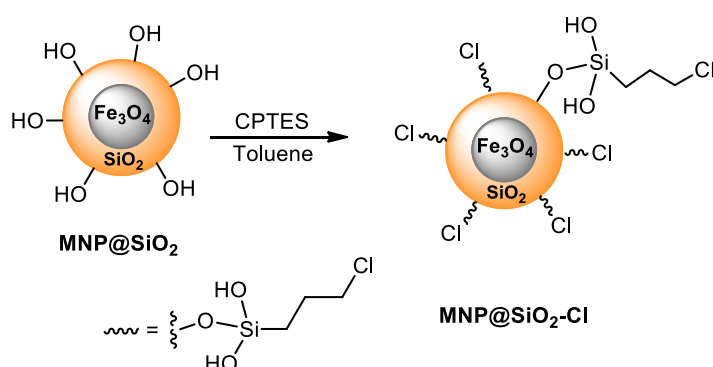


Figure 2.14 – a) TG-DSC curves (weight loss – solid line; heat flow – dashed line) of $\text{MNP@SiO}_2\text{-NH}_2$; b) Infrared spectra of $\text{MNP@SiO}_2\text{-NH}_2$.

The thermogram shows an endothermic peak between 30 °C and 175 °C, attributed to weight loss of physically adsorbed water and solvents. Another weight loss of 4.0% was observed for $\text{MNP@SiO}_2\text{-NH}_2$, attributed to the decomposition of aminopropyl groups grafted at the surface of silica-coated magnetite nanoparticle matrix (1.1% of NH_2 corresponding to 0.68 mmol g^{-1}). The infrared spectrum of $\text{MNP@SiO}_2\text{-NH}_2$ (**Figure 2.14; b**) shows two clear bands at 3300-3400 cm^{-1} and one broad band near 1600 cm^{-1} , typical attributed to N–H stretching and N–H

bending of primary amines, respectively. Additionally, the spectrum also shows broad bands between 3750-3300 cm^{-1} , which are typical of terminal silanol and hydroxyl groups in interaction, and additional signals at 2950-2850 cm^{-1} , which are characteristic of C–H stretching vibrations.

Furthermore, the functionalisation of MNP@SiO_2 with chloro groups was also performed. In a typical experiment, MNP@SiO_2 was reacted with a solution of chloropropyltriethoxysilane (CPTES) 1% (v/v) in refluxing dry toluene (**Scheme 2.12**), providing the desired chloro-functionalised magnetite nanoparticles after usual work-up.



Scheme 2.12 – Synthesis of chloro-functionalised nanoparticles ($\text{MNP@SiO}_2\text{-Cl}$).

The chloro-functionalised silica-coated magnetite nanoparticles ($\text{MNP@SiO}_2\text{-Cl}$) were characterised by thermogravimetry/differential scanning calorimetry (TG-DSC) and Fourier-transform infrared spectroscopy (FT-IR) as show in **figure 2.15; a-b**.

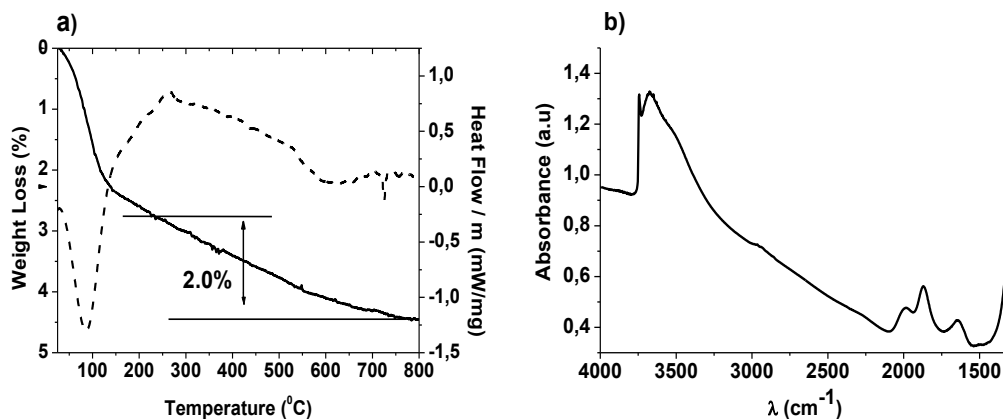


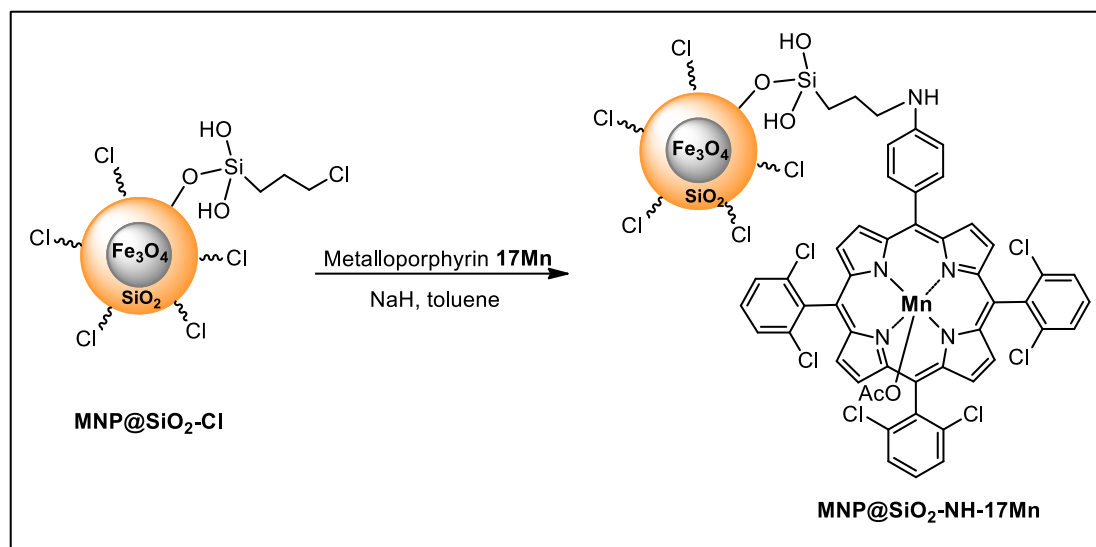
Figure 2.15 – a) TG-DSC curves (weight loss – solid line; heat flow – dashed line) of $\text{MNP@SiO}_2\text{-Cl}$; b) Infrared spectra of $\text{MNP@SiO}_2\text{-Cl}$.

The TG-DSC was used to quantify the organic content of the **MNP@SiO₂-Cl** (**Figure 2.15a**) with several measurements between 25 °C and 800 °C. From the analysis of **MNP@SiO₂-Cl** thermogram (**Figure 2.15; a**), we observed an endothermic peak between 50 °C and 150 °C, attributed to weight loss of physically adsorbed water and solvents. Another weight loss (2.0%) between 200 and 800 °C was also observed, which was attributed to the decomposition of silanol and 3-chloropropyl groups; in this case, the amount of 3-chloropropyl groups could be calculated by the difference between the amount of organic content and the silanol group (**Figure 2.13; a**). The value obtained was 0.4% for 3-chloropropyl groups, corresponding 0.18% (0.052 mmol per gram of material) for chlorine atom. The infrared spectrum of **MNP@SiO₂-Cl** (**Figure 2.15; b**) is similar to **MNP@SiO₂** (**Figure 2.13; b**), and not conclusive since the amount of 3-chloropropyl groups anchored onto magnetic nanoparticles is so low that it is not possible to observe the typical C-Cl stretching vibrations at 600-800 cm⁻¹.

2.3.4 Synthesis of Hybrid Metalloporphyrins Magnetic Catalysts

The hybrid metalloporphyrins magnetic catalysts were prepared using two different approaches: i) by covalently grafting the metalloporphyrins to **MNP@SiO₂-Cl** *via* nucleophilic substitution; ii) by covalent attachment of metalloporphyrins to **MNP@SiO₂-NH₂** *via* β-*ipso*-nitro aromatic nucleophilic substitution.

The **MNP@SiO₂-NH-17Mn** was prepared by the covalent grafting of the amine group at the *meso*-aryl position of the non-symmetric metalloporphyrin **17Mn** to the **MNP@SiO₂-Cl**, using NaH as base and dry toluene as solvent (**Scheme 2.13**). Finally, the hybrid nanocomposite catalyst **MNP@SiO₂-NH-17Mn** was easily collected using an external magnet and washed with ethyl acetate and acetonitrile to rinse away the unreacted metalloporphyrin.



Scheme 2.13 – Immobilization reaction of **17Mn** onto **MNP@SiO₂-Cl**.

The manganese content of **MNP@SiO₂-NH-17Mn** was determined by flame atomic absorption spectroscopy (FAAS), indicating a Mn percentage of 0.090%, which corresponds to the presence 1.5% of porphyrin **17Mn** (0.013 mmol per gram of nanocomposite).

The UV–Vis absorption spectrum of **MNP@SiO₂-NH-17Mn** shows an intense Soret band at 465 nm, in similarity with the non-immobilised metalloporphyrin **17Mn**, whose Soret appears at 480 nm (**Figure 2.16**). This shift can be explained based on the orientation of the nanoparticle molecular dipole with respect to the porphyrin-nanoparticle axis.^[37]

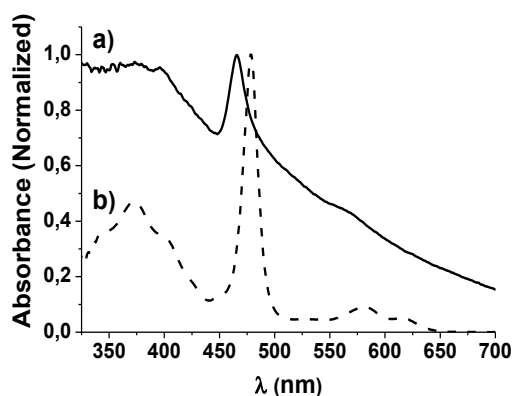


Figure 2.16 – UV-Vis spectra of: a) **MNP@SiO₂-NH-17Mn**, in DMF; b) **17Mn**, in CHCl₃.

Thermogravimetry/differential scanning calorimetry (TG-DSC) was used to quantify the organic content of the nanocomposite material, with several

measurements being carried out between 25 °C and 800 °C, comparatively with the non-immobilized metalloporphyrin **17Mn** and with the “blank” material, *i.e.* 3-chloropropyl functionalised magnetic nanoparticle, denoted as **MNP@SiO₂-Cl** (**Figure 2.17**). All diagrams present an endothermic peak between 50 °C and 200 °C, attributed to the weight loss of physically adsorbed water, while further weight losses (with exothermic peaks) occur between 200 °C and 800 °C, due to organic material decomposition. The metalloporphyrin content in the hybrid porphyrin magnetic nanocomposite could be directly calculated from the TG-DSC diagram of **MNP@SiO₂-NH-17Mn** (**Figure 2.17; a**), in temperature range 200-800 °C, by subtracting the respective “blank” experiment (**Figure 2.17; b**). The value obtained was 1.4%, which was in good agreement with that determined by FAAS.

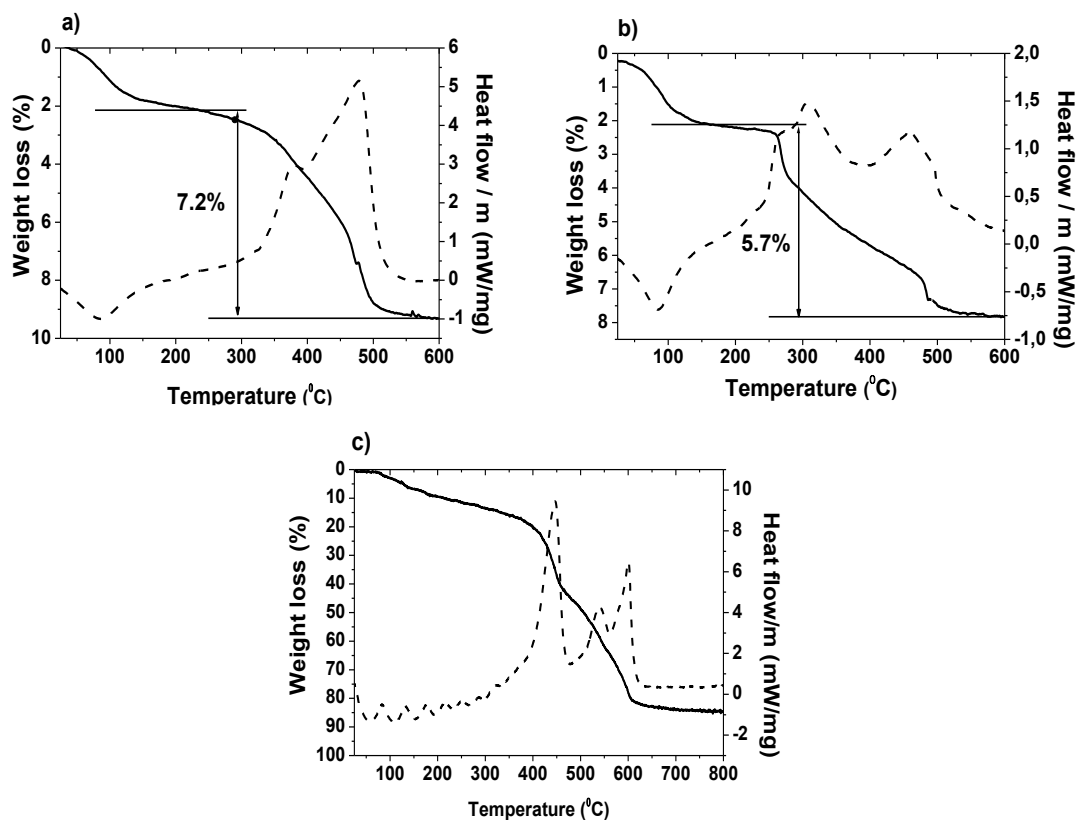


Figure 2.17 – TG-DSC curves (weight loss - solid line; heat flow - dashed line) for: a) **MNP@SiO₂-NH-17Mn**; b) **MNP@SiO₂-Cl** and c) **17Mn**.

The effectiveness of the metalloporphyrin **17Mn** grafting onto the magnetic nanoparticle was further demonstrated by infrared measurements (**Figure 2.18**) of the hybrid material **MNP@SiO₂-NH-17Mn**, compared with the non-functionalised silica-coated magnetite nanoparticles (**MNP@SiO₂**).

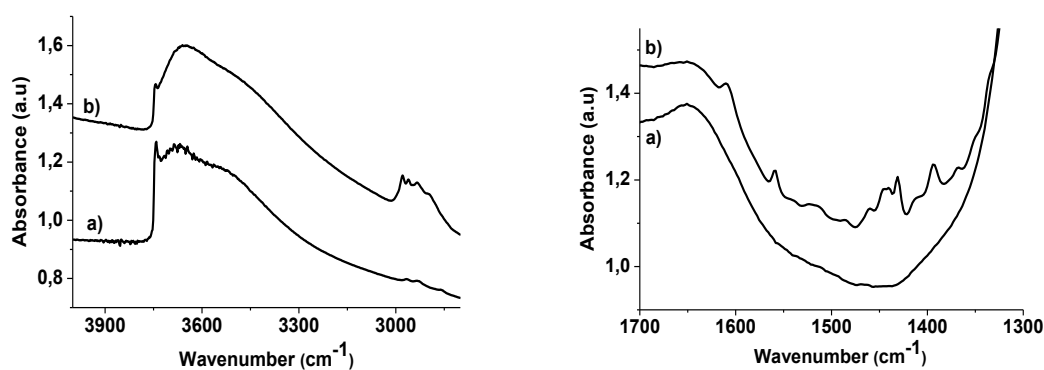
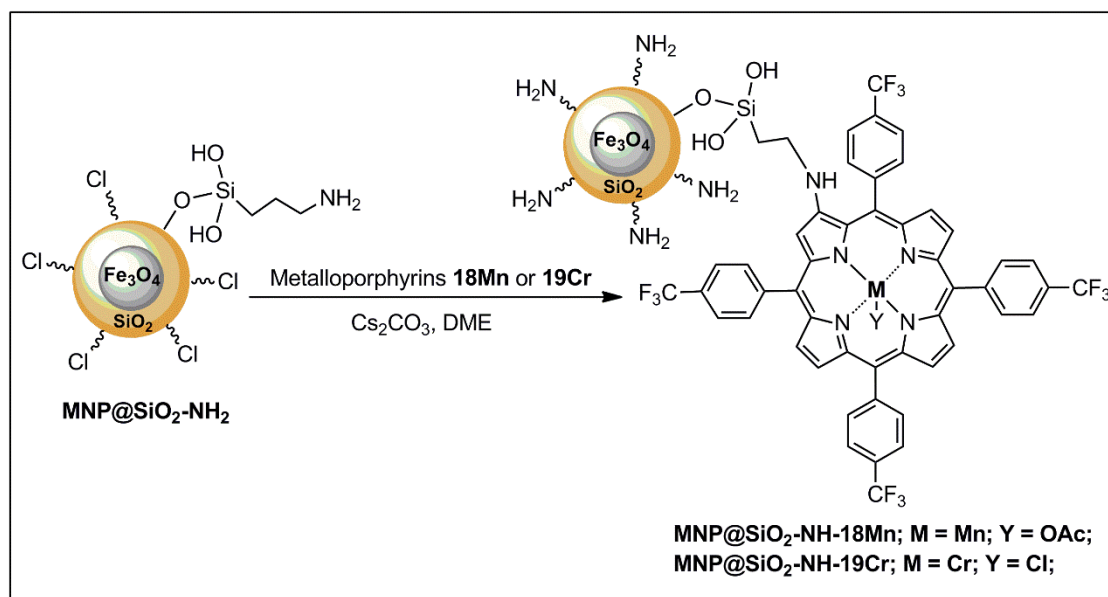


Figure 2.18 – FTIR spectra of: a) **MNP@SiO₂** and b) **MNP@SiO₂-NH-17Mn**, in the regions 4000-2700 (left) and 1700-1300 (right).

In the interval 4000-2700 cm^{-1} (**Figure 2.18; a**), both IR spectra show broad bands between 3750-3300 cm^{-1} , which are typical of terminal silanol and hydroxyl groups in interaction, with the spectrum of **MNP@SiO₂-NH-17Mn** showing additional signals at 2950-2850 cm^{-1} , which are characteristic of C–H stretching vibrations. In the interval 1300-1700 cm^{-1} (**Figure 2.18; b**), no signals were observed in the IR spectrum of **MNP@SiO₂**, while the spectrum of **MNP@SiO₂-NH-17Mn** present several characteristic peaks at: 1560 cm^{-1} (N–H bending), 1450 cm^{-1} (C–H bending), 1410 cm^{-1} (Si–CH₂ bending), 1608 cm^{-1} (pyrrole C=N stretching) and 1508-1465 cm^{-1} (aromatic C=C stretching), which corroborate the presence of metalloporphyrin **17Mn** in the nanocomposite.

Additionally, the **MNP@SiO₂-18Mn** and **MNP@SiO₂-19Cr** were prepared by covalent grafting the **18Mn** and **19Cr** β -nitro-metalloporphyrins onto the aminopropyl-functionalised silica-coated magnetite nanoparticles (**MNP@SiO₂-NH₂**), using cesium carbonate as base and DME as solvent (**Scheme 2.14**).



Scheme 2.14 – Immobilisation reaction of **18Mn** or **19Cr** onto **MNP@SiO₂-NH₂**.

The metal content of the hybrid metalloporphyrin magnetic catalysts was determined by ICP-OES, which indicated a Mn percentage of 0.026% (0.0057 mmol per gram of nanocomposite) in **MNP@SiO₂-18Mn** and a Cr percentage of 0.260% (0.050 mmol per gram of nanocomposite) in **MNP@SiO₂-19Cr**.

The UV-Vis absorption spectra of **MNP@SiO₂-18Mn** and **MNP@SiO₂-19Cr** (**Figure 2.19**) clearly show the Soret bands at 471 nm and at 448 nm, typical of manganese(III) and chromium(III) porphyrins, respectively, in similarity with the corresponding non-immobilised metalloporphyrins **18Mn** and **19Cr**.

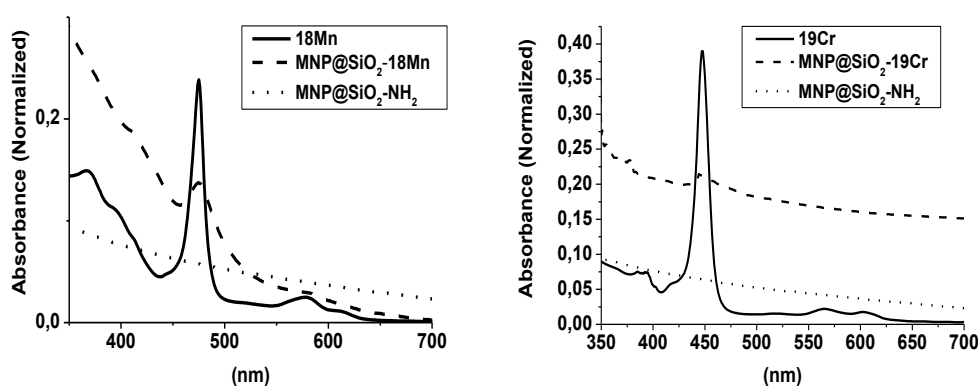


Figure 2.19 – Normalized UV-Vis absorption spectra of: a) **MNP@SiO₂-18Mn** and b) **MNP@SiO₂-19Cr** dispersed in CH₃CN/H₂O (1:1), compared with metalloporphyrins **18Mn** and **19Cr** in CHCl₃.

The quantification of the organic content in the nanocomposite materials was carried out by TG-DSC measurements in the range 25 °C-800 °C (**Figure 2.20**). All diagrams present an endothermic peak between 30 °C and 175 °C, attributed to weight loss of physically adsorbed water and solvents. Another weight loss of 4.0% was observed for **MNP@SiO₂-NH₂** (**Figure 2.20; a**), attributed to the decomposition of aminopropyl groups grafted at the surface of silica-coated magnetite nanoparticle matrix (1.1% of NH₂ corresponding to 0.68 mmol per gram of material). In the TG-DSC curves of **MNP@SiO₂-18Mn** and **MNP@SiO₂-19Cr** (**Figures 2.20; a and b, respectively**), additional weight losses (with exothermic peaks) occurred between 225 °C and 780 °C, which were considered to essentially arise from decomposition of metalloporphyrins **18Mn** or **19Cr**. By comparison with the TG-DSC curve of **MNP@SiO₂-NH₂**, the weight losses of **MNP@SiO₂-18Mn** and **MNP@SiO₂-19Cr** were of 0.6% and 5.1%, respectively, which allowed determining the amount of metalloporphyrins **18Mn** (0.0057 mmol g⁻¹) and **19Cr** (0.050 mmol g⁻¹), grafted onto the magnetic support. These values are in agreement with those obtained by ICP.

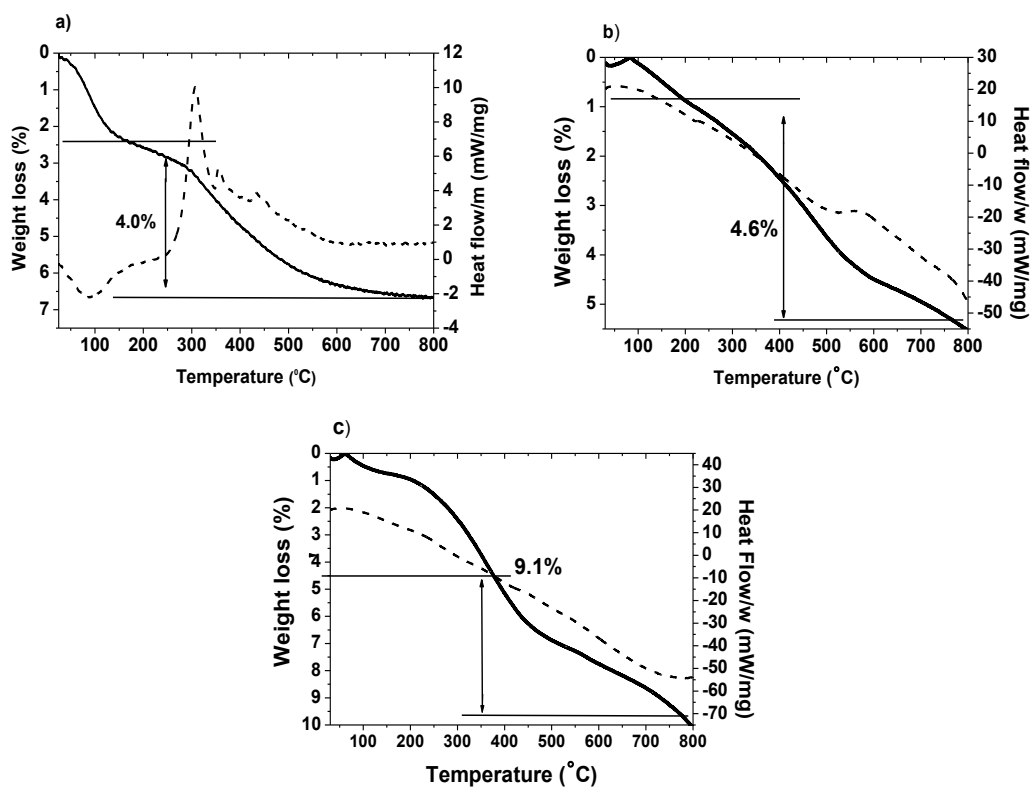


Figure 2.20 – TG-DSC curves (weight loss - solid line; heat flow - dashed line) of: a) **MNP@SiO₂-NH₂**; b) **MNP@SiO₂-18Mn**; c) **MNP@SiO₂-19Cr**.

The effective grafting of metalloporphyrins **18Mn** and **19Cr** onto the magnetic support was confirmed by infrared analysis of the hybrid materials **MNP@SiO₂-18Mn** and **MNP@SiO₂-19Cr**, in contrast with the **MNP@SiO₂-NH₂** (**Figure 2.21**).

In the interval 4000-2500 cm⁻¹ (**Figure 2.21, left**), all IR spectra show broad bands between 3750-3300 cm⁻¹, which are typical of terminal silanol and hydroxyl groups in interaction, and additional signals at 2950-2850 cm⁻¹, which are characteristic of C–H stretching vibrations. The spectrum of **MNP@SiO₂-NH₂** presents two clear bands at 3300-3400 cm⁻¹ (**Figure 2.21, left**) and one broad band close to 1600 cm⁻¹ (**Figure 2.21, right**), typical of N–H stretching of primary amines and N–H bending, respectively. In the interval 1300-1700 cm⁻¹ (**Figure 2.21, right**), both spectra of **MNP@SiO₂-18Mn** and **MNP@SiO₂-19Cr** present characteristic peaks at: 1450 cm⁻¹ (C–H bending), 1410 cm⁻¹ (Si–CH₂ bending) and 1350-1400 cm⁻¹ (C–F stretching), indicating the presence of trifluoromethyl-substituted porphyrins in the nanocomposite materials. It should be noted that, instead of two bands in the region 3300-3400 cm⁻¹, both spectra of **MNP@SiO₂-18Mn** and **MNP@SiO₂-19Cr** present a broad band, attributed to N–H stretching of secondary amines, which corroborate the covalent attachment of the metalloporphyrins, through amino groups, onto the surface of the magnetic support.

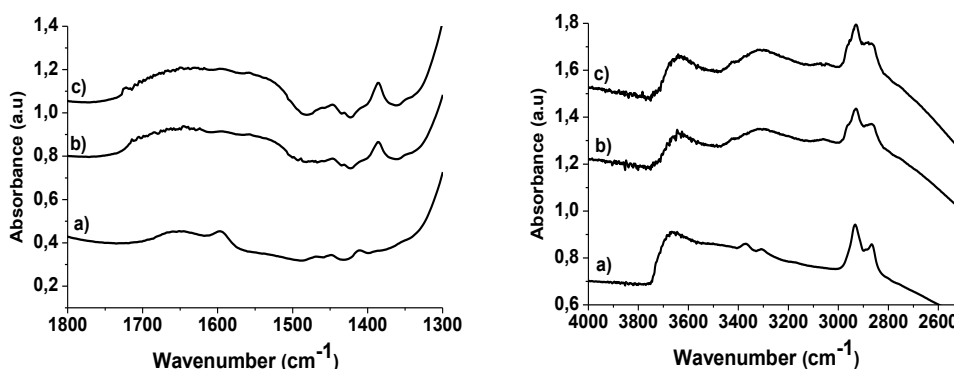


Figure 2.21 – Infrared spectra of: a) **MNP@SiO₂-NH₂**; b) **MNP@SiO₂-18Mn** and c) **MNP@SiO₂-19Cr**, in the regions 4000-2500 cm⁻¹ (left) and 1800-1325 cm⁻¹ (right).

2.4 Conclusions

A family of symmetric and non-symmetric manganese(III) and chromium(III)-porphyrin derivatives were synthesized using efficient methodologies and characterised by spectroscopy/spectrometric techniques aiming their evaluation as bioinspired catalysts in homogenous phase for activation of O₂ and CO₂.

Furthermore, functionalised silica-coated magnetite nanoparticles were prepared and used as solid support for immobilisation of selected manganese(III) and chromium(III) metalloporphyrins. The new hybrid manganese(III) and chromium(III)-porphyrin magnetic nanocomposites were fully characterised by TEM, ICP, TG-DSC, UV-Vis and FT-IR, which demonstrated the effective covalent grating on the silica-coated magnetic support.

In sum, homogeneous and heterogeneous-based metalloporphyrin catalysts were prepared for the further application on biomimetic olefin epoxidation and in CO₂ cycloaddition reaction to epoxide.

2.5 References

- [1] F. L. Jin, X. Li, S. J. Park, *Journal of Industrial and Engineering Chemistry* **2015**, *29*, 1-11.
- [2] A. K. Yudin, *Aziridines and Epoxides in Organic Synthesis*, Wiley-VCH, Weinheim, **2006**.
- [3] E. W. Schultz, M. B. Schwartz, K. M. Yu, *Production of Propylene Oxide from Propylene Using Patented Silver Based Catalyst*, University of Pennsylvania, Pennsylvania, **2016**.
- [4] M. J. F. Calvete, M. Pineiro, L. D. Dias, M. M. Pereira, *ChemCatChem* **2018**, *10*, 3615-3635.
- [5] B. Meunier, *Chemical Reviews* **1992**, *92*, 1411-1456.
- [6] L. Cuesta-Aluja, J. Castilla, A. M. Masdeu-Bulto, C. A. Henriques, M. J. F. Calvete, M. M. Pereira, *Journal of Molecular Catalysis A-Chemical* **2016**, *423*, 489-494.
- [7] R. M. B. Carrilho, L. D. Dias, R. Rivas, M. M. Pereira, C. Claver, A. M. Masdeu-Bulto, *Catalysts* **2017**, *7*, 210-223.
- [8] R. A. Sheldon, *Metalloporphyrins in Catalytic Oxidations*, Marcel Dekker, New York; Basel; Hong Kong, **1994**.
- [9] Q. Liu, L. P. Wu, R. Jackstell, M. Beller, *Nature Communications* **2015**, *6*, 1-15.
- [10] A. Gonsalves, M. M. Pereira, *Journal of Heterocyclic Chemistry* **1985**, *22*, 931-933.
- [11] A. Gonsalves, J. Varejao, M. M. Pereira, *Journal of Heterocyclic Chemistry* **1991**, *28*, 635-640.
- [12] M. Silva, A. Fernandes, S. S. Bebiano, M. J. F. Calvete, M. F. Ribeiro, H. D. Burrows, M. M. Pereira, *Chemical Communications* **2014**, *50*, 6571-6573.
- [13] J. L. Bolton, M. A. Trush, T. M. Penning, G. Dryhurst, T. J. Monks, *Chemical Research in Toxicology* **2000**, *13*, 135-160.
- [14] M. J. F. Calvete, L. D. Dias, C. A. Henriques, S. M. A. Pinto, R. M. B. Carrilho, M. M. Pereira, *Molecules* **2017**, *22*, 741-751.
- [15] O. Cairon, *Physical Chemistry Chemical Physics* **2012**, *14*, 12083-12085.
- [16] F. R. Kooriyaden, S. Sujatha, C. Arunkumar, *Polyhedron* **2015**, *97*, 66-74.
- [17] A. Gonsalves, M. M. Pereira, A. C. Serra, R. A. W. Johnstone, M. Nunes, *Journal of the Chemical Society-Perkin Transactions 1* **1994**, *0*, 2053-2057.
- [18] J. C. P. Grancho, M. M. Pereira, M. D. Miguel, A. M. R. Gonsalves, H. D. Burrows, *Photochemistry and Photobiology* **2002**, *75*, 249-256.
- [19] T. P. Wijesekera, D. Dolphin, *Synthetic Aspects of Porphyrin and Metalloporphyrin Chemistry* Marcel Dekker Inc, New York, **1994**.
- [20] A. D. Adler, F. R. Longo, F. Kampas, J. Kim, *Journal of Inorganic and Nuclear Chemistry* **1970**, *32*, 2443-2445.

- [21] D. Y. Shin, J. H. Yoon, S. H. Kim, H. Baik, S. J. Lee, *Catalysis Science & Technology* **2018**, *8*, 6306-6310.
- [22] X. M. Hu, M. H. Ronne, S. U. Pedersen, T. Skrydstrup, K. Daasbjerg, *Angewandte Chemie-International Edition* **2017**, *56*, 6468-6472.
- [23] D. H. Shen, L. T. Ji, L. L. Fu, X. L. Dong, Z. G. Liu, Q. Liu, S. M. Liu, *Journal of Central South University* **2015**, *22*, 862-867.
- [24] L. M. Rossi, N. J. S. Costa, F. P. Silva, R. Wojcieszak, *Green Chemistry* **2014**, *16*, 2906-2933.
- [25] S. N. Sun, C. Wei, Z. Z. Zhu, Y. L. Hou, S. S. Venkatraman, Z. C. Xu, *Chinese Physics B* **2014**, *23*, -.
- [26] Y. Kobayashi, M. Horie, M. Konno, B. Rodriguez-Gonzalez, L. M. Liz-Marzan, *Journal of Physical Chemistry B* **2003**, *107*, 7420-7425.
- [27] A. H. Lu, W. C. Li, N. Matoussevitch, B. Spliethoff, H. Bonnemann, F. Schuth, *Chemical Communications* **2005**, 98-100.
- [28] N. S. Sobal, M. Hilgendorff, H. Mohwald, M. Giersig, M. Spasova, T. Radetic, M. Farle, *Nano Letters* **2002**, *2*, 621-624.
- [29] Q. X. Liu, Z. H. Xu, J. A. Finch, R. Egerton, *Chemistry of Materials* **1998**, *10*, 3936-3940.
- [30] D. B. Tada, L. L. R. Vono, E. L. Duarte, R. Itri, P. K. Kiyohara, M. S. Baptista, L. M. Rossi, *Langmuir* **2007**, *23*, 8194-8199.
- [31] D. K. Yi, S. S. Lee, G. C. Papaefthymiou, J. Y. Ying, *Chemistry of Materials* **2006**, *18*, 614-619.
- [32] M. J. Jacinto, P. K. Kiyohara, S. H. Masunaga, R. F. Jardim, L. M. Rossi, *Applied Catalysis A-General* **2008**, *338*, 52-57.
- [33] L. T. Zhuravlev, *Colloids and Surfaces a-Physicochemical and Engineering Aspects* **2000**, *173*, 1-38.
- [34] M. Nowostawska, S. A. Corr, S. J. Byrne, J. Conroy, Y. Volkov, Y. K. Gun'ko, *Journal of Nanobiotechnology* **2011**, *9*.
- [35] A. Mourhly, M. Khachani, A. El Hamidi, M. Kacimi, M. Halim, S. Arsalane, *Nanomaterials and Nanotechnology* **2015**, *5*, -.
- [36] K. C. Vrancken, L. Decoster, P. Vandervoort, P. J. Grobet, E. F. Vansant, *Journal of Colloid and Interface Science* **1995**, *170*, 71-77.
- [37] S. Vukovic, S. Corni, B. Mennucci, *Journal of Physical Chemistry C* **2009**, *113*, 121-133.

Chapter 3

Heterobimetallic Dual-Catalyst for Transformation of Olefins into Cyclic Carbonates

3.1 Introduction

The development of efficient and selective catalytic processes able to sequentially promote the synthesis of high value-added cyclic carbonates through olefin epoxidation followed by CO₂ addition, is a very interesting and useful green methodology for modern chemical industry.^[1] In this context, the last two decades have witnessed intense scientific research on the design and synthetic development of catalytic systems capable to promote the epoxidation of olefins ^[2, 3] and CO₂ cycloaddition reaction to epoxides^[4, 5] yielding the desired cyclic carbonates^[6, 7] (**Figure 3.1**).

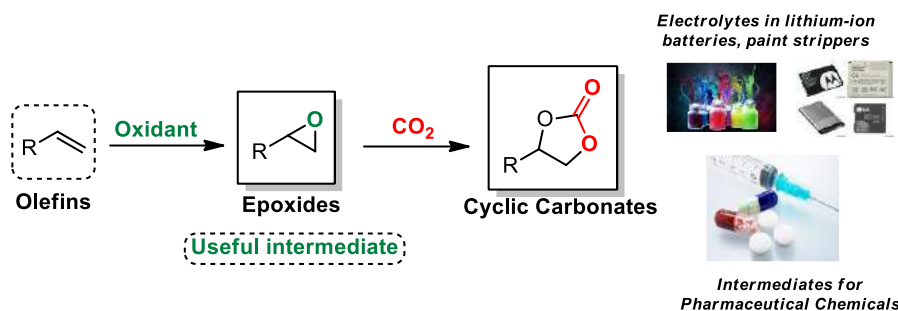


Figure 3.1 – Transformation of olefins into cyclic carbonates, and their general applications.

The five-membered ring cyclic carbonates have extensive chemical applications, namely as intermediates in the production of pharmaceuticals and fine chemicals, including bioactive molecules.^[8, 9] The low toxicities, biodegradability,^[10] and high dielectric constant^[11] of ethylene and propylene carbonates makes them to be among the most attractive sustainable polar aprotic solvents, electrolytes in lithium-ion-based secondary batteries,^[12] degreasers,^[13] paint strippers,^[13] medicinal products,^[13] and also for cosmetic products, like nail polishing.^[10]

Several homogeneous catalysts are applied on olefin epoxidation, followed by CO₂ cycloaddition reactions, aiming the synthesis of cyclic carbonates, including metal oxides^[1, 14], organocatalysts^[15, 16] ionic liquids^[17, 18] organometallic catalysts.^[19, 20] Among them, metalloporphyrins may be considered as the most active and selective bioinspired catalysts for both reactions.^[21-25] Nevertheless, to the best of our knowledge, there are no reports on the application of heterogeneous metalloporphyrin-based recyclable catalysts to promote the sequential transformation of olefins into cyclic carbonates, using green oxidants such as O₂ or H₂O₂, being this one of the main goals of the studies presented and discussed on this thesis.

Thus, aiming the development of an efficient and stable metalloporphyrin-based catalytic system for sequential transformation of olefins into cyclic carbonates, we performed studies regarding the systematic evaluation of a family of metalloporphyrins as catalysts to promote the epoxidation of olefins (using O₂ or H₂O₂ as oxidant) followed by CO₂ cycloaddition reaction, in a sequential process (**Figure 3.2**).

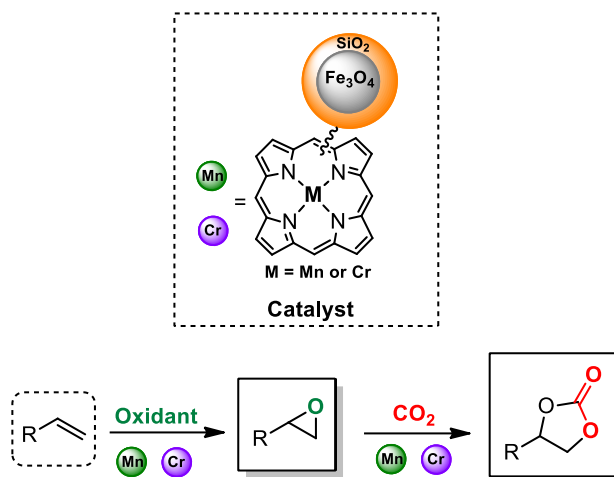


Figure 3.2 – Transformation of olefins into cyclic carbonates catalysed by metalloporphyrin catalysts developed in this work.

In this chapter, we evaluate and discuss the central moiety and the peripheral substitution effects of a set of manganese(III) and chromium(III) metalloporphyrins catalysts in homogeneous olefin epoxidation (using O_2 or H_2O_2 as oxidants), and in CO_2 cycloaddition reaction to epoxide (**Figure 3.2**). Furthermore, the application of hybrid manganese(III) and chromium(III) porphyrin magnetic nanocomposites as reusable catalysts in olefin epoxidation and in CO_2 cycloaddition to epoxides is also described. Finally, a heterobimetallic dual catalyst, prepared by combining the appropriate amounts of Mn(III)-porphyrin and Cr(III)-porphyrin hybrid materials is evaluated in the sequential transformation of vinyl styrene into styrene carbonate. Moreover, studies regarding the magnetic reutilisation of the catalysts are also presented and discussed.

3.2 Catalytic Epoxidation

Initially, a systematic optimisation study on styrene catalytic epoxidation was carried out. In a typical epoxidation reaction using O_2 as oxidant, a round bottom flask was loaded with styrene, the desired metalloporphyrin catalyst, isobutyraldehyde as co-reductant, chlorobenzene as internal standard, and CH_2Cl_2 as solvent. The mixture was stirred at room temperature, with O_2 bubbling. Substrate conversion, along with TON calculations and selectivity were determined by GC analysis, using chlorobenzene as internal standard and the results are presented in **table 3.1**.

Table 3.1 – Epoxidation of styrene with O₂/isobutyraldehyde using Cr(III) or Mn(III) metalloporphyrins as homogeneous catalysts.

Entry	Catalyst	Oxidant	Conv. ^c (%)	Epoxide (%)	TON ^d
1 ^a	-	O ₂	3	78	319
2 ^a	Mn(III)OAc-TPP (9Mn)	O ₂	97	85	10318
3 ^a	Mn(III)OAc-TPP <i>p</i> CF ₃ (11Mn)	O ₂	99	88	10531
4 ^a	Mn(III)OAc-TDFPP (13Mn)	O ₂	99	86	10531
5 ^a	Mn(III)OAc-TDCPP (15Mn)	O ₂	99(0) ^e	92	10531
6 ^a	Cr(III)Cl-TPP (10Cr)	O ₂	12	71	1276
7 ^a	Cr(III)Cl-TPP <i>p</i> CF ₃ (12Cr)	O ₂	15	70	1595
8 ^a	Cr(III)Cl-TDFPP (14Cr)	O ₂	17	73	1807
9 ^a	Cr(III)Cl-TDCPP (16Cr)	O ₂	14	72	1488
10 ^b	Mn(III)OAc-TPP <i>p</i> CF ₃ (11Mn)	H ₂ O ₂	4	90	24
11 ^b	Mn(III)OAc-TDCPP (15Mn)	H ₂ O ₂	99	98	594
12 ^b	-	H ₂ O ₂	-	-	-

Reaction conditions: ^a catalyst (4.7 x 10⁻⁵ mmol), styrene (0.5 mmol), isobutyraldehyde (2.5 mmol), chlorobenzene (0.19 mmol), CH₂Cl₂ (2 mL), 25 °C, 90 min; ^b catalyst (7.48 x 10⁻³ mmol), styrene (4.5 mmol), ammonium acetate (2.91 mmol), chlorobenzene (0.39 mmol), H₂O₂ 30% (2 mmol), CH₃CN (20 mL), 25 °C, 45 min; ^c Calculated by GC; ^d Turnover number (TON) by mol products/mol catalysts; ^e In the absence of isobutyraldehyde.

From the analysis of **table 3.1**, we can conclude that all manganese(III)-porphyrin catalysts **9Mn**, **11Mn**, **13Mn** and **15Mn** (**Table 3.1**, **entries 2-5**) led to almost full conversions (99%) in 90 min, showing good TONs (up to 10531), and also high selectivity for styrene epoxide (**20**) (86-92%), with benzaldehyde being formed as a side-product (8-14%). Furthermore, no significant effects of the manganese(III) porphyrin structure was observed on the catalytic activity, since all

studied *meso*-aryl substituted porphyrins bearing Cl, F or CF₃ substituted groups, showed good activity and selectivity for epoxide.

Diversely, when chromium(III)-porphyrin catalysts (**10Cr**, **12Cr**, **14Cr** and **16Cr**) were evaluated, a strong influence of the central metal in the catalytic activity and selectivity for epoxide was observed. In this case, a significant loss of activity and selectivity towards epoxide, with formation of benzaldehyde in up to 30% was observed, as previously reported^[26] (**Table 3.1, entries 6-9**). Moreover, similarly to results previously obtained with manganese(III)-porphyrin catalysts (**9Mn**, **11Mn**, **13Mn** and **15Mn**), no significant effect of the chromium(III)-porphyrin structure was observed, whether in catalytic activity or in the selectivity for epoxide formation.

Regarding the mechanism of epoxidation reaction with O₂ (**Chapter 1**), the effect of porphyrin structure, central metal, and the reactions conditions on generation of the catalytic active species have been the target of several recent reports.^[27, 28] In this context, the present study corroborates previous observations, in which the use of O₂ as an oxygen donor requires, in general, the presence of an electron source, in this case, an aldehyde.^[29] Herein, the presence of isobutyraldehyde is crucial to obtain an active catalytic system with high selectivity for epoxide formation *via* high-valent metal oxo species, which points toward the involvement of the Mukaiyama mechanism.^[29, 30]

Concerning the evaluation of metalloporphyrin catalyst stability, in homogeneous phase, the UV-Vis analysis show degradation of *ca.* 30% of Cr(III)-porphyrin catalysts **10Cr**, **12Cr**, **14Cr** and **16Cr**, after 90 min reaction. As an example, the **figure 3.3 (a)** shows the degradation UV-Vis spectra of **12Cr**. Furthermore, the Mn(III)-porphyrin catalysts **9Mn**, **11Mn**, and **13Mn** suffer degradation of up to 85%, while the **15Mn**-porphyrin catalyst appeared to be the most stable Mn(III)-porphyrin catalyst, showing only 25% degradation after 90 min reaction (**Figure 3.3; b**).

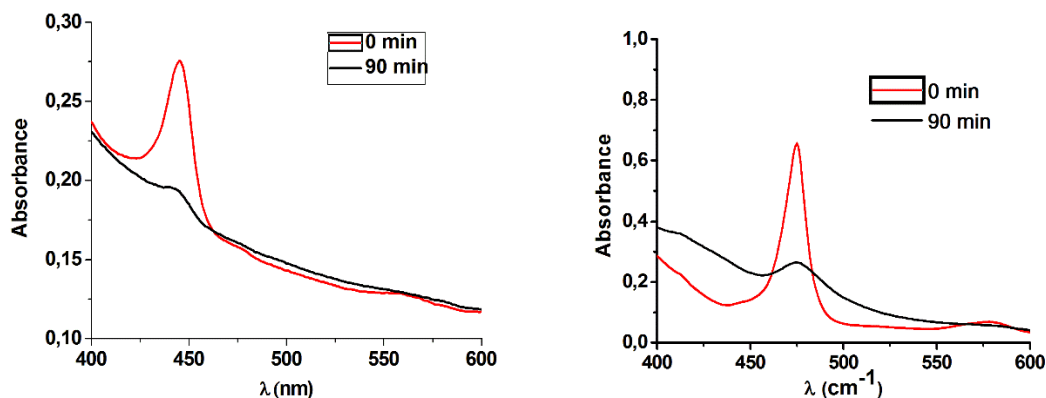


Figure 3.3 – UV-Vis spectrum of metalloporphyrins in catalytic styrene epoxidation using O_2 catalysed by: a) **12Cr**; b) **15 Mn**; (Initial concentration = $2.3 \times 10^{-5}M$).

Then, the effect of the oxidant source was evaluated for the epoxidation of styrene, using the manganese(III) porphyrins **11Mn** and **15Mn** as homogeneous catalysts, under the reaction conditions described above, but using hydrogen peroxide as alternative oxygen source, in absence of co-reductants (**Table 3.1, entries 10-11**). In a model epoxidation experiment, the olefin, the selected metalloporphyrin catalyst and ammonium acetate were dissolved in acetonitrile and stirred at room temperature. Aliquots of hydrogen peroxide solution (30% w/w) in CH_3CN (1:10) were added to the reaction mixture every 15 min, over 45 min. A significant effect of the porphyrin structure was found, as evidenced from the best performing catalyst **15Mn** (MnOAc-TDCPP), which produced full conversion of the olefin in 45 min, with excellent selectivity for epoxide formation (98%), whereas a conversion of only 4% was observed when using catalyst **11Mn** (MnOAc-TPP pCF_3). In this case, the difference of activity may be explained by the higher stability of **15Mn** (MnOAc-TDCPP) (**Figure 3.4; a**) when compared with that of **11Mn** (MnOAc-TPP pCF_3), as corroborated by UV-Vis (**Figure 3.4; b**).

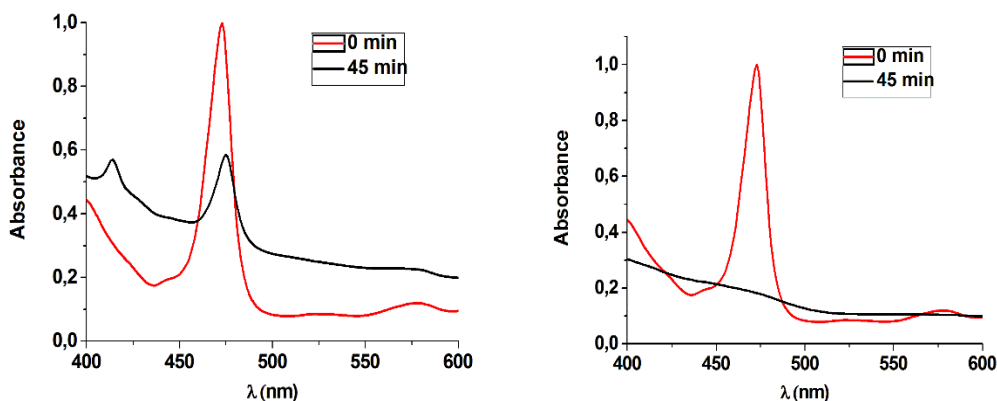


Figure 3.4 – UV-Vis spectrum of metalloporphyrins in catalytic styrene epoxidation using H_2O_2 catalysed by: a) **15Mn**; b) **11 Mn**; (Initial concentration = $3.7 \times 10^{-4}\text{M}$).

The general mechanism of epoxidation using H_2O_2 as oxidant, reported by Pereira^[31, 32] and other authors^[33, 34] (**Figure 3.5**) points out that, under the above-mentioned reaction conditions, using Mn(III)-OAc-TDCPP (**15Mn**) as catalyst, acetonitrile as aprotic solvent, and ammonium acetate as co-axial ligand, the Mn(V)=O oxo species is the active species obtained directly from the reaction of Mn(III)-OAc-TDCPP (**15Mn**) with H_2O_2 (peroxidase route).

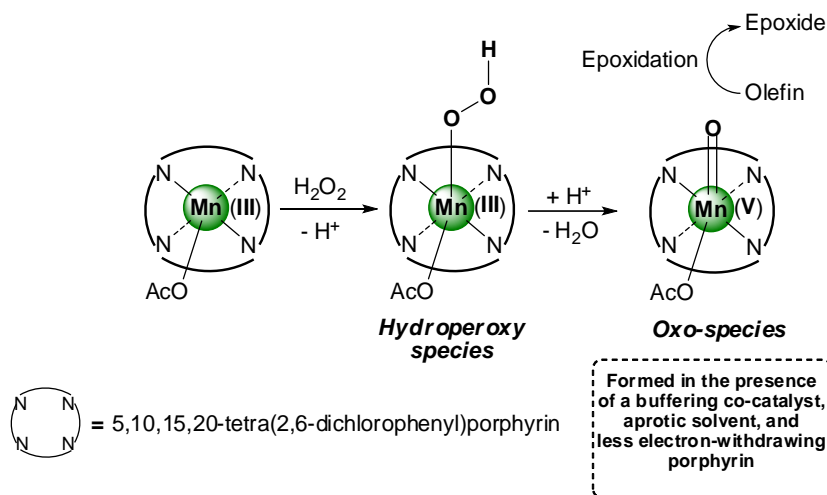


Figure 3.5 – General mechanism for epoxidation reaction using H_2O_2 as oxidant, **15Mn** as catalyst, acetonitrile as solvent and ammonium acetate as co-catalyst.

These homogeneous phase studies allowed us to conclude that Mn(III) metalloporphyrins were found to be the most promising epoxidation catalysts if O_2 was used as oxidant, presenting higher activity and selectivity to epoxides than the Cr(III) counterparts, probably owing to the formation of highly stable and consequently poorly active Cr(V)=O species.^[26] On the other hand, when hydrogen

peroxide was used as oxygen source, only **15Mn** (MnOAc-TDCPP), containing 2,6-dichlorophenyl groups in the *meso* positions induced significant olefin conversion.

Nevertheless, both strategies led to significant catalyst degradation, as it was expected. Therefore, to overcome the intrinsic metalloporphyrin instability and allow their recycling and reutilization, the hybrid heterogeneous catalysts **MNP@SiO₂-17Mn** and **MNP@SiO₂-18Mn**, synthesised in **chapter 2**, were selected to be evaluated in styrene epoxidation, using again molecular oxygen or hydrogen peroxide as oxidants. The results are presented in **table 3.2**.

Table 3.2 – Evaluation of heterogeneous hybrid metalloporphyrin-based magnetic catalysts in styrene epoxidation, using molecular oxygen or hydrogen peroxide as oxidants.

Entry	Catalyst	Oxidant	Conv. ^c (%)	Epoxide (%)	TON ^d
1 ^a	MNP@SiO₂-NH-17Mn	O ₂	99	94	10531
2 ^b	MNP@SiO₂-NH-17Mn	H ₂ O ₂	91	92	546
3 ^a	MNP@SiO₂-NH-18Mn	O ₂	34	85	3616
4 ^b	MNP@SiO₂-NH-18Mn	H ₂ O ₂	2	41	12

Reaction conditions: ^a catalyst (4.7 x 10⁻⁵ mmol), styrene (0.5 mmol), isobutyraldehyde (2.5 mmol), chlorobenzene (0.19 mmol), CHCl₂ (2 mL), 25 °C, 90 min; ^b catalyst (7.48 x 10⁻³ mmol), styrene (4.5 mmol), ammonium acetate (2.91 mmol), chlorobenzene (0.39 mmol), H₂O₂ 30% (2 mmol), CH₃CN (20 mL), 25 °C, 24 h; ^c Calculated by GC; ^d Turnover number (TON) by mol products/mol catalysts;

Using similar reaction conditions as described above for homogeneous system, but using **MNP@SiO₂-NH-17Mn** as heterogeneous catalyst and O₂ as oxidant, high conversion and selectivity (94%) were obtained (**Table 3.2, entry 1**), whereas **MNP@SiO₂-NH-18Mn** showed lower conversion (34%) and selectivity for epoxide (85%). In addition, when hydrogen peroxide was used as oxidant, only the heterogeneous hybrid catalyst containing *meso*-2,6-dichlorophenyl substituents at the porphyrin structure, **MNP@SiO₂-NH-17Mn**, led to high activity, while the trifluoromethyl-substituted manganese(III) porphyrin hybrid catalyst, **MNP@SiO₂-**

NH-18Mn, was inactive (**Table 3.2, entry 4**). These results are in close agreement with those previously observed in homogeneous phase (**Table 3.1, entries 10-11** and **Table 3.2, entries 2 and 4**). The recyclability of **MNP@SiO₂-NH-17Mn** was then evaluated. Recovery of the catalyst after each cycle was performed using an external magnet, followed by washing of the catalyst material with CH₂Cl₂ and CH₃CN, followed by decantation of the supernatant solution (procedure repeated several times). Then, the recovered catalyst material was dried under vacuum, at 60 °C, for 2 h and reused in the next cycle (**Figure 3.6**). When O₂ was used as the oxidant, the catalyst **MNP@SiO₂-NH-17Mn** showed excellent reusability in five consecutive cycles, almost without loss of activity or selectivity for epoxide formation (**Figure 3.6**).

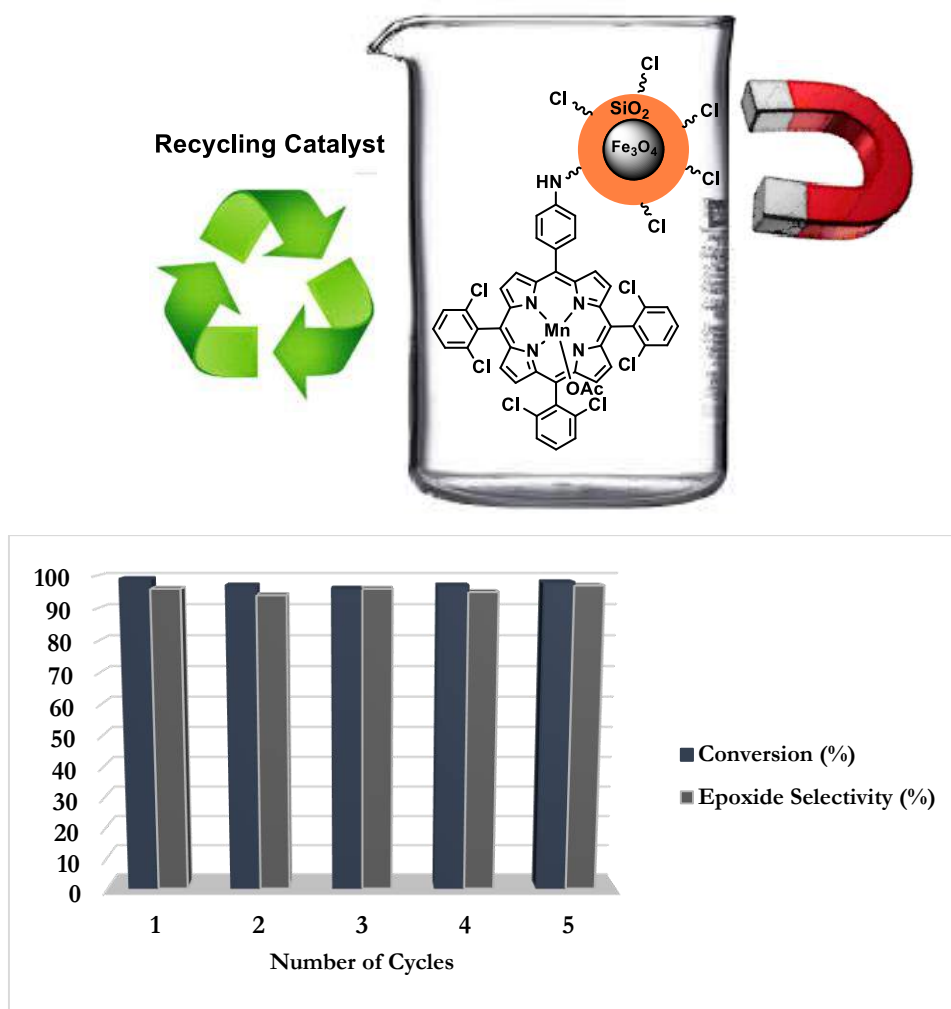


Figure 3.6 – Recycling experiments of **MNP@SiO₂-NH-17Mn** in styrene epoxidation with O₂.

Beyond the high activity and selectivity, it is worth noting the stability of Mn(III) porphyrin magnetic material **MNP@SiO₂-NH-17Mn**, which suffered no leaching or catalyst degradation, as demonstrated by ICP analysis of the liquid supernatant, which showed a negligible metal content in solution (<0.1 μg mL⁻¹). This stabilizing effect may be attributed to the influence of the magnetic support in preventing the formation of catalytically inactive μ-oxo-dimeric metalloporphyrin species^[35] (**Figure 3.7**).

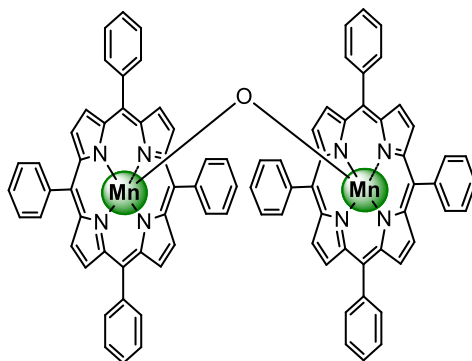


Figure 3.7 – Structure of μ-oxo-bismanganese(III) porphyrin, observed as degradation product of several homogeneous processes.

In contrast, if hydrogen peroxide was used as the oxidant, the catalyst **MNP@SiO₂-NH-17Mn** showed limited reusability, with a sharp decrease in epoxide yield, after the third run (**Figure 3.8**).

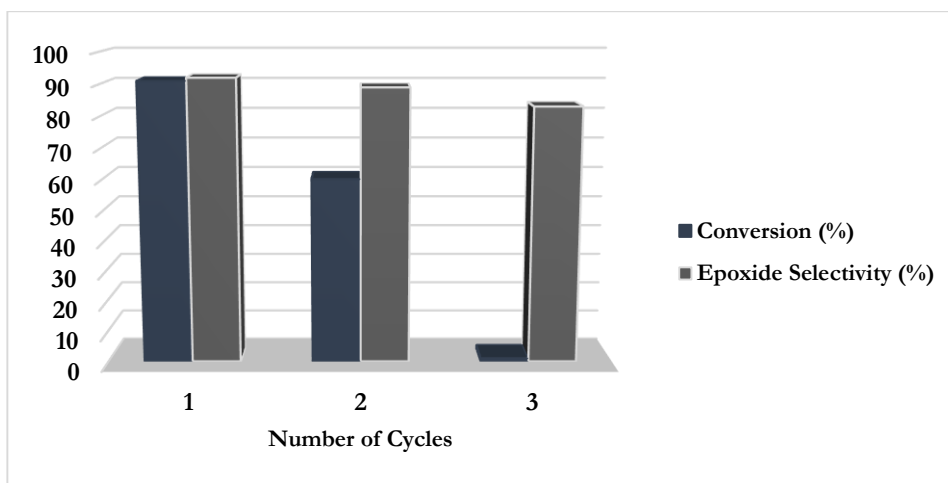


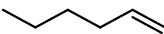
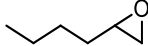
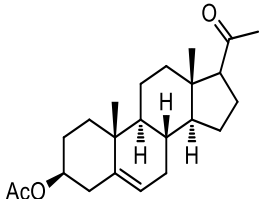
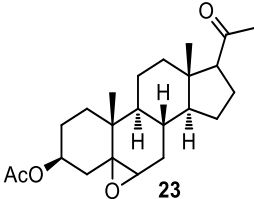


Figure 3.8 – Recycling experiments of **MNP@SiO₂-NH-17Mn** in styrene epoxidation with H₂O₂.

This might be a result of metalloporphyrin degradation due to the formation of hydroxyl radicals ($\cdot\text{OH}$) by homolytic cleavage of H_2O_2 or M-O-O-H . Blank experiments conducted using silica-functionalised magnetite nanoparticles (**MNP@SiO₂-Cl** and **MNP@SiO₂-NH₂**) as catalysts, either with O_2 or H_2O_2 as oxidants, led to conversions below 1%, discarding the involvement of the magnetic supports as reaction catalysts. In sum, when O_2 was used as oxidant, the porphyrin magnetic-nanocomposite **MNP@SiO₂-NH-17Mn** showed excellent stability, activity and reusability in five consecutive cycles, almost without loss of activity or selectivity for epoxide formation. Furthermore, the separation of catalyst using an external magnetic field showed great advantages when compared to other separation procedures, namely by avoiding the use of expensive and toxic solvents and reducing the loss of catalyst between the catalytic cycles, since the separation process can be carried out without removing the catalyst from the reactor.^[36]

Finally, to evaluate the versatility of this synthetic approach for epoxidation using O_2 as a green oxidant, we carried out the epoxidation reaction of olefins, namely 1-hexene, cyclohexene and a steroid derivative (pregnenolone), using the **MNP@SiO₂-NH-17Mn** as catalyst and isobutyraldehyde as co-reductant. The results are summarised in **Table 3.3**.

Table 3.3 – Epoxidation reaction scope catalysed by **MNP@SiO₂-NH-17Mn^a**

Entry	Substrate	Conversion ^b (%)	Product (Yield, %)
1		99	 (97%) 21
2		65	 22 (60%)
3 ^c		99	 23 (57%) <i>d.r.</i> = 71(β) : 29(α)

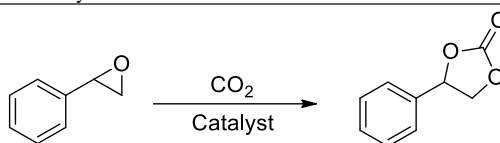
^a **Reactions conditions:** **MNP@SiO₂-NH-17Mn** (4.7×10^{-5} mmol Mn), substrate (0.5 mmol) isobutyraldehyde (2.5 mmol), butyronitrile (2 mL), O₂ bubbling, 25 °C, 2 h. ^b Conversion calculated by GC, based on the substrate, using chlorobenzene (1.95×10^{-1} mmol) as internal standard. ^c 0.25 mmol substrate. Selectivity for epoxide formation was $\geq 97\%$ in all cases. All data were reproduced at least twice and reported as an average.

The epoxidation product of cyclohexene (**21**) was obtained in 97% yield and high selectivity (99%) (**Table 3.3, entry 1**) whereas the epoxidation product (**22**) of the aliphatic terminal olefin 1-hexene (**Table 3.3, entry 2**) was obtained in 65% conversion and 60% yield, as expected for the aerobic epoxidation of terminal alkyl olefins using metalloporphyrin catalysts.^[37] Appreciably, the magnetic catalyst **MNP@SiO₂-NH-17Mn** was effective in promoting the selective epoxidation of 3β-acetoxy-5-pregnen-20-one afforded the respective epoxy steroid (**23**) in 57% isolated yield, with 71% (β) to 29% (α) diastereomeric ratio (**Table 3.3, entry 3**). The stereochemical ratio observed might be explained by the involvement of an oxo species, which approach the double bond preferably from the *cis* side, producing preferentially the β-epoxide.^[31] All epoxidation products were characterised by ¹H- and ¹³C-NMR and the data are presented in the experimental section (**Chapter 5**).

3.3 Catalytic CO₂ Cycloaddition to Epoxides

The effect of activity and selectivity of metalloporphyrin-based on homogeneous catalysts was also evaluated in CO₂ cycloaddition to styrene oxide (**20**), previously prepared under the reaction conditions described in **table 3.1**. The reactions were carried out under mild conditions (10 bar CO₂, 80 °C), using 0.07 mol% catalyst, in presence or absence of bis(triphenylphosphine)iminium chloride (PPNCl) as co-catalyst, and the results are collected in **table 3.3** and **table 3.4**.

Table 3.3 – CO₂ cycloaddition to styrene oxide using manganese(III) metalloporphyrins as homogeneous catalysts.^a

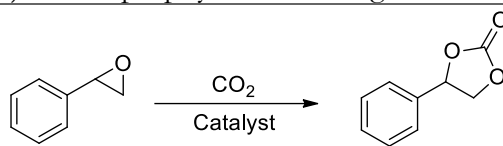


Entry	Catalyst	Co-catalyst	Conv.(%) ^b	TON ^c	TOF ^d
1	-	PPNCl	30	429	18
2	Mn(III)OAc-TTPP (9Mn)	-	7	100	4
3	Mn(III)OAc-TTPP (9Mn)	PPNCl	80	1142	48
4	Mn(III)OAc-TTPP <i>p</i> CF ₃ (11Mn)	-	11	157	7
5	Mn(III)OAc-TTPP <i>p</i> CF ₃ (11Mn)	PPNCl	88	1257	52
6	Mn(III)OAc-TDFPP (13Mn)	-	5	71	3
7	Mn(III)OAc-TDFPP (13Mn)	PPNCl	77	1100	46
8	Mn(III)OAc-TDCPP (15Mn)	-	10	142	5
9	Mn(III)OAc-TDCPP (15Mn)	PPNCl	90	1286	54

Reaction conditions: ^a styrene oxide (35 mmol, 4 mL); catalyst: 2.45 x 10⁻² mmol; co-catalyst (when indicated): 2.45 x 10⁻² mmol PPNCl; 80 °C; CO₂ (10 bar); 24 h. ^b Conversions calculated by GC based on chlorobenzene as internal standard. Selectivity for styrene carbonate, as determined by crude ¹H-NMR, was 100% in all cases; ^c Turnover number (TON) = mol products/mol catalysts; ^d Turnover frequency (TOF) = TON/ number of hours;

From the results presented on **table 3.3**, we can observe that all Mn(III)-porphyrin catalysts presented low conversions in the absence of co-catalyst (**Entries 2, 4, 6 and 8**) but, upon the addition of PPNCl as co-catalyst, a significant increase in their catalytic activity was observed (**Entries 3, 5, 7 and 9**). Moreover, the ligand structure had a moderate influence on the activity of the Mn(III) porphyrins, being the trifluomethylphenyl (**11Mn**) and 2,6-dichlorophenyl-substituted (**15Mn**) metalloporphyrins the most active catalysts, achieving 88% and 90% conversion, respectively (**Table 3.3, entries 5 and 9**). On the other hand, when 2,6-difluorophenyl metalloporphyrin (**13Mn**) was used as catalyst, in presence of PPNCl as co-catalyst, 77% conversion was obtained (**Table 3.3, entry 7**). In addition, full selectivity for the cyclic carbonate was observed with all Mn(III) catalytic systems, under the studied conditions (10 bar CO₂, 80 °C).

In order to evaluate the effect of the central metal, several Cr(III)-porphyrins were also used as catalysts (**10Cr, 12Cr, 14Cr and 16Cr**), under the optimised reactions conditions described above. The results are presented in **table 3.4**.

Table 3.4 – Conversion, TON, TOF obtained in CO₂ cycloaddition to styrene oxide using chromium(III) metalloporphyrins as homogeneous catalysts.^a

Entry	Catalyst	Co-catalyst	Conv.(%) ^b	TON ^c	TOF[h ⁻¹] ^d
1	-	PPNCl	30	429	18
2	Cr(III)Cl-TPP (10Cr)	-	76	1085	45
3	Cr(III)Cl-TPP (10Cr)	PPNCl	100 (85) ^e	1429 (1214) ^e	60 (243) ^e
4	Cr(III)Cl-TPP <i>p</i> CF ₃ (12Cr)	-	88	1257	52
5	Cr(III)Cl-TPP <i>p</i> CF ₃ (12Cr)	PPNCl	100 (91) ^e	1429 (1300) ^e	60 (260) ^e
6	Cr(III)Cl-TDFPP (14Cr)	-	86	1229	51
7	Cr(III)Cl-TDFPP (14Cr)	PPNCl	100 (88) ^e	1429 (1257) ^e	60 (251) ^e
8	Cr(III)Cl-TDCPP (16Cr)	-	78	1128	47
9	Cr(III)Cl-TDCPP (16Cr)	PPNCl	100 (81) ^e	1429 (1157) ^e	60 (231) ^e

Reaction conditions: ^a styrene oxide (35 mmol, 4 mL); catalyst: 2.45 × 10⁻² mmol; co-catalyst (when indicated): 2.45 × 10⁻² mmol PPNCl; 80 °C; CO₂ (10 bar); 24 h. ^b Conversions calculated by GC based on chlorobenzene as internal standard. Selectivity for styrene carbonate, as determined by crude ¹H-NMR, was 100% in all cases; ^c Turnover number (TON) = mol products/mol catalysts; ^d Turnover frequency (TOF) = TON/ number of hours; ^e Reaction time = 5 h.

The Cr(III)-catalytic systems **10Cr**, **12Cr**, **14Cr** and **16Cr**, in the absence of any additive, gave exclusively styrene carbonate in 76%, 88%, 86% and 78% conversion, respectively (**Table 3.4, entries 2, 4, 6 and 8**). Remarkably, the addition of PPNCl led to a significant increase on the activity of all the Cr(III)-porphyrin based catalysts **10Cr**, **12Cr**, **14Cr** and **16Cr** yielding 85%, 91%, 88% and 81% of styrene carbonate, respectively (**Table 3.4, entries 3, 5, 7 and 9**). UV-Vis analysis of aliquots from the crude mixtures showed almost no catalyst degradation, after 24 h, in all cases. From these results, we can conclude that the best catalytic system is **12Cr**/PPNCl, displaying 91% conversion in just 5 h (**Table 3.4, entry 5**), with full selectivity for the formation of styrene carbonate, and without any catalyst degradation (**Figure 3.9**).

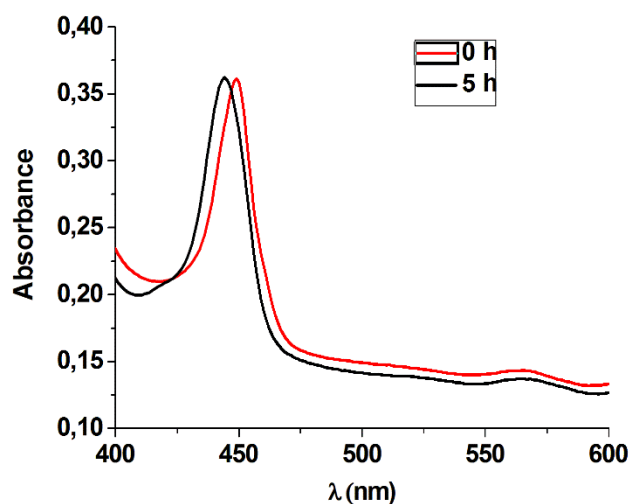


Figure 3.9 – UV-Vis spectra of **12 Cr** as catalyst in the presence of PPNCl in catalytic CO₂ cycloaddition to styrene oxide (Initial concentration = 1.23M).

Based on the homogeneous phase results, the trifluoromethyl-substituted chromium(III) hybrid nanocomposite **MNP@SiO₂-NH-19Cr**, synthesised in **chapter 2** was selected as heterogeneous catalyst, to be evaluated as potential reusable catalyst in CO₂ addition to styrene oxide, under similar homogeneous reaction conditions (10 bar of CO₂, 80 °C). Following a standard procedure, the magnetic catalyst (0.0245 mmol Cr) was introduced in a glass vial inside the autoclave, together with PPNCl (1 equivalent based on Cr) as co-catalyst. The reactor was pressurised with CO₂ (10 bar) and kept under vigorous stirring, at 80 °C. After 24h, a conversion of 55% was observed towards the formation of styrene carbonate through GC analysis of reaction mixture. Moreover, a full selectivity for cyclic carbonate was determined by ¹H-NMR, as can be observed by the signals at δ = 7.50 ppm, 5.66 ppm, 4.79 ppm and 4.33 ppm, typical of styrene carbonate structure (**Figure 3.10**). Moreover, no formation of polycarbonate product was observed, confirmed by the absence of typical signals at δ = 7.44 ppm, 5.79 ppm and 4.32 ppm (**Figure 3.10**).

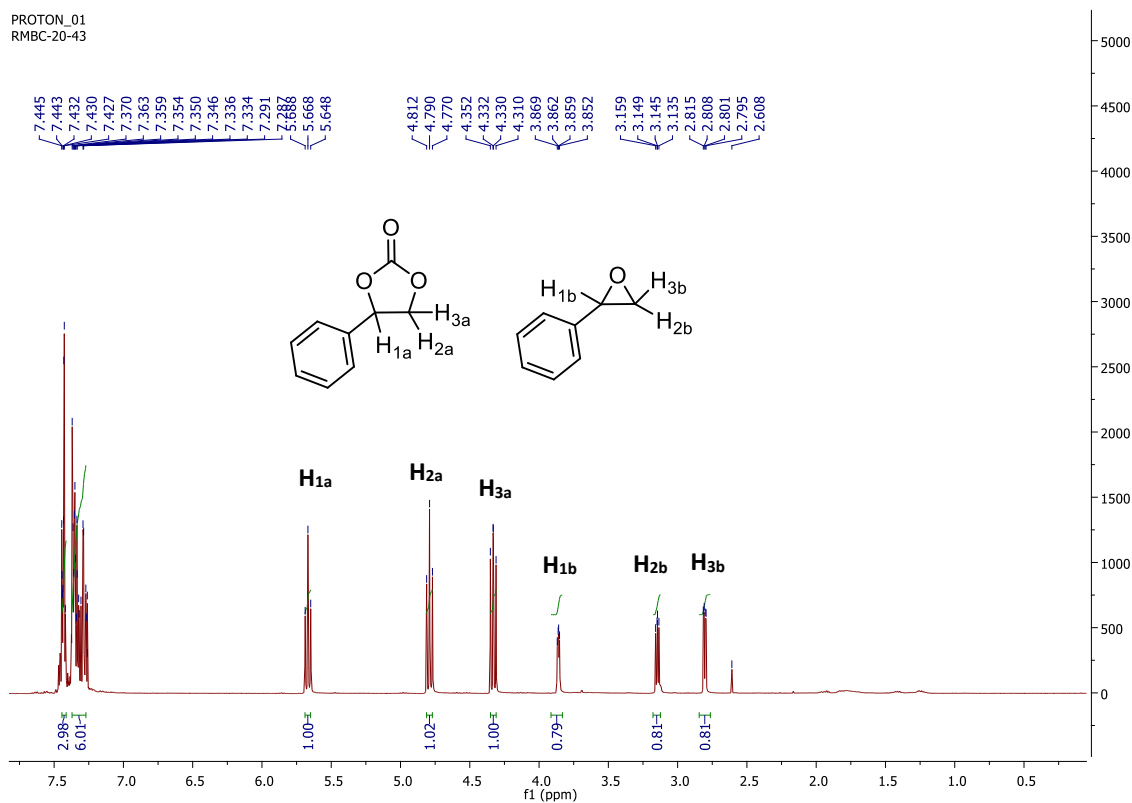


Figure 3.10 – ^1H -NMR of crude in heterogeneous CO_2 cycloaddition reaction in CDCl_3 .

After completing the reaction, the $\text{MNP@SiO}_2\text{-NH-19Cr}$ catalyst was recovered using an external magnet, and the solid catalyst material was washed with CH_2Cl_2 and CH_3CN , followed by decantation of the supernatant solution (procedure repeated several times). Then, the solid material was dried under vacuum, at $60\text{ }^\circ\text{C}$, for 2 h and reused in the next cycle. Remarkably, the nanocomposite showed a notable reusability in four consecutive cycles, without significant loss of activity or selectivity for styrene carbonate (**24**) (**Figure 3.11**).

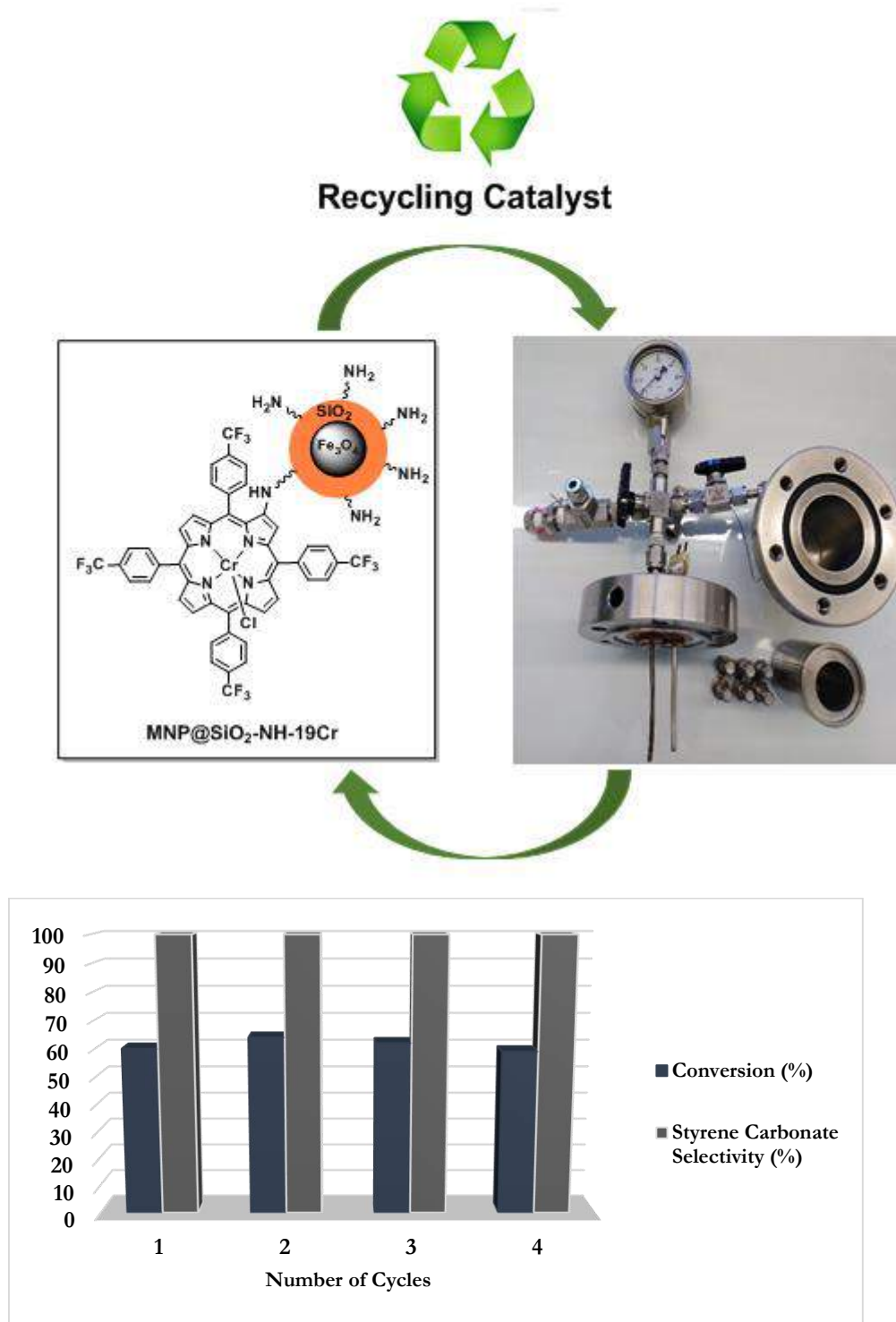


Figure 3.11 – Recycling experiments of **MNP@SiO₂-NH-19Cr** in CO₂ cycloaddition to styrene oxide.

A “blank” experiment was conducted using the aminopropylsilyl-functionalised magnetic nanoparticle (**MNP@SiO₂-NH₂**) as catalyst, whose synthesis was described in **chapter 2**, but practically no conversion (< 1%) was

observed after 24 h, which indicates that the immobilised Cr(III)-porphyrin is the active catalytic site. In summary, these results point out that the hybrid Cr(III)-porphyrin magnetic nanocomposite **MNP@SiO₂-NH-19Cr** is a stable and reusable catalyst for CO₂ cycloaddition to styrene epoxide, with full selectivity for cyclic carbonate.

3.4 Sequential Epoxidation/CO₂ Cycloaddition Reactions

Sequential reactions to promote several different transformations into one single sequence, are one of the most powerful synthetic tools in modern organic chemistry.^[38] In general, these processes are less expensive, relatively simple and readily available; starting from basic substrates to sophisticated targeted molecules that can be obtained without isolation of the intermediates. Therefore, the search of efficient sequential methodologies for the "direct" transformation of olefins into cyclic carbonates is still a great challenge for industrial and academics purposes, being also one of the main goals of the studies described in the present thesis.

Therefore, in pursuing our main goal to develop sustainable catalytic processes for transformation of simple olefins into value-added products, initially we developed studies aiming the development of an ideal route to promote sequential epoxidation/CO₂ addition reactions, under homogeneous conditions.

In a typical experiment, styrene (4.5 mmol) as substrate, the manganese(III)-porphyrin (**15Mn**) (7.48 x 10⁻³ mmol) as the catalyst, ammonium acetate (2.9 mmol) as co-axial ligand and acetonitrile were added in a glass vial, with stirring, at room temperature. Then, to prevent catalyst degradation, a solution (1:20) of H₂O₂ (30%) in acetonitrile, was added in portions to the reaction mixture, every 15 min, for 45 min. At the end of the reaction, the solvent was partially evaporated and the resulting mixture was transferred, without any further purification, to a stainless-steel autoclave containing the chromium(III)-porphyrin catalyst (**12Cr**) (0.07%) and the co-catalyst PPNCl (0.07%), at a temperature of 80 °C and pressure $P(\text{CO}_2) = 10$ bar. After 24 h, the formation of the desired styrene carbonate was observed by GC, being isolated in 70% yield (**Table 3.5, entry 1**).

Table 3.5 – Sequential epoxidation/ CO_2 cycloaddition, catalysed by homogeneous manganese (**15Mn**) and chromium-porphyrin (**12Cr**) catalysts.^a

Entry	Substrate	Conv. ^b (%)	Product	Cyclic Carbonate (%)
1		99		70
2		99		47
3		99		<1
4		93		68

^a **Reaction conditions for epoxidation reaction:** catalyst (7.48×10^{-3} mmol), substrate (4.5 mmol), ammonium acetate (2.91 mmol), chlorobenzene (0.39 mmol), H_2O_2 30% (2 mmol), CH_3CN (20 mL), 25 °C, 45 min. **Reaction conditions for CO_2 cycloaddition:** catalyst: 3.15×10^{-3} mmol; co-catalyst (when indicated): 3.15×10^{-3} mmol PPNCI; 80 °C; CO_2 (10 bar); 24 h. ^b Conversions calculated by GC based on chlorobenzene as internal standard.

To evaluate the versatility of the synthetic process, the scope of this sequential methodology was expanded to a set of vinyl olefins, namely 4-chlorostyrene, 4-methylstyrene and 2-vinylnaphthalene. Remarkably, full conversion of the initial olefin was achieved in most cases, with moderate to good selectivity for cyclic carbonate formation (**24-27**) (47-70%) (**Table 3.5, entries 2-4**). The only exception was obtained with 4-methylstyrene, for which a complex mixture of benzylic

oxidation products, formed during the epoxidation step, was detected by GC/MS analysis, being the aldehyde derivative the major product (35 %) (m/z) = 134.1 (M^+), thus leading to very low selectivity (<1%) for cyclic carbonate formation with aldehyde group (m/z) = 191.1 ($M-H$)⁺ (**Table 3.5, entry 3**).

A different approach was then carried out, by using molecular oxygen instead of hydrogen peroxide as oxidant, and isobutyraldehyde as co-reductant, again using manganese(III)-porphyrin (**15Mn**) as the epoxidation catalyst. In a typical epoxidation reaction, using O₂ as oxidant, a round bottom flask was loaded with the appropriate amounts of styrene, the metalloporphyrin catalyst (**15Mn**), isobutyraldehyde as co-reductant, and CH₂Cl₂ as solvent. The crude mixture was stirred at room temperature, under O₂ bubbling, for 90 min. After this period, the chromium(III)-porphyrin catalyst (**12Cr**) and the co-catalyst PPNCl were added. The subsequent CO₂ cycloaddition proceeded over 24 h, under the following reaction conditions: catalyst and co-catalyst (PPNCl): 0.07 mol%; T = 80 °C; P(CO₂) = 10 bar. GC/MS analysis of the reaction crude showed complete conversion of the initial olefin substrate but a complex mixture of products was observed by GC-MS. This was attributed to epoxide ring-opening due to the presence of isobutyric acid, formed in the first step, which was corroborated by GC-MS where the diol product (m/z) = 138.1 (M^+) was observed as the major product.

Therefore, considering the above results and our goal to develop efficient and reusable catalytic system to sequentially promote the "direct" transformation of olefins into cyclic carbonate, the hybrid metalloporphyrin magnetic nanocomposites **MNP@SiO₂-NH-17Mn** and **MNP@SiO₂-NH-19Cr** were mixed and evaluated as a heterogeneous bimetallic dual catalytic system for styrene epoxidation, with molecular oxygen, followed by CO₂ cycloaddition (**Figure 3.12**).

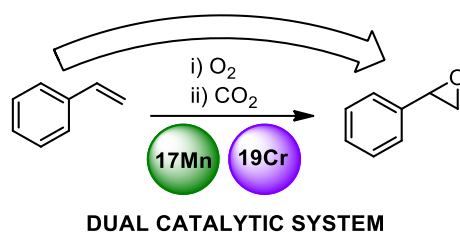


Figure 3.12 – Sequential heterogeneous bimetallic dual catalytic system for direct transformation of styrene into styrene carbonate by sequentially using O₂ and CO₂.

Thus, a mixture containing the two hybrid materials **MNP@SiO₂-NH-17Mn** (8.16×10^{-4} mmol Mn) and **MNP@SiO₂-NH-19Cr** (6.08×10^{-3} mmol Cr) was placed inside the reaction vessel. The epoxidation reaction was performed using molecular oxygen as oxidant and isobutyraldehyde as co-reductant, under the reaction conditions described in **table 3.2**. After 140 minutes, the magnetic hybrid catalyst (containing both Mn(III) and Cr(III)-porphyrin nanoparticles) was collected on the reactor walls with an external magnet and the reaction crude was treated with an aqueous solution of sodium hydrogen carbonate to remove the isobutyric acid formed as side-product. After separation, the organic phase was transferred to the autoclave, already containing the recovered magnetic catalysts and the co-catalyst PPNCl. The reactor was then pressurised with CO₂ (10 bar) and the cycloaddition step was conducted at 80 °C, for 24 h. GC-MS analysis determined complete conversion of the olefin, with formation of styrene carbonate (**24**) as the major product (up to 52%).

After the catalyst's recovery using an external magnet, the dual hybrid material was washed several times with different solvents, dried under vacuum, and reused in the next runs, involving both epoxidation and CO₂ addition as sequential steps. Remarkably, the hybrid material could be reused in several additional consecutive sequential epoxidation/CO₂ addition cycles, almost without loss of catalytic activity and just a slight decrease of selectivity for the formation of styrene carbonate (**24**) (**Figure 3.13**), which demonstrated the recyclability of this heterobimetallic dual catalytic system.

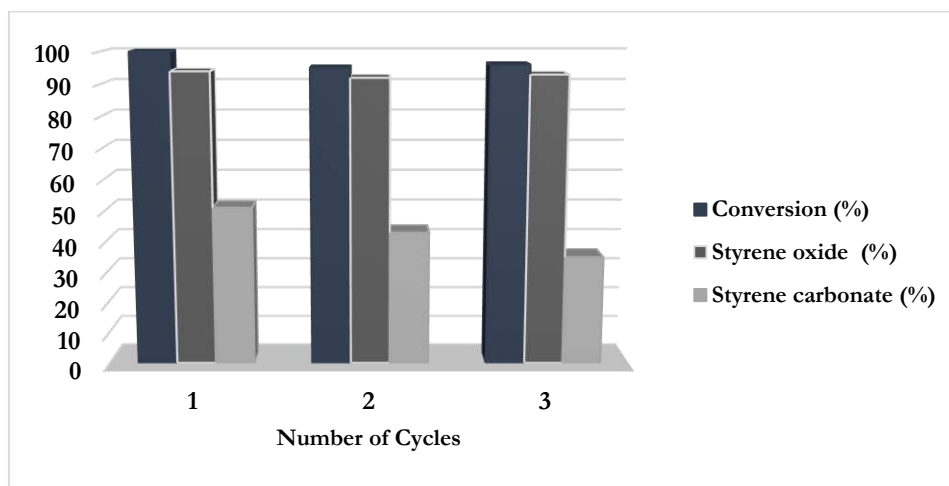


Figure 3.13 – Recycling experiments of the dual catalytic system **MNP@SiO₂-NH-17Mn** + **MNP@SiO₂-NH-19Cr** in styrene sequential epoxidation/CO₂ cycloaddition.

From the final product selectivity, the mechanism of the overall sequential reaction should be similar to the one described for individual steps, in which Mn(V)=O oxo species are the epoxidation active species, obtained by a Mukayama oxygen/aldehyde activation mechanism, and the CO₂ addition to the epoxide is catalysed by the Cr(III) porphyrin (stronger Lewis acid), assisted by the nucleophile PPNCl, as previously described by Pereira.^[39]

3.5 Conclusions

The results presented in **chapter 3** allowed the development of active and selective metalloporphyrin-based homogeneous and heterogeneous catalysts for epoxidation/CO₂ addition sequential reactions, aiming at the direct transformation of olefins into cyclic carbonates, using a heterobimetallic dual-catalyst.

Studies of the styrene epoxidation reaction in homogeneous phase allowed us to conclude that, regardless of the oxidant used (molecular oxygen or hydrogen peroxide), the manganese(III) porphyrins are the most active and selective for epoxide formation. Furthermore, when O₂ was used as oxidant, the catalyst **15Mn** (MnOAc-TDCPP) was the most active, selective, and stable epoxidation catalyst. On the other hand, chromium(III) metalloporphyrins proved to be the most active catalysts for CO₂ addition to styrene oxide. Among the synthesised metalloporphyrins, the best results were obtained with **12Cr** (CrCl-TPP_{*p*}CF₃). Aiming the developing of

sustainable chemical processes, the most promising catalysts for each individual reaction were immobilised onto magnetic nanoparticles to obtain the corresponding reusable heterogeneous hybrid catalysts, which were characterised by several physical/chemical techniques in **chapter 2**.

Although the use of H₂O₂ as oxidant, in homogeneous phase, has allowed the direct transformation of a set of different vinyl olefins into the respective cyclic carbonates in good yields, using **15Mn** and **12Cr** in the epoxidation and CO₂ cycloaddition steps, respectively, the corresponding heterogeneous catalysts showed loss of activity after each recycling experiment. Advantageously, the hybrid catalyst **MNP@SiO₂-NH-17Mn** presented a good performance in styrene epoxidation if O₂ was used as oxidant, maintaining its efficiency in five consecutive runs. So, the results described herein allowed, for the first time, the development of an efficient and reusable heterobimetallic catalytic system, through appropriate combination of two hybrid materials, **MNP@SiO₂-NH-17Mn** and **MNP@SiO₂-NH-19Cr**, capable of sequentially promote the transformation of styrene into epoxide followed by the CO₂ cycloaddition reaction. This dual catalyst could be recycled and reused in several consecutive cycles without significant loss of activity or selectivity.

3.6 References

- [1] M. Aresta, A. Dibenedetto, *Journal of Molecular Catalysis A-Chemical* **2002**, *182*, 399-409.
- [2] K. W. Kwong, T. H. Chen, W. L. Luo, H. Jeddi, R. Zhang, *Inorganica Chimica Acta* **2015**, *430*, 176-183.
- [3] P. J. Thomassen, S. Varghese, E. J. A. Bijsterveld, P. Thordarson, J. Elemans, A. E. Rowan, R. J. M. Nolte, *European Journal of Organic Chemistry* **2015**, *23*, 5246-5253.
- [4] R. R. Shaikh, S. Pornpraprom, V. D'Elia, *ACS Catalysis* **2018**, *8*, 419-450.
- [5] V. B. Saptal, B. M. Bhanage, *Current Opinion in Green and Sustainable Chemistry* **2017**, *3*, 1-10.
- [6] L. Cuesta-Aluja, A. M. Masdeu-Bulto, *ChemistrySelect* **2016**, *1*, 2065-2070.
- [7] K. Jasiak, T. Krawczyk, M. Pawlyta, A. Jakobik-Kolon, S. Baj, *Catalysis Letters* **2016**, *146*, 893-901.
- [8] X. D. Xu, J. A. Moulijn, *Energy & Fuels* **1996**, *10*, 305-325.
- [9] A. A. G. Shaikh, S. Sivaram, *Chemical Reviews* **1996**, *96*, 951-976.
- [10] B. Schaffner, F. Schaffner, S. P. Verevkin, A. Borner, *Chemical Reviews* **2010**, *110*, 4554-4581.
- [11] L. B. Silva, L. C. G. Freitas, *Journal of Molecular Structure-Theochem* **2007**, *806*, 23-34.
- [12] K. Xu, *Chemical Reviews* **2004**, *104*, 4303-4417.
- [13] J. H. Clements, *Industrial & Engineering Chemistry Research* **2003**, *42*, 663-674.
- [14] M. Aresta, A. Dibenedetto, I. Tommasi, *Applied Organometallic Chemistry* **2000**, *14*, 799-802.
- [15] M. Cokoja, M. E. Wilhelm, M. H. Anthofer, W. A. Herrmann, F. E. Kuhn, *ChemSusChem* **2015**, *8*, 2436-2454.
- [16] C. J. Whiteoak, A. Nova, F. Maseras, A. W. Kleij, *ChemSusChem* **2012**, *5*, 2032-2038.
- [17] V. B. Saptal, B. M. Bhanage, *ChemCatChem* **2016**, *8*, 244-250.
- [18] Q. He, J. W. O'Brien, K. A. Kitselman, L. E. Tompkins, G. C. T. Curtis, F. M. Kerton, *Catalysis Science & Technology* **2014**, *4*, 1513-1528.
- [19] J. W. Comerford, I. D. V. Ingram, M. North, X. Wu, *Green Chemistry* **2015**, *17*, 1966-1987.
- [20] X. H. Ji, N. N. Zhu, J. G. Ma, P. Cheng, *Dalton Transactions* **2018**, *47*, 1768-1771.
- [21] M. Zhao, C. D. Wu, *Catalysis Communications* **2017**, *99*, 146-149.
- [22] T. Omagari, A. Suzuki, M. Akita, M. Yoshizawa, *Journal of the American Chemical Society* **2016**, *138*, 499-502.
- [23] S. Rayati, F. Nejabat, *New Journal of Chemistry* **2017**, *41*, 7987-7991.

- [24] Y. J. Chen, R. C. Luo, Q. H. Xu, J. Jiang, X. T. Zhou, H. B. Ji, *Acs Sustainable Chemistry & Engineering* **2018**, *6*, 1074-1082.
- [25] Y. Chen, R. C. Luo, Q. H. Xu, W. Y. Zhang, X. T. Zhou, H. B. Ji, *ChemCatChem* **2017**, *9*, 767-773.
- [26] J. Muzart, *Chemical Reviews* **1992**, *92*, 113-140.
- [27] X. Y. Huang, J. T. Groves, *Chemical Reviews* **2018**, *118*, 2491-2553.
- [28] W. W. Nam, H. J. Kim, S. H. Kim, R. Y. N. Ho, J. S. Valentine, *Inorganic Chemistry* **1996**, *35*, 1045-1049.
- [29] B. B. Wentzel, P. L. Alsters, M. C. Feiters, R. J. M. Nolte, *Journal of Organic Chemistry* **2004**, *69*, 3453-3464.
- [30] L. D. Dias, R. M. B. Carrilho, C. A. Henriques, G. Piccirillo, A. Fernandes, L. M. Rossi, M. F. Ribeiro, M. J. F. Calvete, M. M. Pereira, *Journal of Porphyrins and Phthalocyanines* **2018**, *22*, 331-341.
- [31] S. L. H. Rebelo, M. M. Q. Simoes, M. Neves, A. M. S. Silva, J. A. S. Cavaleiro, A. F. Peixoto, M. M. Pereira, M. R. Silva, J. A. Paixao, A. M. Beja, *European Journal of Organic Chemistry* **2004**, *23*, 4778-4787.
- [32] S. L. H. Rebelo, M. M. Pereira, M. M. Q. Simoes, M. Neves, J. A. S. Cavaleiro, *Journal of Catalysis* **2005**, *234*, 76-87.
- [33] R. De Paula, M. M. Q. Simoes, M. Neves, J. A. S. Cavaleiro, *Journal of Molecular Catalysis A-Chemical* **2011**, *345*, 1-11.
- [34] A. Franke, C. Fertinger, R. van Eldik, *Chemistry-A European Journal* **2012**, *18*, 6935-6949.
- [35] C. G. Sun, B. C. Hu, Z. L. Liu, *Chemical Engineering Journal* **2013**, *232*, 96-103.
- [36] L. M. Rossi, M. A. S. Garcia, L. L. R. Vono, *Journal of the Brazilian Chemical Society* **2012**, *23*, 1959-1971.
- [37] A. Farokhi, H. Hosseini-Monfared, *New Journal of Chemistry* **2016**, *40*, 5032-5043.
- [38] X. M. Zeng, *Chemical Reviews* **2013**, *113*, 6864-6900.
- [39] R. M. B. Carrilho, L. D. Dias, R. Rivas, M. M. Pereira, C. Claver, A. M. Masdeu-Bulto, *Catalysts* **2017**, *7*, 210-222.

Chapter 4

Synthesis of Biologically Active Terpenes through Catalytic Processes

4.1 Introduction

Terpenes represent an important class of organic molecules that led to six major drug classes over the last century, namely steroids, tocopherols, taxanes, artemisinins, ingenanes and cannabinoids.^[1] Hence, the development of catalytic processes to promote the design and synthesis of new biologically active terpene-based compounds is a relevant topic in drug discovery.^[2-5] In this regard, many catalytic transformations able to perform the total synthesis^[6] or specific modification on a terpene scaffold^[7] through a rational medicinal chemistry campaign have been used. Among them, some have aroused much interest, namely catalytic epoxidation,^[8] hydroformylation^[9] and CO₂ cycloaddition^[10] which are able to produce important intermediates and chemical entities with potential anticancer activity.

This chapter describes the optimisation of the aldehyde (co-reductant) and solvent in homogeneous epoxidation, using O₂ as an oxidant and a hybrid magnetic Mn(III)-porphyrin as catalyst. Furthermore, a Mn(III)-porphyrin magnetic

nanocomposite was applied as a reusable catalyst in the epoxidation process of a family of olefins and relevant terpenes, namely α -pinene, (+)-limonene and (–)-isopulegol benzyl ether. Additionally, the hydroformylation reaction of (–)-isopulegol benzyl ether using the catalytic system Rh(I)/(*S*)-phosphite-OBn is described. Finally, the antitumour effect of each epoxide-isopulegol diastereomers against the MG-63 human osteosarcoma cells was evaluated by two complementary biological screening methods (MTT (3-(4,5-dimethylthiazol-2-yl)-2,5-diphenyl tetrazolium bromide) and SRB (Sulforhodamine B)).

4.2 Catalytic Epoxidation of Terpenes using Molecular Oxygen

The development of environmentally and economically sustainable epoxidation processes is a relevant subject in modern chemistry, since epoxides are useful chemical entities, applied as intermediates for fine^[11-13] and bulk chemistry^[14] and are also present in a large array of bioactive molecules, particularly anticancer agent^[15] namely capsaicin epoxide^[16] and carfilzomib^[17] (**Figure 4.1**).

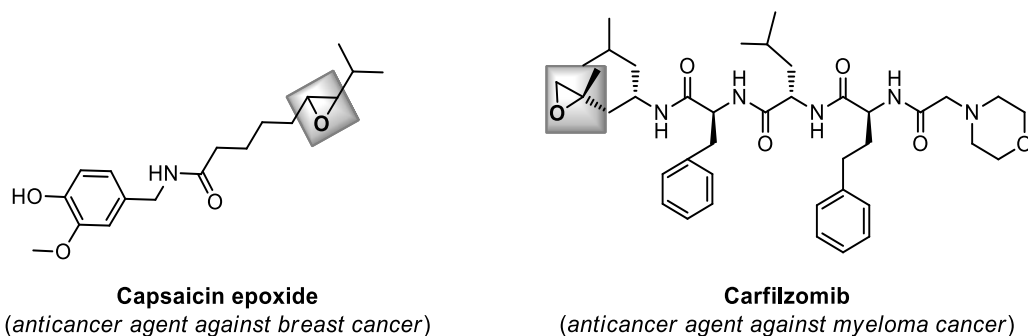


Figure 4.1 – Structure of capsaicin epoxide and carfilzomib.

As previously revised in **chapter 1**, there are multiple reported procedures for epoxide synthesis,^[18, 19] many of these involving stoichiometric and pollutant oxidants such as *m*-chloroperoxybenzoic acid^[20] or iodosylbenzene.^[21] In order to solve this environmental challenge,^[22] the use of a clean catalytic oxidative process based on O₂ as a non-pollutant oxidant catalysed by a immobilised metalloporphyrin onto magnetite nanoparticles is presented and discussed in this chapter (**Figure 4.2**).

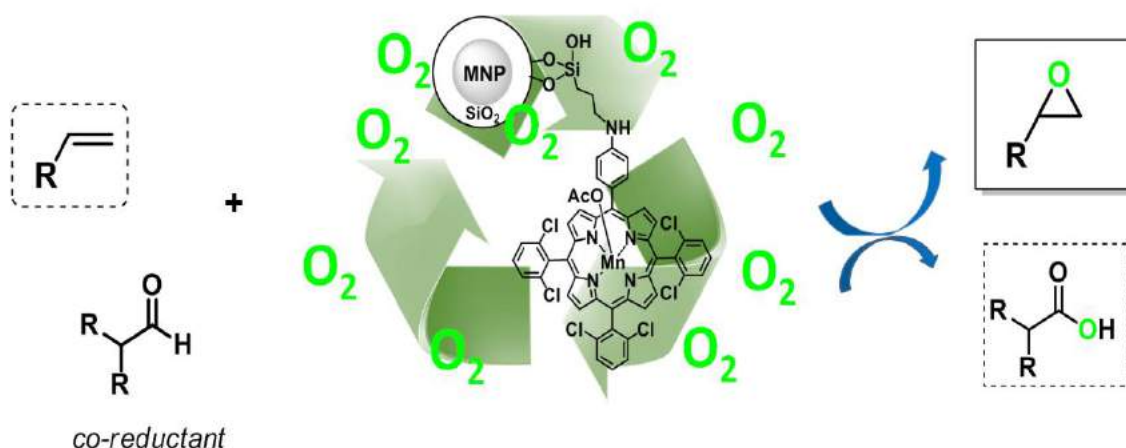
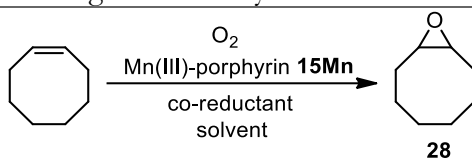


Figure 4.2 – Catalytic epoxidation of olefins developed in this work, using a manganese(III)-porphyrin magnetic nanocomposite as catalyst.

Initially, the epoxidation experiments were performed in homogeneous phase using cyclooctene as the model substrate, in order to evaluate the influence of the solvent and the co-reductant in the activity and selectivity of the catalyst. Typically, a glass vial was loaded with the cyclooctene, Mn(III)OAc-TDCPP (**15Mn**) as the catalyst, an aldehyde as a co-reductant and different solvents. The results and reaction conditions are comprised in **table 4.1**. The reaction mixture was magnetically stirred at room temperature (25 °C), under O₂ bubbling, for 1.5 h. Substrate conversion, TON and TOF calculations were determined by GC, using chlorobenzene as an internal standard (**Equation 1, chapter 5**), the results being summarised in **table 4.1**.

Table 4.1 – Evaluation of different solvents and co-reductants in cyclooctene epoxidation, using **15Mn** as homogeneous catalyst.

Entry	Solvent	Co-reductant	Conv. (%) ^b	TON ^c	TOF ^d
1 ^a	CH ₂ Cl ₂	Isobutyraldehyde	99 (<1) ^e	15532	7021
2 ^a	2-Me-THF	Isobutyraldehyde	36	3830	2553
3 ^a	CH ₃ CN	Isobutyraldehyde	99	15532	7021
4 ^a	CH ₃ CN	3-furfural	0	-	-
5 ^a	CH ₃ CN	2-phenylpropanal	0	-	-
6 ^a	CH ₃ CN	-	0	-	-

Reaction conditions: ^a catalyst **15Mn** (4.7×10^{-5} mmol), cyclooctene (0.5 mmol), co-reductant (2.5 mmol), chlorobenzene (0.19 mmol), solvent (2 mL), 25 °C, 90 min; ^b Calculated by GC; ^c Turnover number (TON) = mol products/mol catalysts; ^d Turnover number frequency (TOF) = TON/time (h); ^e In the absence of catalyst; Selectivity for epoxides was >98% in all cases.

Mn(III)OAc-TDCPP (**15Mn**) was initially used as catalyst in homogeneous phase, and full conversion was obtained with 98% selectivity for cyclooctene oxide (**28**) formation, using dichloromethane as solvent (**Table 4.1, entry 1**). However, searching for a greener reaction solvent,^[23-25] 2-Me-THF and acetonitrile were tested. For 2-Me-THF the conversion was quite low (36%) may be due to coordination of the solvent to the catalyst (**Table 4.1, entry 2**). Regarding acetonitrile the results were similar to those obtained with CH₂Cl₂ (**Table 4.1, entry 3**), which justified the choice of this solvent for the subsequent experiments.

In addition, in order to evaluate the best type of aldehyde as co-reductant, aromatic aldehydes such as 3-furfural and 2-phenylpropanal were appraised, but no conversion was observed in any case (**Table 4.1, entries 4-5**). These results show that, as expected from aldehyde reactivity,^[26] substitution at the α -position of aliphatic aldehydes such as isobutyraldehyde greatly enhance their ability to generate an activated oxygen catalytic species.^[27, 28] Moreover, an experiment was performed in

the absence of aldehyde and no conversion was observed (**Table 4.1, entry 6**), thus corroborating the Mukaiyama mechanism which requires the presence of an electron donor.

The UV-Vis spectrophotometric analysis aiming at assessing the degradation of the **15Mn** catalyst in homogeneous phase (**Figure 4.3**) revealed about 80% degradation during the epoxidation of cyclooctene using O₂ as an oxidant for 90 min.

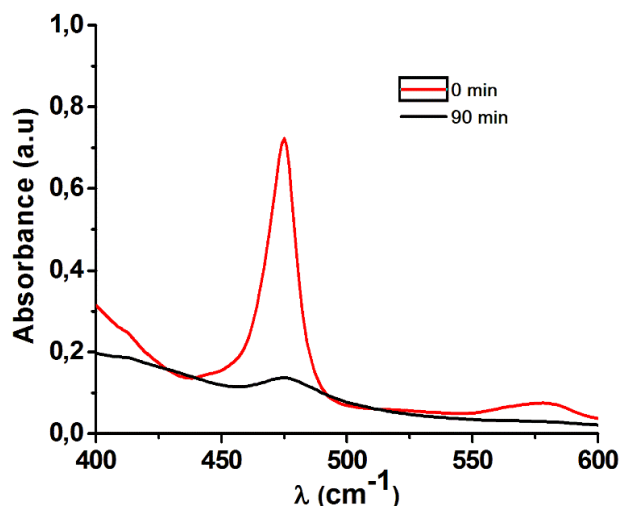
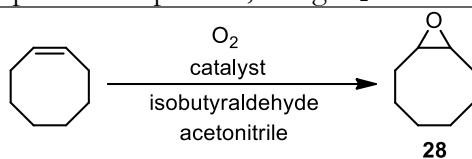


Figure 4.3 – UV-Vis spectra of **15Mn** during the catalytic cyclooctene epoxidation process. (Initial concentration = 5.1×10^{-7} M).

Therefore, to overcome the catalyst's degradation and allow its recycling and reuse, Mn(III)OAc-TDCPP (**15Mn**) was covalently immobilised onto functionalised magnetite nanoparticles, yielding **MNP@SiO₂-NH-17Mn** (**Chapter 2**). This was used as a catalyst in cyclooctene epoxidation, with O₂, the results being presented in **table 4.2**.

Table 4.2 – Evaluation of the heterogeneous hybrid catalyst **MNP@SiO₂-NH-17Mn** in cyclooctene epoxidation process, using O₂ as an oxidant.

Entry	Catalyst	Conv. (%) ^b	TON ^c	TOF ^d
1 ^a	Mn(III)OAc-TDCPP-NH ₂ (17Mn)	98	10426	6951
2 ^a	MNP@SiO ₂ -NH-17Mn	99	10532	7021
3 ^c	MNP@SiO ₂ -NH-17Mn	99 (53) ^f	10532 (5665) ^f	3009 (3777) ^f
4 ^a	MNP@SiO ₂ -Cl	2	213	142

Reaction conditions: ^a catalyst (4.7 × 10⁻⁵ mmol), cyclooctene (0.5 mmol), isobutyraldehyde (2.5 mmol), chlorobenzene (0.19 mmol), acetonitrile (2 mL), 25 °C, 1.5 h; ^b Calculated by GC; ^c Turnover number (TON) = mol products/mol catalysts; ^d Turnover number frequency (TOF) = TON/time (h); ^e scale-up: catalyst MNP@SiO₂-NH-17Mn (8.42 × 10⁻⁴ mmol Mn); cyclooctene (9 mmol), isobutyraldehyde (45 mmol), solvent (36 mL), O₂ bubbling, 25 °C, 3.5 h; ^f conversion at 1.5 h.

Non-symmetric manganese(III)-porphyrin (**17Mn**), which is the homogeneous analogue of the hybrid catalyst **MNP@SiO₂-NH-17Mn**, was then evaluated in cyclooctene epoxidation, providing 98% conversion in 1.5 h and full selectivity for epoxide formation (**Table 4.2, entry 1**). Under the same conditions, the catalyst **MNP@SiO₂-NH-17Mn** also showed an excellent catalytic activity and selectivity, with 99% conversion in 1.5 h and practically exclusive formation of cyclooctene oxide (**28**) (**Table 4.2, entry 2**). The progress of the cyclooctene oxidation reactions using either homogeneous or heterogeneous catalysts (**17Mn** and **MNP@SiO₂-NH-17Mn**, respectively) was evaluated for 90 min (analysing aliquots taken from the reaction mixture every 15 min), the results being depicted in **figure 4.4**.

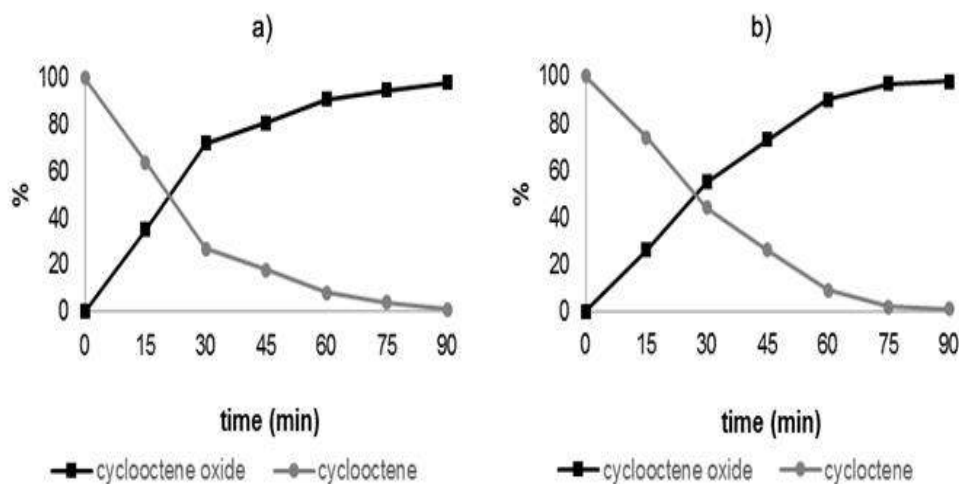


Figure 4.4 – Evolution of cyclooctene epoxidation catalysed by: a) **17Mn**; and b) **MNP@SiO₂-NH-17Mn**.

Analysis of **figure 4.4 (a)** evidences that the homogeneous catalyst **17Mn**, induces a sharp increase of epoxide formation in the first 30 min of reaction (70% conversion), followed by a slower increase after that period which indicates that catalyst degradation might occur or depend on substrate concentration. In order to interpret this result, an UV-Vis analysis was carried out for aliquots taken from the reaction mixture at the start and after 1.5 h, which showed a decrease of *ca.* 80% in the metalloporphyrin Soret band (**Figure 4.5**). Therefore, we concluded that the decrease of the reaction speed with time is due to catalyst degradation.

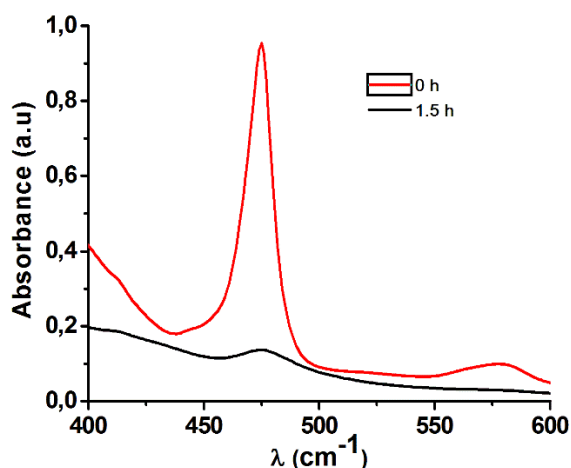
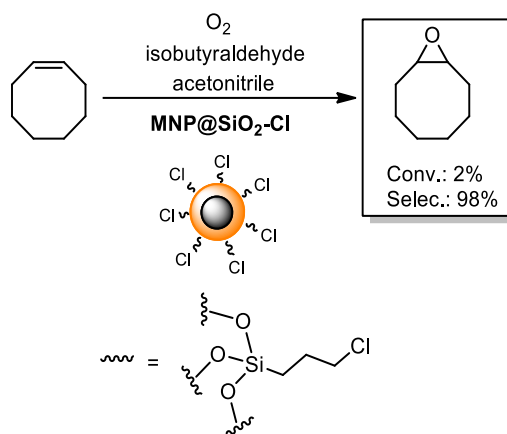


Figure 4.5 – UV-Vis spectra of **17Mn** in solution during the catalytic oxidation of cyclooctene. (Initial concentration = $5.1 \times 10^{-7}\text{M}$).

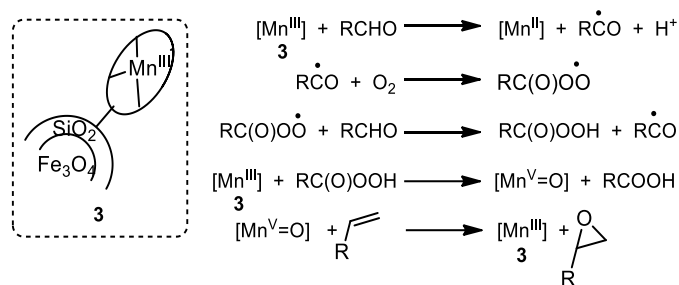
In contrast, the reaction profile obtained with the hybrid nanocomposite catalyst **MNP@SiO₂-NH-17Mn** suggests that catalyst degradation is significantly hindered under these experimental conditions. Moreover, it is worth noticing that the obtained TON values were similar to those corresponding to the **17Mn**-homogeneous system, which suggests that catalyst immobilisation onto a magnetite nanoparticle does not affect catalytic activity.

In addition, in order to evaluate the effect of the solid support in epoxide formation, a “blank” experiment was carried out using the 3-chloropropyl triethoxysilane functionalised magnetite nanoparticle **MNP@SiO₂-Cl** as catalyst, which led to a conversion of only 2% (**Table 4.2, entry 4** and **Scheme 4.1**).



Scheme 4.1 – Epoxidation of cyclooctene catalysed by 3-chloropropyltriethoxysilane functionalized magnetic nanoparticle (**MNP@SiO₂-Cl**).

This result confirms that the Mn(III)-porphyrin magnetic nanocomposite **MNP@SiO₂-NH-17Mn** is the catalytic active site. Furthermore, the requirement for isobutyraldehyde as co-reductant and the high chemoselectivity for epoxide formation suggest that the reaction possibly follows the mechanism previously described by Feiters and coworkers,^[27] depicted in **scheme 4.2**, according to which a peroxyacid species, formed in the presence of molecular oxygen and aldehyde, is assumed to act as an oxygen donor to generate the high-valent Mn(V)-oxo intermediate, that acts as the catalytically active epoxidation species.^[29, 30]



Scheme 4.2 – Mechanism of olefin epoxidation with O_2 . Adapted from [27].

4.2.1 Recyclability and Reusability Tests

In order to evaluate the recyclability of the Mn(III)-porphyrin magnetic nanocomposite **MNP@SiO₂-NH-17Mn**, used as a catalyst in the epoxidation reaction, this magnetic catalyst was applied using the optimized reaction conditions previously described (1.5 h, at 25 °C). After the first cycle, the magnetic nanocomposite was collected by an external magnet in the sidewall of the reaction flask (**Figure 4.6**). After washing the solid material with CH_3CN (3x) and upon subsequent solvent removal, the catalyst **MNP@SiO₂-NH-17Mn** was able to be reused in the next run (**Figure 4.7**).

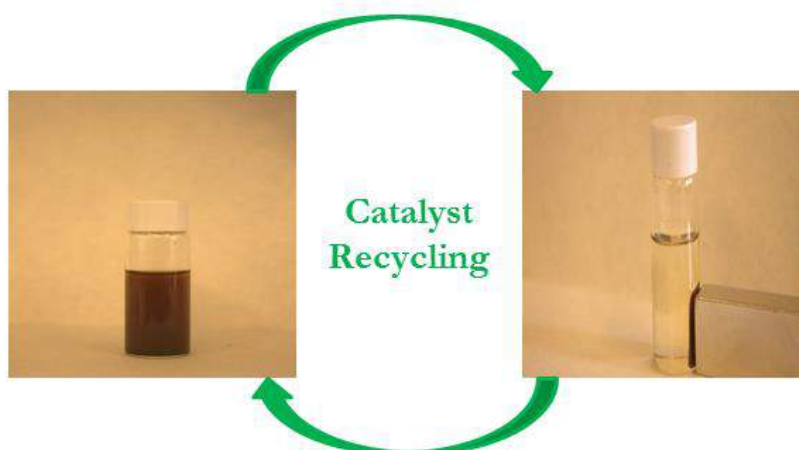


Figure 4.6 – Separation of the magnetic catalyst by application of an external magnetic field.

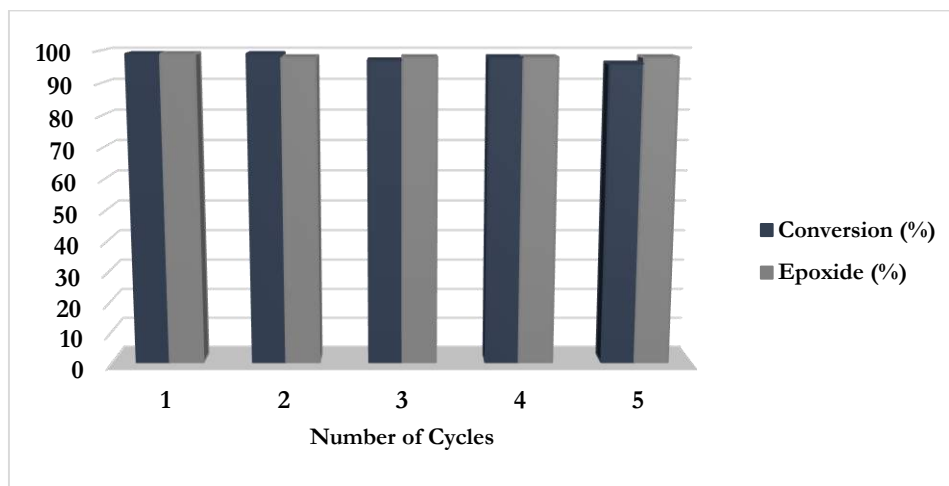


Figure 4.7 – Recycling experiments of $\text{MNP@SiO}_2\text{-NH-17Mn}$ in the cyclooctene epoxidation process with O_2 .

$\text{MNP@SiO}_2\text{-NH-17Mn}$ as a catalyst showed excellent reusability in 5 consecutive reaction cycles, without loss of activity or selectivity for epoxide formation. Therefore, besides its high activity and selectivity, this catalytic unit shows a high stability, with no catalyst leaching being observed as demonstrated by UV-Vis monitoring of the crude reaction using the recycling experiments 1 and 5 (**Figure 4.8**). These findings were confirmed by induced coupling plasma (ICP) analysis, which showed a negligible metal content in the reaction mixture ($< 0.1 \text{ mg mL}^{-1}$).

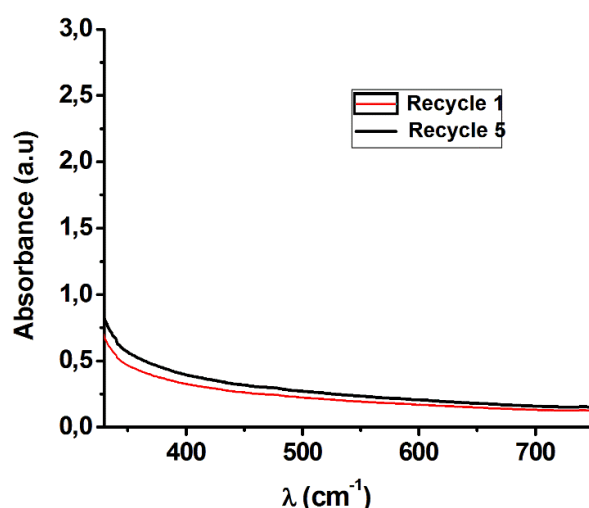


Figure 4.8 – UV-Vis spectra of the crude mixture using $\text{MNP@SiO}_2\text{-NH-17Mn}$ as catalyst, after recycles 1 and 5.

The higher catalyst stability observed when **17Mn** was covalently immobilised onto magnetite nanoparticles was also previously verified by other authors,^[31, 32] and

may be attributed to the beneficial influence of the support in preventing the formation of catalytically inactive μ -oxo-dimeric metalloporphyrin species.^[33]

4.2.2 Scale-up and Experimental Setup for the Recovery of Isobutyric Acid

With a view to develop an oxidative process with potential industrial applications, a reaction scale-up (18x) was performed using the Mn(III)-porphyrin magnetite nanocomposite **MNP@SiO₂-NH-17Mn** as a catalyst. For the one-gram scale cyclooctene oxidation reaction, 99% conversion and 98% selectivity for epoxide were obtained after 3.5 h (TON = 10532) (**Table 4.2, entry 3**). Aiming at achieving a sustainable process, an experimental setup was developed through a simple work-up, which yielded the epoxide with the concomitant recovery of isobutyric acid (**29**), formed during the oxidation reaction (**Figure 4.9**). This showed to be a powerful chemical platform used as raw material for many industrial applications, namely for the production of methyl methacrylate (2.2 million ton per year) and of sucrose acetate isobutyrate (100 000 ton per year).^[34]

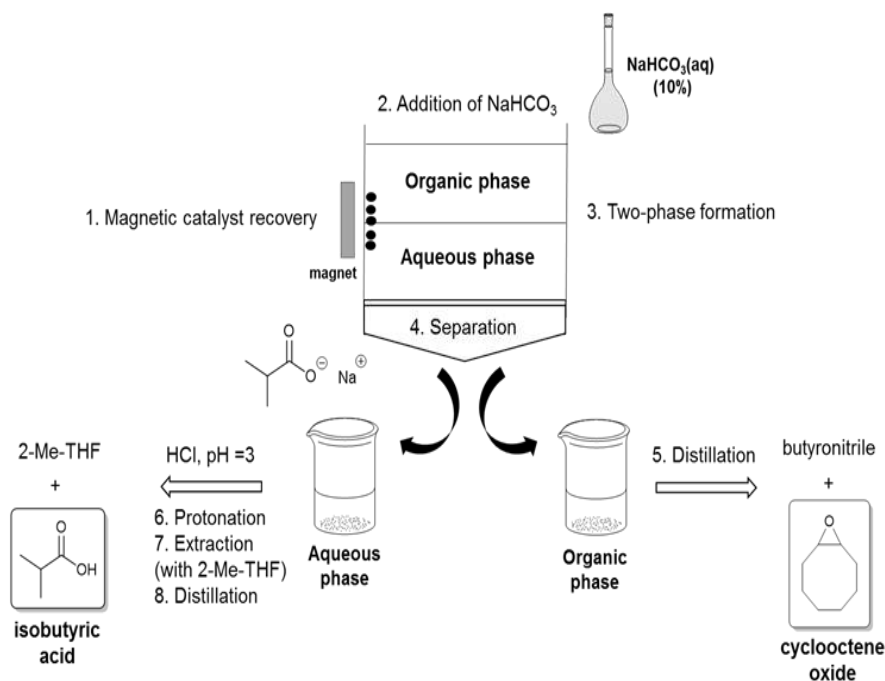


Figure 4.9 – Experimental setup for the cyclooctene oxidation reaction's work-up, yielding cyclooctene oxide (**28**) concomitantly with isobutyric acid (**29**).

The replacement of acetonitrile by a water immiscible analogue as the epoxidation solvent (butyronitrile) was carried out, and similar results were obtained (99% conversion and >98% selectivity for epoxide). The hybrid magnetic catalyst **MNP@SiO₂-NH-17Mn** was recovered in the glass vessel's wall (using an external magnet field), followed by decantation of the liquid mixture into a funnel (**Figure 4.9, step 1**). A sodium hydrogen carbonate saturated aqueous solution (NaHCO₃) was then added into the reaction mixture, leading to the formation of two phases (**Figure 4.9, step 2**), wherein the epoxide remains in the organic phase (butyronitrile) while isobutyric acid stays in the aqueous phase in the ionised form as a sodium salt (**Figure 4.9, step 3**). The cyclooctene epoxide (**28**) was then obtained (with 99% yield, *ca.* 1 gram) by simple distillation (**Figure 4.9, step 4**), whereas the aqueous phase was treated with a 33% HCl solution to adjust the pH at 3.0. Finally, extraction with 2-methyltetrahydrofuran was carried out and, after distillation; the target isobutyric acid (**29**) was obtained in up to 95% yield (**Figure 4.9, step 5**). Thus, the sustainability of the overall process was ensured by the efficient recovery of isobutyric acid, further isolated and characterised by ¹H-NMR (**Figure 4.10**), which shows a singlet signal at $\delta = 11.07$ ppm attributed to one proton of the carboxylic group and two singlet signals at $\delta = 1.17$ and 1.15 ppm corresponding to methyl groups and a multiplet signal at $\delta = 2.55$ corresponding to Ha. Thus, this epoxidation process allows isobutyric acid recovery and reutilization in several industrial chemical processes as described by Zhang and coworkers.^[34]

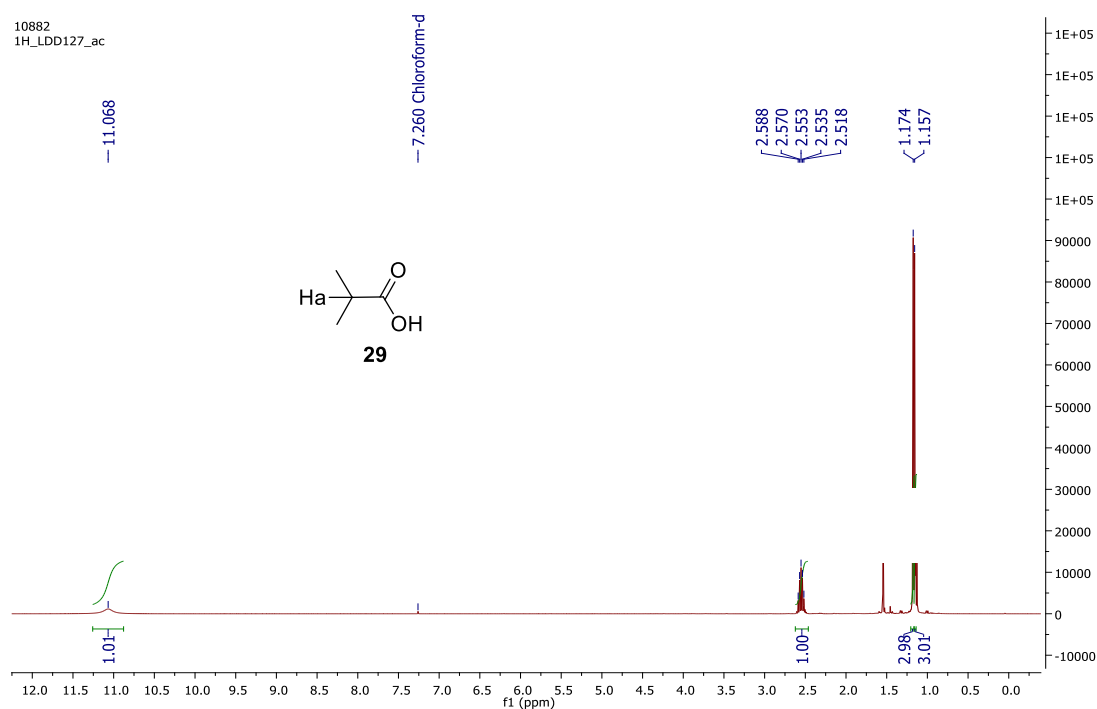

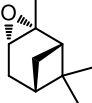
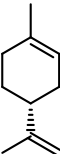
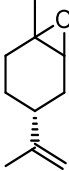
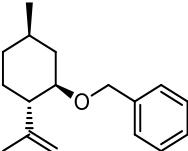
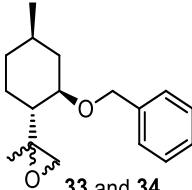


Figure 4.10 – ^1H -NMR spectrum of isobutyric acid (**29**).

In order to evaluate the versatility of the catalytic epoxidation methodology and to obtain biologically active epoxides, the epoxidation reaction of various relevant terpenes was carried out, namely α -pinene, (+)-limonene and (–)-isopulegol benzyl ether (**32**), using **MNP@SiO₂-NH-17Mn** as catalyst, isobutyraldehyde as co-reductant and butyronitrile as solvent, for 2 h, at 25 °C. The results are presented in **table 4.3**.

Table 4.1 – Epoxidation reaction of terpenes catalysed by **MNP@SiO₂-NH-17Mn^a**.

Entry	Substrate	Conversion ^b (%)	Product (yield, %)
1 ^a		99	 30 (96%)
2 ^a		99	 31 (95%)
3 ^{a,c}		99	 33 and 34 (96%)

^a **Reaction conditions:** MNP@SiO₂-NH-17Mn (4.7×10^{-5} mmol Mn), substrate (0.5 mmol) isobutyraldehyde (2.5 mmol), butyronitrile (2 mL), chlorobenzene (0.19 mmol), O₂ bubbling, 25 °C, 2 h.

^b Conversion calculated by GC, based on the substrate, using chlorobenzene (1.95×10^{-1} mmol) as internal standard. Selectivity for epoxide formation was $\geq 97\%$ in all cases. All data were reproduced at least twice and reported as an average. ^c In order to avoid parallel reactions between the hydroxyl group of (–)-isopulegol with the new one functionality group, we carried out the protection reaction of hydroxyl with a benzyl group (described in section 4.3).

Remarkably, the novel hybrid heterogeneous magnetic catalyst **MNP@SiO₂-NH-17Mn** was effective in promoting the selective epoxidation of natural-based substituted olefins, such as α -pinene, (+)-limonene, (–)-isopulegol benzyl ether (**Table 4.3, entries 1-3**) showing excellent conversions (85-99%) and very high selectivity for epoxides ($\geq 97\%$). The epoxidation of α -pinene was easily promoted, giving the corresponding epoxide (**30**) with conversion (99%) and yield (96%) (**Table 4.3, entry 1**). It should be highlighted that the epoxidation process of limonene was 100% selective for the internal C=C double bond, affording exclusively the corresponding epoxide (**31**) isolated in 95% yield (**Table 4.3, entry 2**). The epoxidation of (–)-isopulegol benzyl ether yielded the respective epoxides products (**33** and **34**) in 96% (**Table 4.3, entry 3**). In addition, it is worth mentioning that an

efficient recovery of isobutyric acid (**29**) was achieved in all cases. All epoxidation products were fully characterised by ^1H - and ^{13}C -NMR and these data are presented in the experimental section (**Chapter 5**).

4.3 (–)-Isopulegol Benzyl Ether Derivatives as Potential Anticancer Agents against Osteosarcoma

It is well known that a wide number of compounds isolated from natural products such as terpenes, have a wide array of anticancer effects.^[35, 36] For instance, (–)-isopulegol a type of monoterpene (**Figure 4.11**), approved by Food and Drug Administration (FDA) as a food additive for human consumption,^[37] was described as a useful compound in cosmetic, perfume and fragrances industries. Its use is based on due to its flavour and non-toxic properties showing low oral/dermal toxicity in humans and its use worldwide is about of 1-10 metric tonnes per annum.^[38]

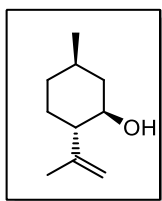


Figure 4.11 – Structure of (–)-isopulegol.

In order to obtain a family of (–)-isopulegol-based terpene as potential antiosteosarcoma agent, we promoted the design and structural transformation of the (–)-isopulegol using different catalytic approaches namely epoxidation, hydroformylation and CO_2 cycloaddition reaction to modulate its anticancer properties.

In this section, we described the epoxidation of (–)-isopulegol derivative to obtain the respective epoxide as a promising biologically active compound and as an important intermediate for drug design (**Figure 4.12; Via A**). Moreover, the hydroformylation reaction was used as a different tool to obtain the respective (–)-isopulegol derivative aldehyde (**Figure 4.12; Via B**) and the epoxide ring-opening

reaction to (–)-isopulegol derivative using an amine as nucleophile (**Figure 4.12; Via C**), yielding the corresponding amino alcohol.

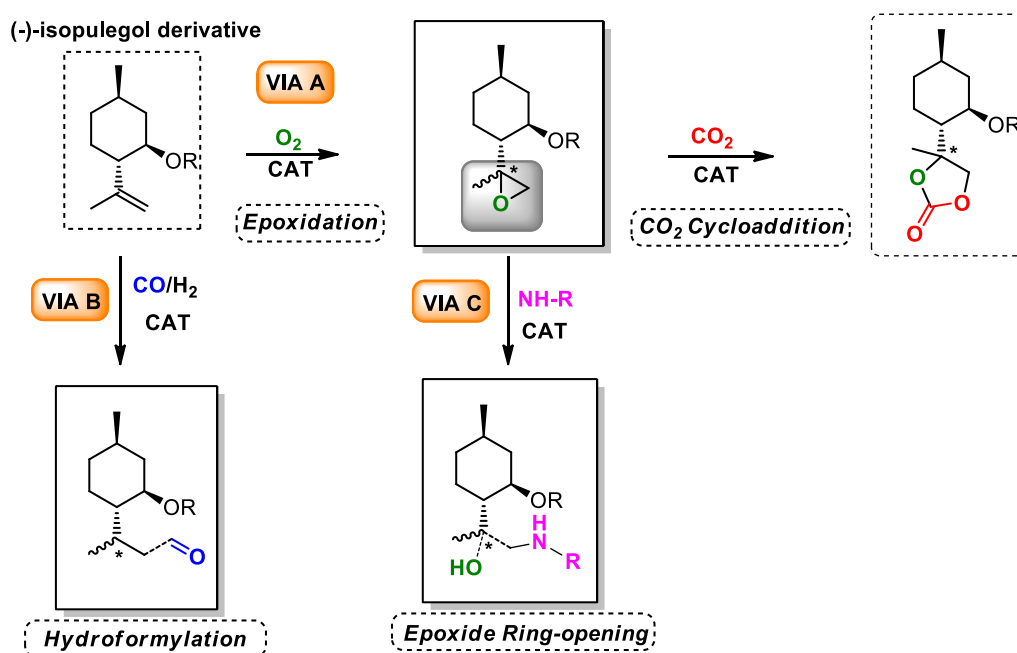


Figure 4.12 – Design and synthesis of (–)-isopulegol derivatives using catalytic processes.

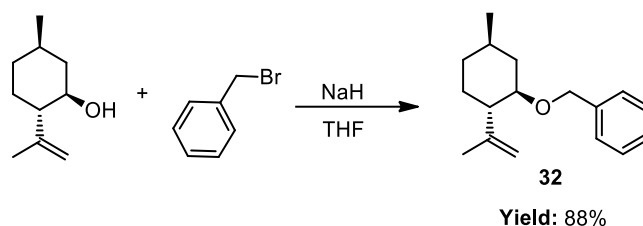
The results and discussion regarding the synthesis and characterisation of the (–)-isopulegol derivatives and the antiosteosarcoma evaluation of newly synthesised (–)-isopulegol benzyl ether epoxide diastereomers on a human osteosarcoma cell line (MG-63) are presented and discussed in the next sections.

The preparation of (–)-isopulegol benzyl carbonate is currently underway in Catalysis & Fine Chemistry Group, Department of Chemistry – University of Coimbra.

4.3.1 Protection Reaction of (–)-Isopulegol

In order to avoid parallel reactions between the hydroxyl group with the new functionality groups formed, we carried out the protection of (–)-isopulegol hydroxyl group with a benzyl (**Scheme 4.3**). In a typical procedure, (–)-isopulegol was dissolved in dry THF and NaH was added. The reaction mixture was kept under

stirring in reflux. Then, benzyl bromide was added dropwise and the reaction's progress was followed by thin layer chromatography (TLC).



Scheme 4.3 – Protection of (–)-isopulegol with a benzyl group (**32**).

Upon complete conversion of the starting material, the reaction crude was extracted with ethyl ether, the organic phase was dried with anhydrous sodium sulphate and the solvent was evaporated under reduced pressure. After purification by silica gel column chromatography, using a mixture of *n*-hexane/ethyl acetate (9:1) as eluent, the product (–)-isopulegol benzyl ether (**32**) was isolated in 88% yield (1.39 g; 5.72 mmol). The (–)-isopulegol benzyl ether (**32**) was characterised by ¹H- and ¹³C-NMR and GC-MS and the characterisation data is described in experimental section (**Chapter 5**).

4.3.2 Synthesis of (–)-Isopulegol Benzyl Ether Epoxides

Considering the high interest in promoting the development of new and more effective antiosteosarcoma drugs using an efficient and eco-friendly approach, the heterogeneous epoxidation methodology, using O₂ as green oxidant, was selected to promote the epoxidation of (–)-isopulegol benzyl ether (**32**).

Thus, the epoxidation of (–)-isopulegol benzyl ether (**32**) using **MNP@SiO₂-NH-17Mn** as catalyst, O₂ (bubbling) as oxidant, at room temperature (25 °C), was carried out and the recycling experiments results are presented in **figure 4.13**. Between each cycle, the solid material was washed with CH₃CN (3x) and subsequent solvent removal, by drying under vacuum at 60 °C, for 12 h, and the **MNP@SiO₂-NH-17Mn** was reused for the next cycle.

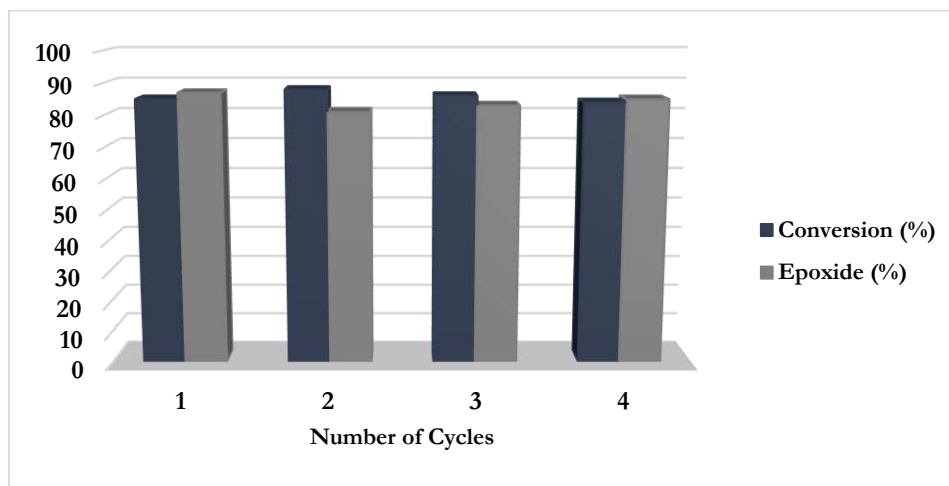
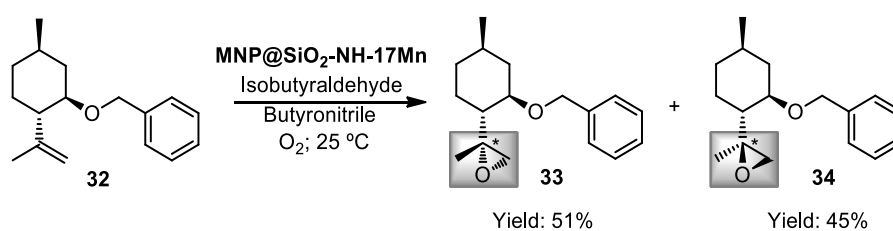


Figure 4.13 – Recycling experiments of **MNP@SiO₂-NH-17Mn** in (–)-isopulegol benzyl ether (**32**) epoxidation with O₂.

MNP@SiO₂-NH-17Mn exhibited an excellent reusability, no loss of activity or selectivity for (–)-isopulegol benzyl ether epoxides, after 4 consecutive runs (**Figure 4.13**). Then, diastereoisomers **33** and **34** of (–)-isopulegol benzyl ether epoxides were separated by silica gel column chromatography, using a mixture of ethyl acetate/*n*-hexane (1:4) as eluent. After evaporation of the solvent obtaining both diastereomers **33** and **34** (**Scheme 4.4**) in combined isolated yields of 51% and 45%, respectively.



Scheme 4.4 – Catalytic epoxidation of (–)-isopulegol benzyl ether catalysed by **MNP@SiO₂-NH-17Mn**.

Each diastereomers **33** and **34** was characterised by ¹H-, ¹³C-NMR and 2D NMR techniques (COSY, NOESY, HMQC and HMBC) and the spectra of ¹H, ¹³C NMR and NOESY for both diastereomers are presented and discussed below (**Figures 4.14-4.19**).

The ¹H-NMR spectrum of diastereomer **33** in CDCl₃, at room temperature (**Figure 4.14**), shows two doublets at δ = 2.76 ppm and δ = 2.68 ppm, assigned to

the epoxide protons (**H9**). In addition, the multiplet at $\delta = 4.76$ - 4.80 from alkene protons of the (-)-isopulegol benzyl ether was not observed. Moreover, new one signal at $\delta = 56.8$ ppm in ^{13}C -NMR spectrum of diastereomer **33** (**Figure 4.15**) were observed and the specific signals at $\delta = 147.9$ ppm of alkene carbon were not evidenced. From this analysis, we observed the epoxide formation through epoxidation reaction of (-)-isopulegol benzyl ether (**32**) using **MNP@SiO₂-17Mn** as catalyst and O₂ as oxidant.

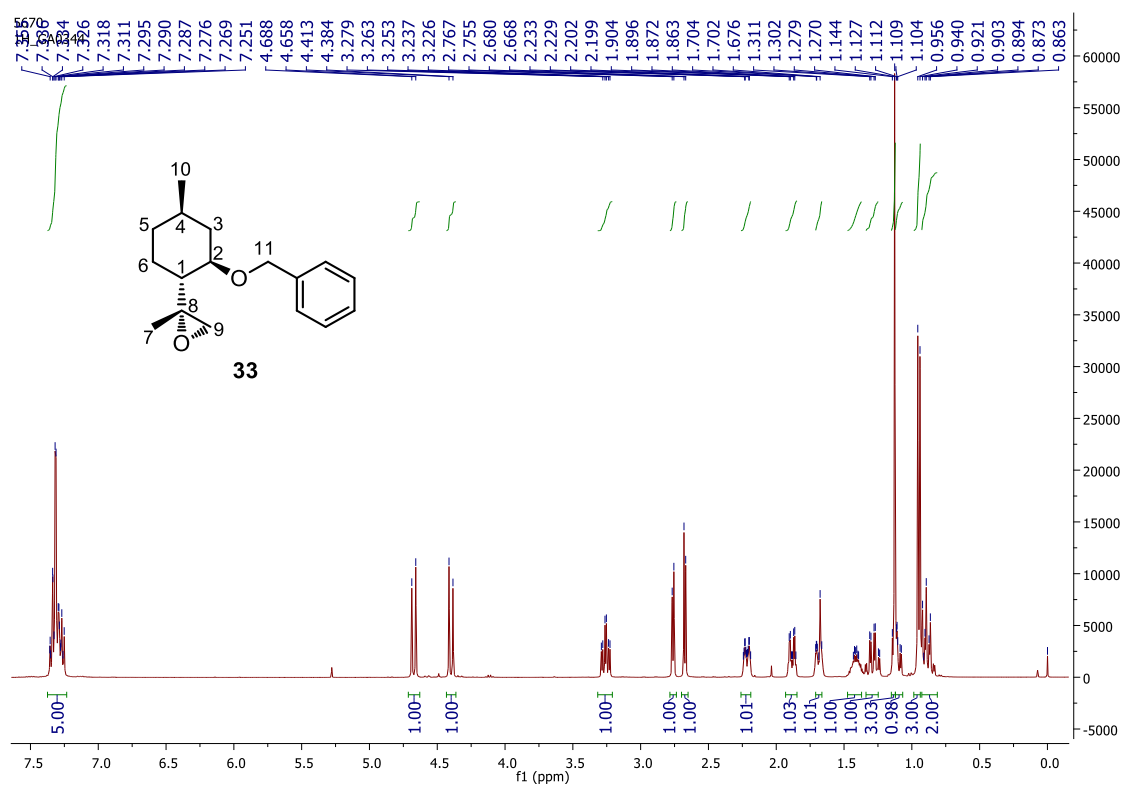


Figure 4.14 – ^1H -NMR spectrum of diastereomer **33**.

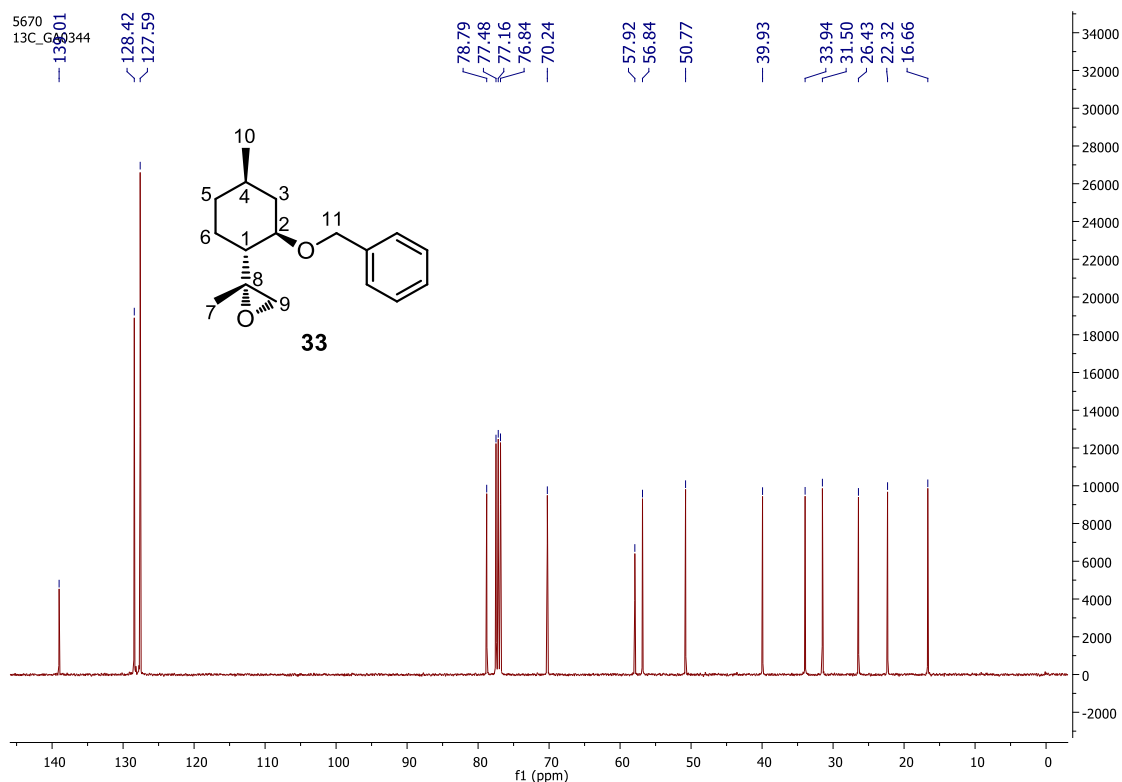


Figure 4.15 – ^{13}C -NMR spectrum of diastereomer **33**.

The stereochemistry of each one diastereomer assigned based on NOEs between relevant protons (H1-H7(CH_3)). NOESY spectra of diastereomer **33** shows an interaction between H1-H7(CH_3), indicating a proximity between these protons, allowing propose its stereochemistry.

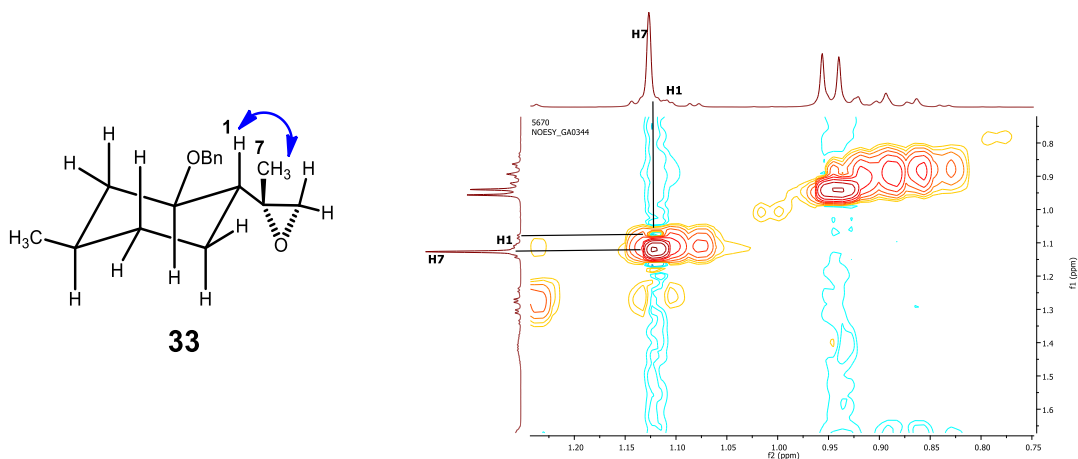


Figure 4.16 – NOESY NMR spectrum of diastereomer **33**.

From the analysis of ^1H - and ^{13}C -NMR spectra of diastereomer **34** (Figures 4.17 and 4.18), we observed at $\delta = 2.76$ ppm a doublet signal assigned to the epoxide protons (H9). On other hand, a multiplet signal at $\delta = 4.76$ -4.80 from alkene protons of the (-)-isopulegol benzyl ether (**32**) was not observed. Furthermore, a signal at $\delta = 52.0$ ppm in ^{13}C -NMR spectrum (Figure 4.18) was observed, whereas at $\delta = 147.9$ ppm was not observed, typical of alkene carbon. In sum, we also observed the epoxide formation through the ^1H - and ^{13}C -NMR spectra of diastereomer **34**.

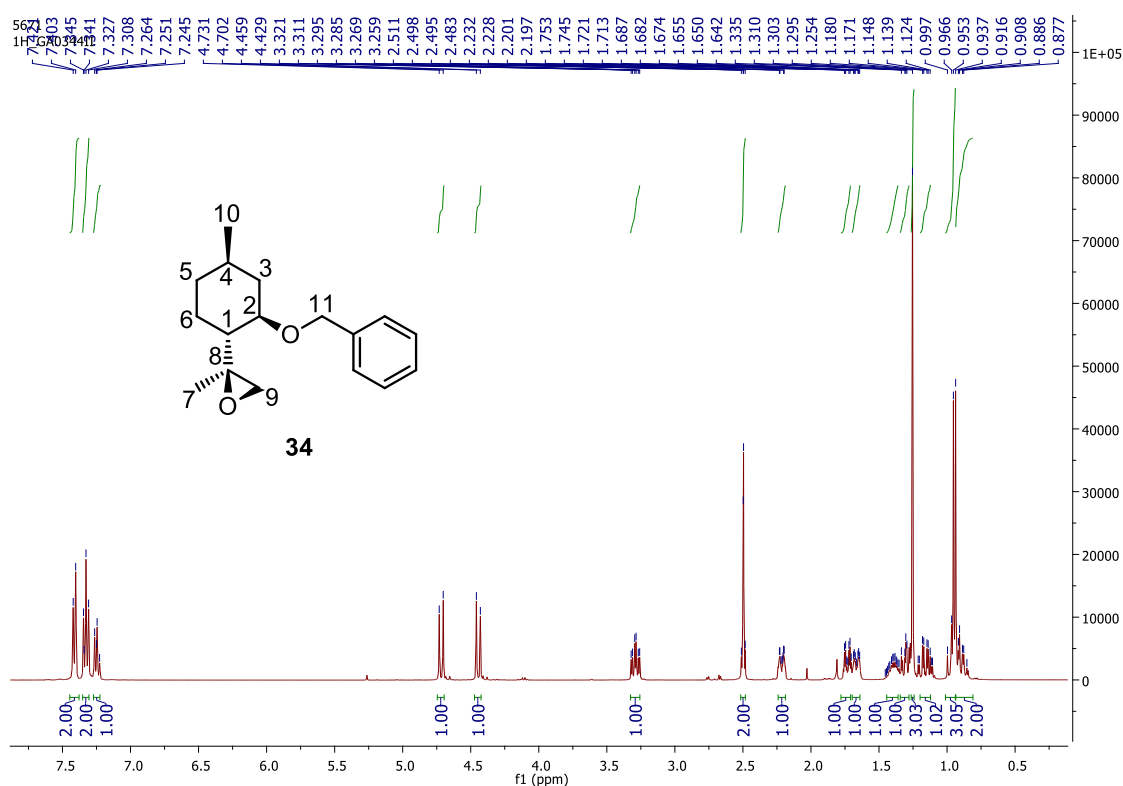


Figure 4.17 – ^1H -NMR spectrum of diastereomer **34**.

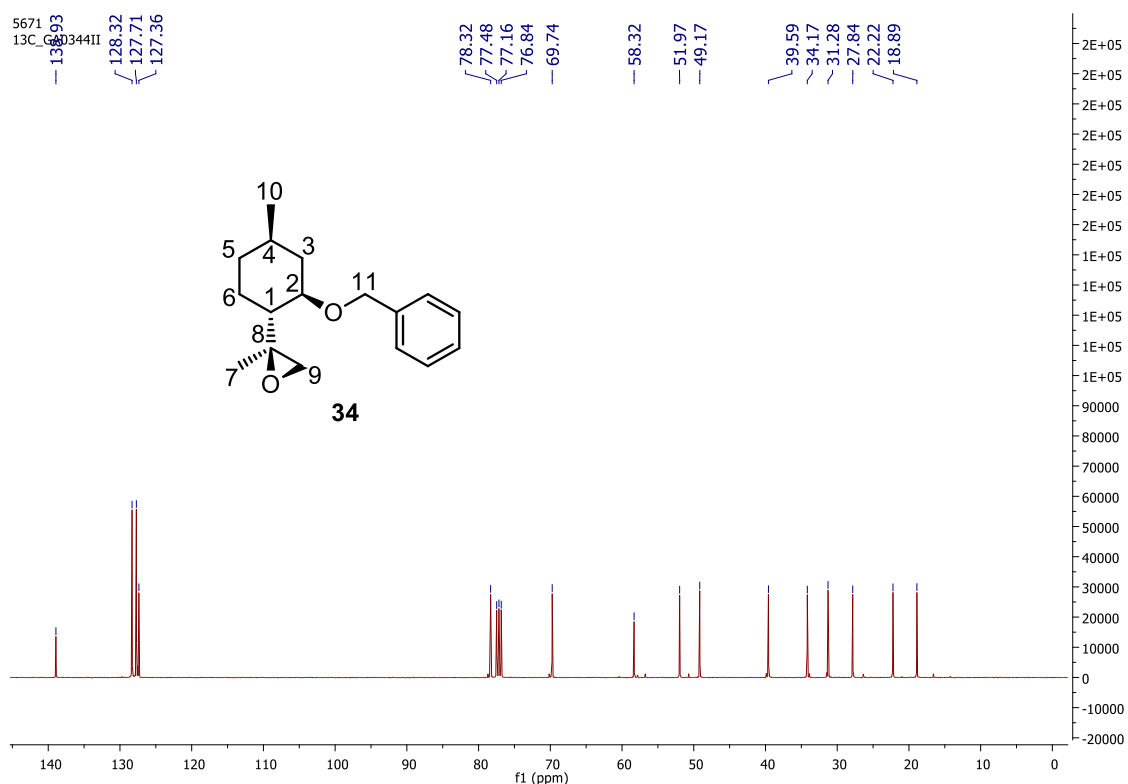


Figure 4.18 – ^{13}C -NMR spectrum of diastereomer **34**.

To determine the stereochemistry of the diastereoisomers **33** and **34**, as mentioned above, we used the interaction between H1-H7(CH₃) as reference. In this case, the NOE H1-H7 (CH₃) was not observed (Figure 4.19) for the diastereoisomer **34**, which allowed us to propose its stereochemistry.

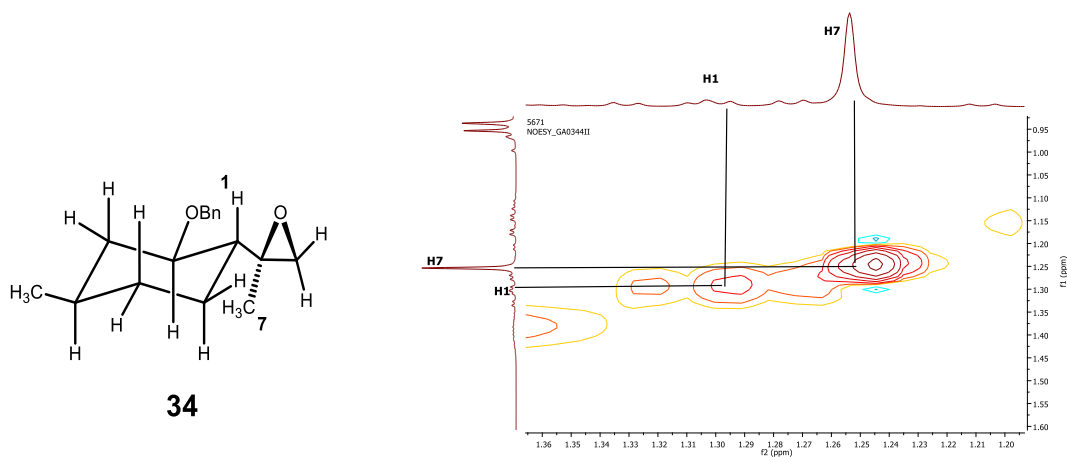
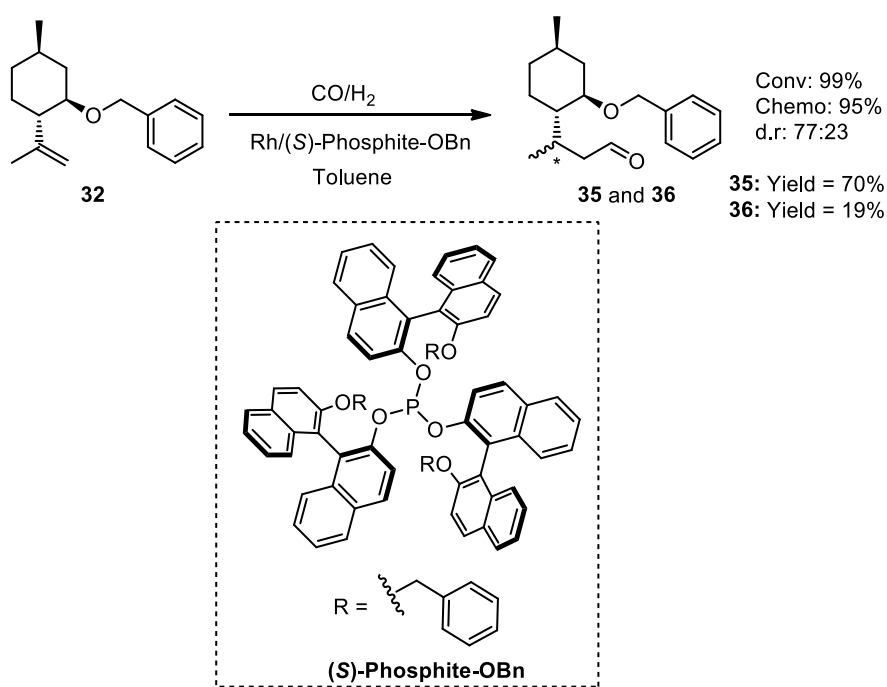


Figure 4.19 – NOESY NMR spectrum of diastereomer **34**.

4.3.3 Hydroformylation of (–)-Isopulegol Benzyl Ether

Regarding our great interest in the preparation of a family of (–)-isopulegol benzyl ether derivatives for development of anticancer agents, the (–)-isopulegol benzyl ether (**32**) was submitted to hydroformylation reaction using Rh(I)/Tris[(*S*)-2'-(benzyloxy)-1,1'-binaphthyl-2-yl]phosphite (provided by Rui Carrilho from Catalysis & Fine Chemistry Group – Department of Chemistry – University of Coimbra) as catalyst (**Scheme 4.5**). In a typical experiment, the autoclave was charged with (*S*)-phosphite-OBn ligand, [Rh(acac)(CO)₂] and toluene as solvent. The reactor was then pressurised with an equimolar mixture of CO/H₂ (25 bar), and the mixture was stirred along 1 h, at 85 °C. After this incubation time, (–)-isopulegol benzyl ether (**32**), dissolved in toluene, was added *via* cannula, and the reaction was conducted at 85 °C, along 12 h, under magnetic stirring. The reaction's progress was analysed by GC.



Scheme 4.5 – Hydroformylation of (–)-isopulegol benzyl ether (**32**).

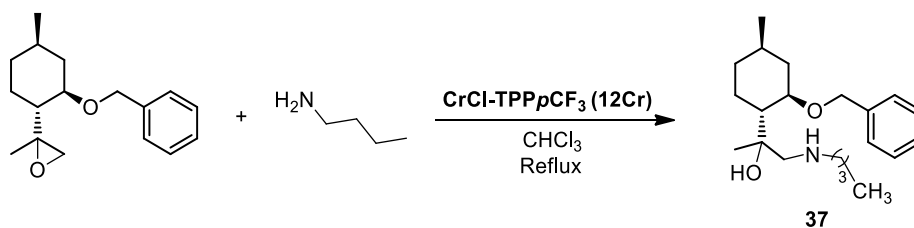
Reaction conditions: (–)-isopulegol benzyl ether: (0.25 mmol); [Rh(acac)(CO)₂] (0.01 mmol); (*S*)-Phosphite-OBn (0.05 mmol); toluene (5 mL); *P* = 25 bar CO/H₂ (1:1).

The catalytic system (Rh(I)/(*S*)-phosphite-OBn) provided 99% conversion in 12 h, with 95% of chemoselectivity for aldehydes **35** and **36**, in a diastereomeric ratio of 77:23 determined by GC. When the reaction was performed with [Rh(acac)(CO)₂]

and the absence of phosphite ligand, no conversion was observed after 12 h, under the same reaction conditions, which clearly evidence of bulk monophosphite the decisive to generate an active catalytic species for hydroformylation as previously observed in our group.^[39, 40] At the end, the autoclave was cooled to room temperature and slowly depressurised. Then, the solvent was evaporated and the crude mixture was purified by column chromatography in silica gel, using a mixture of *n*-hexane/ethyl acetate (4:1) as eluent, affording the isomeric aldehydes **35** and **36**, 70% and 19% yields, respectively. Their full characterisation were carried out by ¹H- and ¹³C-NMR and GC-MS. The characterisation data are described in experimental section (**Chapter 5**). The evaluation of the two-diastereomeric aldehydes as antiosteosarcoma agents is one of our proposal for future work.

4.3.4 Epoxide Ring-opening of (–)-Isopulegol Benzyl Ether Epoxide

In order to obtain the corresponding amine alcohol derivative, epoxide ring-opening reaction of (–)-isopulegol benzyl ether epoxide (**33** and **34**) was carried out using butylamine as nucleophile (**Scheme 4.6**). In a typical reaction, (–)-isopulegol benzyl ether epoxide (50 mg; 0.192 mmol), CrCl-TPPpCF₃ (**12Cr**) (37 mg; 0.0384 mmol) as catalyst, butylamine (14 mg; 0.192 mmol) as nucleophile in chloroform (3 mL) was kept under reflux/stirring and the reaction's progress was followed by TLC using *n*-hexane/ethyl acetate (9:1) as eluent.



Scheme 4.6 – Catalytic epoxide ring-opening reaction of (–)-isopulegol benzyl ether epoxide.

At the end, GC-MS analysis of crude mixture was performed showing full conversion of (–)-isopulegol benzyl ether epoxide, with good selectivity (70%) for amino alcohol derivative (**37**) $m/z = 334.3$ [M+H]⁺. The evaluation of the amino

alcohol derivative as antiosteosarcoma agent is also one of our proposal for future work.

4.4 Anticancer Activity of (-)-Isopulegol Benzyl Epoxides against Human Osteosarcoma Cells

In order to evaluate the activity of (-)-isopulegol benzyl ether epoxides (**33** and **34**) against a human osteosarcoma cell line (MG-63) two complementary biological colorimetric assays were used, namely MTT (3-(4,5-dimethylthiazol-2-yl)-2,5-diphenyltetrazolium bromide) and SRB (Sulforhodamine B) (**Figure 4.20**), in order to assess the effect of each epoxide-isopulegol diastereomer (**33** and **34**).

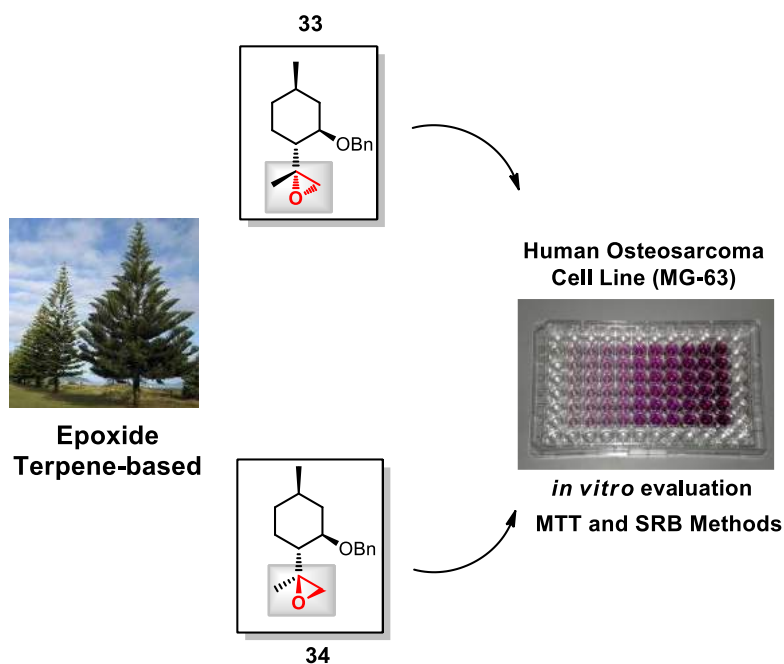


Figure 4.20 – Evaluation of each epoxide-isopulegol diastereomer (**33** and **34**) against the human osteosarcoma cell line (MG-63).

The MTT colorimetric assay used in this work was first reported by Mossmann in 1983.^[41] It is based on the reduction of the water soluble 3-(4,5-dimethylthiazol-2-yl)-2,5-diphenyltetrazolium bromide (MTT) (yellow) yielding insoluble formazan (1-(4,5-dimethylthiazol-2-yl)-3,5-diphenylformazan) crystals (violet), through the cleavage of the tetrazole ring catalysed by mitochondrial NADH-dependent dehydrogenases, which are present in metabolically active cells^[42] (**Figure 4.21**).

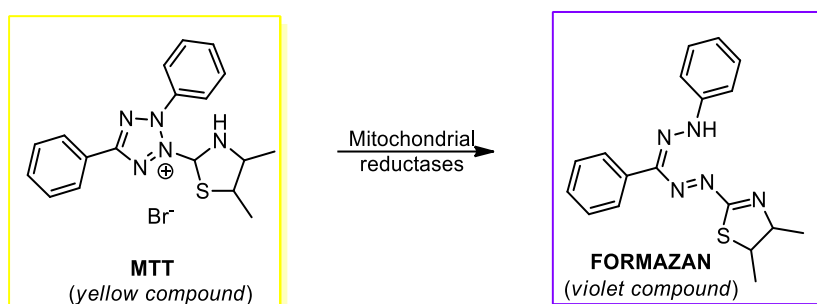


Figure 4.21 – Reduction reaction of MTT to formazan, catalysed by mitochondrial NADH-dependent dehydrogenases.

In this assay, the formazan formed from MTT metabolisation by mitochondrial reductases is quantified spectrophotometrically ($\lambda_{\text{max.}} = 570 \text{ nm}$). In other words, the amount of formazan is directly proportional to the number of viable cells.^[43] In this sense, the MTT method is a quick, accurate and inexpensive method to assess the percentage of viable cells. In this work, the MTT methodology was used to determine cell viability translated into IC_{50} values for each epoxide-isopulegol diastereomer (**33** and **34**) (IC_{50} = inhibition concentration 50, representing the compound concentration corresponding to a 50% reduction of cell viability).

With a view to evaluate cell density, the SRB assay was also used for each epoxide-isopulegol diastereomer. This methodology was first reported by Skehan^[44] in 1989 and is based on the ability of the sulforhodamine B dye (**Figure 4.22**) to bind (electrostatically) to protein basic amino acid residues. Thus, the SRB dye binds to proteins of trichloroacetic (TCA)-fixed cells in acid conditions, being solubilised by bases such as Tris (tris-hydroxymethyl-aminomethane), before optical density measurement.^[45]

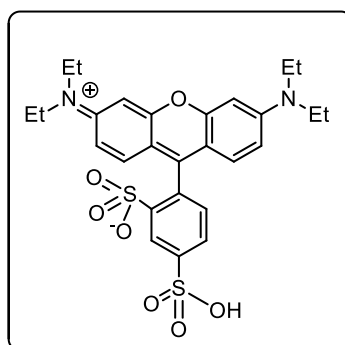


Figure 4.22 – Structure of the sulforhodamine B dye.

This colorimetric assay is stable and allows quantification of cell density, thus yielding quantitative information on cell proliferation upon spectrophotometric measurement ($\lambda_{\text{m\acute{a}x.}} = 540 \text{ nm}$).

As described above, the antitumor effect of the two newly synthesised (–)-isopulegol epoxide diastereomers (**33** and **34**) was assessed through the MTT and SRB assays to determine cell viability, and cell proliferation.

Both diastereomers showed to be moderately active towards the human osteosarcoma MG-63 cell line regarding their impact on cell-growth and viability, with IC_{50} values (at 48 hours of drug exposure) of $114.8 \mu\text{M}$ (SRB)/ $249.8 \mu\text{M}$ (MTT) and $104.0 \mu\text{M}$ (SRB)/ $158.2 \mu\text{M}$ (MTT), respectively for isomers **33** and **34** (Figure 4.23).

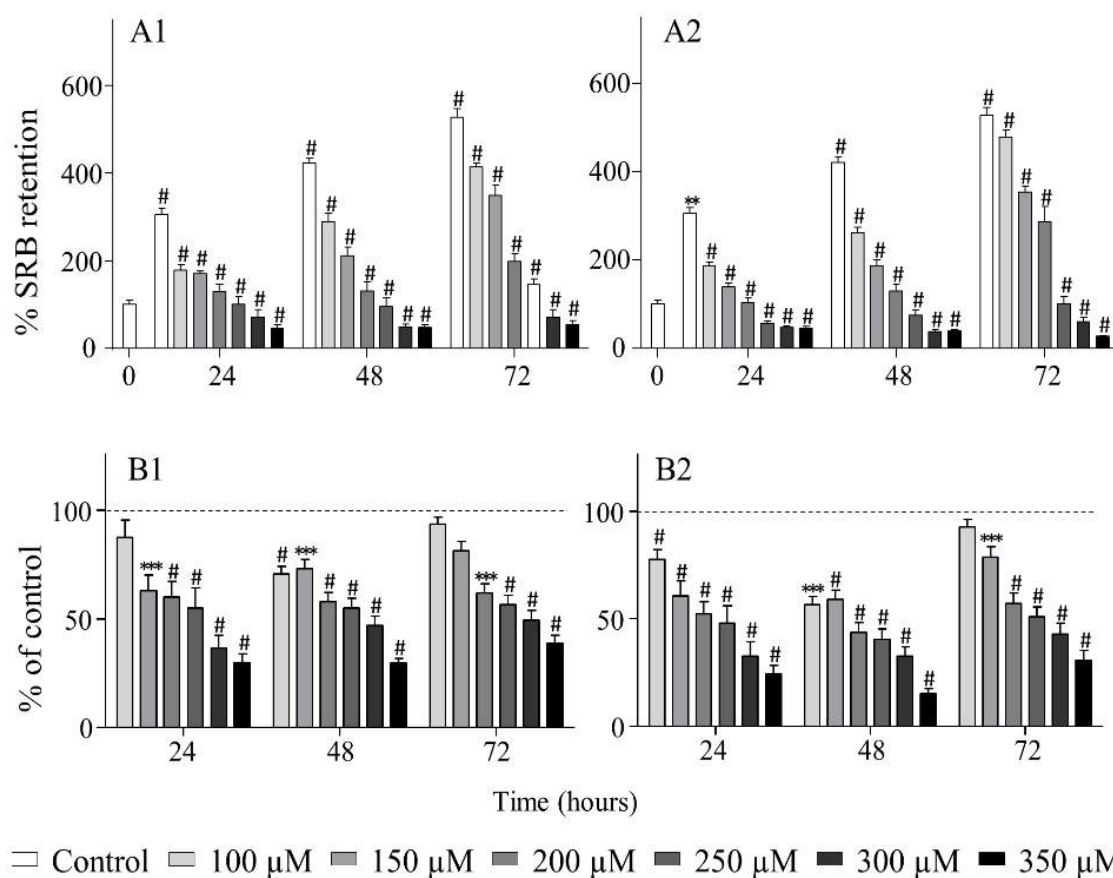


Figure 4.23 – Dose and time-dependent response plots of the effect of the epoxide diastereomers **33** (A1, B1) and **34** (A2, B2) on cell viability in the MG-63 cell line, for dosages between 100 and 350 μM . The results obtained by the SRB (A1, A2) and MTT (B1, B2) assays are represented as a percentage of the control (cells treated with the DMSO vehicle). The data are the mean \pm SEM of the values obtained from 3 independent experiments ($n = 3$), carried out in triplicate. ** $p < 0.01$, *** $p < 0.001$, # $p < 0.0001$ vs the control.

These values are significantly lower than those published for similar compounds, namely for limonene (extracted from mandarin oil) against human lung adenocarcinoma (A549) and hepatocarcinoma (HepG2) cells – IC₅₀ equal to 586 and 889 μM,^[46] respectively (**Figure 4.24**).

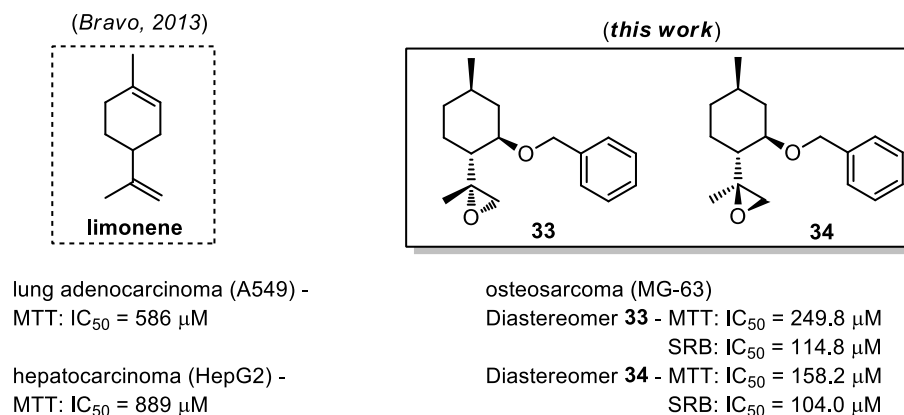


Figure 4.24 – IC₅₀ values for the presently investigated epoxide-isopulegol diastereomers (**33** and **34**) towards osteosarcoma (MG-63) compared to those reported for limonene against lung adenocarcinoma (A549) and hepatocarcinoma (HepG2).

In addition, no significant variation was observed between the antineoplastic activity of each of the two diastereomers. This is in agreement with previous studies on the stereochemistry dependence of the anticancer potency, namely for perillyl alcohol,^[47] tubulysins,^[48] or enigmol.^[49] In fact, although the absolute stereochemistry of a compound may affect its biological activity (with several reported cases), the most relevant structure-activity relationships (SAR's) rely on the specific structural scaffold and functional groups (pharmacophores) of the molecule.

Despite the scarce knowledge on the precise molecular mechanisms underlying the anticancer activity of monoterpenes, some reported studies reveal an impact on key regulatory signal transduction proteins, particularly from the Ras family that regulate fundamental processes such as cell growth, differentiation and survival. Actually, reduced Ras levels (due to decreased up-regulation) were measured in distinct cell lines in the presence of monoterpenes,^[47] with a strong effect on protein synthesis and degradation, and therefore on cell proliferation and viability.

4.5 Conclusions

The hybrid magnetic Mn(III)-porphyrin nanocomposite **MNP@SiO₂-NH-17Mn** was efficiently used as a catalyst in the epoxidation reaction of terpenes (α -pinene, limonene and (–)-isopulegol benzyl ether), using O₂ as a non-pollutant oxidant and isobutyraldehyde as an electron donor (co-reductant). A high catalytic activity and selectivity (similar to homogeneous systems) was found, coupled to a higher stability and recyclability. Furthermore, the magnetic catalyst was easily recovered and reused in five consecutive cycles, without any loss of activity or selectivity. Moreover, the effective recovery of isobutyric acid paves the way for the development of sustainable processes regarding reutilization and application in the bulk chemical industry. The potential applicability and versatility of this catalytic method were demonstrated by its scalability (gram scale). In sum, this methodology constitutes a promising synthetic approach for the preparation of potentially bioactive compounds *via* olefin epoxidation, using O₂ as the oxidant and tetrapyrrolic macrocycle-based hybrid magnetic nanocomposites as reusable catalysts. Regarding the hydroformylation of (–)-isopulegol benzyl ether, the catalytic system (Rh(I)/(*S*)-OBn-monophosphite) demonstrated to be the first example concerning the hydroformylation of highly substituted olefins, of the terpene family, yielding potentially bioactive aldehydes.

Regarding the utilization of epoxide terpene-based derivatives as potential anticancer agents, namely against human osteosarcoma (MG-63 cell line), the two isopulegol epoxide diastereomers were shown to be moderately active regarding both cell-growth and viability. In fact, the IC₅₀ values obtained for these compounds, between 100 and 250 μ M, are quite lower than those previously reported for similar monoterpenes towards different cancer cell lines. In addition, the stereochemical characteristics of the (–)-isopulegol epoxides was found to have a minor effect on its antitumor activity, which is primarily attributed to structural features rather than to optical properties. Although still poorly understood, a suggested mechanism for this cytotoxic activity is related to signal transduction proteins (mainly Ras), that directly affect cell growth and differentiation. The results presently obtained allows us to conclude that these epoxide isomers may be promising agents against human

osteosarcoma, in sole administration. Combined therapeutic schemes with conventional drugs (*e.g.* Doxorubicin or Methotrexate) are envisaged, as a way to increase cancer cell sensitization and enhance therapeutic efficacy.

4.6 References

- [1] P. M. Dewick, *Medicinal Natural Products: A Biosynthetic Approach*, Wiley, West Sussex, UK, **2009**.
- [2] G. M. Cragg, D. G. I. Kingston, D. J. Newman, *Anticancer Agents from Natural Products* Crc Press-Taylor & Francis Group, Boca Raton, **2012**.
- [3] G. M. Cragg, D. J. Newman, *Developments and Future Trends in Anticancer Natural Products Drug Discovery*, Crc Press-Taylor & Francis Group, Boca Raton, **2012**.
- [4] G. Appendino, G. Fontana, F. Pollastro, *Natural Products Drug Discovery*, Elsevier Science Bv, Amsterdam, **2010**.
- [5] A. T. Nguyen, P. Duez, *Cytotoxic Anticancer Drugs from Medicinal Plants*, Nova Science Publishers, Inc, Hauppauge, **2009**.
- [6] K. Chen, Y. Ishihara, M. M. Galan, P. S. Baran, *Tetrahedron* **2010**, *66*, 4738-4744.
- [7] C. Oberhauser, V. Harms, K. Seidel, B. Schroder, K. Ekramzadeh, S. Beutel, S. Winkler, L. Lauterbach, J. S. Dickschat, A. Kirschning, *Angewandte Chemie-International Edition* **2018**, *57*, 11802-11806.
- [8] R. D. Gaikwad, S. S. Kabiraj, S. V. Bhat, *Flavour and Fragrance Journal* **2016**, *31*, 350-355.
- [9] J. G. da Silva, C. G. Vieira, E. N. dos Santos, E. V. Gusevskaya, *Applied Catalysis A-General* **2009**, *365*, 231-236.
- [10] A. W. Kleij, in *Green Synthetic Approaches for Biologically Relevant Heterocycles*, **2015**.
- [11] H. C. Kolb, M. G. Finn, K. B. Sharpless, *Angewandte Chemie-International Edition* **2001**, *40*, 2004-2021.
- [12] P. Tundo, M. Musolino, F. Arico, *Green Chemistry* **2018**, *20*, 28-85.
- [13] G. Fiorani, M. Stuck, C. Martin, M. M. Belmonte, E. Martin, E. C. Escudero-Adan, A. W. Kleij, *ChemSusChem* **2016**, *9*, 1304-1311.
- [14] J. Sanders, E. Scott, R. Weusthuis, H. Mooibroek, *Macromolecular Bioscience* **2007**, *7*, 105-117.
- [15] G. F. Eilon, J. R. Gu, L. M. Slater, K. Hara, J. W. Jacobs, *Cancer Chemotherapy and Pharmacology* **2000**, *45*, 183-191.
- [16] A. Lewinska, P. Chochrek, K. Smolag, E. Rawska, M. Wnuk, *Redox Report* **2015**, *20*, 116-125.
- [17] K. M. Phizackerley, M. Jumaa, A. Lopalco, B. H. Wolfe, C. D. Ablan, V. J. Stella, *Journal of Pharmaceutical Sciences* **2017**, *106*, 1051-1061.
- [18] J. Marco-Contelles, M. T. Molina, S. Anjum, *Chemical Reviews* **2004**, *104*, 2857-2899.
- [19] A. Fingerhut, O. V. Serdyuk, S. B. Tsogoeva, *Green Chemistry* **2015**, *17*, 2042-2058.

- [20] J. T. Groves, M. K. Stern, *Journal of the American Chemical Society* **1987**, *109*, 3812-3814.
- [21] J. T. Groves, T. E. Nemo, *Journal of the American Chemical Society* **1983**, *105*, 5786-5791.
- [22] M. M. Pereira, L. D. Dias, M. J. F. Calvete, *ACS Catalysis* **2018**, *8*, 10784-10808.
- [23] D. Prat, A. Wells, J. Hayler, H. Sneddon, C. R. McElroy, S. Abou-Shehada, P. J. Dunn, *Green Chemistry* **2016**, *18*, 288-296.
- [24] P. G. Jessop, *Green Chemistry* **2011**, *13*, 1391-1398.
- [25] C. Capello, U. Fischer, K. Hungerbuhler, *Green Chemistry* **2007**, *9*, 927-934.
- [26] L. Vanoye, M. Pablos, N. Smith, C. de Bellefon, A. Favre-Reguillon, *RSC Advances* **2014**, *4*, 57159-57163.
- [27] B. B. Wentzel, P. L. Alsters, M. C. Feiters, R. J. M. Nolte, *Journal of Organic Chemistry* **2004**, *69*, 3453-3464.
- [28] L. Vanoye, J. Wang, M. Pablos, C. de Bellefon, A. Favre-Reguillon, *Catalysis Science & Technology* **2016**, *6*, 4724-4732.
- [29] S. I. Murahashi, Y. Oda, T. Naota, *Journal of the American Chemical Society* **1992**, *114*, 7913-7914.
- [30] J. T. Groves, J. B. Lee, S. S. Marla, *Journal of the American Chemical Society* **1997**, *119*, 6269-6273.
- [31] J. Y. Kim, K. Y. Lee, S. Kim, S. J. Lee, *Bulletin of the Korean Chemical Society* **2015**, *36*, 1936-1939.
- [32] A. Farokhi, K. Berijani, H. Hosseini-Monfared, *Catalysis Letters* **2018**, *148*, 2608-2618.
- [33] S. Rayati, F. Nejabat, *New Journal of Chemistry* **2017**, *41*, 7987-7991.
- [34] K. C. Zhang, A. P. Woodruff, M. Y. Xiong, J. Zhou, Y. K. Dhande, *Chemsuschem* **2011**, *4*, 1068-1070.
- [35] B. Orlikova, N. Legrand, J. Panning, M. Dicato, M. Diederich, *Anti-Inflammatory and Anticancer Drugs from Nature*, Springer-Verlag Berlin, Berlin, **2014**.
- [36] Y. Kimura, *Antitumor and Antimetastatic Actions of Various Natural Products*, Elsevier Science Bv, Amsterdam, **2008**.
- [37] CFR - Code of Federal Regulations Title 21; U.S. Food & Drug Administration, Department of Health and Human Services, **2018**.
- [38] S. P. Bhatia, D. McGinty, C. S. Letizia, A. M. Api, *Food and Chemical Toxicology* **2008**, *46*, S185-S189.
- [39] Z. Freixa, M. M. Pereira, A. Pais, J. C. Bayon, *Journal of the Chemical Society-Dalton Transactions* **1999**, 3245-3251.
- [40] G. N. Costa, R. M. B. Carrilho, L. D. Dias, J. C. Viana, G. L. B. Aquino, M. Pineiro, M. M. Pereira, *Journal of Molecular Catalysis A-Chemical* **2016**, *416*, 73-80.
- [41] T. Mosmann, *Journal of Immunological Methods* **1983**, *65*, 55-63.

- [42] K. Prabst, H. Engelhardt, S. Ringgeler, H. Hubner, *Basic Colorimetric Proliferation Assays: MTT, WST, and Resazurin*, Humana Press Inc, Totowa, **2017**.
- [43] M. V. Berridge, A. S. Tan, *Archives of Biochemistry and Biophysics* **1993**, *303*, 474-482.
- [44] P. Skehan, R. Storeng, D. Scudiero, A. Monks, J. McMahon, D. Vistica, J. T. Warren, H. Bokesch, S. Kenney, M. R. Boyd, *Journal of the National Cancer Institute* **1990**, *82*, 1107-1112.
- [45] W. Voigt, *Sulforhodamine B Assay and Chemosensitivity*, Springer Protocols, Switzerland, **2005**.
- [46] C. A. Manassero, J. R. Girotti, S. Mijailovsky, M. G. de Bravo, M. Polo, *Natural Product Research* **2013**, *27*, 1475-1478.
- [47] S. A. Holstein, R. J. Hohl, *Journal of Lipid Research* **2003**, *44*, 1209-1215.
- [48] S. P. Shankar, M. Jagodzinska, L. Malpezzi, P. Lazzari, I. Manca, I. R. Greig, M. Sani, M. Zanda, *Organic & Biomolecular Chemistry* **2013**, *11*, 2273-2287.
- [49] E. C. Garnier-Amblard, S. G. Mays, R. F. Arrendale, M. T. Baillie, A. S. Bushnev, D. G. Culver, T. J. Evers, J. J. Holt, R. B. Howard, L. S. Liebeskind, D. S. Menaldino, M. G. Natchus, J. A. Petros, H. Ramaraju, G. P. Reddy, D. C. Liotta, *ACS Medicinal Chemistry Letters* **2011**, *2*, 438-443.

Chapter 5

Experimental

This chapter is divided according to the experimental procedure carried out for each of the previously discussed chapters (**Chapter 2-4**), as follows:

Chapter 2 – reaction conditions for synthesis of the catalysts (section 5.2);

Chapter 3 – catalytic reaction conditions for epoxidation and sequential epoxidation/ CO_2 cycloaddition reaction and characterisation of the new compounds (section 5.3);

Chapter 4 – catalytic reaction conditions for epoxidation, characterisation of new terpene-based compounds and cell viability studies on human osteosarcoma cells (MG-63) (section 5.4).

5.1 General Information

5.1.1. Solvents and Chemicals

All solvents and chemicals were obtained from Sigma-Aldrich (Portugal), Merck (Portugal), Strem (United Kingdom) or FluoroChem (United Kingdom). Air and moisture sensitive reagents and solutions were handled under nitrogen or argon atmosphere, in a vacuum system, using Schlenk techniques.^[1] All the glassware was dried by heating. The solvents were purified by distillation or, when necessary, dried and distilled using the procedures reported by literature,^[2, 3] described below.

i) Toluene, dimethoxyethane, tetrahydrofuran and 2-methyltetrahydrofuran

The solvent was placed in a round-bottom flask, with sodium flakes and benzophenone. The mixture was kept under reflux until a strong blue colour was observed. After distillation, the solvent was collected and stored, under nitrogen atmosphere, in a vessel containing activated molecular sieves (3Å).

ii) Dichloromethane and chloroform

Chlorinated solvents were placed in a round-bottom flask, with anhydrous calcium sulphate and pumice stone. The mixture was kept under reflux, for two hours. After distillation, the solvent was collected and passed through a column of basic alumina (grade I) and stored in a flask containing activated molecular sieves (3Å).

iii) Ethyl acetate

Ethyl acetate was placed in a round-bottom flask, with anhydrous calcium sulphate and pumice stone. The mixture was kept under reflux, for two hours. After distillation, the solvent was collected and passed through a column of basic alumina (grade I) and stored in a flask containing activated molecular sieves (3Å).

iv) *n*-Hexane and cyclohexane

n-Hexane or cyclohexane was placed in a round-bottom flask, with anhydrous calcium sulphate and pumice stone. The mixture was kept under reflux, for three hours. After distillation, the solvent was collected and passed through a column of

basic alumina (grade I) and stored in a flask containing activated molecular sieves (3Å).

v) Acetonitrile and butyronitrile

Acetonitrile or butyronitrile were placed in a round-bottom flask, with anhydrous potassium carbonate. The mixture was kept under reflux, for three hours. After distillation, the solvent was collected and passed through a column of basic alumina (grade I) and stored in a flask containing activated molecular sieves (3Å).

vi) Acetone

Acetone was placed in a round-bottom flask, with anhydrous calcium sulphate and pumice stone. The mixture was kept under reflux, for two hours. After distillation, the solvent was collected and passed through a column of basic alumina (grade I) and stored in a flask containing activated molecular sieves (3Å).

vii) Ethanol

Ethanol was placed in a round-bottom flask, with anhydrous calcium sulphate and pumice stone. The mixture was kept under reflux, for two hours. After distillation, the solvent was collected and passed through a column of basic alumina (grade I) and stored in a flask containing activated molecular sieves (3Å).

5.1.2. Instrumentation and Methodology

i) Thin Layer Chromatography (TLC)

The reaction control, when necessary, was performed using thin layer chromatography (TLC) plate coated with silica 60 (Sigma-Aldrich), with fluorescence indicator UV₂₅₄ and UV₃₆₆.

ii) Column Chromatography

The catalysts and reaction products, when necessary, were purified by column chromatography using silica gel 60 (particles of size 0.06-0.20 mm) as stationary phase and the appropriate eluent.

iii) Flash Chromatography

The catalysts and reaction products, when necessary, also were purified using a flash chromatography equipment PuriFlash 420® Interchim (Department of Chemistry, University of Coimbra, Portugal), equipped with a UV diode array detector and a HP silica F0004 column (0.15 μm) as stationary phase and the appropriate eluent.

iv) Homogenizer

Magnetite nanoparticles synthesis's procedures were carried out using an Ultra-Turrax® T18 Homogenizer (Institute of Chemistry, University of São Paulo, São Paulo, Brazil).

v) Ultrasound

To facilitate the dissolution of some of the compounds studied, a Bandelin Sonorex TK52 device was used as the ultrasound system.

vi) Nuclear Magnetic Resonance (NMR)

NMR spectra were recorded on Bruker Avance 400 spectrometer (Department of Chemistry, University of Coimbra, Portugal), using CDCl_3 ($\delta = 7.26$ ppm) as deuterated solvent (unless otherwise stated). ^1H and ^{13}C chemical shifts, expressed in ppm, are generally relative to a TMS ($\delta = 0.00$ ppm) internal standard. The data obtained are indicated in the following order: Nucleus (apparatus, solvent): chemical shift (δ , ppm) [multiplicity (s - singlet, d - doublet, dd – double doublet, m - multiplet), coupling constant (J , in Hertz), relative intensity (nH as number of protons), assignment in the structure].

vii) Mass Spectrometry (MS)

High-resolution mass spectrometry was carried out on a Bruker Microtof apparatus, equipped with selective ESI detector (Unidade de Masas e Proteómica, University of Santiago de Compostela, Spain).

viii) Gas Chromatography (GC)

Gas chromatography was carried out on an HP-Agilent 6890 apparatus equipped with a non-polar capillary HP-5 column (5% diphenyl and 95% dimethylpolysiloxane); with 30 m length and 0.32 mm inside diameter and using nitrogen as carrier gas (Department of Chemistry, University of Coimbra, Portugal). The GC analysis for general epoxidation and CO₂ cycloaddition reactions were performed using chlorobenzene as internal standard and the following conditions:

- Initial temperature: 100 °C;
- Rate: 60 °C min⁻¹;
- Final temperature: 280 °C;
- Gas flow: 1.63 mL min⁻¹.

ix) Gas Chromatography Coupled with Mass Spectrometry (GC-MS)

GC-MS spectra were obtained in a Hewlett-Packard 5973 MSD spectrometer, using EI (70 eV), coupled to a Hewlett-Packard Agilent 6890 chromatographer, equipped with a HP-5 MS column (30 m × 0.25 mm × 0.25 μm) (Department of Chemistry, University of Coimbra, Portugal).

The GC analysis for general epoxidation and CO₂ cycloaddition reactions were performed using the following conditions:

- Initial temperature: 100 °C;
- Rate: 60 °C min⁻¹;
- Final temperature: 280 °C;
- Gas flow: 1.63 mL min⁻¹.

The GC analysis for hydroformylation of (–)-isopulegol benzyl ether (**32**) were carried out using the following conditions:

- Initial temperature: 80 °C; 20 °C min until 150 °C;
150 °C; 30 °C min until 200 °C;
200 °C; 20 °C min until 310 °C (10 min);
- Final temperature: 310 °C;
- Gas flow: 1.55 mL min⁻¹.

x) UV-Visible Absorption Spectroscopy (UV-Vis)

UV-visible absorption spectra were obtained on a Hitachi U-2010 and Shimadzu UV-1700 spectrophotometers with 1 cm double-stranded quartz cells with 1 cm optical path and using the respective solvent as reference. For magnetic nanocomposite spectra, material (2 mg) was placed in a solvent DMF, CH₃CN/H₂O or CHCl₃ (5 mL) and submitted to the ultrasound for 1 min.

xi) Transmission Electron Microscopy (TEM)

TEM analyses were performed on a Philips CM 200 (Institute of Chemistry, University of São Paulo, São Paulo, Brazil), operating at an acceleration voltage of 200 KV. Samples were prepared by slow evaporation of one drop of colloidal solution in isopropyl alcohol deposited on the carbon covered copper grid. The size distributions of the nanoparticles were determined through a manual analysis of amplified micrographs using ImageToll software version 3.0 in order to obtain the statistical distribution of the diameter. The mean curve fit was obtained using the Gaussian line shape.

xii) Flame Atomic Absorption Spectroscopy (FAAS)

Determination of the percentage of manganese metal was performed using a Shimadzu AA-6300 atomic absorption spectrophotometer (Institute of Chemistry, University of São Paulo, São Paulo, Brazil). The samples (10 mg) were digested using an acid solution (concentrated nitric acid and hydrochloric acid solution (1:3)) (5 mL) for 3 hours at 100 °C. After this period, it was checked with distilled water to the desired volume (10 mL).

xiii) Inductively Coupled Plasma (ICP)

The percentage of manganese and chromium present on the magnetic nanoparticles or in solution was determined using an ICP Thermo X Series spectrometer (Department of Chemistry, University of Aveiro, Portugal).

xiv) Elemental Analysis

Elemental analysis for carbon, hydrogen and nitrogen were measured on LECO model (CHNS 932) Instruments apparatus (Unidade de Masas e Proteómica, University of Santiago de Compostela, Spain).

xv) Infrared Spectroscopy (IR)

The infrared spectra of nanocomposites were obtained using a Pike Miracle spectrometer (Institute of Chemistry, University of São Paulo, São Paulo, Brazil) which each spectrum were performed with a resolution of 4 cm^{-1} (64 scans). The samples were pressed into thin wafers ($20\text{-}25\text{ mg cm}^{-2}$) and heated in an IR glass cell up to $160\text{ }^{\circ}\text{C}$ using a heating rate of $10\text{ }^{\circ}\text{C min}^{-1}$ during 1 h, under vacuum (10 Pa) before spectra acquisition in transmission mode, in order to remove physically adsorbed water. The infrared spectra of tetrapyrrolic macrocycles also were taken in KBr pellets using an FTIR Nicolet Nexus 670 (Department of Chemistry, University of Coimbra, Portugal) with a resolution of 4 cm^{-1} (64 scans).

xvi) Thermogravimetry-differential Scanning Calorimetry (TG-DSC)

Thermogravimetric analyses were obtained using a Parkin-Elmer STA6000 (Department of Physics, University of Coimbra, Portugal) simultaneous TG-DSC instrument from $25\text{ }^{\circ}\text{C}$ to $800\text{ }^{\circ}\text{C}$ ($10\text{ }^{\circ}\text{C min}^{-1}$) under flow of air (30 mL min^{-1}).

xvii) pH-Meter Instrument

The pH of solutions were measured using a pH-Meter BASIC 20+ (Unidade de I&D Química-Física Molecular, Department of Chemistry, University of Coimbra, Portugal).

xviii) Water Purification Apparatus Milli-Q

The deionised water was obtained using a Water Purification Apparatus Milli-Q (Unidade de I&D Química-Física Molecular, Department of Chemistry, University of Coimbra, Portugal).

xix) Centrifuge

The centrifugation was performed using a centrifuge with cooling (MPW-350R) (Unidade de I&D Química-Física Molecular, Department of Chemistry, University of Coimbra, Portugal).

xx) Incubator

Incubation procedure for biological assays was carried out using an incubator MCO-19AIC (UV) Sanyo under humidified atmosphere (5% CO₂), at 37 °C (Unidade de I&D Química-Física Molecular, Department of Chemistry, University of Coimbra, Portugal).

xxi) Laminar Flow Hood

Biological assay's procedures were performed using a laminar flow hood (BW 100) (flow rate: 1050 m³ h⁻¹) BioWizard (Unidade de I&D Química-Física Molecular, Department of Chemistry, University of Coimbra, Portugal).

xxii) Microplate Reader

Absorbance measure for MTT and SRB biological assays were determined using a Biotek μ Quant MQX200 UV-Visible spectrophotometer, Gen5 software, Biotek (Unidade de I&D Química-Física Molecular, Department of Chemistry, University of Coimbra, Portugal).

xxiii) Microscope

Microscopic analysis were performed using a microscope CRX41 coupled to a DP20 camera Olympus® (Unidade de I&D Química-Física Molecular, Department of Chemistry, University of Coimbra, Portugal).

5.2. Experimental of Chapter 2

5.2.1. Synthesis of Metalloporphyrins for Homogeneous Catalysis

In this section, the synthetic procedures of metalloporphyrins used as catalysts and their full characterisation are provided. 5,10,15,20-tetraarylporphyrins were prepared using three synthetic approaches and reagents ratio, described below.

General Procedure for Nitrobenzene Method:^[4, 5] To a mixture of glacial acetic acid (210 mL) and nitrobenzene (105 mL) under stirring at ≈ 140 °C, aldehyde or a mixture of aldehyde (60 mmol) and pyrrole (60 mmol; 4.2 mL) was added dropwise and the mixture was stirred at ≈ 140 °C, for 1-2 h. Then, the glacial acetic acid and nitrobenzene were evaporated under reduced pressure. For the non-symmetric porphyrins, a column chromatography on silica gel was performed. Regarding symmetric porphyrins, methanol (200 mL) was added and the mixture was putted at 5 °C overnight. At the end, the solid was filtrated.

General Procedure for NaY/Nitrobenzene Method:^[6] A mixture of acetic acid (650 mL) and nitrobenzene (325 mL) was heated at 140 °C. Then, aldehyde (or mixture of aldehydes) (60 mmol), pyrrole (60 mmol) and NaY (30 g) was added. The reaction was stirring at ≈ 140 °C for 1-2 h. After this period, NaY was filtered and methanol (200 mL) was added. Finally, the solid precipitated was isolated by filtration. For the non-symmetric porphyrins, a column chromatography on silica gel was performed.

Reutilisation of NaY Catalyst: After each cycle, the NaY catalyst was collected by filtration and washed with chloroform and tetrahydrofuran, followed by drying of the solid overnight, at 150 °C.

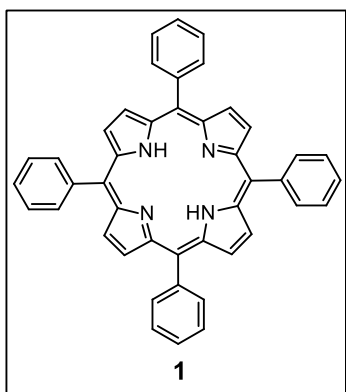
General Procedure for Microwave Method:^[7] Pyrrole (9.8 mmol; 0.68 mL), aldehyde (9.8 mmol) and water (0.2 mL) were added into a microwave vial. For solid aldehydes, the mixture was previously putted under ultrasound for 10-15 min. The mixture was submitted to microwave radiation at 300 W, 200 °C, for 10-20 min. At

the end, the porphyrin was extracted with ethyl lactate (20 mL). After removal of the solvent under reduced pressure, the residue was purified by column chromatography on silica gel, using the appropriate eluent.

Synthesis of Symmetric Porphyrins

5,10,15,20-tetraphenylporphyrin (1)

Following the above-described nitrobenzene, NaY/nitrobenzene and microwave methods and benzaldehyde (6.36 g; 59.93 mmol), (6.36 g; 59.93 mmol), (1.04 g; 9.80 mmol) were used, respectively. At the end, ethanol (15-50 mL) was added and storage at 5 °C. Then, the solid was filtrated, washed with ethanol (5-40 mL) and dried under vacuum.



Yield (%):

Nitrobenzene method: 24% (2.21g; 3.59 mmol);

NaY/Nitrobenzene method: 35% (3.22 g; 5.25 mmol);

Microwave method: 20% (0.30 g; 0.49 mmol);

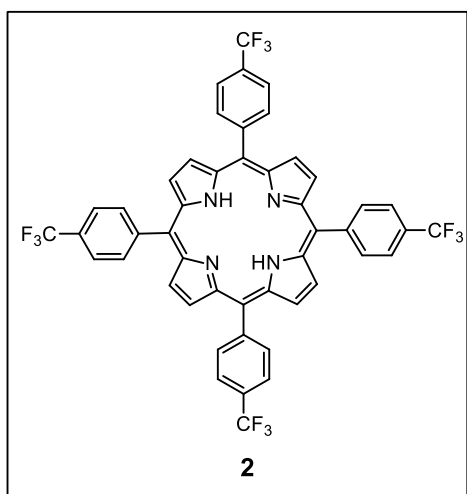
¹H-NMR (400 MHz, CDCl₃, TMS): δ, ppm = 8.80 (s, 8H, β-H), 8.19-8.09 (m, 8H, Ar-H), 7.74-7.62 (m, 12H, Ar-H), -2.80 (s, 2H, NH) (data is in good agreement

with that previously reported).^[8]

5,10,15,20-tetra(4-trifluoromethylphenyl)porphyrin (2)

Following the above described nitrobenzene and NaY methodologies,

4-(trifluoromethyl)benzaldehyde (10.44 g; 60.00 mmol) was used for both methods. At the end, cold water (100 mL) was added and storage at room temperature overnight. Then, the solid was filtrated, and dried under vacuum.



Yield (%):

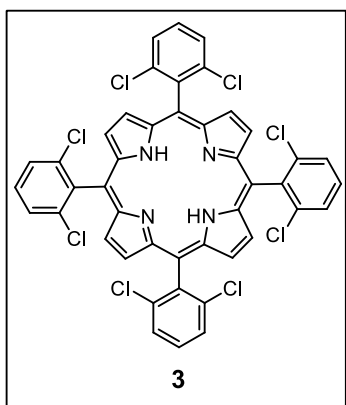
Nitrobenzene method: 8% (1.08 g; 1.22 mmol);

NaY/Nitrobenzene method: 17% (2.26 g; 2.55 mmol);

$^1\text{H-NMR}$ (400 MHz, CDCl_3 , TMS): δ , ppm = 8.79 (s, 8H, β -H), 8.33-8.30 (d, J = 8.0 Hz, 8H, Ar-H), 8.05-8.03 (d, J = 8.0 Hz, 8H, Ar-H), -2.82 (s, 2H, NH) (data is in good agreement with that previously reported).^[9]

5,10,15,20-tetra(2,6-dichlorophenyl)porphyrin (3)

Following the above described nitrobenzene and NaY methods, 2,6-dichlorobenzaldehyde (8.45 g; 48.28 mmol) was used for both methods.



Yield (%):

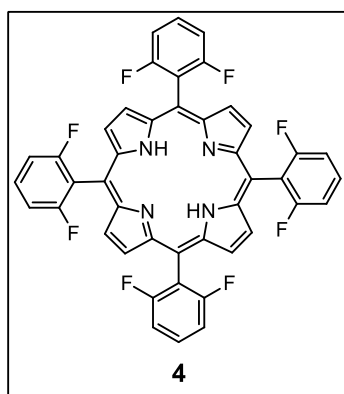
Nitrobenzene method: 6% (0.64 g; 0.72 mmol);

NaY/Nitrobenzene method: 11% (1.17 g; 1.32 mmol);

$^1\text{H-NMR}$ (400 MHz, CDCl_3 , TMS): δ , ppm = 8.68 (s, 8H, β -H), 7.83-7.62 (m, 12H, Ar-H), -2.57 (s, 2H, NH) (data is in good agreement with that previously reported).^[5]

5,10,15,20-tetra(2,6-difluorophenyl)porphyrin (4)

Following the above described nitrobenzene and NaY methodologies, 2,6-difluorobenzaldehyde (8.56 g; 60.23 mmol) was used for both methods.



Yield (%):

Nitrobenzene method: 8% (0.89 g; 1.17 mmol);

NaY/Nitrobenzene method: 17% (1.92 g; 2.53 mmol);

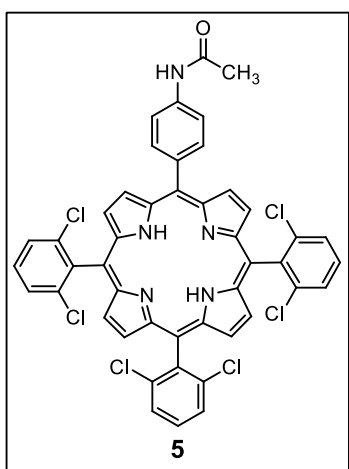
$^1\text{H-NMR}$ (400 MHz, CDCl_3 , TMS): δ , ppm = 8.82 (s, 8H, β -H), 7.83-7.72 (m, 4H, Ar-H), 7.40-7.27 (m, 8H, Ar-H), -2.75 (s, 2H, NH) (data is in good agreement with that previously reported).^[10]

Synthesis of Non-symmetric Porphyrins

5-(4-acetamidophenyl)-10,15,20-tris(2,6-dichlorophenyl)porphyrin (5)

Following the nitrobenzene and NaY methods above described, 2,6-dichlorobenzaldehyde (7.00 g; 40.00 mmol) and 4-acetamidobenzaldehyde (2.17 g; 13.33 mmol) were used for both methods. At the end, the porphyrin was

extracted with ethyl lactate (18 mL). After removal of the solvents under reduced pressure, the residue was purified by column chromatography on silica gel, initially using a mixture of *n*-hexane/dichloromethane (1:1) as eluent, and the red spot was isolated and characterised as 5,10,15,20-tetra(2,6-dichlorophenyl)porphyrin (**3**) in the following yields: nitrobenzene method = 2.4% (0.21 g; 0.24 mmol); NaY method = 3.6% (0.32 g; 0.36 mmol). Then, the eluent was gradually changed to a mixture of ethyl acetate/dichloromethane (1:1), and the desired 5-(4-acetamidephenyl)-10,15,20-tris(2,6-dichlorophenyl)porphyrin (**5**) was isolated.



Yield (%):

Nitrobenzene method = 4% (0.47 g; 0.53 mmol);

NaY/Nitrobenzene method = 9% (1.08 g; 1.23 mmol);

¹H-NMR (400 MHz, CDCl₃, TMS): δ = 8.85 (d, *J* = 4.5 Hz, 2H, β-H), 8.73-8.62 (m, 6H, β-H), 8.13 (d, *J* = 8.0 Hz, 2H, Ar(Acetamide)-H), 7.87 (d, *J* = 7.9 Hz, 2H, Ar(Acetamide)-H), 7.82-7.66 (m, 9H, Ar-H), 2.31 (s, 3H, CH₃), -2.56 (s, 2H, NH). **MS (MALDI-TOF):** *m/z* =

875.039 [M]⁺ calculated for C₄₆H₂₇Cl₆N₅O [M]⁺ = 875.034. **Elemental analysis for C₄₆H₂₇Cl₆N₅O:** C: 62.89; H: 3.10; N: 7.97; found: C: 62.85; H: 3.08; N: 7.99. **UV-Vis (toluene), λ_{máx}/nm (ε/mol⁻¹ cm⁻¹):** 420 (3.6 x 10⁵), 514 (2.3 x 10⁴), 545 (6.1 x 10³), 591 (6.9 x 10³), 656 (4.4 x 10³).

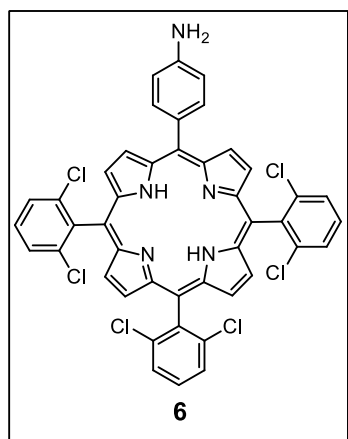
5-(4-aminephenyl)-10,15,20-tris(2,6-dichlorophenyl)porphyrin (6)

The porphyrin (**6**) was obtained through basic and acid hydrolysis of acetamide group from porphyrin (**5**), following the below methods:

Basic Hydrolysis: In a round bottom flask, 5-(4-acetamidephenyl)-10,15,20-tris(2,6-dichlorophenyl)porphyrin (**5**) (1.00 g; 1.13 mmol) was dissolved in THF (100 mL). Then, a saturated solution of 1M potassium hydroxide was added and the reaction was stirred for 72 h at 60 °C, under inert atmosphere. Upon complete conversion of the starting material (observed by TLC), the reaction crude was extracted with dichloromethane (50 mL). The organic phase was washed with a 10% sodium hydrogen carbonate solution (2x 50 mL) and water (2x 30 mL), dried with

anhydrous sodium sulphate and the solvent was evaporated under reduced pressure. After purification by column chromatography in silica gel, using a dichloromethane/ethyl acetate (1:2) mixture as the eluent, the porphyrin (**6**) was obtained.

Acid Hydrolysis: In a round bottom flask, the porphyrin (**5**) (1.00 g; 1.13 mmol) was dissolved in THF (100 mL). Then, a solution of 33% hydrochloric acid (20 mL) was added and the reaction was conducted at 40 °C for 18 h. Upon complete conversion of the starting material (observed by TLC), the reaction crude was extracted with ethyl acetate (100 mL). The organic phase was washed with a 10% sodium hydrogen carbonate solution (4x 50 mL) and water (4x 50 mL), dried with anhydrous sodium sulphate and the solvent was evaporated under reduced pressure.



After purification by column chromatography in silica gel, using a mixture of *n*-hexane/ethyl acetate (1:5) as the eluent, the porphyrin (**6**) was obtained.

Yield (%):

Basic hydrolysis = 77% (0.72 g; 0.87 mmol);

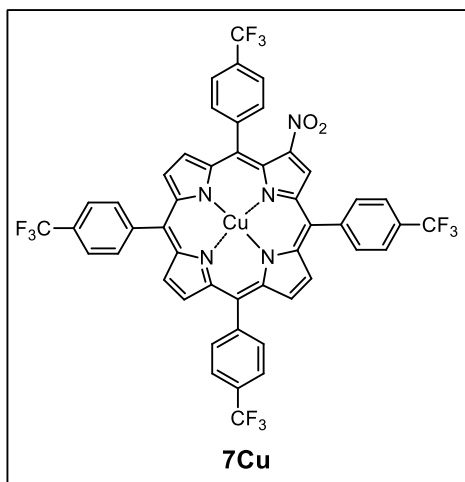
Acid hydrolysis = 91% (0.86 g; 1.03 mmol);

¹H-NMR (400 MHz, CDCl₃, TMS): δ, ppm = 8.96 (d, *J* = 4.6 Hz, 2H, β-H), 8.73-8.62 (m, 6H, β-H), 7.98 (d, *J* = 8.0 Hz, 2H, Ar(Amine)-H), 7.82-7.66 (m, 9H, Ar-H), 7.05 (d, *J* = 8.1 Hz, 2H, Ar(Amine)-H), -2.56 (s, 2H, NH). **HRMS (ESI-FIA-TOF):** *m/z* = 833.0236 [M]⁺calculated for C₄₄H₂₅Cl₆N₅ [M]⁺ = 833.0241. **UV-Vis (toluene), λ_{max}/nm (ε/mol⁻¹ cm⁻¹):** 422 (1.8 x 10⁵), 515 (1.4 x 10⁴), 551 (4.9 x 10³), 593 (4.9 x 10³), 651 (1.4 x 10³).

2-nitro-5,10,15,20-tetra(4-trifluoromethylphenyl)porphyrinato Copper (II) (7Cu)

A solution of copper(II) nitrate trihydrate (0.27 g; 1.12 mmol) in acetic anhydride/acetic acid mixture (50:10 mL) was added to a chloroform solution (500 mL) of 5,10,15,20-tetra-(4-trifluoromethylphenyl)porphyrin (**2**) (500 mg; 0.56 mmol). The reaction was conducted at 60 °C for 24 h. Then, the solution was

concentrated under vacuum and washed with a saturated solution of sodium hydrogen carbonate (2x 50 mL), water (2x 50 mL), and dried with anhydrous sodium sulphate. The crude was then purified by silica gel column chromatography using dichloromethane/*n*-hexane (2:1) as the eluent.



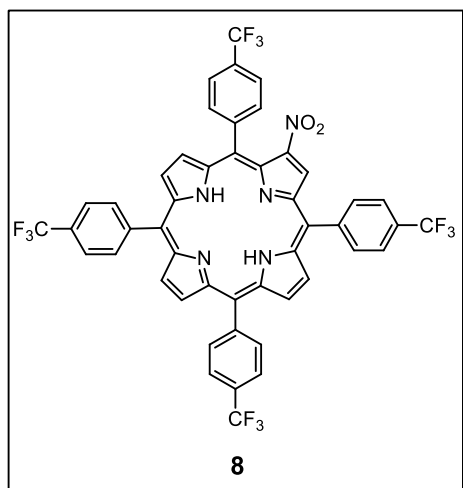
Yield (%): 84% (0.47 g; 0.47 mmol);

HRMS (ESI-FIA-TOF): $m/z = 992.0954$

$[M]^+$ calculated for $C_{48}H_{23}F_{12}N_5O_2Cu$ $[M]^+ = 992.0956$.

2-nitro-5,10,15,20-tetra(4-trifluoromethylphenyl)porphyrin (**8**)

Demetallation reaction was carried out following modified methods described in literature.^[11, 12] A solution of 98% sulphuric acid (5 mL) was added dropwise to a chloroform solution (100 mL) of **7Cu** (250 mg; 0.25 mmol). The reaction was kept at 25 °C for 1 h. Then, the crude was carefully neutralised with a saturated solution of sodium bicarbonate and distilled water. The organic solution was dried with anhydrous sodium sulphate, filtrated and solvent evaporation under reduced pressure. The crude was purified by silica gel column chromatography using dichloromethane/*n*-hexane (2:1) as the eluent.



Yield (%): 88% (0.20 g; 0.22 mmol);

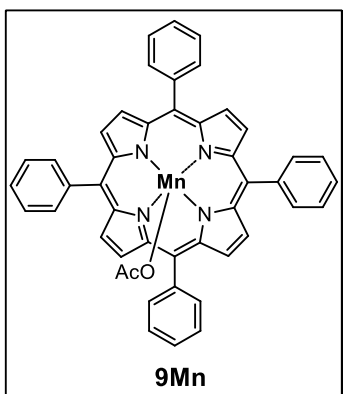
¹H-NMR (400 MHz, CDCl₃): δ, ppm = 9.01 (s, 1H, β-H), 8.96-8.86 (m, 4H, β-H), 8.70-8.67 (m, 2H, β-H), 8.37-8.32 (m, 8H, Ar-H), 8.09-8.06 (m, 6H, Ar-H), 7.99 (d, *J* = 8.0 Hz, 2H, Ar-H), -2.68 ppm (s, 2H). **HRMS (ESI-FIA-TOF):** *m/z* = 932.1889 [M+H]⁺ calculated for C₄₈H₂₅F₁₂N₅O₂ [M+H]⁺ = 932.1817.

Synthesis of Metalloporphyrins

DMF/metallic salts general procedure:^[13] Desired porphyrin was dissolved in DMF under stirring at 160 °C. Then, the desired metallic salt was added. Upon complete metalation (observed by TLC and UV-Vis), the DMF was evaporated under reduced pressure, the crude reaction was dissolved in chloroform and washed with water (3x 100 mL). The organic phase was dried with anhydrous sodium sulphate and solvent was evaporated under reduced pressure. At the end, the crude was purified by silica gel column chromatography using the selected eluent for each case.

5,10,15,20-tetraphenylporphyrinatomanganese(III) Acetate (9Mn)

Following the above described DMF/metallic salt method, 5,10,15,20-tetraphenylporphyrin (**1**) (300 mg; 0.48 mmol) and tetrahydrate manganese (II) acetate (0.88 g; 3.6 mmol) were added in DMF (20 mL), and the reaction was stirring for 18 h. The crude reaction was purified by silica gel column chromatography using ethyl acetate as eluent.

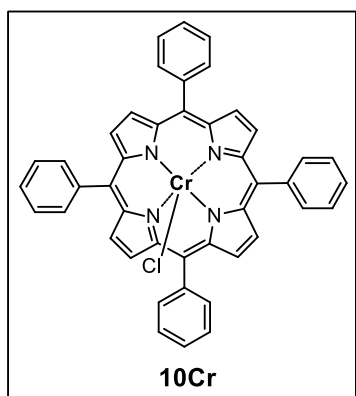


Yield (%): 89% (310 mg; 0.43 mmol);

Mass (FAB) $C_{46}H_{31}N_4MnO_2$: $m/z = 667$ (100) $[M-OAc]^+$; **Elemental analysis for $C_{46}H_{31}N_4MnO_2$:** C: 76.03; H: 4.30; N: 7.71; found: C: 75.87; H: 4.22; N: 7.58 (data is in good agreement with that previously reported).^[14]

5,10,15,20-tetraphenylporphyrinatochromium(III) Chloride (10Cr)

Following the above described DMF/metallic salts method, 5,10,15,20-tetraphenylporphyrin (**1**) (400 mg; 0.65 mmol) and chromium(II) chloride (95 mg; 0.77 mmol) were added in DMF (15 mL), and the reaction was stirring in reflux for 30 min, under argon atmosphere. Then, chromium(II) chloride (73 mg; 0.59 mmol) was added and the reaction was stirring in reflux for 20 min. The crude reaction was purified by silica gel column chromatography using ethyl acetate as eluent.



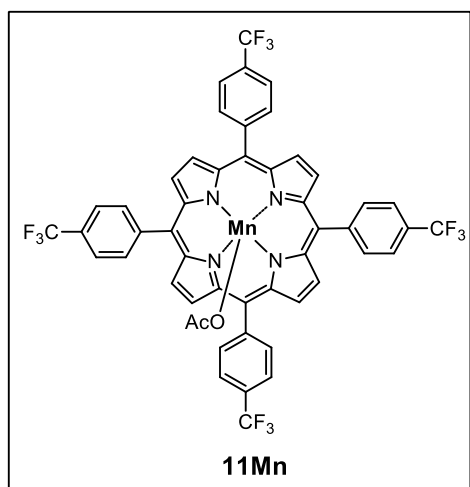
Yield (%): 86% (398 mg; 0.56 mmol);

HRMS (ESI-FIA-TOF): $m/z = 723.1327$ $[M+Na]^+$ calculated for $C_{44}H_{28}ClCrN_4$ $[M+Na]^+ = 723.1305$. (data is in good agreement with that previously reported).^[15]

5,10,15,20-tetra(4-trifluoromethylphenyl)porphyrinatomanganese(III) Acetate (11Mn)

Following the above described DMF/metallic salt method, 5,10,15,20-tetra(4-trifluoromethylphenyl)porphyrin (**2**) (300 mg; 0.33 mmol) and tetrahydrate manganese (II) acetate (0.88 g; 3.6 mmol) were added in DMF (20 mL),

and the reaction was stirring for 22 h. The crude reaction was purified by silica gel column chromatography using ethyl acetate as eluent.



Yield (%): 85% (279 mg; 0.28 mmol);

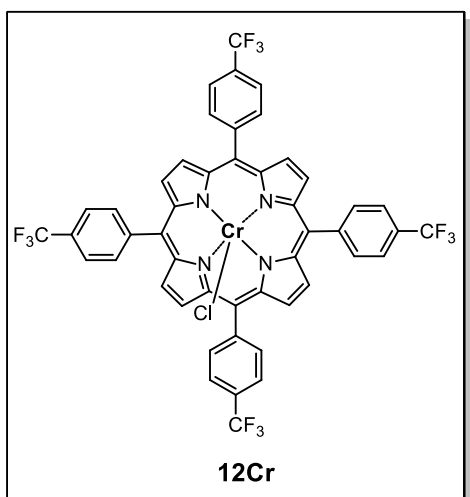
HRMS (ESI-FIA-TOF): $m/z = 1021.2432$

$[M+Na]^+$ calculated for $C_{50}H_{27}F_{12}MnN_4O_2$

$[M+Na]^+ = 1021.1220$ (data is in good agreement with that previously reported).^[16]

5,10,15,20-tetra(4-trifluoromethylphenyl)porphyrinatochromium(III) Chloride (12Cr)

Following the above described DMF/metallic salt method, 5,10,15,20-tetra(4-trifluoromethylphenyl)porphyrin (**2**) (400 mg; 0.45 mmol) and chromium(II) chloride (95 mg; 0.77 mmol) were added in DMF (15 mL), and the reaction was stirring in reflux for 30 min, under argon. Then, chromium(II) chloride (73 mg; 0.59 mmol) was added and the reaction was stirring in reflux for 5 h, under argon atmosphere. The crude reaction was purified by silica gel column chromatography using ethyl acetate as eluent.



Yield (%): 96% (418 mg; 0.43 mmol);

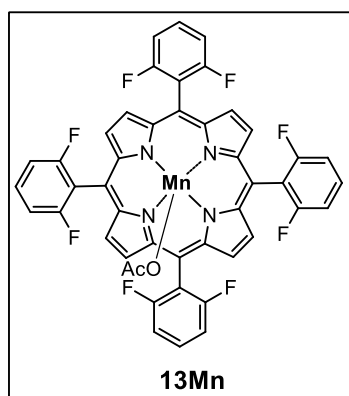
HRMS (ESI-FIA-TOF): $m/z = 1018.1738$

$[M+2Na]^+$ calculated for $C_{48}H_{24}ClCrF_{12}N_4$

$[M+2Na]^+ = 1018.0687$; **Elemental analysis for $C_{48}H_{24}ClCrF_{12}N_4$:** C: 53.0; H: 2.5; N: 5.1; found: C: 50.2; H: 2.4; N: 5.2 (data is in good agreement with that previously reported).^[17]

5,10,15,20-tetra(2,6-difluorophenyl)porphyrinat manganese(III) Acetate (13Mn)

Following the above described DMF/metallic salt method, 5,10,15,20-tetra(2,6-difluorophenyl)porphyrin (**4**) (350 mg; 0.46 mmol) and tetrahydrate manganese(II) acetate (0.88 g; 3.6 mmol) were added in DMF (20 mL), and the reaction was stirring for 20 h. The crude reaction was purified by silica gel column chromatography using ethyl acetate as eluent.



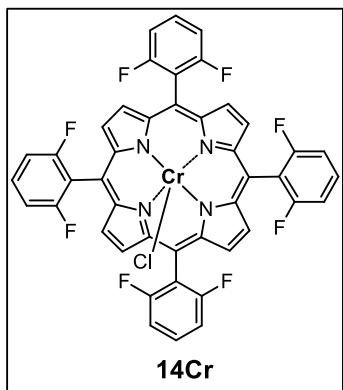
Yield (%): 89% (356 mg; 0.41 mmol);

Mass (FAB) = 811(100) [M-OAc]⁺ calculated for

C₄₆H₂₃F₈MnN₄O₂ [M-OAc]⁺ = 811.0941 (data is in good agreement with that previously reported).^[18]

5,10,15,20-tetra(2,6-difluorophenyl)porphyrinato chromium(III) Chloride (14Cr)

Following the above described DMF/metallic salt method, 5,10,15,20-tetra(2,6-difluorophenyl)porphyrin (**4**) (400 mg; 0.61 mmol) and chromium(II) chloride (95 mg; 0.77 mmol) were added in DMF (15 mL), and the reaction was stirring in reflux for 30 min, under argon atmosphere. Then, chromium(II) chloride (73 mg; 0.59 mmol) was added and the reaction was stirring in reflux for 4 h. The crude reaction was purified by silica gel column chromatography using ethyl acetate as eluent.

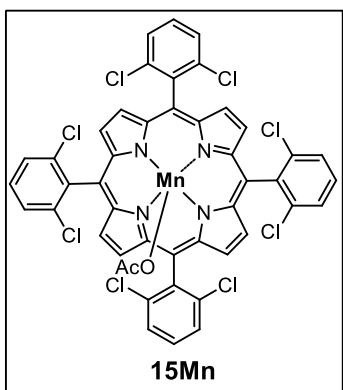


Yield (%): 87% (447 mg; 0.53 mmol);

HRMS (ESI-FIA-TOF): $m/z = 891.1512$ $[M+2Na]^+$
 calculated for $C_{44}H_{20}ClCrF_8N_4$ $[M+2Na]^+ = 891.0448$
 (data is in good agreement that previously reported).^[19]

5,10,15,20-tetra(2,6-dichlorophenyl)porphyrinatomanganese Acetate (15Mn)

Following the above described DMF/metallic salt method, 5,10,15,20-tetra(2,6-dichlorophenyl)porphyrin (**4**) (300 mg; 0.33 mmol) and tetrahydrate manganese(II) acetate (0.88 g; 3.6 mmol) were added in DMF (20 mL), and the reaction was stirring for 20 h. The crude reaction was purified by silica gel column chromatography using ethyl acetate as eluent.



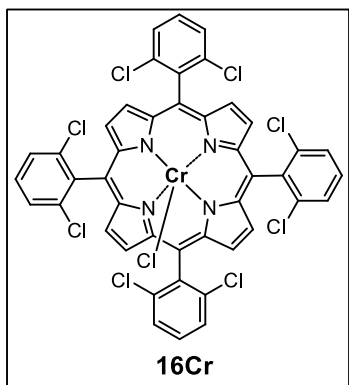
Yield (%): 88% (290 mg; 0.29 mmol);

Elemental analysis for $C_{46}H_{23}Cl_8MnN_4O_2$: C: 55.12;
 H: 2.31; N: 5.59; found: C: 55.02; H: 2.10; N: 5.42. (data
 is in good agreement that previously reported).^[20]

5,10,15,20-tetra(2,6-dichlorophenyl)porphyrinatochromium Chloride (16Cr)

Following the above described DMF/metallic salts method, 5,10,15,20-tetra(2,6-dichlorophenyl)porphyrin (**3**) (450 mg; 0.50 mmol) and chromium(II) chloride (95 mg; 0.77 mmol) were added in DMF (15 mL), and the reaction was stirring in reflux for 30 min. Then, chromium (II) chloride (73 mg; 0.59 mmol) was added and the reaction was stirring in reflux for 5 h, under argon atmosphere. The

crude reaction was purified by silica gel column chromatography using ethyl acetate as eluent.

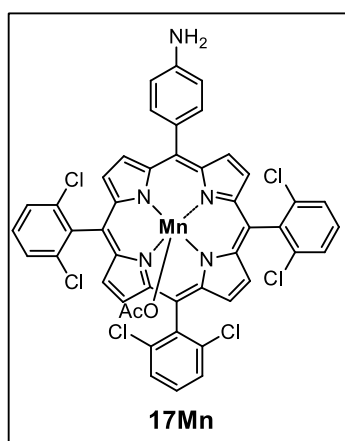


Yield (%): 72% (351 mg; 0.36 mmol);

HRMS (ESI-FIA-TOF): $m/z = 1016.7564$ $[M+2Na]^+$
calculated for $C_{44}H_{20}Cl_9CrN_4$ $[M+2Na]^+ = 1016.8084$
(data is in good agreement that previously reported).^[21]

5-(4-aminephenyl)-10,15,20-tris(2,6-dichlorophenyl)porphyrinatomanganese (III) Acetate (17Mn)

Following the above described DMF/metallic salt method, 5-(4-aminephenyl)-10,15,20-tetra(2,6-dichlorophenyl)porphyrin (**6**) (600 mg; 0.72 mmol) and tetrahydrate manganese(II) acetate (1.76 g; 7.2 mmol) were added in DMF (30 mL), and the reaction was stirring for 18 h. The crude reaction was purified by silica gel column chromatography using ethyl acetate as eluent.



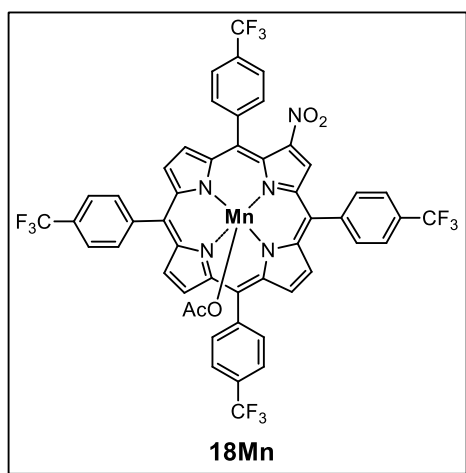
Yield (%): 78% (531 mg; 0.56 mmol)

Elemental analysis for $C_{46}H_{26}Cl_6N_5O_2Mn$: C: 58.26; H: 2.76; N: 7.38; found: C: 59.17; H: 2.51; N: 7.35.

UV-Vis (toluene), λ_{max}/nm ($\epsilon/mol^{-1} cm^{-1}$): 371 (2.2×10^4), 480 (4.8×10^4), 586 (4.4×10^3), 621 (2.8×10^3).

2-nitro-5,10,15,20-tetra(4-trifluoromethylphenyl)porphyrinatomanganese Acetate (18Mn)

Following the above described DMF/metallic salt method, 2-nitro-5,10,15,20-tetra(4-trifluoromethylphenyl)porphyrin (**8**) (320 mg; 0.37 mmol) and tetrahydrate manganese(II) acetate (0.88 g; 3.6 mmol) were added in DMF (20 mL), and the reaction was stirring for 18 h. The crude reaction was purified by silica gel column chromatography using ethyl acetate as eluent.

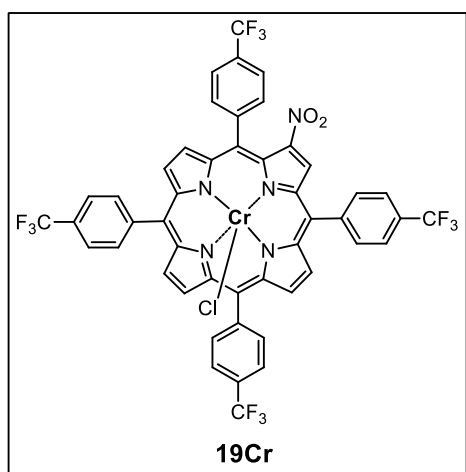


Yield (%): 76% (292 mg; 0.28 mmol)

MS (ESI-FIA-TOF): $m/z = 984.0883$
 [M-OAc] calculated for $C_{50}H_{26}F_{12}N_5O_4Mn$
 [M-OAc] = 984.1041.

2-nitro-5,10,15,20-tetra(4-trifluoromethylphenyl)porphyrinatochromium Acetate (19Cr)

Following the above described DMF/metallic salts method, 2-nitro-5,10,15,20-tetra(4-trifluoromethylphenyl)porphyrin (**8**) (350 mg; 0.37 mmol) and chromium(II) chloride (181 mg; 1.48 mmol) were added in DMF (20 mL), and the reaction was stirring in reflux for 5 h, under argon atmosphere. The crude reaction was purified by silica gel column chromatography using ethyl acetate as eluent.

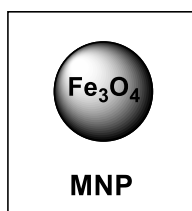


Yield (%): 89% (335 mg; 0.33 mmol).

MS (ESI-FIA-TOF): $m/z = 1017.0837$
 $[M+H]$ calculated for $C_{48}H_{23}ClF_{12}N_5O_2Cr = 1017.0754$.

5.2.2. Synthesis of Hybrid Metalloporphyrins for Heterogeneous Catalysis

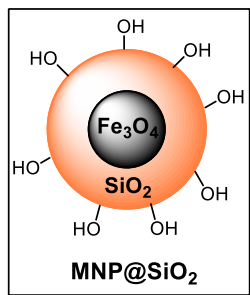
Synthesis of Magnetite Nanoparticles (MNP)



Magnetite nanoparticles (**MNP**) were prepared using a method described by Rossi.^[22] A mixture of aqueous solution of 1M $FeCl_3$ (10 mL) and a 2M HCl solution of $FeCl_2$ (2.5 mL) was added to 1M NH_4OH (250 mL) under mechanical stirring (10 000 rpm), along 30 min. Then, **MNP** were magnetically recovered and washed with distilled water (3×250 mL), following by dispersion in distilled water (250 mL). Subsequently, a solution of oleic acid (2 mL; 7 mmol) in acetone (5 mL) was added dropwise into the aqueous dispersion containing the **MNP**, under vigorous stirring. Finally, the resulting precipitate was magnetically separated, washed with acetone (3×25 mL) and dissolved in cyclohexane (15 mL). The final solution was centrifuged (2000 rpm; 30 min) to remove the non-stabilized particles and was stocked under air. After solvent evaporation, a stock solution containing 45 mg of **MNP** mL^{-1} of cyclohexane was obtained.

The size distributions of the nanoparticles were determined through a manual analysis of TEM images using ImageToll software version 3.0, showing a size of 7 ± 2 nm.

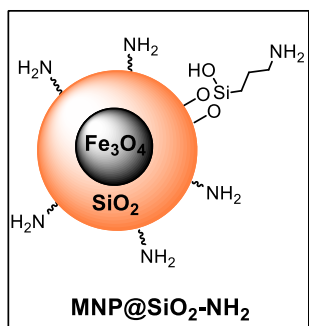
Synthesis of Silica-Coated Magnetite Nanoparticles ($\text{MNP}@SiO_2$)



The silica-coated magnetite nanoparticles were prepared by reverse microemulsion process^[23] and the optimisation studies are described in **chapter 2**. Igepal CO-520 (178.4 g), **MNP** (800 mg; 17.7 mL of stock solution in cyclohexane) and 29% ammonium hydroxide (38 mL) were added in cyclohexane (2.8 L). Then, tetraethyl orthosilicate (TEOS) (30.8 mL) was added dropwise and the mixture was kept under slow stirring (≈ 300 rpm), along 6-16 h. The solid was precipitated with methanol (≈ 250 mL), recovered by centrifugation (7000 rpm; 30 min) and washed with ethanol (3x). Finally, the solid material was dried open air for 24 h, at room temperature, and then calcined in the oven at 500 °C for 2 h giving the magnetic nanoparticles coated with silica ($\text{MNP}@SiO_2$). The size distributions of the coating magnetic nanoparticles with silica ($\text{MNP}@SiO_2$) were determined after silica coating process optimisation, through a manual analysis of TEM images using the ImageToll software version 3.0. The $\text{MNP}@SiO_2$ also were characterised by infrared spectra, presenting broad bands between 3750-3300 cm^{-1} , which are typical of terminal silanol and hydroxyl groups, and additional signals at 2950-2850 cm^{-1} , characteristic of C–H stretching vibrations. Furthermore, peaks at 2000 and 1870 cm^{-1} are attributed to Si–O–Si elongation harmonic and the 1640 cm^{-1} band is typical of O–H.

Functionalisation of Silica-coated Magnetite Nanoparticles

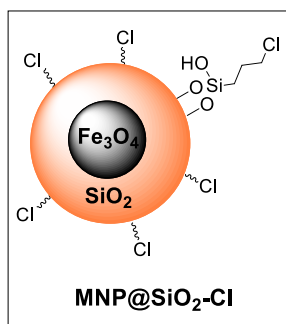
Synthesis of $\text{MNP}@SiO_2\text{-NH}_2$



$\text{MNP}@SiO_2$ (1 g) and (3-aminopropyl)triethoxysilane (APTES) (0.5 mL; 2.13 mmol) were added in dry toluene and kept under stirring, at reflux, for 12 h. Then, the amine-functionalised magnetite nanoparticles ($\text{MNP}@SiO_2\text{-NH}_2$) was washed with toluene (3x 30 mL), separated by centrifugation, and dried at 100 °C for 20 h. The $\text{MNP}@SiO_2\text{-NH}_2$ were characterised by FT-IR, presenting bands between 3300-

3400 cm^{-1} (N-H stretching of primary amines) and one broad band at 1600 cm^{-1} (N-H bending). The **MNP@SiO₂-NH₂** also were characterised by TG-DSC, aiming quantify the 3-aminopropyl group, showing a weight loss of 4.0% (1.1% of NH₂ corresponding to 0.68 mmol g⁻¹).

Synthesis of **MNP@SiO₂-Cl**

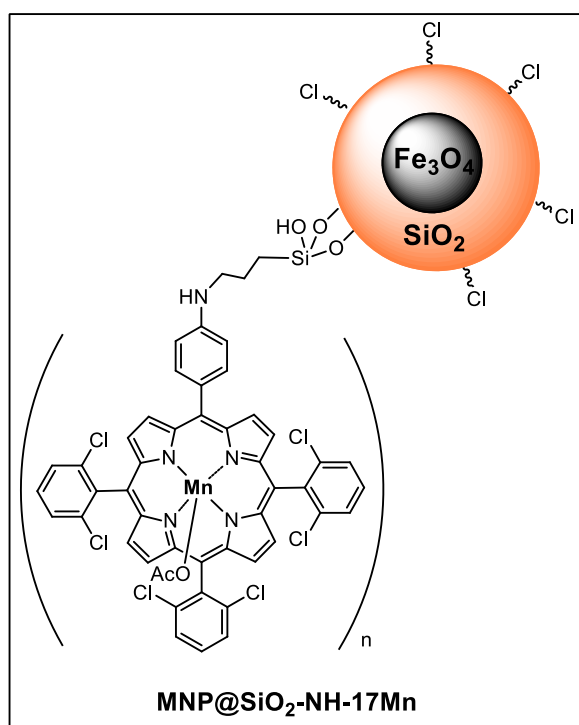


MNP@SiO₂ (1 g) and (3-chloropropyl)triethoxysilane (CPTES) (0.5 mL; 2.07 mmol) were added in dry toluene (40 mL) and kept under stirring at 110 °C, for 12 h. The resulting material was magnetically collected and washed several times with ethyl acetate and acetonitrile. Finally, the solid was dried under vacuum for 24 h. The

MNP@SiO₂-Cl were characterised by TG-DSC, aiming quantify the 3-chloropropyl functionalisation, showing a functionalisation percentage of 0.4% (0.18% of Cl corresponding to 0.052 mmol g⁻¹).

Synthesis of Hybrid Metalloporphyrin Magnetic Catalysts

Synthesis of $\text{MNP@SiO}_2\text{-NH-17Mn}$

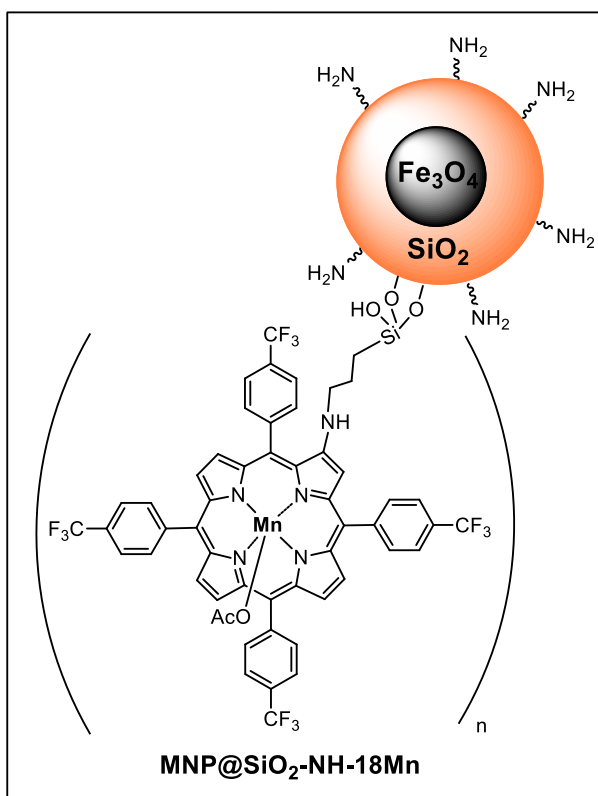


Metalloporphyrin (**17Mn**) (470 mg; 45 mmol) and NaH (60% dispersion in mineral oil) (25 mg) in dry toluene (80 mL) was heated at room temperature along 1 h. Then, **MNP@SiO₂-Cl** (1 g; 0.052 mmol of Cl g⁻¹) was added and the reaction was stirring for 24 h, under reflux. The magnetic material was magnetically collected and washed several times with acetonitrile, ethyl acetate, and dichloromethane to rinse away excess of metalloporphyrins (**17Mn**). The

final material **MNP@SiO₂-NH-17Mn** was dried under vacuum for 24 h and characterised by UV-Vis, FT-IR, TG-DSC and ICP.

- **UV-Vis:** 465 nm (Soret band);
- **FT-IR:** 3750-3300 cm⁻¹ (Si-OH and OH - Broad bands); 2950-2850 cm⁻¹ (C-H stretching); 1608 cm⁻¹ (pyrrole C=N stretching); 1560 cm⁻¹ (N-H bending); 1508-1465 cm⁻¹ (aromatic C=C stretching); 1450 cm⁻¹ (C-H bending); 1410 cm⁻¹ (Si-CH₂ bending);
- **TG-DSC** (25 °C-800 °C): 50 °C-200 °C (endothermic peak-water and solvents); 200 °C-800 °C (exothermic peak-organic material);
- **ICP:** manganese percentage: 0.090% (0.013 mmol per gram of nanocomposite).

Synthesis of **MNP@SiO₂-NH-18Mn**

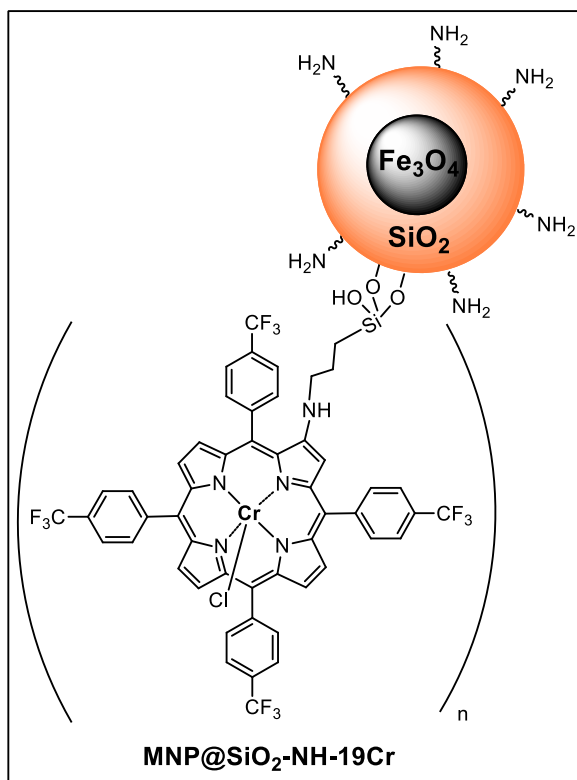


In a round-bottom flask, the 3-aminopropylsilyl functionalized magnetite material **MNP@SiO₂-NH₂** (1 g) was added to a solution of **18Mn** (230 mg, 0.22 mmol) and cesium carbonate (310 mg, 0.95 mmol) in dry 1,2-dimethoxyethane (50 mL). The mixture was kept under stirring at 85 °C for, 24 h. Then, the magnetic solid material was collected using an external magnet and washed several times with acetonitrile, ethyl acetate, and dichloromethane to rinse away excess non-immobilised metalloporphyrin. Finally, the

resulting hybrid metalloporphyrin magnetic **MNP@SiO₂-NH-18Mn** was dried under vacuum for 24 h and characterised by UV-Vis, FT-IR, TG-DSC and ICP.

- **UV-Vis:** 471 nm (Soret band);
- **FT-IR:** 3750-3300 cm⁻¹ (Si-OH and OH - Broad bands); 3400-3300 cm⁻¹ (secondary N-H stretching); 2950 2850 cm⁻¹ (C-H stretching); 1450 cm⁻¹ (C-H bending); 1410 cm⁻¹ (Si-CH₂ bending); 1350-1400 cm⁻¹ (C-F stretching);
- **TG-DSC** (25 °C-800 °C): 30 °C-175 °C (endothermic peak-water and solvents); 225 °C-780 °C (exothermic peak-metalloporphyrin **18Mn**);
- **ICP:** manganese percentage: 0.026% (0.0057 mmol per gram of nanocomposite).

Synthesis of $\text{MNP@SiO}_2\text{-NH-19Cr}$



In a round-bottom flask, the 3-aminopropylsilyl functionalised magnetite material $\text{MNP@SiO}_2\text{-NH}_2$ (1.5 g) was added to a solution of **19Cr** (300 mg, 0.35 mmol) and cesium carbonate (388 mg, 1.19 mmol) in dry 1,2-dimethoxyethane (100 mL). The mixture was kept under stirring at 85 °C for 24 h. Then, the magnetic solid material was collected using an external magnet and washed several times with acetonitrile, ethyl acetate, and dichloromethane to rinse away excess non-immobilized metalloporphyrins.

Finally, the resulting hybrid metalloporphyrin magnetic $\text{MNP@SiO}_2\text{-NH-19Cr}$ was dried under vacuum for 24 h and characterised by UV-Vis, FT-IR, TG-DSC and ICP.

- **UV-Vis:** 448 nm (Soret band);
- **FT-IR:** 3750-3300 cm^{-1} (Si-OH and OH - Broad bands); 3400-3300 cm^{-1} (secondary N-H stretching); 2950-2850 cm^{-1} (C-H stretching); 1450 cm^{-1} (C-H bending); 1410 cm^{-1} (Si-CH₂ bending); 1350-1400 cm^{-1} (C-F stretching);
- **TG-DSC** (25 °C-800 °C): 30 °C-175 °C (endothermic peak – water and solvents); 225 °C-780 °C (exothermic peak – metalloporphyrin **19Cr**);
- **ICP:** chromium percentage: 0.260% (0.050 mmol per gram of nanocomposite).

5.3 Experimental of Chapter 3

In this section, general reaction conditions for catalytic epoxidation using O_2 and H_2O_2 , catalytic CO_2 cycloaddition reaction to epoxide and sequential epoxidation/cycloaddition CO_2 are described, for homogeneous and heterogeneous phases. In turn, a high-pressure system (**Figure 5.1**) and a high-pressure reactor (**Figure 5.2**) (Department of Chemistry, University of Coimbra, Portugal) were used to perform the catalytic CO_2 cycloaddition reaction to epoxide and sequential epoxidation/ CO_2 cycloaddition reactions.



Figure 5.1 – High-pressure system for catalytic sequential epoxidation/ CO_2 cycloaddition (Department of Chemistry, University of Coimbra, Portugal).

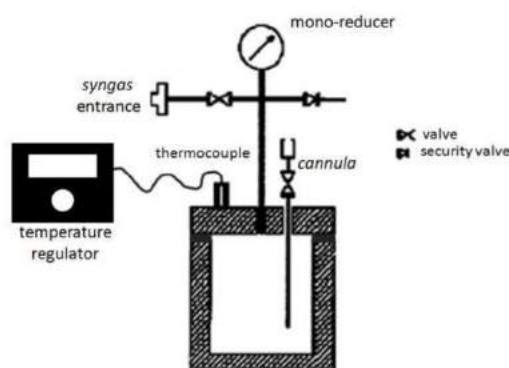


Figure 5.2 – Schematic representation of the reactor for high-pressure CO_2 cycloaddition reactions and sequential epoxidation/ CO_2 cycloaddition reactions.

At the end of each reaction, the samples were analysed by GC and GC-MS, using chlorobenzene (internal standard) to determine conversion (**Equation 1**), selectivity (**Equation 2**) and TON (**Equation 3**), based on peaks areas through the following equations.

$$\text{Conversion (\%)} = \frac{(\text{substrate/standard})_{t=0h} - (\text{substrate/standard})_{t=xh}}{(\text{substrate/standard})_{t=0h}} \times 100$$

(Equation 1)

$$\text{Selectivity (\%)} = \frac{\text{product peak area}}{\text{total product peak area}} \times 100$$

(Equation 2)

$$\text{TON} = \frac{\text{mol of products}}{\text{mol of catalyst}}$$

(Equation 3)

5.3.1 General Procedures for Catalytic Epoxidation Reaction

Homogeneous Epoxidation with O₂

A glass vial was charged with the olefin substrate (0.5 mmol) and homogeneous metalloporphyrin catalyst (4.7 x 10⁻⁵ mmol), solvent (2 mL), isobutyraldehyde (0.18 g; 2.5 mmol) and chlorobenzene (21 mg; 0.19 mmol) as inert internal standard. The reaction was conducted under stirring, at room temperature (25 °C) along 90 min, with a constant bubbling of molecular oxygen. Conversion and selectivity were determined by GC, based on peak areas, using chlorobenzene as internal standard. Products identification was performed by GC analysis against standards and by ¹H- and ¹³C-NMR of isolated products.

Homogeneous Epoxidation with H₂O₂

The olefin substrate (4.5 mmol), ammonium acetate (225 mg; 2.91 mmol), the metalloporphyrin catalyst (7.48 x 10⁻³ mmol), and chlorobenzene (44 mg; 0.39 mmol)

were dissolved in acetonitrile (20 mL). The mixture was introduced into a glass vial and a hydrogen peroxide (2 mmol) solution (30% w/w), diluted with acetonitrile (1:10), was slowly added to the reaction mixture, in 2.25 mL aliquots, until complete substrate conversion. The reaction was conducted at 25 °C, under stirring, for the desired time (45 min with homogeneous catalysts or 24 h with heterogeneous catalysts). Conversion and selectivity were determined by GC, by using chlorobenzene as internal standard. The products identification was performed by GC-MS and GC analysis against standards.

Heterogeneous Epoxidation with O₂

A glass vial was charged with the olefin substrate (0.5 mmol) and metalloporphyrin hybrid magnetic catalyst (4.7×10^{-5} mmol of manganese), solvent (2 mL), isobutyraldehyde (0.18 g; 2.5 mmol) and chlorobenzene (21 mg; 0.19 mmol) as inert internal standard. The reaction was conducted under vigorously stirring, at room temperature (25 °C) for 90-120 min, with a constant bubbling of molecular oxygen. At the end, the hybrid magnetic catalyst was recovered using an external magnet field. Conversion and selectivity were determined by GC, based on peak areas, using chlorobenzene as internal standard. Products identification was performed by GC analysis against standards and by ¹H- and ¹³C-NMR of isolated products.

Heterogeneous Epoxidation with H₂O₂

The olefin substrate (4.5 mmol), ammonium acetate (225 mg; 2.91 mmol), the metalloporphyrin hybrid magnetic catalyst (7.48×10^{-3} mmol metal), and chlorobenzene (44 mg; 0.39 mmol) were dissolved in acetonitrile (20 mL). The mixture was introduced into a glass vial and a hydrogen peroxide (2 mmol) solution (30% w/w), diluted with acetonitrile (1:10), was slowly added to the reaction mixture, in 2.25 mL aliquots, until complete substrate conversion. The reaction was conducted at 25 °C, under stirring, for the desired time (45 min with homogeneous catalysts or 24 h with heterogeneous catalysts). At the end, the hybrid magnetic catalyst was recovered using an external magnet field. Conversion and selectivity were determined by GC, by using chlorobenzene as internal standard. The products identification was performed by GC-MS and GC analysis against standards.

Recycling and Reuse of Heterogeneous Magnetic Catalysts

After the first run of each catalytic experiment, the heterogeneous catalysts **MNP@SiO₂-17Mn** or **MNP@SiO₂-18Mn** were separated from the crude mixtures using an external magnet field, followed by decantation of the supernatant solution. Then, the solid magnetic material was washed with CH₂Cl₂ (3x 4 mL) and CH₃CN (3x 4 mL), dried under vacuum, at 60 °C, for 2 h and reused in the next run.

5.3.2. General Procedures for Catalytic CO₂ Cycloaddition Reaction

Homogeneous CO₂ Cycloaddition to Epoxide

The metalloporphyrin catalyst (2.45×10^{-2} mmol) and the co-catalyst PPnCl (2.45×10^{-2} mmol; if indicated) were placed inside a 100 mL stainless-steel autoclave and kept for 3 h under vacuum, at 80 °C. Then, styrene epoxide (4 mL; 35 mmol), previously dried over alumina and stored under inert atmosphere, was introduced using a cannula into the autoclave. The autoclave was pressurised with CO₂ (10 bar) and the reaction was conducted under stirring (700 rpm), at 80 °C, for 24 h. At the end, the autoclave was cooled in an ice bath and slowly depressurized. Conversion was determined by GC, by using chlorobenzene as internal standard, and selectivity was determined by ¹H-NMR spectroscopy, through integral ratio.

Heterogeneous CO₂ Cycloaddition to Epoxide

The metalloporphyrin hybrid magnetic catalyst (2.45×10^{-2} mmol metal) and the co-catalyst PPnCl (2.45×10^{-2} mmol; if indicated) were placed inside a 100 mL stainless-steel autoclave and kept for 3 h under vacuum, at 80 °C. Then, styrene epoxide (4 mL; 35 mmol), previously dried over alumina and stored under inert atmosphere, was introduced using a cannula into the autoclave. The autoclave was pressurized with CO₂ (10 bar) and the reaction was conducted under stirring (700 rpm), at 80 °C, for 24 h. At the end, the autoclave was cooled in an ice bath and slowly depressurized and the hybrid magnetic catalyst was recovered using an external magnet field. Conversion was determined by GC, by using chlorobenzene as internal

standard, and selectivity was determined by ^1H NMR spectroscopy, through integral ratio.

Recycling and Reuse of Heterogeneous Magnetic Catalysts

After the first run of each catalytic experiment, the heterogeneous catalyst **MNP@SiO₂-19Cr** were separated from the crude mixtures by using an external magnet, followed by decantation of the supernatant solution. Then, the solid magnetic material was washed with CH_2Cl_2 (3x 4 mL) and CH_3CN (3x 4 mL), dried under vacuum, at 60 °C, for 2 h and reused in the next run.

5.3.3. General Procedures for Sequential Epoxidation/ CO_2 Cycloaddition Reaction

Homogeneous Sequential Epoxidation/ CO_2 Cycloaddition with O_2 as the Oxidant

A dichloromethane or butyronitrile solution (2 mL) containing styrene (1 mL; 8.69 mmol), the catalyst **15Mn** (0.8 mg; 8.16×10^{-4} mmol), isobutyraldehyde (3.1 g; 43.4 mmol), and chlorobenzene (21 mg; 0.19 mmol) was introduced into an autoclave. The reaction was conducted with stirring at 25 °C, under oxygen bubbling, for 4 h. Meanwhile, the catalyst **12Cr** (5.9 mg; 6.08×10^{-3} mmol) and **PPNCl** (6.08×10^{-3} mmol) were placed inside a 100 mL stainless-steel autoclave and kept for 3 h under vacuum, at 80 °C. Then, the epoxidation crude mixture was transferred using a cannula into the autoclave. The reactor was pressurized with CO_2 (10 bar) and the reaction was conducted at 80 °C for 24 h. At the end, the autoclave was cooled in an ice bath and slowly depressurised. The product identification was performed by GC-MS and GC analysis against standards. Conversion was determined by GC, by using chlorobenzene as internal standard, and selectivity was determined by ^1H -NMR spectroscopy, through peak integral ratio.

Homogeneous Sequential Epoxidation/ CO_2 Cycloaddition with H_2O_2 as the Oxidant

The olefin substrate (4.5 mmol), ammonium acetate (225 mg; 2.91 mmol), the catalyst **15Mn** (7.5 mg; 7.48×10^{-3} mmol), and chlorobenzene (44 mg; 0.39 mmol)

were dissolved in CH₃CN (20 mL). The mixture was then introduced into an autoclave and an aqueous hydrogen peroxide (2 mmol) solution (30% w/w), diluted with acetonitrile (1:10), was slowly added to the reaction mixture, in 2.25 mL aliquots, every 15 min. The reaction was conducted with stirring at 25 °C, for 45 min. Then, the crude mixture was dried over anhydrous sodium sulfate, concentrated to a total volume of 2.5 mL, and stored under inert atmosphere. Meanwhile, the catalyst **12Cr** (3.0 mg; 3.15 x 10⁻³ mmol) and the co-catalyst PPNCl (1.8 mg; 3.15 x 10⁻³ mmol) were placed inside a 100 mL stainless-steel autoclave and kept for 3 h under vacuum, at 80 °C. Then, the epoxidation crude mixture was transferred using a cannula into the autoclave. The reactor was pressurized with CO₂ (10 bar) and the reaction was conducted at 80 °C for 24 h. At the end, the autoclave was cooled in an ice bath, and slowly depressurized. Conversion was determined by GC, by using chlorobenzene as internal standard, and selectivity was determined by ¹H-NMR spectroscopy, through peak integral ratio.

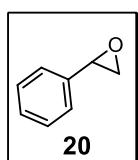
Heterogeneous Sequential Epoxidation/CO₂ Cycloaddition with O₂ as the Oxidant

Styrene (1 mL, 8.69 mmol), the hybrid catalysts **MNP@SiO₂-17Mn** (66 mg; 8.16 x 10⁻⁴ mmol Mn) and **MNP@SiO₂-19Cr** (122 mg; 6.08 x 10⁻³ mmol Cr), isobutyraldehyde (3.1 g; 43.4 mmol), chlorobenzene (0.4 g; 3.32 mmol), and dichloromethane were introduced into a glass vial, inside an autoclave and the reaction was conducted with stirring at 25 °C, under oxygen bubbling, for 4 h. After this period, the hybrid solid material (containing both catalysts **MNP@SiO₂-17Mn** and **MNP@SiO₂-19Cr**) was collected at the autoclave walls, by using an external magnet, and the liquid was decanted. Then, PPNCl (6.08 x 10⁻³ mmol) was added to the stainless-steel autoclave containing the hybrid magnetic catalysts and the reactor was kept under vacuum, at 80 °C, for 3 h. Next, the crude mixture obtained in the epoxidation step was treated with a saturated sodium hydrogen carbonate solution (30 mL). After phase separation, the organic phase was dried over sodium sulfate anhydrous and introduced using a cannula into the stainless-steel autoclave containing the recovered hybrid catalysts. Then, the reactor was pressurised with CO₂ (10 bar) and the reaction was conducted at 80 °C for 24 h. At the end, the autoclave was cooled

and slowly depressurized. Finally, the mixture of magnetic catalysts (**MNP@SiO₂-17Mn** and **MNP@SiO₂-19Cr**) was separated from the reaction mixture by using an external magnet. The recovered solid material was washed with dichloromethane (3x 4 mL), dried in vacuum for 2 h at 60 °C, and reused in the next run. Conversion was determined by GC, by using chlorobenzene as internal standard, and selectivity was determined by ¹H-NMR spectroscopy, through peak integral ratio.

Styrene oxide (20)

The catalytic epoxidation of styrene was performed using the general procedure for epoxidation with O₂ and H₂O₂ as the oxidant, above described. After work-up and purification by column chromatography in silica gel, using a mixture of ethyl acetate/*n*-hexane (1.5:1) as eluent.



Yield (%):

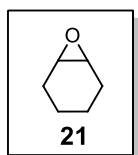
Catalytic epoxidation with O₂ = 99% (59 mg; 0.49 mmol);

Catalytic epoxidation with H₂O₂ = 99% (535 mg; 4.45 mmol);

¹H-NMR (400 MHz, CDCl₃, TMS): δ, ppm = 7.17-7.10 (m, 5H), 3.65 (m, 1H), 2.92 (m, 1H), 2.59 (m, 1H); **¹³C-NMR (100 MHz, CDCl₃):** δ, ppm = 137.6, 128.3, 128.0, 125.4, 52.1, 50.9 (data is in good agreement that previously reported).^[24]

1,2-cyclohexene oxide (21)

The catalytic epoxidation of cyclohexene (41 mg; 0.50 mmol) was performed using the general procedure for epoxidation with O₂ as the oxidant, above described. After work-up and purification by column chromatography in silica gel, using a mixture of ethyl acetate/*n*-hexane (1:1) as eluent.

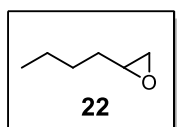


Yield (%): 97% (48 mg; 0.48 mmol);

¹H-NMR (400 MHz, CDCl₃, TMS): δ, ppm = 2.94-2.93 (m, 2H), 1.76-1.73 (m, 2H), 1.66-1.65 (m, 2H), 1.26-1.22 (m, 2H), 1.11-1.03 (m, 2H); **¹³C-NMR (100 MHz, CDCl₃):** δ, ppm = 51.8, 24.3, 19.3 (data is in good agreement that previously reported).^[25]

1,2-hexene oxide (22)

The 1,2-hexene oxide (**22**) was synthesized through the epoxidation of 1,2-hexene (55 mg; 0.50 mmol) using the O₂ as the oxidant, above described. After work-up and purification by column chromatography in silica gel, using a mixture of ethyl acetate/*n*-hexane (1.5:5) as eluent.

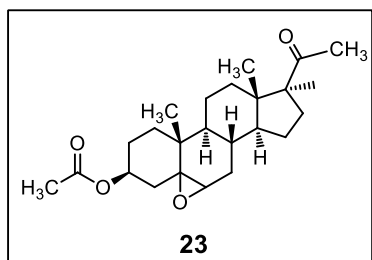


Yield (%): 60% (30 mg; 0.30 mmol);

¹H-NMR (400 MHz, CDCl₃, TMS): δ, ppm = 2.81-2.77 (m, 1H), 2.63 (dd, *J*₁ = 4.9 Hz, *J*₂ = 4.2 Hz, 1H), 2.35 (dd, *J*₁ = 4.9 Hz, *J*₂ = 2.7 Hz, 1H), 1.44 – 1.41 (m, 2H), 1.39-1.27 (m, 2H), 0.82 (t, *J* = 7.1 Hz, 3H); **¹³C-NMR (100 MHz, CDCl₃):** δ, ppm = 52.2, 46.9, 32.1, 28.0, 22.5, 13.9 (data is in good agreement that previously reported).^[25]

β- and α-Pregnenolone acetate oxide (23)

The catalytic epoxidation of pregnenolone acetate (89 mg; 0.25 mmol) was performed using the general procedure for epoxidation with O₂, above described. After work-up and purification by column chromatography in silica gel, using a mixture of ethyl acetate/*n*-hexane (1:5) as eluent.

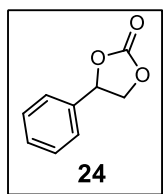


Yield (%): 57% (54 mg; 0.14 mmol);

¹H-NMR (400 MHz, CDCl₃, TMS): δ, ppm = 4.99-4.74 (m, 1H), 3.08 (d, *J* = 4.3 Hz, 1H), 2.91 (d, *J* = 1.8 Hz, 1H), 2.50-2.48 (m, 1H), 2.19-1.97 (m, 11H), 1.70-1.60 (m, 4H), 1.55-1.01 (m, 16H), 0.89-0.68 (m, 1H), 0.58 (d, *J* = 13.3 Hz, 3H); **¹³C-NMR (100 MHz, CDCl₃):** δ, ppm = 209.6, 209.5, 170.7, 170.4, 71.4, 65.3, 63.8, 63.5, 59.1, 57.1, 56.4, 51.0, 44.1, 44.0, 42.5, 39.0, 38.6, 36.9, 36.2, 35.3, 35.2, 32.3, 31.7, 31.6, 30.0, 29.9, 28.7, 27.3, 24.5, 24.4, 22.8, 22.0, 21.5, 20.8, 17.2, 16.0, 13.4, 13.3 (data is in good agreement that previously reported).^[26]

Styrene carbonate (24)

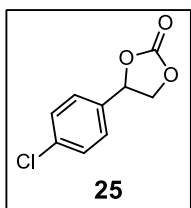
The catalytic CO₂ cycloaddition of styrene oxide (4.2 g; 35 mmol) and the sequential epoxidation/CO₂ cycloaddition of styrene (0.47g; 4.5 mmol) with O₂ as the oxidant were performed using the general procedures, above described. After 24 h, a sample from crude reaction was analysed by GC-MS.



MS (EI) m/z: 164.1, 119.1, 105.1, 90.1, 78.1, 65.1, 51.1, 39.1, 30.1
(data is in good agreement that previously reported).^[27]

4-chlorostyrene carbonate (25)

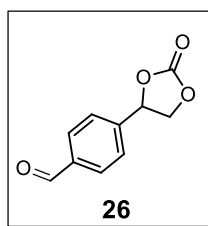
The 4-chlorostyrene carbonate (25) was synthesised by sequential process epoxidation/CO₂ cycloaddition of 4-chlorostyrene (0.6 g; 4.5 mmol) with H₂O₂ as the oxidant, above described. After 24 h, a sample from crude reaction was analysed by GC-MS.



MS (EI) m/z: 198.0, 163.1, 139.0, 124.1, 112.1, 101.1, 89.1, 75.1, 63.1, 50.1, 39.1 (data is in good agreement that previously reported).^[27]

4-methylstyrene carbonate (26)

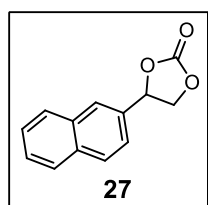
The sequential epoxidation/CO₂ cycloaddition of 4-methylstyrene (0.53 g; 4.5 mmol) with H₂O₂ as the oxidant was performed using the general procedure above described. After 24 h, a sample from crude reaction was analysed by GC-MS.



MS (EI) m/z: 191.1, 163.0, 147.0, 133.1, 105.1, 76.1.

2-naphthalene carbonate (27)

The sequential epoxidation /CO₂ cycloaddition of 2-vinylnaphthalene (0.69 g; 4.5 mmol) with H₂O₂ as the oxidant was performed using the general procedure above described. After 24 h, a sample from crude reaction was analysed by GC-MS.



MS (EI) m/z: 214.1, 169.1, 155.1, 140.1, 115.1, 101.1, 77.1, 63.1, 39.1 (data is in good agreement that previously reported).^[28]

5.4 Experimental of Chapter 4

5.4.1. Catalytic Epoxidation of Terpenes

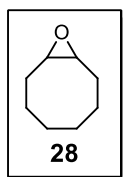
The epoxidation reaction with O₂ of cyclooctene (model substrate) and a family of terpenes (α -pinene, limonene and (-)-isopulegol benzyl ether) were carried out according to the general procedure for catalytic epoxidation reaction, described in section 5.3.1.

Scale-up and Experimental Setup for the Recovery of Isobutyric Acid

The scale-up epoxidation of cyclooctene was performed as the general procedure for heterogeneous catalytic epoxidation with O₂ described above, using cyclooctene (0.992 g; 9 mmol), isobutyraldehyde (3.245 g; 45 mmol), **MNP@SiO₂-NH-17Mn** (64.8 mg; 8.42×10^{-4} mmol Mn), butyronitrile (36 mL) as the solvent and chlorobenzene (3.51 mmol) as internal standard. Then, a sodium bicarbonate saturated solution (50 mL) was added to the crude reaction, leading to the formation of two phases. The target epoxide was then isolated from the organic phase by simple distillation, while the aqueous phase was treated with a 33% HCl solution, to adjust the solution pH value to 3. Finally, extraction with 2-methyltetrahydrofuran was performed and, after distillation, isobutyric acid was obtained with 99% yield (3.921 g; 44.5 mmol) and characterised by ¹H- and ¹³C-NMR spectroscopy.

Cyclooctene oxide (28)

The catalytic epoxidation of *cis*-cyclooctene (55 mg; 0.50 mmol) was performed using the general procedure for epoxidation with O₂ as the oxidant, above described. After work-up and purification by column chromatography in silica gel, using a mixture of ethyl acetate/*n*-hexane (1:1) as eluent.



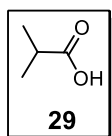
Yield (%): 95% (59 mg; 0.47 mmol);

¹H-NMR (400 MHz, CDCl₃, TMS): δ , ppm = 2.91-2.88 (m, 2H), 2.16-2.12 (m, 2H), 1.63-1.44 (m, 8H), 1.29-1.26 (m, 2H); **¹³C-NMR**

(100 MHz, CDCl₃): δ , ppm = 55.8, 26.7, 26.4, 25.7 (data is in good agreement that previously reported).^[29]

Isobutyric acid (29)

The isobutyric acid (**29**) was obtained through scale-up and experimental setup process, described above. After extraction with 2-methyltetrahydrofuran and distillation.



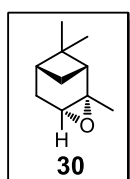
Yield(%): 95% (3.766 g; 42.7 mmol);

¹H-NMR (400 MHz, CDCl₃, TMS): δ, ppm = 11.07 (s, 1H), 2.55 (m, 1H), 1.17 (s, 3H), 1.15 (s, 3H); **¹³C-NMR (100 MHz, CDCl₃):** δ, ppm =

55.8, 26.7, 26.4, 25.7

α-pinene oxide (30)

The catalytic epoxidation of α-pinene (68 mg; 0.50 mmol) was performed using the general procedure for epoxidation with O₂, above described. After work-up and purification by column chromatography in silica gel, using a mixture of ethyl acetate/*n*-hexane (1:3) as eluent.



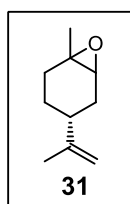
Yield (%): 96% (73 mg; 0.48 mmol);

¹H-NMR (400 MHz, CDCl₃, TMS): δ, ppm = 2.97 (d, *J* = 4.1 Hz, 1H), 1.94-1.79 (m, 4H), 1.68-1.59 (m, 1H), 1.54 (d, *J* = 9.5 Hz, 1H), 1.25

(s, 3H), 1.20 (s, 3H), 0.85 (s, 3H). **¹³C-NMR (100 MHz, CDCl₃):** δ, ppm = 60.2, 56.8, 45.1, 40.5, 39.7, 27.6, 26.7, 25.8, 22.4, 20.2 (data is in good agreement that previously reported).^[30]

(+)-Limonene oxide (31) (mixture of isomers)

The (+)-limonene oxide (**31**) was synthesized through the epoxidation of (+)-limonene (68 mg; 0.50 mmol) using the O₂ as the oxidant, above described. After work-up and purification by column chromatography in silica gel, using a mixture of ethyl acetate/*n*-hexane (1:4) as eluent.



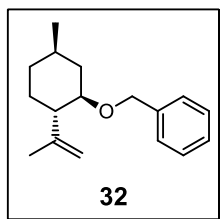
Yield (%): 95% (72 mg; 0.47 mmol);

¹H-NMR (400 MHz, CDCl₃, TMS): δ, ppm = 4.61-4.55 (m, 2H), 2.93-2.85 (m, 1H), 2.00-1.89 (m, 2H), 1.74-1.70 (m, 1H), 1.59-1.54 (m, 5H), 1.27-1.17 (m, 5H). **¹³C-NMR (100 MHz, CDCl₃):** δ, ppm =

148.9, 148.7, 109.0, 60.3, 59.0, 57.3, 57.1, 40.6, 36.1, 30.67, 30.6, 29.8, 28.5, 25.8, 24.2, 24.2, 23.0, 21.0, 20.1 (data is in good agreement that previously reported).^[31]

(–)-Isopulegol benzyl ether (**32**)

(–)-isopulegol (1.0 g; 6.5 mmol) and NaH (0.192 g; 8.0 mmol) was added in dried THF (25 mL) and kept in reflux under stirring. Then, benzyl bromide (1.36 g; 8.0 mmol) was added dropwise and the reaction's progress was followed by TLC using mixture a of *n*-hexane/ethyl acetate (9:1) as the eluent. Upon complete conversion of the starting material, the reaction crude was extracted with ethyl ether (50 mL), the organic phase was dried with anhydrous sodium sulphate and the solvent was evaporated under reduced pressure. After purification by silica gel column chromatography, using mixture of *n*-hexane/ethyl acetate (9:1) as eluent, the product (–)-isopulegol benzyl ether (**32**) was obtained.



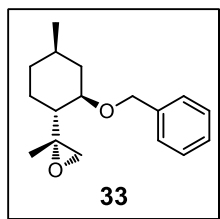
Yield (%): 88% (1.39 g; 5.72 mmol);

¹H-NMR (400 MHz, CDCl₃, TMS): δ , ppm = 0.84-1.05 (m, 2H, CH), 0.94 (d, J = 6.6 Hz, 3H, CH₃), 1.21-1.48 (m, 2H, CH), 1.56-1.67 (m, 2H, CH), 1.67-1.70 (m, 3H, CH₃), 2.01-2.20 (m, 2H, CH), 3.28 (td, J_1 = 10.5, J_2 = 4.1 Hz, 1H, CHOBn), 4.41 (d, J = 11.7 Hz, 1H, CHPh), 4.59 (d, J = 11.5 Hz, 1H, CHPh), 4.80 (m, 2H, =CH₂), 7.16-7.37 (m, 5H, ArH).
¹³C-NMR (100 MHz, CDCl₃): δ , ppm = 19.9, 22.2, 30.9, 31.4, 34.3, 40.1, 51.7, 70.3, 79.1, 110.9, 127.1, 127.5, 128.0, 139.0, 147.7. **MS (EI) m/z:** 244.1, 229.0, 153.1, 138.1, 123.1, 91.1, 69.1, 41.1.

(–)-Isopulegol-benzyl ether epoxides (**33** and **34**)

The catalytic epoxidation of (–)-isopulegol benzyl ether (**32**) (122 mg; 0.50 mmol) was performed using the general procedure for epoxidation with O₂, above described. Then, a solution of sodium bicarbonate saturated (50 mL) was added to the crude mixture, leading the formation of two phases and solvent evaporated. After purification by column chromatography in silica gel, using a mixture of ethyl acetate/*n*-hexane (1:4) as eluent, the diastereoisomers of (–)-isopulegol benzyl ether epoxides were isolated.

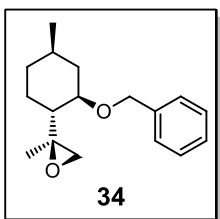
Diastereoisomer **A (33)**: (*R*)-2-((1*R*,2*R*,4*R*)-2-(benzyloxy)-4-methylcyclohexyl)-2-methyloxirane.



Yield (%): 51% (67 mg; 0.26 mmol);

¹H-NMR (400 MHz, CDCl₃, TMS): δ, ppm = 7.35-7.25 (m, 5H, HAr), 4.67 (d, *J* = 12.0 Hz, 1H, H11), 4.40 (d, *J* = 12.0 Hz, 1H, H11), 3.26 (ddd, *J*₁ = 10.8 Hz, *J*₂ = 10.8 Hz, *J*₃ = 4.4 Hz, H2), 2.76 (d, *J* = 4.8 Hz, 1H, H9), 2.68 (d, *J* = 4.8 Hz, 1H, H9), 2.24-2.18 (m, 1H, H3eq), 1.91-1.85 (m, 1H, H6eq), 1.70-1.66 (m, 1H, H5eq), 1.46-1.36 (m, 1H, H6ax), 1.34-1.23 (m, 1H, H4), 1.14-1.07 (m, 1H, H1), 1.12 (s, 3H, CH₃-7), 0.94 (d, *J* = 6.4 Hz, 3H, CH₃-10), 0.92-0.83 (m, 2H, H3ax, H5ax). **¹³C-NMR (100 MHz, CDCl₃)**: δ, ppm = 16.7 (C-7), 22.3 (C-10), 26.4 (C-6), 31.5 (C-4), 33.9 (C-5), 39.9 (C-3), 50.8 (C-1), 56.8 (C-9), 57.9 (C-8), 70.2 (C-11), 78.8 (C-2), 127.6 (C-Ar), 128.4 (C-Ar), 139.0 (C-Ar). **(ESI-FIA-TOF)**: *m/z* = 283.1669 [M+Na]⁺ calculated for C₁₇H₂₄O₂ [M+Na]⁺ = 283.1669.

Diastereoisomer **B (34)**: (*S*)-2-((1*R*,2*R*,4*R*)-2-(benzyloxy)-4-methylcyclohexyl)-2-methyloxirane.



Yield (%): 45% (60 mg; 0.23 mmol);

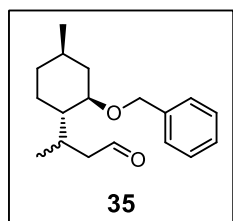
¹H-NMR (400 MHz, CDCl₃, TMS): δ, ppm = 7.41 (d, *J* = 8.0 Hz, 2H, HAr), 7.35-7.31 (m, 2H, HAr), 7.26-7.25 (m, 1H, HAr), 4.72 (d, *J* = 12.0 Hz, 1H, H11), 4.44 (d, *J* = 12.0 Hz, 1H, H11), 3.29 (ddd, *J*₁ = 10.4 Hz, *J*₂ = 10.4 Hz, *J*₃ = 4.0 Hz, H2), 2.76 (d, *J* = 4.8 Hz, 2H, H9), 2.24 – 2.19 (m, 1H, H3eq), 1.76 – 1.70 (m, 1H, H6eq), 1.69 – 1.64 (m, 1H, H5eq), 1.44 – 1.35 (m, 1H, H4), 1.34 – 1.28 (m, 1H, H1), 1.25 (s, 3H, CH₃-7), 1.20 – 1.11 (m, 1H, H6ax), 0.95 (d, *J* = 6.4 Hz, 3H, CH₃-10), 0.97 – 0.88 (m, 2H, H3ax, H5ax). **¹³C-NMR (100 MHz, CDCl₃)**: δ, ppm = 18.9 (C-7), 22.2 (C-10), 27.8 (C-4), 31.3 (C-6), 34.2 (C-5), 39.6 (C-3), 49.2 (C-1), 52.0 (C-9), 58.3 (C-8), 69.7 (C-11), 78.3 (C-2), 127.4 (C-Ar), 127.7 (C-Ar), 128.3 (C-Ar), 138.9 (C-Ar). **MS (ESI-FIA-TOF)**: *m/z* = 283.1669 [M+Na]⁺ calculated for C₁₇H₂₄O₂ [M+Na]⁺ = 283.1669.

5.4.2. Catalytic Hydroformylation of (–)-Isopulegol Benzyl Ether

The rhodium precursor $[\text{Rh}(\text{acac})(\text{CO})_2]$ (3.0 mg; 1×10^{-2} mmol) and the bulk monophosphite ligand (*S*)-L2-OBn (57 mg; 5×10^{-2} mmol) were added into a stainless steel autoclave. Then, toluene (3 mL) was placed under vacuum, the reactor was pressurized with CO/H_2 (30 bar) (1:1) and the mixture remained under stirring at 80 °C, during 1 h. After incubation period, (–)-isopulegol benzyl ether (**32**) (61 mg; 0.25 mmol) and toluene (2 mL) were added into reactor. The reaction mixture was kept under magnetic stirring, at 80 °C and with 25 bar of CO/H_2 , for 12 h. At the end, the autoclave was cooled at 25 °C and depressurised. Finally, the solvent was evaporated and the crude mixture was purified by column chromatography in silica gel, using a mixture of *n*-hexane/ethyl acetate (4:1) as the eluent, yielding the isomeric aldehydes **35** and **36** with 95% of chemoselectivity and a diastereomeric ratio of 77:23, respectively.

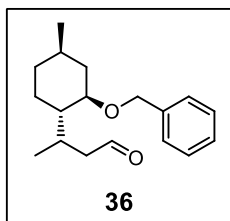
(–)-Isopulegol-benzyl ether aldehydes (**35** and **36**)

Diastereoisomer **35**



Yield (%): 70% (48 mg; 0.176 mmol);

$^1\text{H-NMR}$ (400 MHz, CDCl_3 , TMS): δ , ppm = 0.73 (d, $J = 7.1$ Hz, 3H, CH_3), 0.77-1.09 (m, 2H, CH), 0.93 (d, $J = 6.2$ Hz, 3H, CH_3), 1.23-1.42 (m, 2H, CH), 1.46-1.57 (m, 1H, CH_3CHCH_2), 1.59-1.70 (m, 1H, CH), 2.14-2.34 (m, 3H, $\text{CH}_2\text{C}=\text{O}$ and CH), 2.69-2.86 (m, 1H, CH), 3.17 (td, $J_1 = 10.5$ Hz, $J_2 = 4.05$ Hz, 1H, CHOBn), 4.37 (d, $J = 11.6$ Hz, 1H, OCHHBn), 4.65 (d, $J = 11.6$ Hz, 1H, OCHHBn), 7.16-7.41 (m, 5H, CHAr), 9.66 (t, $J = 2.5$ Hz, 1H, CHO). **$^{13}\text{C-NMR}$ (100 MHz, CDCl_3)**: δ , ppm = 13.79, 22.01, 23.48, 25.84, 31.06, 34.04, 39.70, 46.85, 49.22, 69.88, 77.61, 127.17, 127.50, 128.08, 138.59, 202.62. **MS (EI) m/z** : 274.1, 256.0, 201.1, 183.1, 167.1, 107.1, 91.0, 69.0, 41.0.

Diastereoisomer **36**

Yield (%): 19% (13 mg; 0.048 mmol);

¹H-NMR (400 MHz, CDCl₃, TMS): δ , ppm = 0.91 (d, J = 7.1 Hz, 3H, CH₃), 0.94 (d, J = 6.4 Hz, 3H, CH₃), 0.84-0.98 (m, 3H, CH), 1.25-1.47 (m, 2H, CH), 1.61-1.71 (m, 2H, CH), 1.94-2.09 (m, 1H, CH₃CHCH₂), 2.13-2.28 (m, 2H, CH₂C=O), 2.55-2.71 (m, 1H, CH), 3.11 (td, J_1 = 10.5, J_2 = 4.2 Hz, 1H, CHOBN), 4.33 (d, J = 11.6 Hz, 1H, OCHHPh), 4.65 (d, J = 11.6 Hz, 1H, OCHHBn) 7.20-7.39 (m, 5H, CHAr), 9.54 (dd, J_1 = 3.2 Hz, J_2 = 1.5 Hz, 1H, HC=O). **¹³C-NMR (100 MHz, CDCl₃):** δ , ppm = 17.86, 22.10, 25.02, 26.56, 31.20, 34.31, 39.65, 46.40, 69.67, 76.57, 127.46, 127.95, 128.23, 138.52, 203.31. **MS (EI) m/z:** 274.1, 256.1, 213.1, 183.1, 167.1, 107.1, 91.0, 79.0, 41.0.

5.4.3. Biological Assays of (-)-Isopulegol Benzyl Ether

Epoxides

This section describes the procedures performed in this work, regarding preparation of solutions, cell growth and drug exposure protocols with an osteosarcoma cell line (MG-63).

Preparation of solutions

Table 5.1 – Preparation of solutions for biological assays.

Solution	Components	pH	Storage
Phosphate Buffered Saline (PBS) 10x	2.0 g KH ₂ PO ₄ (15 mM) 6.1 g Na ₂ HPO ₄ (43 mM) 2.0 g KCl (27 mM) 87.7 g NaCl (1.5 M) 1000.0 mL ultrapure water	7.4	Room temperature
PBS 1x	100.0 mL PBS 10x 900.0 mL ultrapure water	7.4	Room temperature
DMEM-HG	13.4 g DMEM-HG 1.5 g NaHCO ₃ 1000.0 mL (final volume) ultrapure water	7.4	4 °C
DMEM-HG 10% (v/v) FBS/1% Pen/Strep	890.0 mL DMEM-HG 100.0 mL FBS 10.0 mL Pen/Strep	7.4	4 °C
Trypsin-EDTA 1x	90.0 mL PBS 1x 10.0 mL Trypsin 10 x 20.0 mg EDTA	7.4	4 °C
Methanol 1% (v/v) in Acetic Acid	495.0 mL Methanol 5.0 mL Acetic acid	-	-20 °C
1% Acetic Acid	990.0 mL deionised water 10.0 mL Acetic acid	-	Room temperature
SRB 0.5%	2.5 g Sulforhodamine B 500.0 mL 1% Acetic acid solution	-	Room temperature
Tris 10mM	1.2 g Tris base 1000.0 mL ultrapure water	10	Room temperature

MG-63 Cell Line

The human osteosarcoma cells (MG-63) morphologically present as elongated shape cells being classified as fibroblasts and were established from an osteosarcoma of a 14 year old Causacian male.^[32] The MG-63 cells line has a population doubling

time of approximately 24 hours and can be used for many tens of passages, preserving its morphological proprieties. These characteristics justify its use as a model cell lines in different research contexts.

Cell Culture

The MG-63 is an adherent cell line that grows in monolayers and was acquired from the HPA Collections (Sigma-Aldrich, Portugal). Osteosarcoma cells were grown using Minimum Essential Medium (MEM) (Sigma-Aldrich, Portugal), complemented with (10%) heat-inactivated fetal bovine serum (FBS) (Alfagene, Portugal), 1 mM sodium pyruvate (Sigma-Aldrich, Portugal), 1 mM non-essential amino acids (Sigma-Aldrich, Portugal) and penicillin-streptomycin (Sigma-Aldrich, Portugal) and were kept at 5% CO₂ and 37 °C, under humidified atmosphere, using a MCO-19A Incubator (SanyoElectric Co., Ltd.). The MG-63 cells line was grown in 150 cm² cultures flasks and when a confluence of approximately 80% was reached, the cells were washed using a solution of phosphate buffered saline (PBS, pH = 7.4) (Sigma-Aldrich, Portugal), following by addition of a 0.05% trypsin/ethylenediaminetetraacetic acid (EDTA) (Sigma-Aldrich, Portugal) solution. Then, after detachment of the cells, trypsin was neutralized by addition (2x) of complete MEM. The cells suspension was centrifuged (1100 rpm, 5 min, 21 °C), followed by resuspension in a known volume of MEM, from which 100 µL were taken for cell counting using the Trypan blue assay, described below.

Trypan Blue Assay

In order to assess the number of morphologically intact cells, the Trypan blue colorimetric assay was used.^[33] For this purpose, after washed steps, the cells were incubated using a solution of Trypan blue dye (0.4% w/v), followed by counting using a Neubauer-counting chamber (Boeco) under an optical microscope. Thus, the number of cells with intact membranes and, therefore, dye excluding was expressed in mean ± standard deviation (SD).

Cytotoxic Evaluation and Antiproliferative Effects (IC₅₀ Determination)

Cytotoxic: MTT Assay

The MTT assay^[34] was used to determine the IC₅₀ concentration for (–)-isopulegol epoxide diastereomers (**33** and **34**). MG-63 cells cultures were established in 24-well plates (1 mL/well) at a density of 3 x 10⁴ cells/cm². Cells were allowed to attach for 24 h, treated with six different concentrations (350, 300, 250, 200, 150 and 100 μM) and incubated in a humidified atmosphere (5% CO₂), at 37 °C. All experiments were carried out in triplicate and both epoxides (**33** and **34**) were solubilised in DMSO (concentration never exceeding 0.1% (v/v) in the cell cultures). After 24 h of drug exposure (24, 48 and 72 h), cells were washed using a solution of PBS (1 mL), MTT solution in PBS (0.5 mg/mL – 500 μL) (Sigma-Aldrich, Portugal) was added to each well and plates were incubated for 3 h. The violet MTT formazan precipitate was then solubilised by addition of dimethylsulfoxide (500 μL) (Sigma-Aldrich, Portugal) to each well and absorbance was measured at 570 nm on a microplate reader Biotek μQuant MQX200.

Antiproliferative Activity Evaluation: SRB Assay

The colorimetric SRB assay^[35] is complementary to previous MTT assay and was also used to assess the IC₅₀ concentration of (–)-isopulegol epoxide diastereomers (**33** and **34**). MG-63 cells cultures were established in 24-well plates (1 mL/well) at a density of 3 x 10⁴ cells/cm². Cells were allowed to attach for 24 h, treated with six different concentrations (350, 300, 250, 200, 150 and 100 μM) and incubated in a humidified atmosphere (5% CO₂), at 37 °C. All experiments were carried out in triplicate and both epoxides (**33** and **34**) were solubilised in DMSO (concentration never exceeding 0.1% (v/v) in the cell cultures). After 24 h of drug exposure (24, 48 and 72 h), cells were washed with PBS (2x) and miliQ water (1x). Then, the cells were put in the incubator (10 min) for remaining water evaporation and fixed (overnight) using a solution of 1% acetic acid in methanol (2 mL/well), at -20 °C. After this period, the solvent excess was discarded, the plate was left to dry at room temperature

and a solution of 0.5% SRB in acetic acid (1 mL) was added to each well, following by the incubation in the dark at 37 °C, for 1 hour. Then, the MG-63 cells were washed with a solution of 1% acetic acid aiming to remove non-bonded SRB and dried (12 h, room temperature). The amount of SRB bounded to cells proteins was dissolved by addition of a solution 10 mM Tris at pH = 10 (2 mL), and the absorbance was measured at 540 nm. The calculation of cell density (%) was determined according to the following **equation 4**:

$$\text{Cell Density (\%)} = \frac{\text{Abs}_{\text{treated}} - \text{Abs}_{0\text{h}}}{\text{Abs}_{\text{control}} - \text{Abs}_{0\text{h}}} \times 100$$

(Equation 4)

5.5. References

- [1] D. F. Shriver, M. A. Drezdson, *The Manipulation of Air-Sensitive Compounds*, Wiley and Sons, New York, **1986**.
- [2] H. D. Burrows, M. M. Pereira, *Química: Síntese e Estrutura- Uma abordagem prática*, Escolar Editora, Coimbra, **2006**.
- [3] W. L. F. Armarego, D. D. Perrin, *Purification of Laboratory Chemicals*, Butterworth Heinemann, Oxford, **1996**.
- [4] A. Gonsalves, J. Varejao, M. M. Pereira, *Journal of Heterocyclic Chemistry* **1991**, *28*, 635-640.
- [5] A. Gonsalves, M. M. Pereira, A. C. Serra, R. A. W. Johnstone, M. Nunes, *Journal of the Chemical Society-Perkin Transactions 1* **1994**, 2053-2057.
- [6] M. Silva, A. Fernandes, S. S. Bebiano, M. J. F. Calvete, M. F. Ribeiro, H. D. Burrows, M. M. Pereira, *Chemical Communications* **2014**, *50*, 6571-6573.
- [7] C. A. Henriques, S. M. A. Pinto, G. L. B. Aquino, M. Pineiro, M. J. F. Calvete, M. M. Pereira, *Chemsuschem* **2014**, *7*, 2821-2824.
- [8] R. A. W. Johnstone, M. Nunes, M. M. Pereira, A. Gonsalves, A. C. Serra, *Heterocycles* **1996**, *43*, 1423-1437.
- [9] F. R. Kooriyaden, S. Sujatha, C. Arunkumar, *Polyhedron* **2015**, *97*, 66-74.
- [10] J. C. P. Grancho, M. M. Pereira, M. D. Miguel, A. M. R. Gonsalves, H. D. Burrows, *Photochemistry and Photobiology* **2002**, *75*, 249-256.
- [11] A. Giraudeau, H. J. Callot, J. Jordan, I. Ezhar, M. Gross, *Journal of the American Chemical Society* **1979**, *101*, 3857-3862.
- [12] H. K. Hombrecher, V. M. Gherdan, S. Ohm, J. A. S. Cavaleiro, M. Neves, M. D. Condesso, *Tetrahedron* **1993**, *49*, 8569-8578.
- [13] Z. C. Sun, Y. B. She, Y. Zhou, X. F. Song, K. Li, *Molecules* **2011**, *16*, 2960-2970.
- [14] H. Sugimoto, H. Ohshima, S. Inoue, *Journal of Polymer Science Part A-Polymer Chemistry* **2003**, *41*, 3549-3555.
- [15] P. Chen, M. H. Chisholm, J. C. Gallucci, X. Y. Zhang, Z. P. Zhou, *Inorganic Chemistry* **2005**, *44*, 2588-2595.
- [16] K. Sugiura, S. Mikami, T. Tanaka, M. Sawada, J. L. Manson, J. S. Miller, Y. Sakata, *Chemistry Letters* **1997**, 1071-1072.
- [17] D. J. Liston, B. O. West, *Inorganic Chemistry* **1985**, *24*, 1568-1576.
- [18] L. Cuesta-Aluja, J. Castilla, A. M. Masdeu-Bulto, C. A. Henriques, M. J. F. Calvete, M. M. Pereira, *Journal of Molecular Catalysis A-Chemical* **2016**, *423*, 489-494.
- [19] R. M. B. Carrilho, L. D. Dias, R. Rivas, M. M. Pereira, C. Claver, A. M. Masdeu-Bulto, *Catalysts* **2017**, *7*, 210-222.
- [20] N. K. Boen, M. A. Hillmyer, *Macromolecules* **2003**, *36*, 7027-7034.

-
- [21] T. G. Traylor, A. R. Miksztal, *Journal of the American Chemical Society* **1989**, *111*, 7443-7448.
- [22] L. M. Rossi, L. L. R. Vono, F. P. Silva, P. K. Kiyohara, E. L. Duarte, J. R. Matos, *Applied Catalysis A-General* **2007**, *330*, 139-144.
- [23] D. K. Yi, S. S. Lee, G. C. Papaefthymiou, J. Y. Ying, *Chemistry of Materials* **2006**, *18*, 614-619.
- [24] A. Nodzevska, M. Watkinson, *Chemical Communications* **2018**, *54*, 1461-1464.
- [25] L. D. Dias, R. M. B. Carrilho, C. A. Henriques, G. Piccirillo, A. Fernandes, L. M. Rossi, M. F. Ribeiro, M. J. F. Calvete, M. M. Pereira, *Journal of Porphyrins and Phthalocyanines* **2018**, *22*, 331-341.
- [26] S. Kim, E. Ma, *Molecules* **2009**, *14*, 4655-4668.
- [27] B. Gabriele, R. Mancuso, G. Salerno, L. Veltri, M. Costa, A. Dibenedetto, *Chemsuschem* **2011**, *4*, 1778-1786.
- [28] J. Wu, J. A. Kozak, F. Simeon, T. A. Hatton, T. F. Jamison, *Chemical Science* **2014**, *5*, 1227-1231.
- [29] Y. Güneş, E. Şenocak, C. Tosun, Y. Taşkesenligil, *Organic Communications* **2009**, *2*, 79-83.
- [30] S. Qiu, G. N. Li, P. Liu, C. H. Wang, Z. C. Feng, C. Li, *Physical Chemistry Chemical Physics* **2010**, *12*, 3005-3013.
- [31] E. E. Ferrandi, C. Marchesi, C. Annovazzi, S. Riva, D. Monti, R. Wohlgemuth, *ChemCatChem* **2015**, *7*, 3171-3178.
- [32] A. Billiau, V. G. Eddy, H. Heremans, J. Vandamme, J. Desmyter, J. A. Georgiades, P. Desomer, *Antimicrobial Agents and Chemotherapy* **1977**, *12*, 11-15.
- [33] W. Strober, *Current Protocols in Immunology* **1997**, *21*, A.3A.1-A.3A.2.
- [34] T. Mosmann, *Journal of Immunological Methods* **1983**, *65*, 55-63.
- [35] P. Skehan, R. Storeng, D. Scudiero, A. Monks, J. McMahon, D. Vistica, J. T. Warren, H. Bokesch, S. Kenney, M. R. Boyd, *Journal of the National Cancer Institute* **1990**, *82*, 1107-1112.